Advances in Well Test Analysis

Robert C. Earlougher, Jr.

Senior Research Engineer

Marathon Oil Co.

Second Printing

Henry L. Doherty Memorial Fund of AIME

Society of Petroleum Engineers of AIME

New York **1977** **Dallas**

DEDICATION

To Evelyn, whose patience, understanding, and encouragement were essential to completion of this monograph.

ISBN 0-89520-204-2

Contents

SPE Monograph Series

The Monograph Series of the Society of Petroleum Engineers of AIME was established in 1965 by action of the SPE Board of Directors. The Series is intended to provide members with an authoritative, up-to-date treatment of the fundamental principles and state of the art in selected fields of technology. The work is directed by the Society's Monograph Committee, one of 40 national committees, through a Committee member designated as Monograph Coordinator. Technical evaluation is provided by the Monograph Review Committee. Below is a listing of those who have been most closely involved with the preparation of this book.

Monograph Coordinator

William C. Miller, Shell Development Co., Houston

Monograph Review Committee

Earl E. Morris, chairman, Amoco Production Co., Houston
John M. Campbell, Continental Oil Co., Houston
Vance J. Driscoll, Amoco Production Co., Houston
Bruce B. McGlothlin, Gulf Research & Development Co., Houston
L. J. Sanders, Amoco Production Co., Houston
Juris Vairogs, Cities Service Oil Co., Tulsa
Jerry L. Zink, Continental Oil Co., Houston

SPE Monograph Staff

Thomas A. Sullivan
Technical Services
Manager-Editor

Ann Gibson
Production Manager

Georgeann Bilich
Project Editor

Acknowledgments

This manuscript exists only because of significant support from many individuals. In particular, I am indebted to three of my Marathon colleagues, H. C. Bixel, Hossein Kazemi, and Shri B. Mathur,* who have heavily influenced the content and philosophy of this monograph. The four of us have worked closely in well test analysis for many years. As a team, we have prepared company handbooks and presented training courses in well test analysis for Marathon engineers. In so doing, we have developed a philosophy for presenting well test analysis material, and have learned which techniques are most successful and which are least successful for conveying information in an understandable and useable fashion. That philosophy and background pervade this monograph — it is impossible to separate my contributions from those of Messrs. Bixel, Kazemi, and Mathur. Additionally, Messrs. Bixel, Kazemi, and Mathur have contributed significantly to the presentation of much of the material in the monograph, if not in detail at least in substance. I very much appreciate all they have contributed toward making this a useful book.

The material presented in this monograph has been reviewed by members of the SPE-AIME Monograph Review Committee. They have spent hundreds of hours reading, checking, and critically commenting on all aspects of the material and its presentation. There is no doubt that the monograph is a much better volume than it would have been without their aid.

Marie E. LeBlanc typed the many versions of the manuscript required to reach the final form. Her secretarial skills and command of the English language have enabled preparation of this volume to proceed smoothly and on schedule.

Sally M. Andrews illustrated the monograph. Besides preparing all the original illustrations, she redrew many illustrations taken from the references to provide a consistent nomenclature and format. Her artist's viewpoint, her skill, and her highly accurate work have added substantially to this monograph.

*Presently with Shell Oil Co.

Preface

By about 1973, recent publications and advances in well test analysis were numerous enough to justify some type of update to C. S. Matthews' and D. G. Russell's monograph, *Pressure Buildup and Flow Tests in Wells*. In 1974, the Monograph Committee asked me to prepare an updated monograph that would include enough information to stand alone, rather than to just be a supplement or an update to the Matthews-Russell monograph. Although this book draws heavily on information in *Pressure Buildup and Flow Tests in Wells*, it is my belief that it can be used for most well test analysis situations without requiring other material.

In the mid-1960's, when the Matthews-Russell monograph was being prepared, reservoir simulation, and particularly the application of reservoir simulation to well test problems, was in its infancy. Subsequently, there has been a significant expansion of knowledge about well testing, much of it a result of the application of reservoir simulators. Publication of this monograph does not imply the belief that such advances will not continue, for they certainly will. I expect that there will be updated well test analysis monographs at regular intervals for many years to come.

The subject of this monograph is a broad and general one that is hard to define completely and concisely. I have attempted to present a valid and useful range of information rather than a completely comprehensive treatment (which would require many times the present length). As a result, there are many compromises. A high degree of technical accuracy (not always available) is sometimes sacrificed to provide methods with practical utility. Many available testing and analysis techniques are just referenced, while only the essence of others is presented, without consideration of minor qualifications and special cases that often appear in the original articles. In writing this book, I have made many value judgments, not only as to the accuracy and validity of a particular technique, but also as to its practical application and utility to the engineer. In general, I have attempted to provide information that can be used readily for practical and real problems. Most parts of the monograph give guidelines for applicability of various analysis techniques. One set of nomenclature is applied to all types of well testing. To show the interrelation and the minor differences between various tests, I include in Appendix E a comparison table that should be useful to the frequent monograph user.

The monograph is not written as a textbook or to provide theoretical background. There are no derivations, although the method for deriving some of the equations is suggested. The reader must return to the original reference material cited to find derivations. Worked examples are an important part of this monograph — more than 50 are included to illustrate analysis techniques presented and, frequently, to emphasize practical problems that arise in well test analysis.

I believe that most users of this monograph will find it logically organized and readily applicable to many well testing problems. Nevertheless, there will arise many situations for which the answer does not appear in this monograph and which will require further research on the part of the reader. As years pass, many currently unanswered questions will be answered; it is hoped that the next volume covering this subject will include many of those new answers.

Littleton, Colorado — ROBERT C. EARLOUGHER, JR.

February, 1976

Chapter 1

Introduction

1.1 Purpose

In 1967, Matthews and Russell published the first complete, cohesive treatment of well testing and analysis.[1] The Matthews-Russell monograph has become a standard reference for many petroleum engineers. Since the publication of that monograph, more than 150 additional well test analysis technical papers have been published. Those papers have extended the scope of well test analysis, publicized many new problems, provided solutions for previously unsolved problems, and changed the approach to some phases of well test analysis. Thus, it is appropriate to provide an updated monograph dealing with advances in well test analysis in a manner that presents an up-to-date treatment of the state of the art.

Enough material is presented so that this book can be used alone rather than solely as a supplement to the Matthews-Russell monograph. Matthews and Russell have presented the applicable history, the theoretical background of fluid flow, and the derivation of most of the equations used in well test analysis. Therefore, this monograph does not treat those subjects in detail, but refers to more rigorous treatment. The theory is brief and simple and derivations are minimized, since a detailed understanding of the mathematics involved in developing well test analysis equations is not necessary for correct engineering application. However, an understanding is often required of what a given method physically represents for appropriate engineering application. Thus, an attempt is made to be conceptually clear about different analysis techniques and to present estimates of the range of applicability. Examples illustrate most analysis techniques.

1.2 Use of Pressure Transient Testing in Petroleum Engineering

Reliable information about in-situ reservoir conditions is important in many phases of petroleum engineering. The reservoir engineer must have sufficient information about the reservoir to adequately analyze reservoir performance and predict future production under various modes of operation. The production engineer must know the condition of production and injection wells to coax the best possible performance from the reservoir. Much of that information can be obtained from pressure transient tests.

Pressure transient testing techniques, such as pressure buildup, drawdown, injectivity, falloff, and interference, are an important part of reservoir and production engineering. As the term is used in this monograph, pressure transient testing includes generating and measuring pressure variations with time in wells and, subsequently, estimating rock, fluid, and well properties. Practical information obtainable from transient testing includes wellbore volume, damage, and improvement; reservoir pressure; permeability; porosity; reserves; reservoir and fluid discontinuities; and other related data. All this information can be used to help analyze, improve, and forecast reservoir performance.

It would be a mistake to either oversell or undersell pressure transient testing and analysis. It is one of the most important in a spectrum of diagnostic tools. In certain situations it is indispensable for correct well or reservoir analysis; for example, in definition of near-wellbore and interwell conditions as opposed to composite properties that would be indicated by steady-state productivity index data. In other cases, a simpler approach is adequate, or a different or combined approach is needed to solve a problem.

Consider the case of a pumping oil well with substantial production decline. It usually would be inappropriate to run a pressure buildup test without first determining whether the problem was merely a worn pump and high working fluid level or some other mechanical problem. If a simple approach fails to identify the problem, a pressure buildup test could be indispensable in pinpointing that the specific problem is related to damage at or near the formation face rather than to rapid reservoir depletion.

On the other hand, even with the most complex and thorough transient analysis, a unique solution often is not possible without considering other information. Pressure interference or pulse testing could establish the possible existence and orientation of vertical fractures in a reservoir. However, other information (such as profile surveys, production logs, stimulation history, well production tests, borehole televiewer surveys or impression packer tests, core descriptions, and other geological data about reservoir lithology and continuity) would be useful in distinguishing between directional permeability and fractures or estimating

whether the fractures were induced or natural.

In practice, engineering application of pressure transient analysis is often limited by (1) insufficient data collection; (2) inappropriate application of analysis techniques; or (3) failure to integrate other available or potentially available information. Most practicing engineers are aware of instances where a definitive analysis has been precluded by a lack of accurate early pressure and withdrawal information or prior base data for comparative purposes.

It is generally good practice to run a base pressure transient test on a producing well shortly after completion or on an injection well after a suitable period of injection. This can lead to early recognition and correction of many problems, of which insufficient stimulation is only the most obvious. Such tests also provide in-situ data for reservoir simulation and a base for comparison with reservoir or well problems as they arise.

1.3 Organization, Scope, and Objectives

The data in this monograph should enable the petroleum engineer to design, conduct, and analyze pressure transient tests to obtain reliable information about reservoir and well conditions. Each chapter is, as nearly as possible, an independent unit. For completeness, Chapter 1 includes a short discussion of unit conversion factors and the SI (metric) unit system. Appendix A provides a list of conversion factors and a tabulation of some of the more important equations in oilfield units, groundwater units, and three sets of metric units.

Chapter 2 is a summary of transient fluid flow behavior and sets the stage for all transient test analysis procedures in the text. The approach is a pragmatic one that provides the reader with material to derive methods of test analysis and to calculate expected transient response in wells. Since recent advances have modified some older methods, we attempt to integrate and present what appears to be best current engineering practice. Many research studies, invaluable in themselves for providing insight or cross-checks on the validity of other work, are not necessarily suitable for direct field application. Others, although complex, provide ways to estimate important reservoir properties. In situations where only minor differences in accuracy would result by using simpler methods, preference has been given to the simpler method. Nevertheless, test analysis procedures in the monograph may be used without complete understanding of Chapter 2. Appendix B presents a detailed theoretical treatment of the use of superposition to generate new solutions that may be useful to some readers. Appendix C presents a wide range of dimensionless solutions incorporating various geometries and boundary conditions.

The chapters describing basic testing and analysis techniques utilize the flow theory of Chapter 2, but otherwise stand alone. Since the primary thrust of the monograph is toward the practicing engineer, an effort has been made to set bounds and define the range of applicability of various solutions or techniques. Chapter 3 covers pressure drawdown testing, the most theoretically simple form of pressure transient testing. It also introduces type-curve matching. That relatively new (to the petroleum industry) approach allows the engineer to effectively use more sophisticated transient solutions incorporating wellbore storage effects, deep fracturing, complex boundary conditions, etc., when simpler analysis techniques are not applicable.

Chapter 4 covers multiple-rate testing and discusses how superposition may be used where variable rates are involved. Chapter 5 treats pressure buildup test analysis; and Chapter 6 presents methods for estimating average pressure for well drainage areas and the entire reservoir. Chapter 7 deals with injection well testing, a matter of ever-increasing importance. Chapter 8 discusses drillstem test analysis.

Chapter 9 gives transient testing techniques utilizing more than one well. Chapter 10 covers the effects of reservoir heterogeneities on pressure behavior. Chapter 11 provides more detailed information on the effects of wellbore storage and induced fractures on pressure transient behavior. Chapter 12 briefly discusses computer methods; and Chapter 13 considers design and instrumentation of pressure transient tests.

Appendix D presents methods and correlations for estimating many reservoir rock and fluid properties; and Appendix E summarizes well test analysis equations.

1.4 Nomenclature and Units

As much as possible, the standard symbols adopted by the Society of Petroleum Engineers of AIME[2-4] are used throughout this monograph. "Oilfield units" are used in equations *consistently:* flow rate, q, is in stock-tank barrels per day; permeability, k, is in millidarcies; time, t, is in hours; viscosity, μ, is in centipoise; compressibility, c, is in volume/volume/pounds per square inch; and porosity, ϕ, is always used as a fraction. Units are included in the nomenclature list. Occasionally, different units are used to be consistent with industry usage; such cases are clearly identified.

Throughout the monograph, a positive flow rate, $q > 0$, signifies production, while a negative flow rate, $q < 0$, designates injection. The sign convention requires that the correct sign be given to slopes of various data plots. That results in some equations that are slightly different from forms commonly seen in the literature. However, this is a practical way to approach transient test analysis.

We expect that metric units eventually will be the only accepted units in engineering. For that reason, Appendix A provides information outlining the definition of the "SI" units of weights and measures, along with factors for converting to SI from customary units. SI is the official abbreviation, *in all languages*, for the International System of Units (les Systéme International d'Unités). The International System is neither the centimetre-gram-second (cgs) system nor the metre-kilogram-second (mks) system, but is a modernized version of mks. A complete description of SI is presented by Hopkins.[5] The American Petroleum Institute has proposed a set of metric standards for use in the petroleum industry.[6] Most nations are gravitating toward exclusive use of SI, so SI units are given top billing in the conversion tables in Appendix A.

Tables A.1 and A.2 provide general information about the SI system. Table A.3 gives values for physical constants useful in petroleum engineering. Table A.4 gives general

conversion factors. Table A.5 presents conversion factors that include permeability. Table A.6 deals with temperature scales and conversions. Finally, Table A.7 compares units and equations for well testing from five unit systems. Oilfield units are used *exclusively* throughout the remainder of this monograph.

In this monograph, the term permeability (k) is sometimes used even though the terms mobility (k/μ) or mobility-thickness product (kh/μ) may be more appropriate. This is done because permeability is a property of the rock rather than a combined property of rock and fluid. Even though this convention is used, it is important to recognize that the mobility-thickness product almost always appears as a unit in the flow and transient test analysis equations. Similarly, porosity (ϕ) is sometimes used rather than the commonly associated porosity-thickness product (ϕh) or porosity-compressibility-thickness ($\phi c_t h$) product.

References

1. Matthews, C. S. and Russell, D. G.: *Pressure Buildup and Flow Tests in Wells*, Monograph Series, Society of Petroleum Engineers of AIME, Dallas (1967) **1.**
2. "Letter Symbols for Petroleum Reservoir Engineering, Natural Gas Engineering, and Well Logging Quantities," Society of Petroleum Engineers of AIME, Dallas (1965).
3. "Supplements to Letter Symbols and Computer Symbols for Petroleum Reservoir Engineering, Natural Gas Engineering, and Well Logging Quantities," Society of Petroleum Engineers of AIME, Dallas (1972).
4. "Supplements to Letter Symbols and Computer Symbols for Petroleum Reservoir Engineering, Natural Gas Engineering, and Well Logging Quantities," Society of Petroleum Engineers of AIME, Dallas (1975).
5. Hopkins, Robert A.: *The International (SI) Metric System and How It Works*, Polymetric Services, Inc., Tarzana, Calif. (1974).
6. "Conversion of Operational and Process Measurement Units to the Metric (SI) System," *Manual of Petroleum Measurement Standards*, Pub. API 2564, American Petroleum Institute (March 1974) Chap. 15, Sec. 2.

Chapter 2

Principles of Transient Test Analysis

2.1 Introduction

This chapter summarizes the basic transient flow theory for the well testing and analysis techniques presented in this monograph. An understanding of the following material should clarify the techniques presented later, as well as allow the reader to devise additional testing and analysis techniques. Nevertheless, it is possible to use the material in Chapters 3 through 13 without a thorough reading and understanding of this chapter.

All basic theory needed in the monograph is summarized here. We neither derive the basic flow equations nor show how to solve them. Rather, a general equation is used for transient pressure behavior with dimensionless pressure solutions for the specific conditions desired. Some important dimensionless pressure functions are presented in this chapter and in Appendix C, and references to others are provided. The dimensionless pressure approach provides a way to calculate pressure response and to devise techniques for analyzing transient tests in a variety of systems.

Sections covering wellbore storage effects and wellbore damage and improvement are included, since those effects have a significant influence on transient well response. The reader is encouraged to study those sections, even if he only scans the rest of the chapter. Chapter 11 provides additional information about the effects of those two quantities.

2.2 Basic Fluid-Flow Equation

The differential equation for fluid flow in a porous medium, the diffusivity equation, is a combination of the law of conservation of matter, an equation of state, and Darcy's law.[1-4] When expressed in radial coordinates, the diffusivity equation is*

$$\frac{\partial^2 p}{\partial r^2} + \frac{1}{r}\frac{\partial p}{\partial r} = \frac{1}{0.0002637}\,\frac{\phi\mu c_t}{k}\,\frac{\partial p}{\partial t} \quad \ldots\ldots\ldots (2.1)$$

Matthews and Russell[1] present a derivation of Eq. 2.1 and point out that it assumes horizontal flow, negligible gravity effects, a homogeneous and isotropic porous medium, a single fluid of small and constant compressibility, and applicability of Darcy's law, and that μ, c_t, k, and ϕ are independent of pressure. As a result of those assumptions, and since the common boundary conditions are linear, Eq. 2.1 is linear and readily solved. Therefore, solutions (dimensionless pressures) may be added together to form new solutions, as indicated in Section 2.9. If ϕ, μ, c_t, or k are strong functions of pressure, or if varying multiple fluid saturations exist, Eq. 2.1 must be replaced by a nonlinear form. That equation usually must be solved using computer analysis methods (numerical reservoir simulation) beyond the scope of this monograph.

Boundary conditions are an important factor in solutions to Eq. 2.1. Most transient-test analysis techniques assume a single well operating at a constant flow rate in an infinite reservoir. That boundary condition is useful because every well transient is like that of a single well in an infinite reservoir — at early time. At later times the effects of other wells, of reservoir boundaries, and of aquifers influence well behavior and cause it to deviate from the "infinite-acting" behavior. Thus, different solutions to Eq. 2.1 are required for longer time periods. Superposition or other solutions are needed to include other factors, such as gradually changing rate at the formation face (wellbore storage), hydraulic fractures, layered systems, or the presence of multiple fluids or boundaries. Many of those solutions are presented in Appendix C and Chapters 10 and 11; Matthews and Russell[1] present others. The solution for a constant-pressure well is given in Chapter 4.

Although Eq. 2.1 appears to be severely restricted by its basic assumptions, under certain circumstances it can be applied to both multiple-phase flow and gas flow, as indicated in Sections 2.10 and 2.11.

2.3 Solutions to the Flow Equation — Dimensionless Quantities

Comprehensive treatments of transient well testing normally use a general approach for providing solutions to the diffusivity equation, Eq. 2.1. Such an approach provides a convenient way of summarizing the increasing number of solutions being developed to more accurately depict well or reservoir pressure behavior over a broad range of time, boundary, and geometry conditions. The general solutions

*Symbols and units are defined in the Nomenclature. Normally, only deviations from that list are discussed in the text.

rely on the concepts of dimensionless pressure and dimensionless time, explained later in this section. Some solutions are identical to others in certain time ranges, but are significantly different in others. Thus, throughout the monograph, guidelines indicate where complex solutions are needed and where the simpler solutions normally give adequate results.

An unfortunate consequence of the generalized dimensionless-solution approach is that the dimensionless parameters do not provide the engineer with the physical feel available when normal dimensional parameters are used. For example, a real time of 24 hours may correspond to a dimensionless time range from about 300 for a tight gas reservoir to more than 10^7 for a highly permeable oil reservoir. The pressure corresponding to a 24-hour time in those two situations might vary by hundreds of pounds per square inch. Fortunately, after one works long enough with dimensionless variables, one does begin to get a feel for them. Nevertheless, it is always good practice to calculate physical quantities from dimensionless ones; that is easily done because physical quantities are *directly proportional* to dimensionless quantities.

The dimensionless-solution approach can be illustrated by starting with the familiar steady-state radial flow equation:

$$q = 0.007082 \frac{kh(p_e - p_w)}{B\mu \ln(r_e/r_w)}.$$

This equation may be solved for the pressure difference,

$$p_e - p_w = 141.2 \frac{qB\mu}{kh} \ln(r_e/r_w).$$

Changing to dimensionless form, the radial flow equation becomes

$$p_e - p_w = 141.2 \frac{qB\mu}{kh} p_D,$$

where

$$p_D = \ln(r_e/r_w).$$

Thus, the physical pressure drop in the steady-state radial-flow situation is equal to a dimensionless pressure drop, which in this case is simply $\ln(r_e/r_w)$, times a scaling factor. The scaling factor depends on flow rate and reservoir properties only. The same concept applies to transient flow and to more complex situations — only the dimensionless pressure is different. It is this generality that makes the dimensionless-solution approach useful.

The advantages of the dimensionless form occur, as indicated previously, when situations get more complex. In general terms, the pressure at any point in a single-well reservoir being produced at constant rate, q, is described with the generalized solution of Eq. 2.1:

$$p_i - p(t,r) = 141.2 \frac{qB\mu}{kh} \left[p_D(t_D, r_D, C_D, \text{geometry}, \ldots) + s\right], \quad \ldots\ldots\ldots (2.2)$$

where p_i is the initial, *uniform* pressure existing in the reservoir before production or injection; q is the *constant* surface flow rate; k, h, and μ are *constant* reservoir properties; p_D is the dimensionless-pressure solution to Eq. 2.1 for the appropriate boundary conditions; and s is the skin effect, a dimensionless pressure drop assumed to occur at the wellbore face as a result of wellbore damage or improvement.[5,6] Skin effect, s, only appears in Eq. 2.2 when $r_D = 1$. (See Section 2.5.)

In *transient* flow, p_D is *always* a function of dimensionless time,

$$t_D = \frac{0.0002637\,kt}{\phi\mu c_t r_w^2}, \quad \ldots\ldots\ldots\ldots\ldots\ldots (2.3a)$$

when based on wellbore radius, or

$$t_{DA} = \frac{0.0002637\,kt}{\phi\mu c_t A} = t_D \left(\frac{r_w^2}{A}\right), \quad \ldots\ldots\ldots (2.3b)$$

when based on total drainage area. Dimensionless pressure also varies with location in the reservoir, as indicated in Eq. 2.2 by the dimensionless radial distance from the operating well,

$$r_D = r/r_w. \quad \ldots\ldots\ldots\ldots\ldots\ldots\ldots\ldots\ldots (2.4)$$

The point location also may be expressed in Cartesian coordinates. Dimensionless pressure is also affected by system geometry, other system wells, the wellbore storage coefficient of the producing well, anisotropic reservoir characteristics, fractures, radial discontinuities, and other physical features.

Dimensionless pressure, p_D, is a solution to Eq. 2.1 for specific boundary conditions and reservoir geometry. Practically speaking, dimensionless pressure is just a number given by an equation, a table, or a graph. Some expressions for p_D are given in Sections 2.4, 2.7, and 2.8, and Appendix C. The dimensionless-pressure approach is used throughout this monograph because of its simplicity and general applicability in well-test development and analysis. The approach, which is easy to apply, results in simple, general equations that apply to any set of reservoir properties. It is easily adapted to mathematical manipulation and superposition (Section 2.9), so more complex systems can be considered. For simplicity, the following conventions apply throughout this monograph:

1. Although dimensionless pressure is generally a function of time, location, system geometry, and other variables, we commonly write $p_D(t_D, \ldots)$, $p_D(t_D)$, or just p_D. Dimensionless pressure, p_D, is a number that may be obtained from an equation, figure or table; it scales linearly to real pressure.

2. The symbol t_D always refers to dimensionless time calculated from Eq. 2.3a using the *wellbore radius*. It is clearly indicated when dimensionless time is based on some other dimension. Dimensionless time is just real time multiplied by a scale factor that depends on reservoir properties.

3. Eq. 2.2 includes the van Everdingen-Hurst[5,6] skin factor. That factor appears only when calculating Δp for a producing or injecting well. In general, s is not shown in equations unless it is specifically used. The reader should recognize that adding s is necessary under the appropriate circumstances.

The following example illustrates the use of Eq. 2.2 to estimate flowing well pressure in a closed system.

Example 2.1 Estimating Well Pressure

Estimate the pressure at a well located in the center of a closed-square reservoir after it has produced 135 STB/D of dry oil for 15 days. Other data are*

$p_i = 3{,}265$ psi	$\phi = 0.17$
$k_o = 90$ md	$c_t = 2.00 \times 10^{-5}$ psi^{-1}
$\mu_o = 13.2$ cp	$r_w = 0.50$ ft
$B_o = 1.02$ RB/STB	$A = 40$ acres $= 1{,}742{,}400$ sq ft
$h = 47$ ft	$s = 0$.

Curve A of Fig. C.13 is used for p_D since it applies to a closed-square system with a well at the center.

Using Eq. 2.3b,

$$t_{DA} = \frac{(0.0002637)(90)(15 \times 24)}{(0.17)(13.2)(2.00 \times 10^{-5})(1{,}742{,}400)}$$

$$= 0.109.$$

From Curve A of Fig. C.13, $p_D(t_{DA} = 0.109) = 6.95$. Rearranging Eq. 2.2 and substituting values,

$$p_{wf}(t, r_w) = 3{,}265 - \frac{(141.2)(135)(1.02)(13.2)}{(90)(47)}(6.95)$$

$$= 2{,}843 \text{ psi}.$$

Fig. 2.1 schematically illustrates three transient flow regimes for a closed drainage system. Dimensionless pressure is shown as a function of both t_{DA} and log (t_{DA}). The portion marked A is the early transient or infinite-acting flow regime; we prefer the term "infinite-acting", since all wells act as if they were alone in an infinite system at short flow times. The infinite-acting period is characterized by a straight line on the semilog plot, Fig. 2.1b. The portion of the curves labeled C in Fig. 2.1 is the pseudosteady-state flow regime that occurs in all closed systems. During pseudosteady-state flow, pressure changes linearly with time, as shown in Fig. 2.1a. The B portion of the curves is the transition period between infinite-acting and pseudosteady-state flow.

In Fig. 2.1, flow is transient *at all times*. Some systems exhibit true steady-state behavior with p_D constant. Those systems are most commonly observed in laboratory core flooding and permeability measurement experiments; they also may exist in fluid injection projects with balanced production and injection and in reservoirs with a strong natural water drive.

*In the examples in this monograph, data values are not always stated to their full number of significant digits. In such cases, values are assumed to have three significant digits with significant zeroes omitted. Computations are usually done using the intermediate values shown. When intermediate values are not shown, all computed digits have been used and the final result has been rounded off.

2.4 Dimensionless Pressure During the Infinite-Acting Flow Period

Fig. 2.2 is a schematic representation of a single well producing at constant rate q in an infinite, horizontal, thin reservoir containing a single-phase, slightly compressible fluid. When the assumptions of Eq. 2.1 are satisfied, Eq. 2.2, with p_D from Fig. 2.3, describes the pressure behavior at any point in the system. Fig. 2.3 shows p_D is a function of t_D and of r_D, the dimensionless radial distance from the well, for the infinite-acting system. (Fig. C.1 is a full-scale gridded version of Fig. 2.3.) When $r_D \geq 20$ and $t_D/r_D^2 \geq 0.5$, or when $t_D/r_D^2 \geq 25$, the $r_D = 20$ and the "exponential-integral solution" lines on Figs. 2.3 and C.1 are essentially the same, so p_D depends only on t_D/r_D^2 under those conditions.[8] The exponential-integral solution[1,4] (also called the line-source or the Theis[9] solution) to the flow equation is

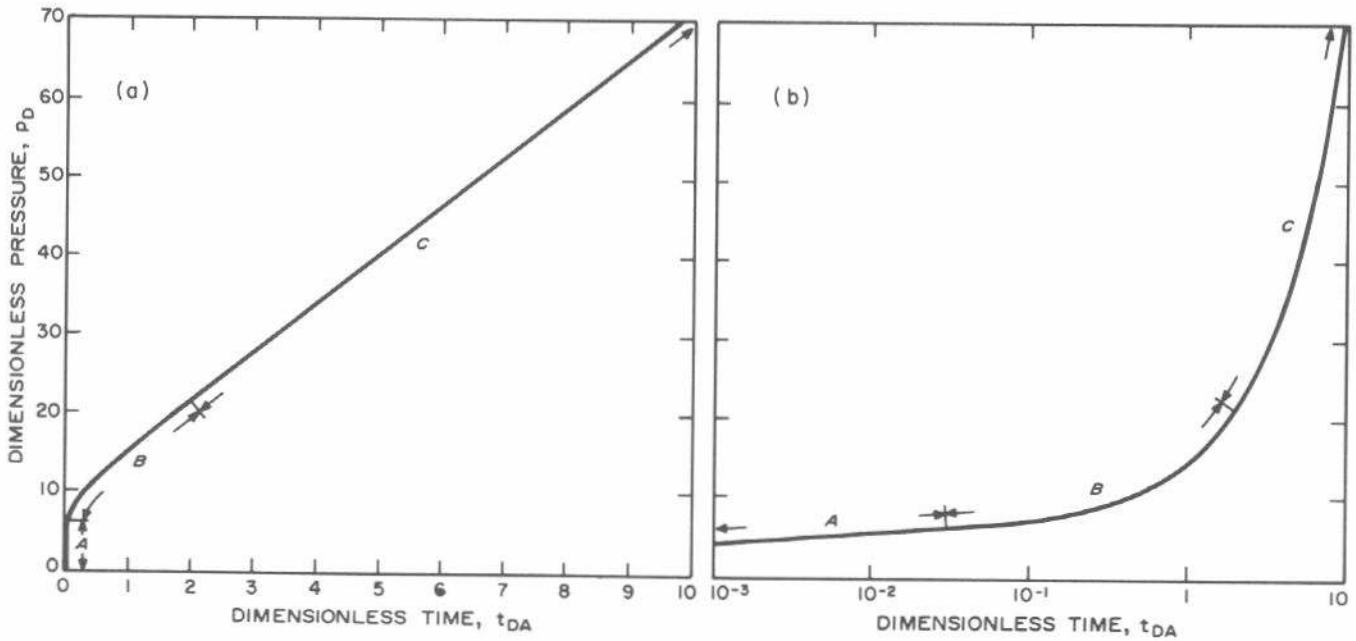

Fig. 2.1 Transient flow regimes: A — infinite acting; B — transition; C — pseudosteady state. Data from Earlougher and Ramey[7] for a 4:1 rectangle with the well at $x/L = 0.75$, $y/W = 0.5$.

$$p_D(t_D, r_D) = -\frac{1}{2}\,\mathrm{Ei}\left(\frac{-r_D^2}{4t_D}\right), \quad \ldots\ldots\ldots\ldots\ldots (2.5a)$$

$$\simeq \frac{1}{2}\left[\ln(t_D/r_D^2) + 0.80907\right]. \quad \ldots\ldots\ldots (2.5b)$$

Eq. 2.5b may be used when

$$t_D/r_D^2 > 100, \quad \ldots\ldots\ldots\ldots\ldots\ldots\ldots\ldots\ldots (2.6)$$

but the difference between Eq. 2.5a and Eq. 2.5b is only about 2 percent when $t_D/r_D^2 > 5$. Thus, for *practical* purposes, the log approximation to the exponential integral is satisfactory when the exponential integral is satisfactory. Nevertheless, the more accurate limit of Eq. 2.6 is used in this monograph.

The exponential integral is defined by

$$\mathrm{Ei}(-x) = -\int_x^\infty \frac{e^{-u}}{u}\,du. \quad \ldots\ldots\ldots\ldots\ldots (2.7a)$$

Values may be taken from tables[10] or may be approximated from

$$\mathrm{Ei}(-x) \simeq \ln(x) + 0.5772 \quad \text{for } x < 0.0025. \quad \ldots\ldots (2.7b)$$

At the operating well $r_D = 1$, so $t_D/r_D^2 = t_D$. Since $t_D > 100$ after only a few minutes for most systems, there is practically no difference between the two forms of Eq. 2.5, as illustrated by the following example.

Example 2.2 Estimating Pressure vs Time History of a Well

Use the exponential-integral solution and the data of Example 2.1 to estimate the pressure vs time relationship for a well in an infinite-acting system.

We calculate p_{wf} at 1 minute and at 10 hours to illustrate the procedure; final results are shown in Fig. 2.4. From Eq. 2.3a,

$$t_D = \frac{(0.0002637)(90)\,t}{(0.17)(13.2)(2.00\times 10^{-5})(0.50)^2}$$

$$= 2{,}115\,t.$$

At 1 minute, $t_D = (2{,}115)(1/60) = 35.25$. The exponential-integral solution, Eq. 2.5a, applies because $t_D/r_D^2 = 35.25/1 > 25$. However, since $t_D/r_D^2 = 35.25 < 100$, the log approximation, Eq. 2.5b, should not be used. Using Eq. 2.5a and evaluating p_D from Fig. C.1, we get $p_D(t_D = 35.25) = 2.18$. Then, rearranging Eq. 2.2,

$$p_{wf}(t = 1 \text{ minute}) = 3{,}265 - \frac{(141.2)(135)(1.02)(13.2)}{(90)(47)} \quad (2.18)$$

$$= 3{,}265 - (60.67)(2.18) = 3{,}133 \text{ psi}.$$

At 10 hours, $t_D = (2{,}115)(10) = 21{,}150$ and the log approximation, Eq. 2.5b, can be used:

$$p_D = \frac{1}{2}\left[\ln(21{,}150/1) + 0.80907\right]$$

$$= 5.384,$$

so

$$p_{wf}(t = 10 \text{ hours}) = 3{,}265 - (60.67)(5.384)$$

$$= 2{,}938 \text{ psi}.$$

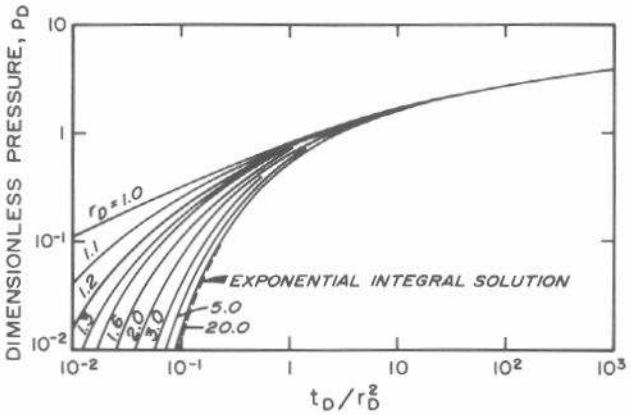

Fig. 2.3 Dimensionless pressure function at various dimensionless distances from a well located in an infinite system. After Mueller and Witherspoon.[8]

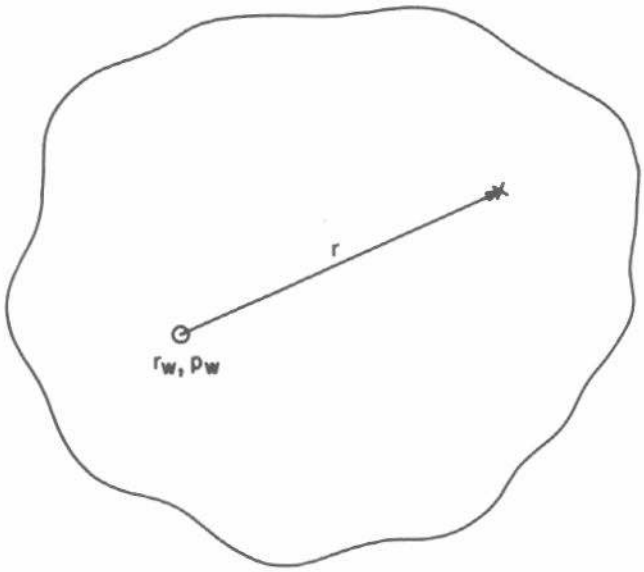

Fig. 2.2 Infinite system with a single well.

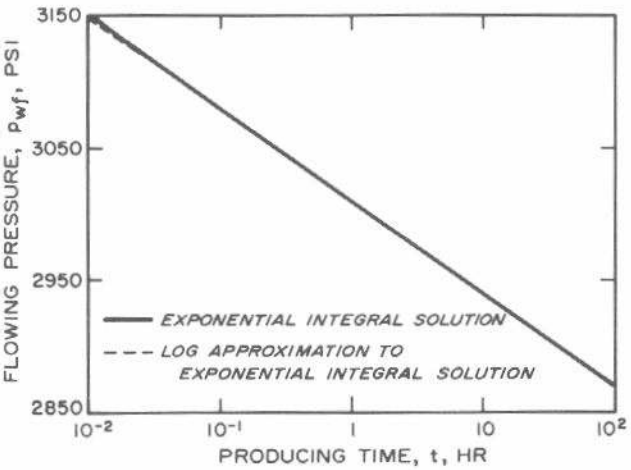

Fig. 2.4 Calculated pressure response for a well in an infinite-acting system. Example 2.2.

The response from 0.01 hour (0.6 minute) to 100 hours is shown in Fig. 2.4. The dashed line is the log approximation for $t_D/r_D^2 < 100$; after that time the two lines coincide. Note how well the two solutions (Eqs. 2.5a and 2.5b) agree, even for $t_D/r_D^2 = (2,115)(0.01)/1 = 21$.

As mentioned previously, all wells are infinite-acting for some time after a change in rate. For drawdown, the duration of the infinite-acting period may be estimated from

$$t_{eia} = \frac{\phi\mu c_t A}{0.0002637k}(t_{DA})_{eia}, \quad \ldots\ldots\ldots\ldots\ldots\ldots (2.8a)$$

where t_{DA} at the end of the infinite-acting period is given in the "Use Infinite System Solution With Less Than 1% Error for $t_{DA} <$" column of Table C.1. For a well in the center of a closed circular reservoir, $(t_{DA})_{eia} = 0.1$ and

$$t_{eia} \simeq \frac{380\ \phi\mu c_t A}{k}. \quad \ldots\ldots\ldots\ldots\ldots\ldots (2.8b)$$

Equations for buildup are given in Section 5.3.

2.5 Wellbore Damage and Improvement Effects

There are several ways to quantify damage or improvement in operating (producing or injecting) wells. A favored method represents the wellbore condition by a steady-state pressure drop at the wellface in addition to the normal transient pressure drop in the reservoir. The additional pressure drop, called the "skin effect," occurs in an infinitesimally thin "skin zone."[5,6] In the flow equation, Eq. 2.2, the degree of damage (or improvement) is expressed in terms of a "skin factor," s, which is positive for damage and negative for improvement. It can vary from about -5 for a hydraulically fractured well to $+\infty$ for a well that is too badly damaged to produce. Eq. 2.2 indicates the pressure drop at a damaged (or improved) well differs from that at an undamaged well by the additive amount

$$\Delta p_s = \frac{141.2\ qB\mu}{kh}\, s \quad \ldots\ldots\ldots\ldots\ldots\ldots (2.9)$$

Fig. 2.5A illustrates the idealized pressure profile for a damaged well ($s > 0$). Since the damage-zone thickness is considered to be infinitesimal, the entire pressure drop caused by the skin occurs at the wellface. The thin-skin approximation results in a pressure gradient reversal for wellbore improvement ($s < 0$), shown in Fig. 2.5B. Although this situation is physically unrealistic, the skin-factor concept is valuable as a measure of wellbore improvement. A more physically realistic pressure profile for the negative skin situation is also shown in Fig. 2.5B.

If the skin is viewed as a zone of finite thickness with permeability k_s, as shown in Fig. 2.6, then[11]

$$s = \left(\frac{k}{k_s} - 1\right)\ln\left(\frac{r_s}{r_w}\right). \quad \ldots\ldots\ldots\ldots\ldots\ldots (2.10)$$

Either s, k_s, or r_s may be estimated from Eq. 2.10 if the other two parameters are known.

It is also possible to define an apparent wellbore radius for use in Eqs. 2.3 and 2.4 so the correct pressure drop at the well results when $s = 0$ is used in Eq. 2.2:[12]

$$r_{wa} = r_w e^{-s}. \quad \ldots\ldots\ldots\ldots\ldots\ldots\ldots\ldots (2.11)$$

For positive s, $r_{wa} < r_w$; for negative s, $r_{wa} > r_w$.

Eqs. 2.2 and 2.9 show that the skin factor simply increases or decreases the pressure change at a well proportional to the flow rate of that well. When dimensionless pressure functions include the skin factor (for example,

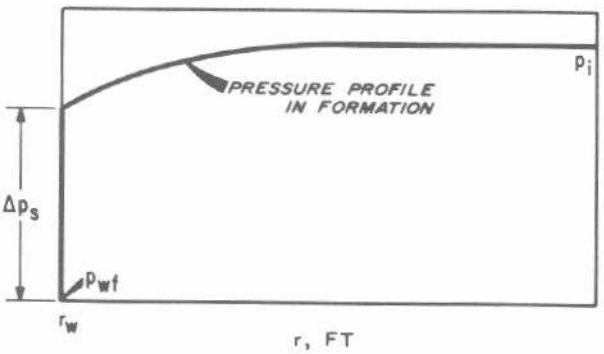

Fig. 2.5A Pressure distribution around a well with a positive skin factor.

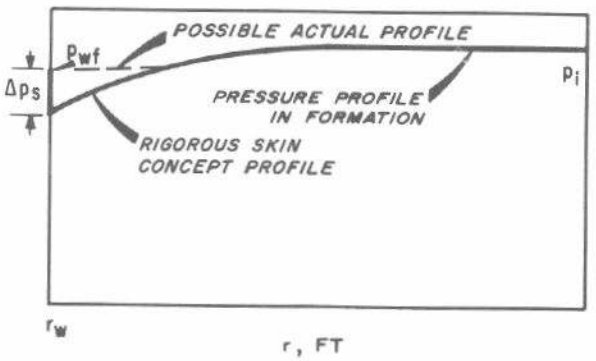

Fig. 2.5B Pressure distribution around a well with a negative skin factor.

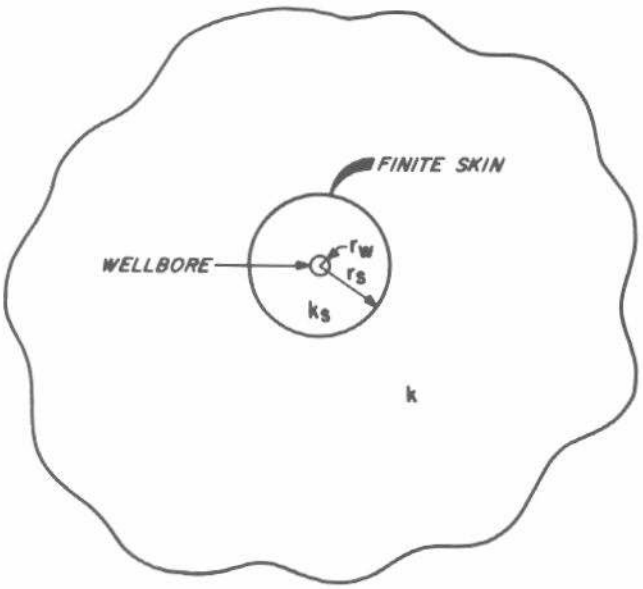

Fig. 2.6 Skin zone of finite thickness.

Figs. C.6 and C.7), it should not be included explicitly in Eq. 2.2. Dimensionless pressure functions that include the skin factor are particularly useful when the skin zone extends for some distance rather than being concentrated within a few feet of the wellbore. The skin-factor concept is used only for pressures at the well. When the skin affects some r_s around the well, the pressure profile in that region will be modified (for example, see Fig. 2.5B). In such situations, special p_D functions that include s must be used to determine pressures near the well. When using Eq. 2.2 to estimate pressure at distances greater than r_w or r_{wa}, the s term is omitted, and normal p_D's are used.

The *flow efficiency* (also called the condition ratio) indicates the approximate fraction of a well's undamaged producing capacity. It is defined as the ratio of the well's actual productivity index to its productivity index if there were no skin.[1] For closed systems, the *flow efficiency* is

$$\frac{J_{\text{actual}}}{J_{\text{ideal}}} = \frac{\bar{p} - p_{wf} - \Delta p_s}{\bar{p} - p_{wf}} \quad \ldots\ldots\ldots\ldots (2.12)$$

Although the drainage-area average pressure, $\bar{p}$, should be used in Eq. 2.12, it is frequently permissible to use the extrapolated buildup pressure,[1] p^*. Flow efficiency depends on the flowing pressure, p_{wf}, and thus it depends on how long the well has been operating unless the well is at pseudosteady-state conditions. (At pseudosteady state, $\bar{p} - p_{wf}$ is constant.) For wells operating at true steady state, $\bar{p}$ should be replaced by p_e, the pressure that the area will reach after extended shut-in.

The *damage ratio* and *damage factor* are also relative indicators of wellbore condition. The inverse of the flow efficiency is the *damage ratio*:

$$\frac{J_{\text{ideal}}}{J_{\text{actual}}} = \frac{\bar{p} - p_{wf}}{\bar{p} - p_{wf} - \Delta p_s} \quad \ldots\ldots\ldots\ldots (2.13)$$

By subtracting the flow efficiency from 1, we obtain the *damage factor*:

$$1 - \frac{J_{\text{actual}}}{J_{\text{ideal}}} = \frac{\Delta p_s}{\bar{p} - p_{wf}} \quad \ldots\ldots\ldots\ldots\ldots (2.14)$$

The following example illustrates the wellbore damage indicators.

Example 2.3 Wellbore Damage Indicators

A pressure buildup-test analysis for a well with $q = 83$ STB/D, $B = 1.12$ RB/STB, $\mu = 3.15$ cp, $h = 12$ ft, $r_w = 0.265$ ft, and $\bar{p} - p_{wf} = 265$ psi gave $k = 155$ md and $s = 2.2$. Find the pressure drop across the skin, the flow efficiency, the damage ratio, the damage factor, and the apparent wellbore radius.

Using Eq. 2.9,

$$\Delta p_s = \frac{(141.2)(83)(1.12)(3.15)}{(155)(12)}(2.2) = 49 \text{ psi}.$$

The flow efficiency is estimated from Eq. 2.12:

$$\frac{265 - 49}{265} = 0.82 = 82 \text{ percent}.$$

Using Eq. 2.13, the damage ratio is

$$\frac{1}{0.82} = 1.22,$$

and using Eq. 2.14, the damage factor is

$$1 - 0.82 = 0.18.$$

The apparent wellbore radius is estimated from Eq. 2.11:

$$r_{wa} = 0.265\, e^{-2.2} = 0.03 \text{ ft}.$$

Damage at this well is reducing production to about 82 percent of the value that could be expected without damage or stimulation.

Wells completed with only a part of the formation thickness open to the wellbore can appear to be damaged. Partial penetration (wells not drilled completely through the productive interval) and partial completion (entire productive interval not perforated) are examples.[13] (See Section 11.4 for more information and references.) Fig. 2.7 shows theoretical "pseudoskin" factors for partially penetrating wells. The skin factor estimated from a transient test would be that given by Fig. 2.7 if there were no true *physical* damage (or improvement) at the well. If there is physical damage, the calculated skin factor is higher than indicated by Fig. 2.7.

Skin factors estimated from transient tests on hydrauli-

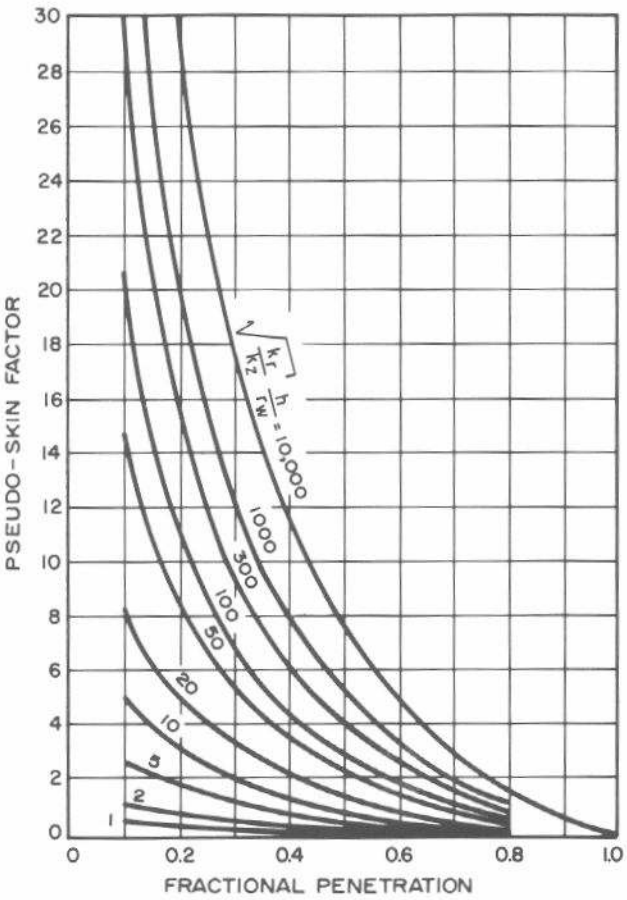

Fig. 2.7 Pseudoskin factor for partially penetrating wells. After Brons and Marting.[13]

cally fractured wells are generally negative. Fig. 2.8 compares the dimensionless pressure for an ideal, undamaged, unstimulated well with that for a hydraulically fractured well with a half-fracture length of 31.63 r_w. At small t_D, the difference between the two dimensionless pressure curves, which is s (Eq. 2.2), varies; at larger t_D that difference is constant. This indicates that reasonable skin values can be estimated from transient tests for many hydraulically fractured wells. However, when large fracture jobs are known to have been performed, the fracture should be accounted for by analyzing well tests using the type-curve matching method (Section 3.3) with Figs. C.3, C.4, C.5, C.17, C.18, or C.19. An important feature of all the log-log plots of fractured-well p_D data is the slope of ½ at small t_D. This slope also will be observed on a log-log plot of transient *pressure difference* data from fractured wells, unless it is obscured by wellbore storage. Section 11.3 provides additional details.

2.6 Wellbore Storage

Wellbore storage, also called afterflow, afterproduction, afterinjection, and wellbore unloading or loading, has long been recognized as affecting short-time transient pressure behavior.[2,14] More recently, several authors[15-26] have considered wellbore storage in detail. It is easy to see that liquid is stored in the wellbore when the liquid level rises. That situation occurs when a pumping well without a packer is shut in; indeed, bottom-hole pressure is often deduced by measuring liquid level. When wellbore storage is significant, it must be considered in transient test design and analysis. If it is not considered, the result may be an analysis of the wrong portion of the transient test data, the deduction of nonexistent reservoir conditions (faults, boundaries, etc.), or an analysis of meaningless data. Fortunately, the effects of wellbore storage usually can be accounted for in test analysis — or can be avoided by careful test design.

The wellbore storage constant (coefficient, factor) is defined[16] by

$$C = \frac{\Delta V}{\Delta p}, \quad \ldots\ldots\ldots\ldots\ldots\ldots\ldots\ldots\ldots\ldots (2.15)$$

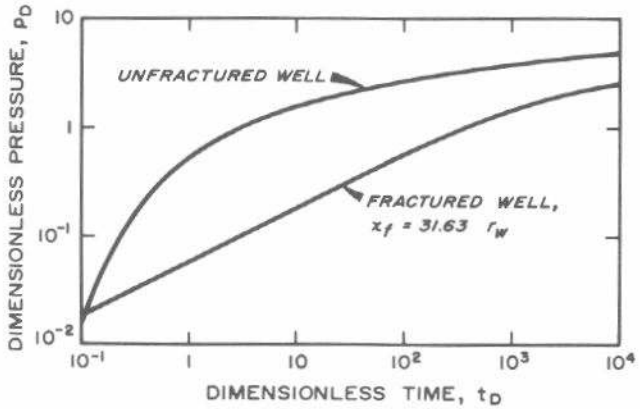

Fig. 2.8 Comparison of dimensionless pressures for an ideal well and for a well with a single vertical fracture. Infinite-acting system.

where C = wellbore storage constant (coefficient, factor), bbl/psi,
ΔV = change in volume of fluid in the wellbore, *at wellbore conditions*, bbl, and
Δp = change in bottom-hole pressure, psi.

Applying Eq. 2.15 to a wellbore with a changing liquid level,[16]

$$C = \frac{V_u}{\left(\frac{\rho}{144}\,\frac{g}{g_c}\right)}, \quad \ldots\ldots\ldots\ldots\ldots\ldots\ldots\ldots\ldots\ldots (2.16)$$

where V_u is the wellbore volume per unit length in barrels per foot. Eq. 2.16 is valid for both rising and falling liquid levels. When the wellbore is completely full of a single-phase fluid, Eq. 2.15 becomes[16]

$$C = V_w c, \quad \ldots\ldots\ldots\ldots\ldots\ldots\ldots\ldots\ldots\ldots (2.17)$$

where V_w is the total wellbore volume in barrels and c is the compressibility of the fluid *in the wellbore* at wellbore conditions. Throughout this monograph, the wellbore storage coefficient, C, has units of barrels per psi; some authors prefer cubic feet per psi. The compressibility in Eq. 2.17 is for the fluid in the wellbore; it is *not* c_t for the reservoir. Since the wellbore fluid compressibility is pressure dependent (Appendix D), the wellbore storage coefficient may vary with pressure. Fortunately, such variation in wellbore storage coefficient is generally important only in wells containing gas or in wells that change to a falling or rising liquid level during the test. Those conditions are considered in Section 11.2.

Some dimensionless pressure functions (Appendix C) for systems with wellbore storage use a dimensionless wellbore storage coefficient,

$$C_D = \frac{5.6146\,C}{2\pi\,\phi c_t h r_w^2}. \quad \ldots\ldots\ldots\ldots\ldots\ldots\ldots\ldots\ldots\ldots (2.18)$$

Note that the total compressibility for the reservoir system, c_t, is used in this definition.

Wellbore storage causes the sand-face flow rate to change

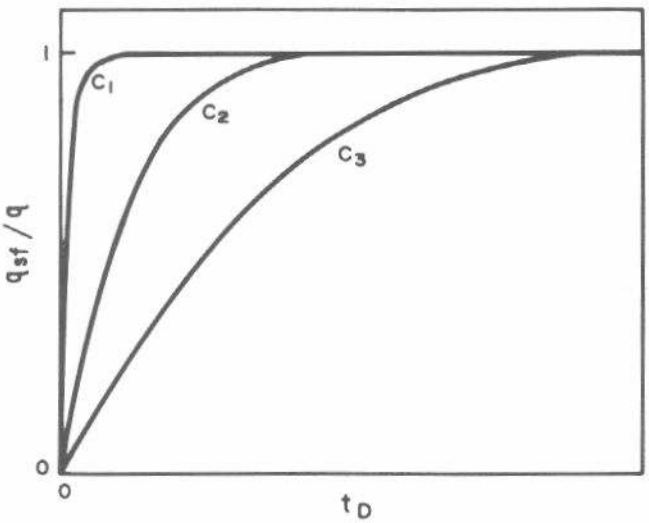

Fig. 2.9 Effect of wellbore storage on sand-face flow rate, $C_3 > C_2 > C_1$.

more slowly than the surface flow rate. Fig. 2.9 schematically shows the ratio of sand-face to surface rate when the surface rate is changed from 0 to q at time 0. When $C = 0$, $q_{sf}/q = 1$ at all times. For $C > 0$, the flow-rate ratio changes gradually from 0 to 1. The larger C, the longer the transition, as indicated in Fig. 2.9. The sand-face flow rate may be calculated from

$$q_{sf} = q + \frac{24C}{B}\frac{dp}{dt}$$

$$= q\left[1 - C_D \frac{d}{dt_D} p_D(t_D, C_D, \ldots)\right]. \quad \ldots\ldots (2.19)$$

Eq. 2.2 relates flowing well pressure to time for a constant flow rate, q. Since Eq. 2.19 indicates that q varies with t and p, it appears that Eq. 2.2 may not be useable. Fortunately, the problem is avoided by using a dimensionless pressure that accounts for wellbore storage and, thus, for the change in flow rate. Such $p_D(t_D, C_D, \ldots)$ are shown in Fig. 2.10, a simplified version of Figs. C.6 and C.7. The effect of wellbore storage on p_D is clear in those figures.

Fig. 2.10 has a characteristic that is diagnostic of wellbore storage effects: the slope of the p_D vs t_D graph on log-log paper is 1.0 during wellbore storage domination. Since p_D is proportional to Δp and t_D is proportional to time (see Eqs. 2.2 and 2.3), Fig. 2.10 indicates a way to estimate when wellbore storage is dominant during a transient test. On log-log paper, plot the pressure change during the test, $p_w - p_w(\Delta t = 0)$, (as a positive number) against test time, Δt, and observe where that plot has a slope of one cycle in pressure change per cycle in time. (Note that the nomenclature has been generalized here: p_w is the bottom-hole pressure during the test, be it flowing or static; $p_w(\Delta t = 0)$ is the pressure at the instant before the start of the test, be it static or flowing; and Δt is running test time, with the test starting at $\Delta t = 0$.) Well test data falling on the unit slope of the log-log plot reveal *nothing* about formation properties, since essentially all production is from the wellbore during that time. The location of the log-log unit slope can be used to estimate the apparent wellbore storage coefficient from[16]

$$C = \frac{qB\Delta t}{24\Delta p}, \quad \ldots\ldots (2.20)$$

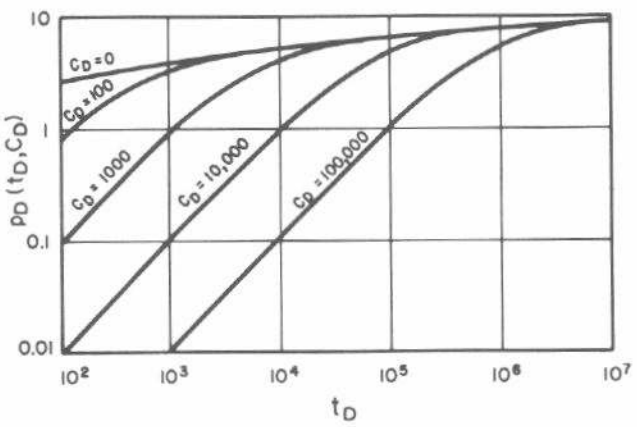

Fig. 2.10 Dimensionless pressure including wellbore storage, $s = 0$. After Wattenbarger and Ramey.[21]

where Δt and Δp are values read from a *point* on the log-log *unit-slope straight line*. C calculated from Eq. 2.20 should agree fairly well with C calculated from Eq. 2.16 or Eq. 2.17. If it does not, a reason should be sought. We have observed that wells producing at high gas-liquid ratios, highly stimulated wells, and wells used for viscous fluid injection commonly indicate wellbore storage coefficients from the log-log data plot that are much higher than those predicted from Eqs. 2.16 and 2.17.

The log-log data plot is a valuable aid for recognizing wellbore storage effects in transient tests when early-time pressure data are available. Thus, throughout this monograph, it is recommended that this plot be made a part of transient test analysis. It often helps the engineer avoid serious analysis mistakes by delineating the period of wellbore storage dominance as a unit-slope straight line. As wellbore storage effects become less severe, the formation begins to influence the bottom-hole pressure more and more, and the data points on the log-log plot fall below the unit-slope straight line and finally approach the slowly curving line for zero wellbore storage. Such behavior is illustrated by Fig. 2.10 for varying degrees of wellbore storage. Sometimes pressure data between the unit-slope line and the zero wellbore-storage line can be analyzed for formation properties, but the analysis may be tedious. The Gladfelter-Tracy-Wilsey[15] and the type-curve matching techniques[18-24] (Sections 3.3 and 8.3) apply in this region. Once the final portion of the log-log plot is reached ($C_D = 0$ line), wellbore storage is no longer important and standard semilog data-plotting analysis techniques apply. As a rule of thumb, that time usually occurs about 1 to 1½ cycles in time after the log-log data plot starts deviating significantly from the unit slope. The time may be estimated from

$$t_D > (60 + 3.5s)C_D, \quad \ldots\ldots (2.21a)$$

or approximately,

$$t > \frac{(200{,}000 + 12{,}000\,s)\,C}{(kh/\mu)}, \quad \ldots\ldots (2.21b)$$

for drawdown and injection tests. For pressure buildup and falloff tests, Chen and Brigham[25] state that a reasonably accurate analysis is possible when

$$t_D > 50\,C_D\,e^{0.14s}, \quad \ldots\ldots (2.22a)$$

or approximately when

$$t > \frac{170{,}000\,C\,e^{0.14s}}{(kh/\mu)}. \quad \ldots\ldots (2.22b)$$

Note that skin factor influences pressure buildup (falloff) much more than drawdown (injection).

Fig. C.5 for a horizontally fractured well *without* wellbore storage shows unit-slope straight lines for small h_D. Thus, factors other than wellbore storage can cause the unit-slope straight line on the log-log plot. Fortunately, horizontal fractures are thought to occur rarely.

Example 2.4 Computing Wellbore Storage Coefficients From Well Data

Water is injected into a sand at 2,120 ft through 4.75-in.,

16.00-lb_m casing. Estimate the wellbore storage coefficient for (1) a wellhead injection pressure of 400 psi, and (2) a wellhead vacuum. Use $\phi = 0.15$, $h = 30$ ft, and $r_w = 3.5$ in. to calculate the dimensionless wellbore storage coefficient.

1. When the wellhead pressure is greater than zero, Eq. 2.17 is used to estimate C. Water compressibility is estimated to be 3.25×10^{-6} psi^{-1} from data in Appendix D. For 4.75-in., 16-lb_m casing, $V_u = 0.0161$ bbl/ft, so $V_w = (0.0161)(2{,}120) = 34.1$ bbl. Using Eq. 2.17,

$$C = (34.1)(3.25 \times 10^{-6}) = 1.11 \times 10^{-4} \text{ bbl/psi}.$$

From Eq. 2.18,

$$C_D = \frac{(5.6146)(1.11 \times 10^{-4})}{2\pi(0.15)(3.25 \times 10^{-6})(30)(3.5/12)^2} = 80.$$

2. In this second case there is a changing liquid level in the well, so Eq. 2.16 is used:

$$C = \frac{0.0161}{\left(\frac{62.4}{144}\right)\left(\frac{32.17}{32.17}\right)} = 0.0372 \text{ bbl/psi}.$$

$$C_D = \frac{(5.6146)(0.0372)}{2\pi(0.15)(3.25 \times 10^{-6})(30)(3.5/12)^2}$$

$$= 2.7 \times 10^4.$$

In this case, there is a factor of about 340 difference between compressive and changing-liquid-level storage. Note, we assumed $c_t \simeq c_w$, which is not always a valid assumption.

Example 2.5 Computing Wellbore Storage Coefficient From Well Test Data

Use the log-log data plot shown in Fig. 2.11 to estimate a wellbore storage coefficient. That well has 2.5-in. tubing in 8⅛-in., 35.5-lb_m casing.

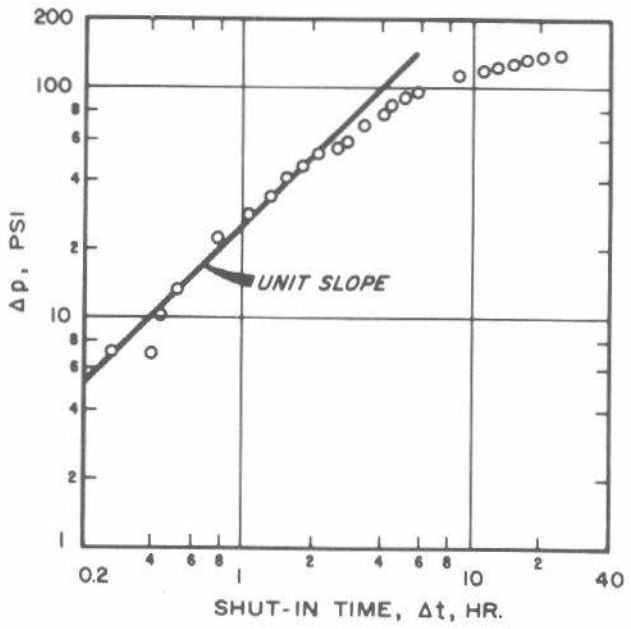

Fig. 2.11 Log-log data plot for Example 2.5. Pressure buildup test in a sandstone reservoir with $B = 1.0$ RB/STB; $q = 66$ STB/D; $h = 20$ ft; and depth = 980 ft.

At $\Delta t = 1$ hour, $\Delta p = 26$ psi on the unit-slope straight line. Using Eq. 2.20 and the data values in the figure caption, the wellbore storage coefficient is estimated as

$$C = \frac{(66)(1)}{(24)}\frac{1}{26} = 0.106 \text{ bbl/psi}.$$

Using Eq. 2.16 and $\rho = 62.4$ lb_m/cu ft,

$$V_u = C\left(\frac{\rho}{144}\frac{g}{g_c}\right) = (0.106)\left(\frac{62.4}{144}\frac{32.17}{32.17}\right)$$

$$= 0.0459 \text{ bbl/ft}.$$

This indicates that fluid is rising in the annulus between the tubing and casing (V_u for that annulus is 0.0435 bbl/ft). The well is completed without a packer, so the result is reasonable.

For this well, $c_t \simeq 10^{-5}$ psi^{-1}, $\phi = 0.20$, and $r_w = 0.36$ ft, so from Eq. 2.18,

$$C_D = \frac{(5.6146)(0.106)}{2\pi(0.20)(10^{-5})(20)(0.36)^2} = 18{,}300.$$

The wellbore storage coefficient can change during transient testing. For example, consider a falloff test in a water injection well with a high wellhead pressure during injection. When the well is shut in, surface pressure is high initially but could decrease to atmospheric and go on vacuum if the static formation pressure is below hydrostatic. The liquid level must start falling as soon as the wellhead pressure drops below atmospheric. As a result, the wellbore storage coefficient increases from one for fluid compression (Eq. 2.17) to one for a falling liquid level (Eq. 2.16); the second storage coefficient easily could be a hundred to a thousand times the first. The reverse situation can occur as well, with a high, rising-liquid-level storage at the beginning of injection changing to fluid-compression storage as the wellhead pressure begins to increase. Fig. 2.12 schematically illustrates dimensionless pressure behavior when the wellbore storage coefficient changes. When the wellbore storage coefficient increases (from C_1 to C_2 in Fig. 2.12), p_D (or Δp) flattens, begins to increase again, and finally approaches the response curve for the larger storage coefficient. When the wellbore storage coefficient decreases,

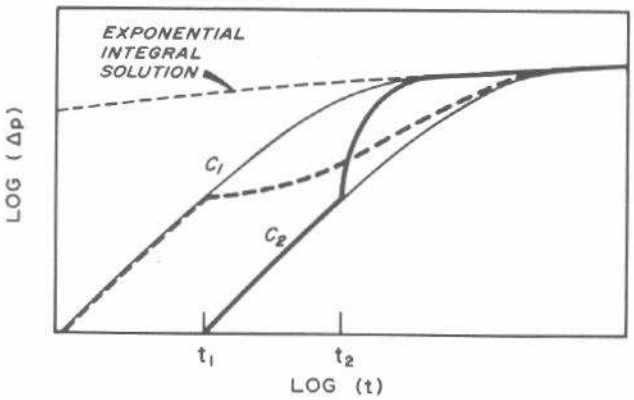

Fig. 2.12 Theoretical pressure response for both increasing and decreasing wellbore storage; $C_2 > C_1$. Adaptation of data from Earlougher, Kersch, and Ramey.[26]

there is a rapid p_D (or Δp) increase as the pressure response approaches the low wellbore storage curve. More discussion about this is given in Ref. 26 and in Section 11.2

Stegemeier and Matthews[27] showed that gas-liquid (phase) redistribution in the wellbore causes anomalous pressure-buildup curves of the form shown in Fig. 2.13. Fig. 2.14 indicates that phase redistribution is similar to wellbore storage, although it is probably more complex than anything else presented in this section. It is important to understand that the behavior illustrated in Fig. 2.13 is wellbore, not formation, dominated. Pitzer, Rice, and Thomas[28] demonstrated this by testing a well once with surface shut in and a second time with bottom-hole shut in.

In summary, wellbore storage effects always should be considered in transient test design and analysis and in computing the expected pressure response of wells. In some cases, transient tests must be designed to minimize or alleviate wellbore storage, or no useful information will be obtained. Wellbore storage effects can be recognized on log-log data plots if sufficient short-time pressure data are available. No information about the formation can be determined from transient test data falling on the unit slope of such a data plot.

2.7 Dimensionless Pressure During the Pseudosteady-State Flow Period

Fig. 2.1 indicates that in closed systems a transition period follows the infinite-acting transient response. That is followed by the pseudosteady-state flow period, a transient flow regime when the pressure change with time, dp/dt, is constant at all points in the reservoir. (That is equivalent to the right-hand side of Eq. 2.1 being constant.) This flow period occasionally has been mistakenly called steady state, although at true steady state pressure is constant with time everywhere in the reservoir (Section 2.8).

Fig. 2.15 schematically shows a single producing well in the center of a closed-square drainage area. Fig. 2.16, a plot of p_D vs t_D at Points A, B, C, and D of Fig. 2.15, illustrates two properties common to all closed systems. First, at small dimensionless times, p_D at the well is given by Eq. 2.5 if $\sqrt{A}/r_w > 50$; the well behaves as if it were alone in an infinite system. Second, at large dimensionless times, p_D *at any point* in the system varies linearly with t_{DA}. This is the pseudosteady-state flow period, which can occur only in bounded systems. During pseudosteady state, dimensionless pressure is given by[29]

$$p_D = 2\pi t_{DA} + \frac{1}{2}\ln\left(\frac{A}{r_w^2}\right) + \frac{1}{2}\ln\left(\frac{2.2458}{C_A}\right) . \quad \ldots\ldots\ldots\ldots\ldots (2.23)$$

C_A, the shape factor, is a geometric factor characteristic of the system shape and the well location. Values are given by Brons and Miller,[12] Dietz,[30] and others.[7,31] Both C_A and the final term in Eq. 2.23 are given in Table C.1. Eq. 2.23 may be used for any closed system with known shape factor. If 31.62, the C_A value for a well in the center of a circular system, is used in Eq. 2.23, the last two terms become the familiar $\ln(r_e/r_w) - 0.75$.

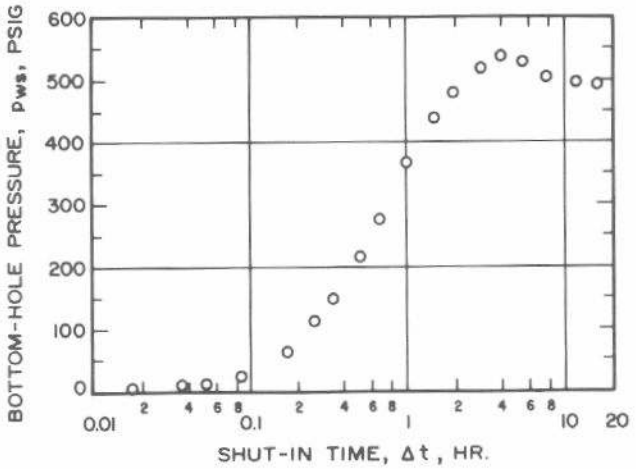

Fig. 2.13 Pressure buildup behavior showing the effect of fluid segregation in the wellbore. After Matthews and Russell.[1]

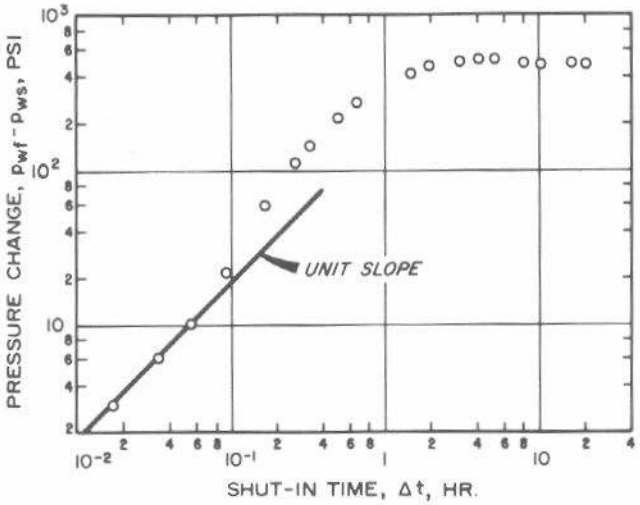

Fig. 2.14 Log-log plot of Fig. 2.13 data.

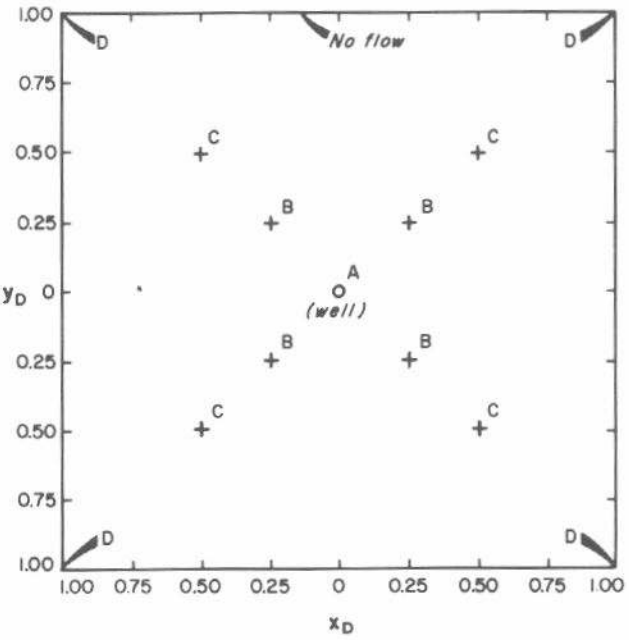

Fig. 2.15 Well in center of a closed square.

Eq. 2.23 applies any time after pseudosteady-state flow begins; that time may be estimated from

$$t_{pss} = \frac{\phi\mu c_t A}{0.0002637\,k}\,(t_{DA})_{pss}\,, \quad \ldots\ldots\ldots\ldots (2.24)$$

where $(t_{DA})_{pss}$ is given in the "Exact for t_{DA} >" column of Table C.1. Both C_A and $(t_{DA})_{pss}$ depend on reservoir shape and well location.

Dimensionless pressure data at the well and at several other points in closed rectangular systems are given in Ref. 7.

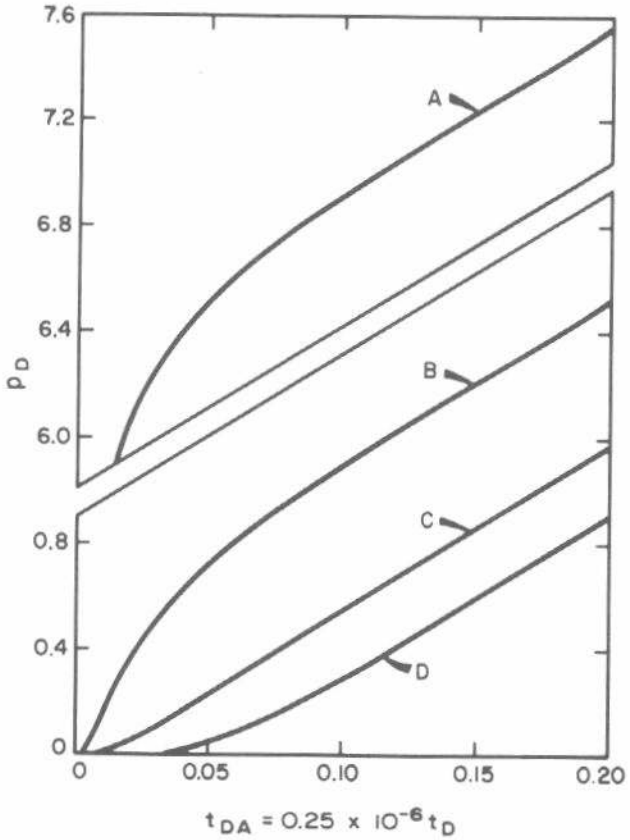

Fig. 2.16 Dimensionless pressure at various points in a closed square caused by a producing well in the center. A, B, C, and D identified in Fig. 2.15; $\sqrt{A}/r_w = 2{,}000$. After Earlougher, Ramey, Miller and Mueller.[31]

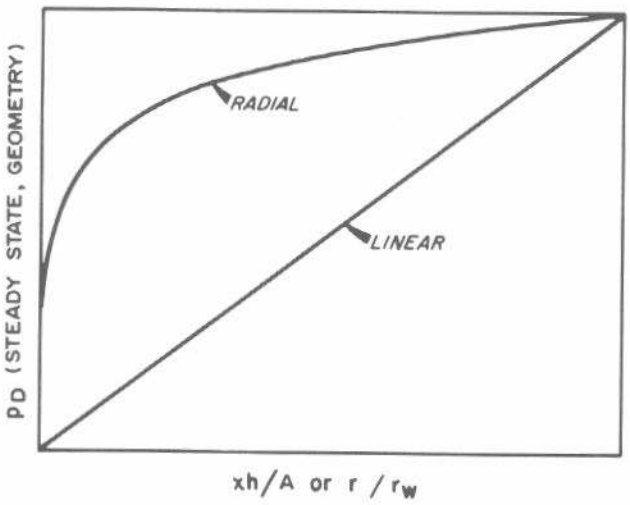

Fig. 2.17 Dimensionless pressure distribution in linear and radial steady-state flow.

Example 2.6 Estimating Well Pressure During Pseudosteady-State Flow

Using the data of Example 2.1, estimate flowing well pressure after 60 days. From Eq. 2.3b,

$$t_{DA} = \frac{(0.0002637)(90)(60 \times 24)}{(0.17)(13.2)(2.00 \times 10^{-5})(1{,}742{,}400)}$$

$$= 0.437.$$

Table C.1 indicates pseudosteady state exists after $t_{DA} = 0.1$ for a well in the center of a square, so Eq. 2.23 applies. From Table C.1, $C_A = 30.8828$. Using Eq. 2.23,

$$p_D = 2\pi(0.437) + \frac{1}{2}\ln\left(\frac{1{,}742{,}400}{(0.50)^2}\right)$$

$$+ \frac{1}{2}\ln\left(\frac{2.2458}{30.8828}\right) = 9.31.$$

Then, from Eq. 2.2,

$$p_{wf}(t, r_w) = 3{,}265 - \frac{(141.2)(135)(1.02)(13.2)}{(90)(47)}(9.31)$$

$$= 2{,}700 \text{ psi}.$$

2.8 Steady-State Flow

When the pressure at every point in a system does not vary with time (that is, when the right-hand side of Eq. 2.1 is zero), flow is said to be steady state. Linear and radial steady-state flow, whose dimensionless pressure distributions are illustrated in Fig. 2.17, usually occur only in laboratory situations. The dimensionless-pressure functions are

steady state, linear

$$(p_D)_{ssL} = 2\pi\frac{Lh}{A}\,, \quad \ldots\ldots\ldots\ldots (2.25)$$

steady state, radial

$$(p_D)_{ssr} = \ln\left(\frac{r_e}{r_w}\right). \quad \ldots\ldots\ldots\ldots (2.26a)$$

When Eq. 2.26a is used in Eq. 2.2, we obtain after rearrangement

$$q = \frac{0.007082\,kh\,(p_e - p_w)}{B\mu\,\ln(r_e/r_w)}\,, \quad \ldots\ldots\ldots\ldots (2.26b)$$

the familiar radial form of Darcy's law.[32]

In reservoirs, steady-state flow can occur only when the reservoir is completely recharged by a strong aquifer or when injection and production are balanced. Muskat[33] relates flow rate to interwell pressure drop for several flooding patterns. His equations are easily converted to the dimensionless pressure approach used in this monograph. Perhaps the most useful is the dimensionless pressure expression for a *five-spot flooding pattern at steady state* with unit mobility ratio and with r_w the same in all wells:

$$(p_D)_{ss5} = \ln\left(\frac{A}{r_w{}^2}\right) - 1.9311. \quad \ldots\ldots\ldots\ldots (2.27)$$

Here, A is the five-spot pattern area, not the area per well.

It is useful to recognize that Higgins-Leighton[34] geometric factors are dimensionless pressures for cells within streamtubes operating at steady state. By appropriate addition of available Higgins-Leighton geometric factors, such as those in Ref. 35, one can calculate dimensionless pressures for many irregular steady-state systems.

$$(p_D)_{ss} = \sum_i \left(\frac{2\pi}{\sum_j F_{HLi,j}} \right) , \quad \ldots\ldots\ldots\ldots (2.28)$$

where $F_{HLi,j}$ is the Higgins-Leighton geometric factor for cell j in streamchannel i of the pattern. The sums are taken over all cells and all channels. If the pattern is symmetric, the right-hand side of Eq. 2.28 must be multiplied by the number of symmetry units. For the confined five-spot pattern flood of Ref. 35, we calculate $p_D = 10.498$; here, $\sqrt{A}/r_w = 500$. Eq. 2.27 gives the same result to three decimal places.

2.9 The Principle of Superposition

So far, only systems with a single well operating at a constant rate from time zero onward have been considered. Since real reservoir systems usually have several wells operating at varying rates, a more general approach is needed to study the problems associated with transient well testing. Fortunately, because Eq. 2.1 is linear, multiple-rate, multiple-well problems can be considered by applying the principle of superposition. The mathematical basis for this technique is explained by van Everdingen and Hurst,[2] Collins,[36] and others.[1,4,31]

As used here, the superposition principle states that adding solutions to a linear differential equation results in a new solution to that differential equation, but for different boundary conditions. Eq. 2.2 is a solution to Eq. 2.1 for a single well producing at constant rate q. Superposition can be applied to include more than one well, to change rates, and to impose physical boundaries. Superposition is easily applied to infinite systems; but for bounded systems it must be used with more care — not because the principle is different, but because p_D solutions frequently do not give the necessary information for correct superposition.

To illustrate the principle of superposition in space, consider the three-well infinite system in Fig. 2.18. At $t = 0$, Well 1 starts producing at rate q_1, and Well 2 starts producing at rate q_2. We wish to estimate the pressure at the shut-in observation point, Well 3. To do this, we add the *pressure change* at Well 3 caused by Well 1 to the *pressure change* at Well 3 caused by Well 2:

$$\Delta p_3 = \Delta p_{3,1} + \Delta p_{3,2} . \quad \ldots\ldots\ldots\ldots\ldots\ldots (2.29)$$

To use Eq. 2.29 we must substitute Eq. 2.2 for Δp. Then, extending to an arbitrary number of wells, $j = 1, 2, \ldots, n$,

$$\Delta p(t, r) = \frac{141.2\mu}{kh} \sum_{j=1}^{n} q_j B_j p_D(t_D, r_{Dj}) , \quad \ldots\ldots (2.30)$$

where r_{Dj} is the dimensionless distance from Well j to the point of interest. Note that Eqs. 2.29 and 2.30 add *pressure changes* (or dimensionless pressures), not pressures. If the point of interest is an operating well, the skin factor must be added to the dimensionless pressure for *that well only*.

Fig. 2.19 graphically illustrates the use of Eqs. 2.29 and

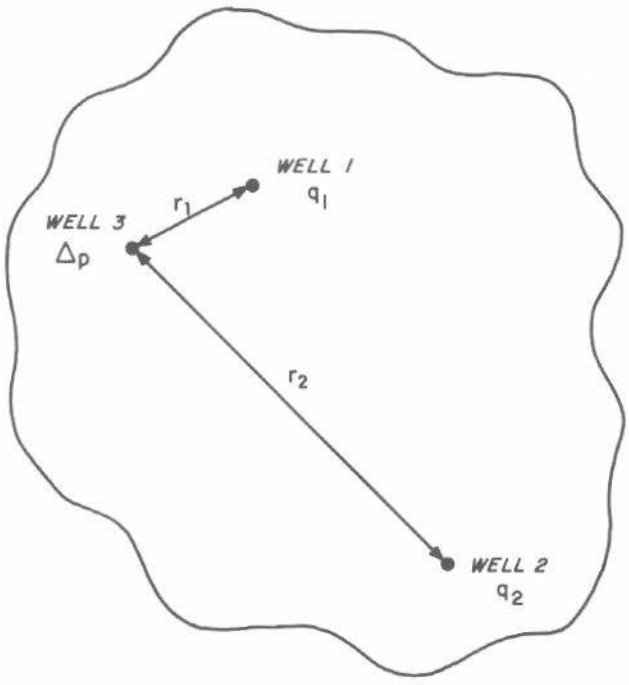

Fig. 2.18 Multiple-well infinite system for superposition explanation.

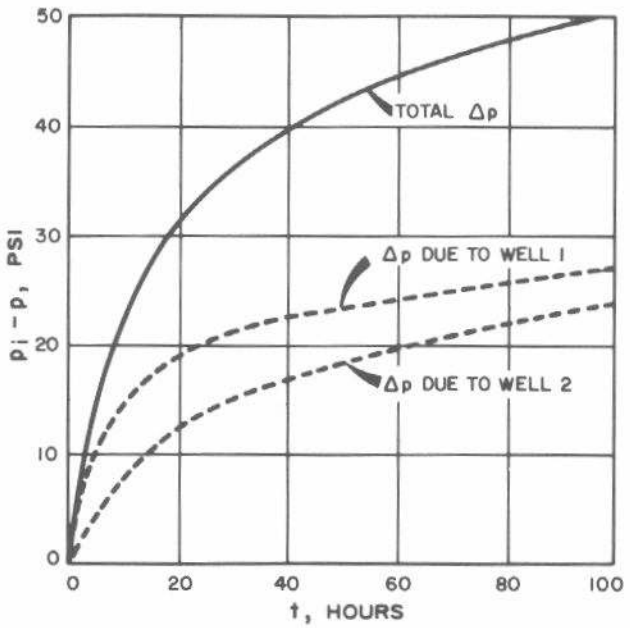

Fig. 2.19 Calculation of pressure change at observation well of Fig. 2.18. $q_1 = 100$ STB/D; $r_1 = 100$ ft; $q_2 = 150$ STB/D; $r_2 = 316$ ft; $k = 76$ md; $\mu = 1.0$ cp; $\phi = 0.20$; $c_t = 10 \times 10^{-6}$ psi^{-1}; $B = 1.08$ RB/STB; $h = 20$ ft; and $s = 0$.

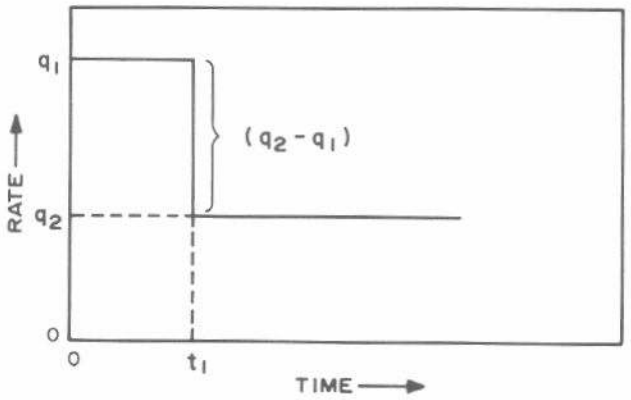

Fig. 2.20 Variable rate schedule for superposition explanation.

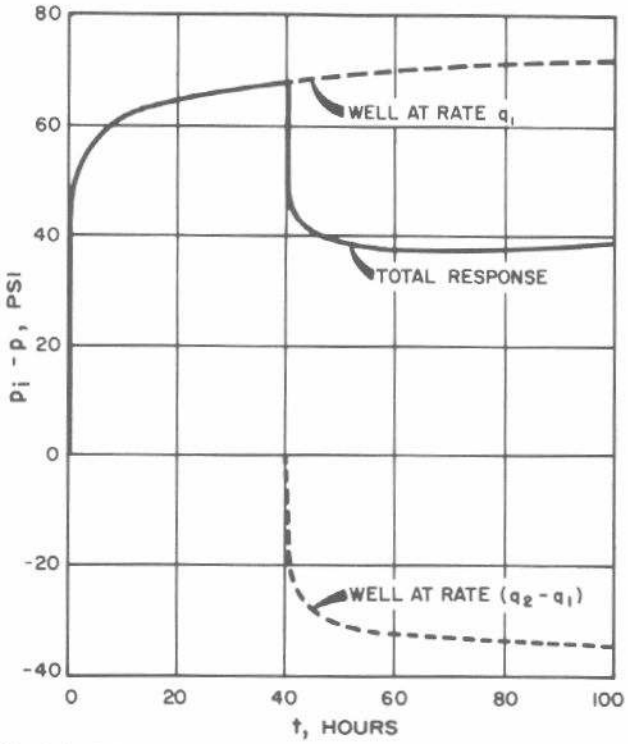

Fig. 2.21 Calculation of pressure change at producing well with the rate history of Fig. 2.20. $q_1 = 100$ STB/D; $q_2 = 50$ STB/D; $k = 76$ md; $\mu = 1.0$ cp; $\phi = 0.20$; $c_t = 10 \times 10^{-6}$ psi^{-1}; $B = 1.08$ RB/STB; $h = 20$ ft; and $s = 0$.

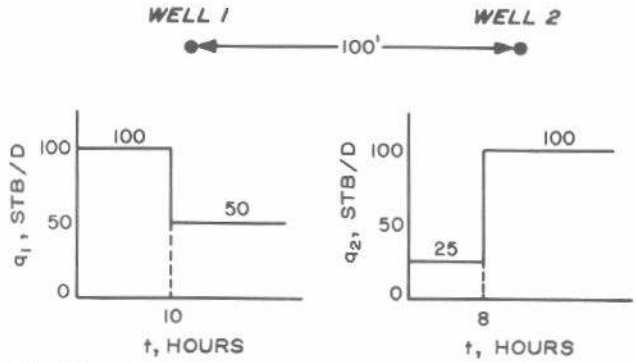

Fig. 2.22 Example superposition calculation for two wells, each produced at two rates. Well 1: $s = 5$, $r_w = 1$ ft. Well 2: $s = 1.7$, $r_w = 1$ ft. $k = 76$ md; $\mu = 1.0$ cp; $\phi = 0.20$; $c_t = 10 \times 10^{-6}$ psi^{-1}; $B = 1.08$ RB/STB; $h = 20$ ft; and $p_i = 2{,}200$ psi.

2.30 for the system of Fig. 2.18 and the exponential integral p_D (Eq. 2.5). The lowest curve in Fig. 2.19 is the pressure change at Well 3 caused by Well 2. The upper dashed curve is the pressure change at Well 3 caused by Well 1. Using Eq. 2.29, we add the two pressure changes to get the solid curve, the total pressure change observed at Well 3.

To illustrate an application of the principle of superposition to varying flow rates, consider a single-well system with the production-rate schedule shown in Fig. 2.20. The production rate is q_1 from $t = 0$ to $t = t_1$ and q_2 thereafter. To perform the superposition calculation the single well may be visualized as two wells located at the same point, with one well producing at rate q_1 from $t = 0$ to t and the second (imaginary) well producing at rate $(q_2 - q_1)$, starting at t_1 and continuing for a time period $(t - t_1)$. The net rate after time t_1 would be $q_1 + (q_2 - q_1) = q_2$. As in the previous illustration, Δp's are added for these conditions. The general form of the equation for N rates, with changes at t_j, $j = 1, 2, \ldots N$, is

$$\Delta p = \frac{141.2\,\mu}{kh} \sum_{j=1}^{N} \left\{ (q_j B_j - q_{j-1} B_{j-1}) \left[p_D\left([t - t_{j-1}]_D \right) + s \right] \right\}. \quad \ldots\ldots\ldots\ldots\ldots\ldots (2.31)$$

In Eq. 2.31, $[t - t_1]_D$ is the dimensionless time calculated at time $(t - t_1)$. For Fig. 2.20, $N = 2$ and only two terms of the summation are needed. Fig. 2.21 illustrates the calculation. The upper dashed curve (including the first portion of the solid curve) is the pressure change caused by rate q_1. The lower dashed curve is the pressure change caused by rate $q_2 - q_1$ after $t = 40$ hours; that Δp is negative because $(q_2 - q_1) < 0$. The sum of the two dashed curves, the solid curve, is the pressure response for the two-rate schedule.

To combine varying rates and multiple wells, first apply Eq. 2.31 for each well in the system to estimate Δp caused by that well at the point desired. Then add the Δp for all wells, as in Eq. 2.30, to get the total Δp caused by all wells and all rates. The double summation process is conceptually simple, but can be tedious in application, as illustrated by the following example.

Example 2.7 Principle of Superposition

For the conditions shown in Fig. 2.22, estimate the pressure at Well 1 after 7 hours and at Well 2 after 11 hours. Assume that the system behaves as an infinite one at these short times.

Start by computing the coefficients in the Δp and t_D equations, Eqs. 2.2 and 2.3. Then, at a given time, estimate Δp at the desired well caused by both Well 1 and Well 2; that calculation of Δp may require use of Eq. 2.31 to account for varying rates.

From Eq. 2.3a,

$$t_D = \frac{0.0002637\,kt}{\phi\mu c_t r_w^2} = \frac{(0.0002637)(76)t}{(0.2)(1)(10 \times 10^{-6})(1)^2}$$

$$= 10{,}000\,t.$$

From Eq. 2.2,

$$\Delta p = \frac{141.2\, qB\mu}{kh}\left[p_D(t_D, \ldots)\right]$$

$$= \frac{(141.2)(1.08)(1)q}{(76)(20)}\, p_D(t_D, r_D, \ldots)$$

$$= 0.1\, q\, p_D(t_D, r_D, \ldots).$$

Recall that s_j must be added to p_D to get Δp at Well j (unless p_D is a function of s, as are some that are given in Appendix C). The appropriate r also must be used to calculate r_D, depending on the p_D function we use.

At $t = 7$ hours, there is a Δp contribution at Well 1 from a single rate at Well 1 and a single rate at Well 2; so the over-all pressure change would be (Eq. 2.30)

$$\Delta p\ (7 \text{ hours}, r_D = 1)$$

$$= \frac{141.2\, q_1 B_1 \mu}{kh}\left[p_D(t_D, r_D = 1) + s\right]$$

$$+ \frac{141.2\, q_2 B_2 \mu}{kh}\, p_D(t_D, r_D = 100/1).$$

For the contribution of Well 1, $t_D = (10{,}000)(7) = 70{,}000$. Since $t_D > 100$ Eq. 2.5b is used:

$$p_D(t_D = 70{,}000, r_D = 1)$$

$$= \frac{1}{2}\left[\ln(70{,}000) + 0.80907\right]$$

$$= 5.98.$$

For the contribution of Well 2, at a distance of 100 ft,

$$\frac{t_D}{r_D^2} = \frac{(70{,}000)}{(100/1)^2} = 7.$$

Since $r_D > 20$, we can use the line-source solution, Eq. 2.5a, but we should not use Eq. 2.5b unless $t_D/r_D^2 > 100$. From Fig. C.1 or Fig. C.2 for $t_D/r_D^2 = 7$ and $r_D = 100$,

$$p_D(t_D = 7, r_D = 100) = 1.40.$$

Calculating Δp at Well 1,

$$\Delta p(\text{Well 1, 7 hours}) = (0.1)(100)(5.98 + 5) + (0.1)(25)(1.40) = 113.3 \text{ psi}.$$

The pressure at Well 1 at 7 hours is

$$p_w\ (7 \text{ hours}, r_D = 1) = p_i - \Delta p = 2{,}200 - 113.3 = 2{,}086.7 \text{ psi}.$$

At $t = 11$ hours, we wish to estimate p at Well 2. We must consider two rates at each well:

$$\Delta p(11 \text{ hours}, r_D = 1)$$

$$= (0.1)(100)\, p_D(\text{Well 1}, t = 11 \text{ hours}, r_D = 100)$$

$$+ (0.1)(50-100)\, p_D(\text{Well 1}, t = [11-10] \text{ hours}, r_D = 100)$$

$$+ (0.1)(25)\left[p_D(\text{Well 2}, t = 11 \text{ hours}, r_D = 1) + s\right]$$

$$+ (0.1)(100-25)\left\{p_D(\text{Well 2}, t = [11-8] \text{ hours}, r_D = 1) + s\right\}.$$

For Well 1, use Fig. C.2:

$$t_D(11 \text{ hours})/r_D^2 = \frac{(10{,}000)(11)}{(100)^2} = 11.$$

$$p_D(\text{Well 1}, t_D = 11, r_D = 100) = 1.61.$$

$$t_D(11-10 \text{ hours})/r_D^2 = \frac{(10{,}000)(1)}{(100)^2} = 1.$$

$$p_D(\text{Well 1}, t_D = 1, r_D = 100) = 0.522.$$

For Well 2, $r_D = 1$:

$$t_D(11 \text{ hours}) = (10{,}000)(11) = 110{,}000.$$

Since $t_D > 100$, we use Eq. 2.5b:

$$p_D(\text{Well 2}, t_D = 110{,}000, r_D = 1)$$

$$= \frac{1}{2}\left[\ln(t_D) + 0.80907\right]$$

$$= 6.21.$$

$$t_D(11-8 \text{ hours}) = (10{,}000)(3) = 30{,}000.$$

$$p_D(t_D = 30{,}000, r_D = 1)$$

$$= \frac{1}{2}\left[\ln(30{,}000) + 0.80907\right]$$

$$= 5.56.$$

Estimating Δp at Well 2,

$$\Delta p(\text{Well 2, 11 hours}) = (0.1)(100)(1.61) + (0.1)(50-100)(0.522) + (0.1)(25)(6.21 + 1.7) + (0.1)(100-25)(5.56 + 1.7) = 87.7 \text{ psi}.$$

$$p_w(\text{Well 2, 11 hours}) = 2{,}200 - 87.7 = 2{,}112.3 \text{ psi}.$$

Additional applications of the principle of superposition and the method of images are shown in Appendix B.

2.10 Application of Flow Equations to Gas Systems

Although this monograph is concerned only with liquid systems, much of the material presented can be applied to dry gas systems if modified slightly.

Gas viscosity and density vary significantly with pressure, so the assumptions of Eq. 2.1 are not satisfied for gas systems and the equation does not apply directly to gas flow in porous media. That difficulty is avoided by defining a "real gas potential" (also commonly referred to as the real gas pseudopressure or just pseudopressure):[37,38]

$$m(p) = 2\int_{p_b}^{p} \frac{p}{\mu(p)z(p)}\, dp, \quad \ldots\ldots\ldots\ldots (2.32)$$

where p_b is an arbitrary base pressure. When the real gas potential is used, Eq. 2.1 essentially retains its form but with $m(p)$ replacing p. That equation can be solved and an analog to Eq. 2.2 can be written with $m_D(t_D)$ in place of $p_D(t_D)$. For radial gas flow it has been shown[37,39,40] that when $t_D < (t_D)_{pss}$,

$$m_D(t_D) = p_D(t_D), \quad \ldots\ldots\ldots\ldots (2.33)$$

where $p_D(t_D)$ is the liquid flow dimensionless pressure.

Using Eq. 2.33, the gas analog of Eq. 2.2, and substituting the appropriate gas properties, the flow equation for a real gas is

$$m(p_{wf}) = m(p_i) - 50{,}300 \frac{p_{sc}}{T_{sc}} \frac{qT}{kh} \left[p_D(t_D) + s + D|q|\right], \quad \ldots\ldots\ldots\ldots\ldots (2.34)$$

where q is in Mscf/D. In Eq. 2.34, the term $D|q|$ accounts for non-Darcy flow around the wellbore. Otherwise, the form is like the liquid flow equation. To use Eq. 2.34 it is necessary to construct a high-resolution graph of $m(p)$ vs p from the viscosity and z factor for the gas. If μ and z are not known, information presented by Zana and Thomas[41] may be used to estimate $m(p)$ vs p.

As a result of the characteristics of the real gas potential, Eq. 2.34 can be simplified for certain pressure ranges. Fig. 2.23 shows μz as a function of pressure for a typical gas. At low pressures μz is essentially constant, while at high pressures it is essentially directly proportional to pressure. When this behavior is used in Eq. 2.32, Eq. 2.34 can be simplified to

$$p_{wf} = p_i - 50{,}300 \frac{z_i \mu_{gi}}{2p_i} \frac{p_{sc}}{T_{sc}} \frac{qT}{kh} \left[p_D(t_D) + s + D|q|\right], \quad \ldots\ldots\ldots\ldots\ldots (2.35)$$

at high pressures, while at low pressures it becomes

$$p_{wf}^2 = p_i^2 - 50{,}300\,(z_i\mu_{gi}) \frac{p_{sc}}{T_{sc}} \frac{qT}{kh} \left[p_D(t_D) + s + D|q|\right]. \quad \ldots\ldots\ldots\ldots\ldots (2.36)$$

As a rule of thumb,[40] Eq. 2.36 generally applies when $p < 2{,}000$ psi, while Eq. 2.35 generally applies for $p > 3{,}000$ psi; for $2{,}000 < p < 3{,}000$ use Eq. 2.34. We suggest that the μz vs p plot be made for the particular gas flowing before choosing between the equations. If neither situation prevails at the pressure level observed or expected, then the real gas potential, $m(p)$, must be used. Eqs. 2.34, 2.35, or 2.36 may be used with liquid dimensionless pressure for most gas systems.

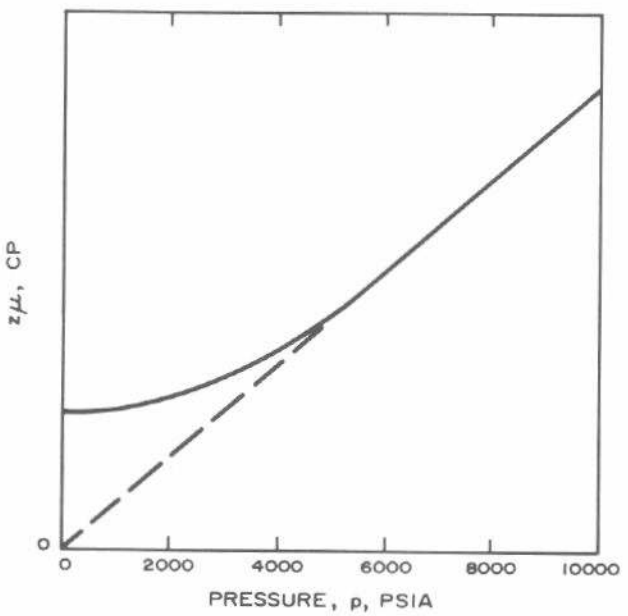

Fig. 2.23 Isothermal variation of μz with pressure.

2.11 Application of Flow Equations to Multiple-Phase Flow

Eqs. 2.1 and 2.2 and the dimensionless pressure information in this monograph are derived for single-phase flow. However, they may be used for certain multiple-phase flow situations with some modifications.[42-45] The basic approach is to replace the mobility terms in Eqs. 2.1 through 2.3 by the total flowing mobility,

$$\lambda_t = \lambda_o + \lambda_g + \lambda_w, \quad \ldots\ldots\ldots\ldots\ldots\ldots (2.37a)$$

or

$$\left(\frac{k}{\mu}\right)_t = k\left(\frac{k_{ro}}{\mu_o} + \frac{k_{rg}}{\mu_g} + \frac{k_{rw}}{\mu_w}\right), \quad \ldots\ldots\ldots (2.37b)$$

and to replace the total system compressibility by

$$c_t = S_o c_{oa} + S_w c_{wa} + S_g c_g + c_f. \quad \ldots\ldots\ldots\ldots (2.38a)$$

$$c_t = S_o\left[\frac{B_g}{B_o}\left(\frac{\partial R_s}{\partial p}\right) - \frac{1}{B_o}\left(\frac{\partial B_o}{\partial p}\right)\right] + S_w\left[\frac{B_g}{B_w}\left(\frac{\partial R_{sw}}{\partial p}\right) - \frac{1}{B_w}\left(\frac{\partial B_w}{\partial p}\right)\right] + S_g\left[-\frac{1}{B_g}\left(\frac{\partial B_g}{\partial p}\right)\right] + c_f. \quad \ldots\ldots\ldots\ldots (2.38b)$$

With these modifications, single-phase liquid dimensionless pressures may be used to describe multiple-phase systems containing immiscible fluids with fairly uniform saturation distribution. The same modifications are made when analyzing transient well test data. For example, mobility estimating equations take the form

$$\left(\frac{k}{\mu}\right)_o = \pm \frac{162.6\, q_o B_o}{mh} \quad \ldots\ldots\ldots\ldots\ldots\ldots (2.39a)$$

$$\left(\frac{k}{\mu}\right)_g = \pm \left\{162.6\,(1{,}000)\left[q_g - 0.001\,(q_o R_s + q_w R_{sw})\right] B_g\right\} \Big/ mh \quad \ldots\ldots (2.39b)$$

$$\left(\frac{k}{\mu}\right)_w = \pm \frac{162.6\, q_w B_w}{mh}. \quad \ldots\ldots\ldots\ldots\ldots\ldots (2.39c)$$

The $\pm$ sign in Eq. 2.39 indicates application to any of the various test analysis techniques.

2.12 Radius of Drainage and Stabilization Time

The concepts of stabilization time and radius of drainage are commonly used in petroleum engineering and in transient testing. These quantities are frequently used without appropriate understanding of their actual meaning and limitations. It is beyond the scope of this monograph to investigate the problems associated with radius of drainage and stabilization time. However, because of their wide use, the quantities are defined and equations are given for them in this section.

Stabilization time has been defined in many ways by various authors.[46,47] Most definitions correspond to the beginning of the pseudosteady-state flow period. Using that as the definition of stabilization time, we can estimate the

stabilization time for any shape given in Table C.1 from Eq. 2.24. For a well in the center of most symmetrical shapes, drawdown stabilization time is estimated from

$$t_s \simeq 380 \frac{\phi\mu c_t A}{k}, \quad \ldots\ldots\ldots\ldots\ldots\ldots \quad (2.40a)$$

where t_s is in hours. If we assume the system is radial,

$$t_s \simeq 1{,}200 \frac{\phi\mu c_t r_e^2}{k}. \quad \ldots\ldots\ldots\ldots\ldots\ldots \quad (2.40b)$$

For stabilization time in days the coefficient in Eq. 2.40b is 50 and the equation takes the form given by van Poollen.[46] It is important to recognize that stabilization time can be considerably longer than indicated by Eq. 2.40 when the shape is not a symmetrical one with the well in the center, or if two or more noncommunicating layers intersect the wellbore.[48,49]

Radius of drainage is also defined in several ways. Many definitions are presented by van Poollen,[46] Kazemi,[50] and Gibson and Campbell.[51] In most definitions, the radius of drainage defines a circular system with a pseudosteady-state pressure distribution from the well to the "drainage radius." As time increases, more of the reservoir is influenced by the well and the radius of drainage increases, as given by

$$r_d = 0.029 \sqrt{\frac{kt}{\phi\mu c_t}}, \quad \ldots\ldots\ldots\ldots\ldots\ldots \quad (2.41)$$

where r_d is the radius of drainage in feet and t is in hours. If t is expressed in days, the constant 0.029 rounds to 0.14, and Eq. 2.41 corresponds to equations given in Refs. 46, 50, and 51. Eventually, r_d must stop increasing — either when reservoir boundaries or drainage regions of adjacent wells are encountered, so Eq. 2.41 can only apply until t_{pss}.

Example 2.8 Radius of Drainage

Estimate the radius of drainage created during a 72-hour test on a well in a reservoir with $k/\mu = 172$ md/cp and $\phi c_t = 0.232 \times 10^{-5}$ psi^{-1}. Using Eq. 2.41,

$$r_d = 0.029 \sqrt{\frac{(172)(72)}{0.232 \times 10^{-5}}}$$

$$= 2{,}100 \text{ ft}.$$

This estimate is valid only if no boundaries are within about 2,100 ft of the test well, and if no other operating wells are within about 4,200 ft.

In systems completely recharged by an aquifer or when production and injection are balanced, the concepts of stabilization time and radius of drainage are meaningless. However, Ramey, Kumar, and Gulati[52] define a readjustment time, the time required for a short-lived transient to die out, for such systems. For a single well in the center of a constant-pressure square, which is equivalent to a balanced five-spot water injection pattern with unit mobility ratio, the readjustment time is[52]

$$t_R = 946 \frac{\phi\mu c_t A}{k}. \quad \ldots\ldots\ldots\ldots\ldots\ldots \quad (2.42)$$

In this equation, A would be approximately one-half the five-spot pattern area.

2.13 Numerical Solution of the Diffusivity Equation

It is possible to obtain analytical solutions to Eq. 2.1 only for the simplest systems. Most dimensionless-pressure functions are from numerical solutions of Eq. 2.1 or its analogs for gas and multiple-phase flow. Computer solution is the only practical method for obtaining dimensionless pressures for extremely heterogeneous systems, layered systems, systems with two or three phases flowing, systems with water or gas coning, or systems with significant gravity effects, for example. During the past several years, many papers that discuss various kinds of reservoir simulators have appeared in the petroleum literature. Three of the classics are by Aronofsky and Jenkins,[53] Bruce, Peaceman, Rachford, and Rice[54], and West, Garvin, and Sheldon.[55] Many facets of reservoir simulation were summarized by van Poollen, Bixel, and Jargon[56] in a series of articles appearing in the *Oil and Gas Journal*. The SPE-AIME Reprint Series booklet[57] on numerical simulation contains many useful papers.

Chapter 12 of this monograph presents some information about the application of computers to transient well testing.

2.14 Summary — A Physical Viewpoint

After presenting the dimensionless-parameter approach to solution of transient flow problems and explaining some of the factors that influence those solutions, it seems worthwhile to summarize the situation from a physical viewpoint.

Fluid withdrawal from a well penetrating a pressurized petroleum reservoir containing a compressible fluid results in a pressure disturbance. Although we might expect that disturbance to move with the speed of sound, it is quickly attenuated, so for any given length of production time there is some distance, the radius of drainage, beyond which no appreciable pressure change can be observed. As fluid withdrawal continues, the disturbance moves farther into the reservoir, with pressure continuing to decline at all points that have started to experience pressure decline. When a closed boundary is encountered, the pressure within the boundary continues to decline, but at a more rapid rate than if the boundary had not been encountered. If, on the other hand, the transient pressure response reaches a replenishable outcrop that maintains constant pressure at some point, pressures nearer the withdrawal well will decline more slowly than if a no-flow boundary had been encountered. Rate changes or additional wells will cause additional pressure transients that affect both pressure decline and pressure distribution. Each well will establish a drainage area that supplies all fluid removed from that well — if there is no fluid injection into the system.

When boundaries are encountered (either no-flow or constant-pressure), the pressure gradient — *not the pressure level* — tends to stabilize after a sufficiently long production time, the stabilization time. For the closed-boundary case, the pressure behavior reaches pseudosteady state with a constant gradient and an over-all pressure decline every-

where that is linear with time. For reservoirs with constant-pressure boundaries, a steady state may be approached. In that case, both pressure gradient and absolute pressure values become constant with time. The pseudosteady-state and steady-state solutions to Eq. 2.1 have a simple form and represent the simplest approach to future performance predictions, when they are applicable.

References

1. Matthews, C. S. and Russell, D. G.: *Pressure Buildup and Flow Tests in Wells*, Monograph Series, Society of Petroleum Engineers of AIME, Dallas (1967) **1**, Chap. 2.
2. van Everdingen, A. F. and Hurst, W.: "The Application of the Laplace Transformation to Flow Problems in Reservoirs," *Trans.*, AIME (1949) **186**, 305-324.
3. Hubbert, M. King: "The Theory of Ground-Water Motion," *J. of Geol.* (Nov.-Dec. 1940) **XLVIII**, 785-944.
4. Horner, D. R.: "Pressure Build-Up in Wells," *Proc.*, Third World Pet. Cong., The Hague (1951) Sec. II, 503-523. Also *Reprint Series, No. 9 — Pressure Analysis Methods*, Society of Petroleum Engineers of AIME, Dallas (1967) 25-43.
5. van Everdingen, A. F.: "The Skin Effect and Its Influence on the Productive Capacity of a Well," *Trans.*, AIME (1953) **198**, 171-176. Also *Reprint Series, No. 9 — Pressure Analysis Methods*, Society of Petroleum Engineers of AIME, Dallas (1967) 45-50.
6. Hurst, William: "Establishment of the Skin Effect and Its Impediment to Fluid Flow Into a Well Bore," *Pet. Eng.* (Oct. 1953) B-6 through B-16.
7. Earlougher, R. C., Jr., and Ramey, H. J., Jr.: "Interference Analysis in Bounded Systems," *J. Cdn. Pet. Tech.* (Oct.-Dec. 1973) 33-45.
8. Mueller, Thomas D. and Witherspoon, Paul A.: "Pressure Interference Effects Within Reservoirs and Aquifers," *J. Pet. Tech.* (April 1965) 471-474; *Trans.*, AIME, **234.**
9. Theis, Charles V.: "The Relation Between the Lowering of the Piezometric Surface and the Rate and Duration of Discharge of a Well Using Ground-Water Storage," *Trans.*, AGU (1935) 519-524.
10. Abramowitz, Milton and Stegun, Irene A. (ed.): *Handbook of Mathematical Functions With Formulas, Graphs and Mathematical Tables*, National Bureau of Standards Applied Mathematics Series-55 (June 1964) 227-253.
11. Hawkins, Murray F., Jr.: "A Note on the Skin Effect," *Trans.*, AIME (1956) **207**, 356-357.
12. Brons, F. and Miller, W. C.: "A Simple Method for Correcting Spot Pressure Readings," *J. Pet. Tech.* (Aug. 1961) 803-805; *Trans.*, AIME, **222.**
13. Brons, F. and Marting, V. E.: "The Effect of Restricted Fluid Entry on Well Productivity," *J. Pet. Tech.* (Feb. 1961) 172-174; *Trans.*, AIME, **222.** Also *Reprint Series, No. 9 — Pressure Analysis Methods*, Society of Petroleum Engineers of AIME, Dallas (1967) 101-103.
14. Chatas, Angelos T.: "A Practical Treatment of Non-Steady State Flow Problems in Reservoir Systems," *Pet. Eng.*, Part 1 (May 1953) B-42 through B-50; Part 2 (June 1953) B-38 through B-50; Part 3 (Aug. 1953) B-44 through B-56.
15. Gladfelter, R. E., Tracy, G. W., and Wilsey, L. E.: "Selecting Wells Which Will Respond to Production-Stimulation Treatment," *Drill. and Prod. Prac.*, API (1955) 117-129.
16. Ramey, H. J., Jr.: "Non-Darcy Flow and Wellbore Storage Effects in Pressure Build-Up and Drawdown of Gas Wells," *J. Pet. Tech.* (Feb. 1965) 223-233; *Trans.*, AIME, **234.** Also *Reprint Series, No. 9 — Pressure Analysis Methods*, Society of Petroleum Engineers of AIME, Dallas (1967) 233-243.
17. Papadopulos, Istavros S. and Cooper, Hilton H., Jr.: "Drawdown in a Well of Large Diameter," *Water Resources Res.* (1967) **3**, No. 1, 241-244.
18. Cooper, Hilton H., Jr., Bredehoeft, John D., and Papadopulos, Istavros S.: "Response of a Finite-Diameter Well to an Instantaneous Charge of Water," *Water Resources Res.* (1967) **3**, No. 1, 263-269.
19. Ramey, H. J., Jr.: "Short-Time Well Test Data Interpretation in the Presence of Skin Effect and Wellbore Storage," *J. Pet. Tech.* (Jan. 1970) 97-104; *Trans.*, AIME, **249.**
20. Agarwal, Ram G., Al-Hussainy, Rafi, and Ramey, H. J., Jr.: "An Investigation of Wellbore Storage and Skin Effect in Unsteady Liquid Flow: I. Analytical Treatment," *Soc. Pet. Eng. J.* (Sept. 1970) 279-290; *Trans.*, AIME, **249.**
21. Wattenbarger, Robert A. and Ramey, H. J., Jr.: "An Investigation of Wellbore Storage and Skin Effect in Unsteady Liquid Flow: II. Finite Difference Treatment," *Soc. Pet. Eng. J.* (Sept. 1970) 291-297; *Trans.*, AIME, **249.**
22. McKinley, R. M.: "Wellbore Transmissibility From Afterflow-Dominated Pressure Buildup Data," *J. Pet. Tech.* (July 1971) 863-872; *Trans.*, AIME, **251.**
23. Barbe, J. A. and Boyd, B. L.: "Short-Term Buildup Testing," *J. Pet. Tech.* (July 1971) 800-804.
24. Earlougher, Robert C., Jr., and Kersch, Keith M.: "Analysis of Short-Time Transient Test Data by Type-Curve Matching," *J. Pet. Tech.* (July 1974) 793-800; *Trans.*, AIME, **257.**
25. Chen, Hsiu-Kuo and Brigham, W. E.: "Pressure Buildup for a Well With Storage and Skin in a Closed Square," paper SPE 4890 presented at the SPE-AIME 44th Annual California Regional Meeting, San Francisco, April 4-5, 1974.
26. Earlougher, Robert C., Jr., Kersch, K. M., and Ramey, H. J., Jr.: "Wellbore Effects in Injection Well Testing," *J. Pet. Tech.* (Nov. 1973) 1244-1250.
27. Stegemeier, G. L. and Matthews, C. S.: "A Study of Anomalous Pressure Build-Up Behavior," *Trans.*, AIME (1958) **213**, 44-50. Also *Reprint Series, No. 9 — Pressure Analysis Methods*, Society of Petroleum Engineers of AIME, Dallas (1967) 75-81.
28. Pitzer, Sidney C., Rice, John D., and Thomas, Clifford E.: "A Comparison of Theoretical Pressure Build-Up Curves With Field Curves Obtained From Bottom-Hole Shut-In Tests," *Trans.*, AIME (1959) **216**, 416-419. Also *Reprint Series, No. 9 — Pressure Analysis Methods*, Society of Petroleum Engineers of AIME, Dallas (1967) 83-86.
29. Ramey, H. J., Jr., and Cobb, William M.: "A General Buildup Theory for a Well in a Closed Drainage Area," *J. Pet. Tech.* (Dec., 1971) 1493-1505.
30. Dietz, D. N.: "Determination of Average Reservoir Pressure From Build-Up Surveys," *J. Pet. Tech.* (Aug. 1965) 955-959; *Trans.*, AIME, **234.**
31. Earlougher, Robert C., Jr., Ramey, H. J., Jr., Miller, F. G., and Mueller, T. D.: "Pressure Distributions in Rectangular Reservoirs," *J. Pet. Tech.* (Feb. 1968) 199-208; *Trans.*, AIME, **243.**
32. Amyx, James W., Bass, Daniel M., Jr., and Whiting, Robert L.: *Petroleum Reservoir Engineering: Physical Properties*, McGraw-Hill Book Co., Inc. New York (1960) 78-79.

33. Muskat, Morris: *Physical Principles of Oil Production*, McGraw-Hill Book Co., Inc., New York (1949) Ch. 12.

34. Higgins, R. V. and Leighton, A. J.: "A Method of Predicting Performance of Five-Spot Waterfloods in Stratified Reservoirs Using Streamlines," *Report of Investigations 5921*, USBM (1962).

35. Higgins, R. V., Boley, D. W., and Leighton, A. J.: "Aids to Forecasting the Performance of Water Floods," *J. Pet. Tech.* (Sept. 1964) 1076-1082; *Trans.*, AIME, **231.**

36. Collins, Royal Eugene: *Flow of Fluids Through Porous Materials*, Reinhold Publishing Corp., New York (1961) 108-123.

37. Al-Hussainy, R., Ramey, H. J., Jr., and Crawford, P. B.: "The Flow of Real Gases Through Porous Media," *J. Pet. Tech.* (May 1966) 624-636; *Trans.*, AIME, **237.**

38. Russell, D. G., Goodrich, J. H., Perry, G. E., and Bruskotter, J. F.: "Methods for Predicting Gas Well Performance," *J. Pet. Tech.* (Jan. 1966) 99-108; *Trans.*, AIME, **237.**

39. Al-Hussainy, R. and Ramey, H. J., Jr.: "Application of Real Gas Flow Theory to Well Testing and Deliverability Forecasting," *J. Pet. Tech.* (May 1966) 637-642; *Trans.*, AIME, **237.** Also *Reprint Series, No. 9 — Pressure Analysis Methods*, Society of Petroleum Engineers of AIME, Dallas (1967) 245-250.

40. Wattenbarger, Robert A. and Ramey, H. J., Jr.: "Gas Well Testing With Turbulence, Damage and Wellbore Storage," *J. Pet. Tech.* (Aug. 1968) 877-887; *Trans.*, AIME, **243.**

41. Zana, E. T. and Thomas, G. W.: "Some Effects of Contaminants on Real Gas Flow," *J. Pet. Tech.* (Sept. 1970) 1157-1168; *Trans.*, AIME, **249.**

42. Martin, John C.: "Simplified Equations of Flow in Gas Drive Reservoirs and the Theoretical Foundation of Multiphase Pressure Buildup Analyses," *Trans.*, AIME (1959) **216,** 309-311.

43. Miller, C. C., Dyes, A. B., and Hutchinson, C. A., Jr.: "The Estimation of Permeability and Reservoir Pressure From Bottom Hole Pressure Build-Up Characteristics," *Trans.*, AIME (1950) **189,** 91-104. Also *Reprint Series, No. 9 — Pressure Analysis Methods*, Society of Petroleum Engineers of AIME, Dallas (1967) 11-24.

44. Perrine, R. L.: "Analysis of Pressure Buildup Curves," *Drill. and Prod. Prac.*, API (1956) 482-509.

45. Earlougher, R. C., Jr., Miller, F. G., and Mueller, T. D.: "Pressure Buildup Behavior in a Two-Well Gas-Oil System," *Soc. Pet. Eng. J.* (June 1967) 195-204; *Trans.*, AIME, **240.**

46. van Poollen, H. K.: "Radius-of-Drainage and Stabilization-Time Equations," *Oil and Gas J.* (Sept. 14, 1964) 138-146.

47. Mathur, Shri B.: "Determination of Gas Well Stabilization Factors in the Hugoton Field," *J. Pet. Tech.* (Sept. 1969) 1101-1106.

48. Cobb, William M., Ramey, H. J., Jr., and Miller, Frank G.: "Well-Test Analysis for Wells Producing Commingled Zones," *J. Pet. Tech.* (Jan. 1972) 27-37; *Trans.*, AIME, **253.**

49. Earlougher, Robert C., Jr., Kersch, K. M., and Kunzman, W. J.: "Some Characteristics of Pressure Buildup Behavior in Bounded Multiple-Layer Reservoirs Without Crossflow," *J. Pet. Tech.* (Oct. 1974) 1178-1186; *Trans.*, AIME, **257.**

50. Kazemi, Hossein: "Pressure Buildup in Reservoir Limit Testing of Stratified Systems," *J. Pet. Tech.* (April 1970) 503-511.

51. Gibson, J. A. and Campbell, A. T., Jr.: "Calculating the Distance to a Discontinuity From D.S.T. Data," paper SPE 3016 presented at the SPE-AIME 45th Annual Fall Meeting, Houston, Oct. 4-7, 1970.

52. Ramey, Henry J., Jr., Kumar, Anil, and Gulati, Mohinder S.: *Gas Well Test Analysis Under Water-Drive Conditions*, AGA, Arlington, Va. (1973).

53. Aronofsky, J. A. and Jenkins, R.: "A Simplified Analysis of Unsteady Radial Gas Flow," *Trans.*, AIME (1954) **201,** 149-154. Also *Reprint Series, No. 9 — Pressure Analysis Methods*, Society of Petroleum Engineers of AIME, Dallas (1967) 197-202.

54. Bruce, G. H., Peaceman, D. W., Rachford, H. H., Jr., and Rice, J. D.: "Calculations of Unsteady-State Gas Flow Through Porous Media," *Trans.*, AIME (1953) **198,** 79-92.

55. West, W. J., Garvin, W. W., and Sheldon, J. W.: "Solution of the Equations of Unsteady State Two-Phase Flow in Oil Reservoirs," *Trans.*, AIME (1954) **201,** 217-229.

56. van Poollen, H. K., Bixel, H. C., and Jargon, J. R.: "Reservoir Modeling — 1: What It Is, What It Does," *Oil and Gas J.* (July 28, 1969) 158-160. (See bibliography for complete series.)

57. *Reprint Series, No. 11 — Numerical Simulation*, Society of Petroleum Engineers of AIME, Dallas (1973).

Chapter 3

Pressure Drawdown Testing

3.1 Introduction

Often, the first significant transient event at a production well is the initial production period that results in a *pressure drawdown* at the formation face. Thus, it seems logical to investigate what can be learned about the well and reservoir from pressure drawdown data. Matthews and Russell[1] state that infinite-acting, transition, and pseudosteady-state pressure drawdown data all may be analyzed for reservoir information. This chapter considers drawdown test analysis for the infinite-acting and pseudosteady-state periods; the transition period (late-transient period) analysis is given in Section 5.2 of Ref. 1. This chapter treats constant-rate drawdown testing only; variable-rate drawdown testing is covered in Chapter 4.

Although drawdown testing is not limited to the initial productive period of a well, that may be an ideal time to obtain drawdown data. Properly run drawdown tests may provide information about formation permeability, skin factor, and the reservoir volume communicating with the well.

Fig. 3.1 schematically illustrates the production and pressure history during a drawdown test. Ideally, the well is shut in until it reaches static reservoir pressure before the test. That requirement is met in new reservoirs; it is less often met in old reservoirs. Fortunately, when the requirement is not satisfied, data may be analyzed by the techniques of Chapter 4. The drawdown test is run by producing the well at a constant flow rate while continuously recording bottomhole pressure. In this type of test, well-completion data details must be known so the effect and duration of wellbore storage may be estimated.

While most reservoir information obtained from a drawdown test also can be obtained from a pressure buildup test (Chapter 5), there is an economic advantage to drawdown testing since the well is produced during the test. The main technical advantage of drawdown testing is the possibility for estimating reservoir volume. The major disadvantage is the difficulty of maintaining a constant production rate.

3.2 Pressure Drawdown Analysis in Infinite-Acting Reservoirs

The pressure at a well producing at a constant rate in an infinite-acting reservoir is given by Eq. 2.2:

$$p_i - p_{wf} = 141.2 \frac{qB\mu}{kh} \left[p_D(t_D, \ldots) + s\right], \quad \ldots\ldots (3.1)$$

if the reservoir is at p_i initially. The dimensionless pressure at the well ($r_D = 1$) is given by Eq. 2.5b:

$$p_D = \frac{1}{2}\left[\ln(t_D) + 0.80907\right], \quad \ldots\ldots\ldots\ldots (3.2)$$

when $t_D/r_D^2 > 100$ and after wellbore storage effects have diminished. Dimensionless time is given by Eq. 2.3a:

$$t_D = \frac{0.0002637\,kt}{\phi\mu c_t r_w^2}. \quad \ldots\ldots\ldots\ldots\ldots\ldots (3.3)$$

Eqs. 3.1 through 3.3 may be combined and rearranged to a familiar form of the pressure drawdown equation:[1]

$$p_{wf} = p_i - \frac{162.6\,qB\mu}{kh}\left[\log t + \log\left(\frac{k}{\phi\mu c_t r_w^2}\right) - 3.2275 + 0.86859\,s\right]. \quad \ldots\ldots\ldots\ldots (3.4)$$

Eq. 3.4 describes a straight-line relationship between p_{wf} and $\log t$. By grouping the intercept and slope terms together, it may be written as

$$p_{wf} = m \log t + p_{1hr}. \quad \ldots\ldots\ldots\ldots\ldots\ldots (3.5)$$

Theoretically, a plot of flowing bottom-hole pressure data vs the logarithm of flowing time (commonly called the "semilog plot") should be a straight line with slope m and intercept p_{1hr}. Fig. 3.2 indicates that the straight-line portion (the "semilog straight line") does appear after wellbore damage and storage effects have diminished; no data are shown after the end of the infinite-acting period. The slope of the semilog straight line in Fig. 3.2 and Eq. 3.5 may be determined from Eq. 3.4 to be

$$m = -\frac{162.6\,qB\mu}{kh}. \quad \ldots\ldots\ldots\ldots\ldots\ldots (3.6)$$

The intercept at $\log t = 0$, which occurs at $t = 1$, is also determined from Eq. 3.4:

$$p_{1hr} = p_i + m\left[\log\left(\frac{k}{\phi\mu c_t r_w^2}\right) - 3.2275 + 0.86859\,s\right]. \quad \ldots\ldots\ldots\ldots (3.7)$$

Two graphs of pressure drawdown data are required for test analysis. The log-log data plot $[\log(p_i - p_{wf})$ vs $\log t]$ is used to estimate when wellbore storage effects are no longer important (Section 2.6). When the slope of that plot is one cycle in Δp per cycle in t, wellbore storage dominates and test data give no information about the formation. The wellbore storage coefficient may be estimated from the unit-slope straight line with Eq. 2.20. The semilog straight line should begin about 1 to 1.5 cycles in t after the data start deviating from the unit slope. That corresponds to a low-slope, slightly curving line on the log-log plot. Alternatively, the beginning time of the semilog straight line may be estimated from Eq. 2.21b:

$$t > \frac{(200{,}000 + 12{,}000s)C}{(kh/\mu)} \quad \ldots\ldots\ldots\ldots\ldots\ldots (3.8)$$

The second required graph is the semilog plot, p_{wf} vs $\log t$. The slope, m, of the correct straight line is measured from this graph, and formation permeability is estimated from

$$k = -\frac{162.6\,qB\mu}{mh} \quad \ldots\ldots\ldots\ldots\ldots\ldots\ldots\ldots (3.9)$$

Clearly, kh/μ, kh, or k/μ also may be estimated.

The skin factor is estimated from a rearranged form of Eq. 3.7:

$$s = 1.1513\left[\frac{p_{1\text{hr}} - p_i}{m} - \log\left(\frac{k}{\phi\mu c_t r_w^2}\right) + 3.2275\right]. \quad \ldots\ldots\ldots\ldots\ldots\ldots\ldots\ldots (3.10)$$

In Eq. 3.10, $p_{1\text{hr}}$ must be from the semilog straight line. If pressure data measured at 1 hour do not fall on that line, the line *must be extrapolated* to 1 hour and the extrapolated value of $p_{1\text{hr}}$ must be used in Eq. 3.10. This procedure is necessary to avoid calculating an incorrect skin by using a wellbore-storage-influenced pressure. Fig. 3.2 illustrates the extrapolation to $p_{1\text{hr}}$.

If the drawdown test is long enough, bottom-hole pressure will deviate from the semilog straight line and make the transition from infinite-acting to pseudosteady state. If reservoir geometry and properties are known, the end of the semilog straight line may be estimated from Eq. 2.8a.

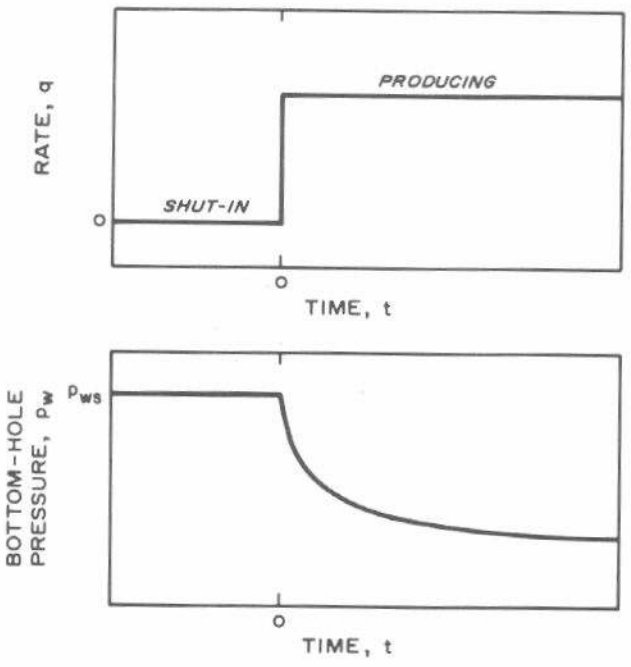

Fig. 3.1 Idealized rate schedule and pressure response for drawdown testing.

Example 3.1 Drawdown Testing in an Infinite-Acting Reservoir

Estimate oil permeability and skin factor from the drawdown data of Figs. 3.3 and 3.4. (Data are from Figs. 5.4 and 5.5 of Ref. 1.) Fig. 3.3, the log-log plot, indicates that wellbore storage effects are not significant for $t > 1$ hr.

Known reservoir data are

$h = 130$ ft	$\phi = 20$ percent
$r_w = 0.25$ ft	$p_i = 1{,}154$ psi
$q_o = 348$ STB/D	$m = -22$ psi/cycle (Fig. 3.4)
$B_o = 1.14$ RB/STB	$p_{1\text{hr}} = 954$ psi (Fig. 3.4).
$\mu_o = 3.93$ cp	
$c_t = 8.74 \times 10^{-6}$ psi^{-1}	

Using Eq. 3.9,

$$k_o = -\frac{(162.6)(348)(1.14)(3.93)}{(-22)(130)} = 89 \text{ md}.$$

Eq. 3.10 gives

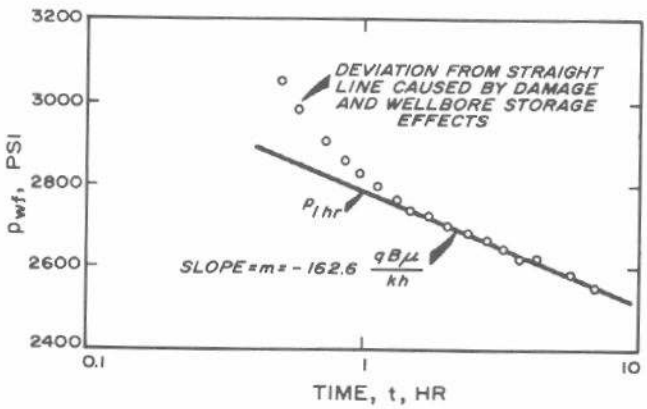

Fig. 3.2 Semilog plot of pressure drawdown data for a well with wellbore storage and skin effect.

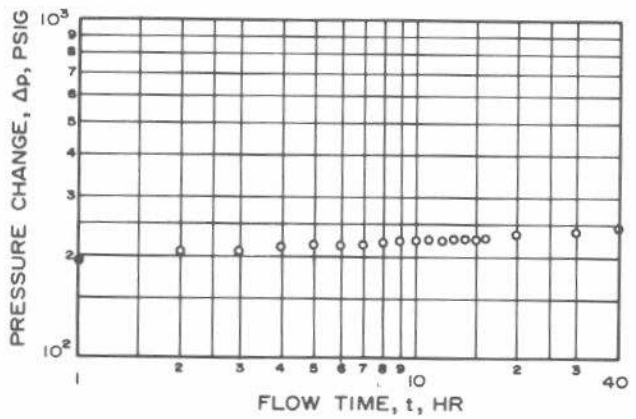

Fig. 3.3 Log-log data plot for Example 3.1.

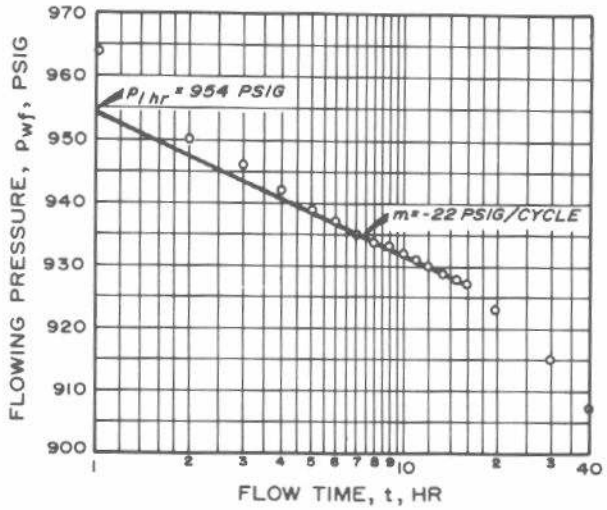

Fig. 3.4 Semilog data plot for the drawdown test of Example 3.1.

$$s = 1.1513\left\{\left(\frac{954 - 1{,}154}{-22}\right) - \log\left[\frac{89}{(0.2)(3.93)(8.74 \times 10^{-6})(0.25)^2}\right] + 3.2275\right\} = 4.6.$$

3.3 Pressure Drawdown Analysis by Type-Curve Matching

When a drawdown test is too short for the semilog straight line to develop, the data cannot be analyzed with the methods of Section 3.2. *Type-curve matching* techniques[2-9] provide a method for analyzing such data. The general method applies to many kinds of transient well tests for any system with known p_D vs t_D. Type-curve matching may be used for drawdown, buildup, interference, and constant-pressure testing. For single-well testing, type-curve matching should be used only when conventional analysis techniques, such as those illustrated in Section 3.2, cannot be used. In such cases, type-curve analysis can provide approximate results even though normal analysis techniques would fail. The type-curve matching technique has been described[2-9] in many ways; the method outlined here is specifically for use with Figs. C.6 through C.8 for drawdown testing in a well with wellbore storage and skin. The material presented is detailed enough so the reader can devise specific curve-matching techniques for other type curves.* Although the type-curve matching process appears awkward and difficult when described in writing, it is really quite straightforward. The reader is urged to try the method using the step-by-step description and data of Example 3.2.

First, we outline a general type-curve analysis approach for p_D vs t_D type curves similar to those in Figs. C.6 and C.7. Then, we give an explanation and an example of type-curve analysis using Fig. C.8. The general approach to type-curve analysis follows. Fig. 3.5 photographically illustrates the steps.

1. Choose the type curve, usually a log-log plot of p_D vs t_D. To provide specific details, the method is illustrated using Fig. C.6, the type curve for a single well with wellbore storage and skin effect in an infinite system. We must plot observed test data as Δp vs test time, t, on the same size scale as the base type curve. For drawdown tests, the pressure difference is

$$\Delta p = p_i - p_{wf}(t) \quad \ldots\ldots\ldots\ldots\ldots\ldots\ldots\ldots (3.11)$$

In general, for any kind of test,

$$\Delta p = |p_w(\Delta t = 0) - p_w(\Delta t)| \quad \ldots\ldots\ldots\ldots\ldots\ldots (3.12)$$

Note that Δp is always calculated as a positive number. The time parameter is the running test time, Δt. To plot the data, use tracing paper placed over the desired type curve (Fig. 3.5b); first trace the major grid lines from the type curve for reference (Fig. 3.5c) and mark the Δp (psi) and Δt (hours) scales (Fig. 3.5d). Use the type-curve grid showing through the tracing paper as a guide for plotting the Δp vs Δt data (Fig. 3.5e). This process guarantees that the data plot and the type curve have the same scale. Ignore the curves and the scale on the type curve during the plotting stage; use only the base grid.

2. Slide the tracing paper with the plotted data, keeping the grids parallel, until the data points match one of the type curves (Fig. 3.5f). The type curves are usually similarly shaped, so the matching process can be difficult. After the match is completed, trace the matched curve (Fig. 3.5g) and pick a convenient "match point" on the data plot, such as an intersection of major grid lines. Record values at that point on the data plot $[(\Delta p)_M$ and $(\Delta t)_M]$ and the corresponding values lying beneath that point on the type-curve grid $[(p_D)_M$ and $(t_D)_M]$ (Fig. 3.5h). The match-point data are used to estimate formation properties.

3. In Fig. C.6 (most other Appendix C figures also could be used), the ordinate of the type curve is dimensionless pressure,

$$p_D = \frac{\Delta p k h}{141.2\, q B \mu} \quad \ldots\ldots\ldots\ldots\ldots\ldots\ldots\ldots (3.13)$$

By substituting match-point values from Step 2 and rearranging Eq. 3.13, we estimate formation permeability:

$$k = 141.2\,\frac{qB\mu}{h}\,\frac{(p_D)_M}{(\Delta p)_M} \quad \ldots\ldots\ldots\ldots\ldots\ldots (3.14)$$

4. Similarly, use the definition on the abscissa on the type curve, the dimensionless time in Fig. C.6,

$$t_D = \frac{0.0002637\, kt}{\phi \mu c_t r_w^{\,2}}, \quad \ldots\ldots\ldots\ldots\ldots\ldots (3.15)$$

with the time-scale match-point data and the permeability just determined, to estimate the reservoir porosity-compressibility product:

$$\phi c_t = \left[\frac{0.0002637\, k}{\mu r_w^{\,2}}\right]\frac{(\Delta t)_M}{(t_D)_M} \quad \ldots\ldots\ldots\ldots\ldots\ldots (3.16)$$

5. If the type curve is one of several on the graph and is

*Large-scale copies of Figs. 4.12, 8.8A through 8.8C, C.2, C.3, C.5 through C.9, and C.17 through C.19 are available. Information about ordering a packet containing these figures can be obtained by writing to Order Dept. SPE-AIME.

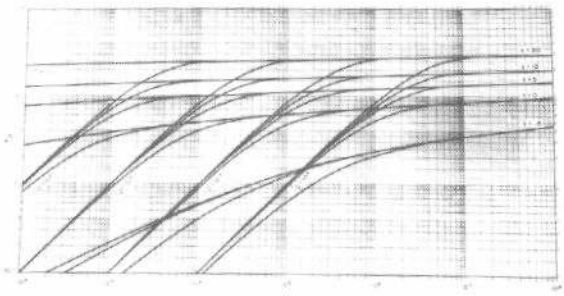

(a) Choose a type curve.

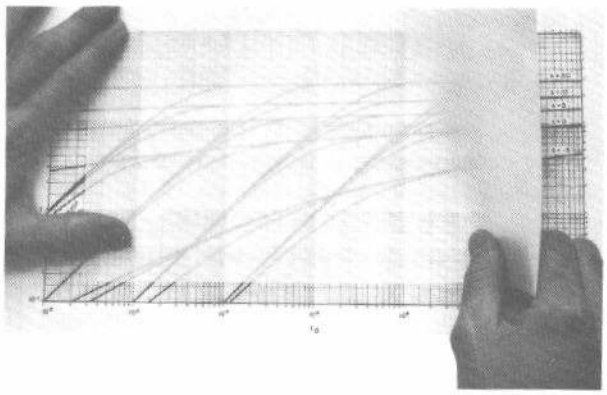

(b) Overlay with tracing paper.

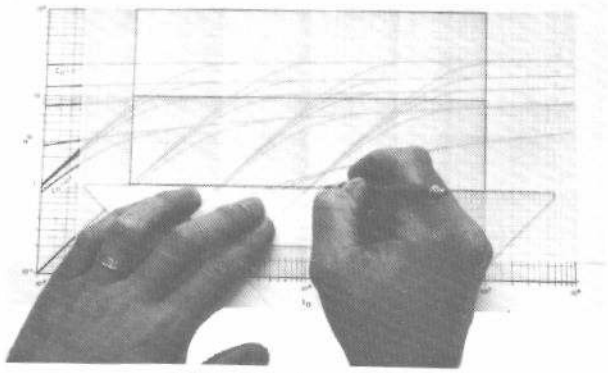

(c) Trace major grid lines.

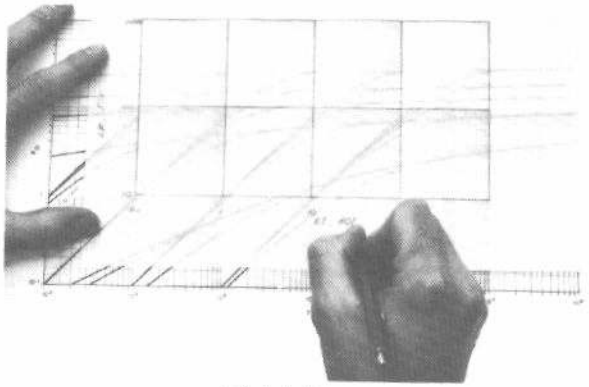

(d) Label axes.

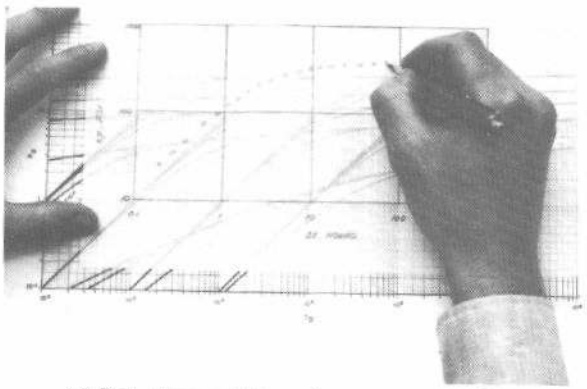

(e) Plot observed data using type-curve grid.

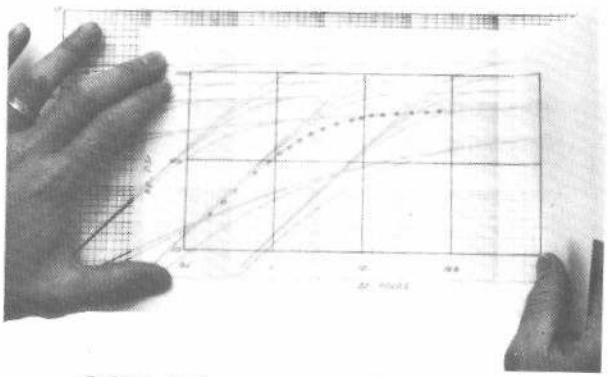

(f) Slide tracing paper to match a type curve.

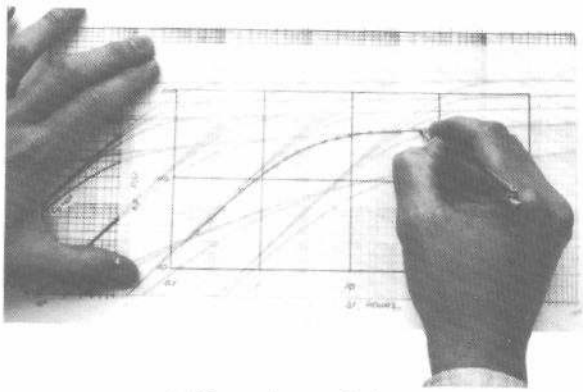

(g) Trace the matched curve.

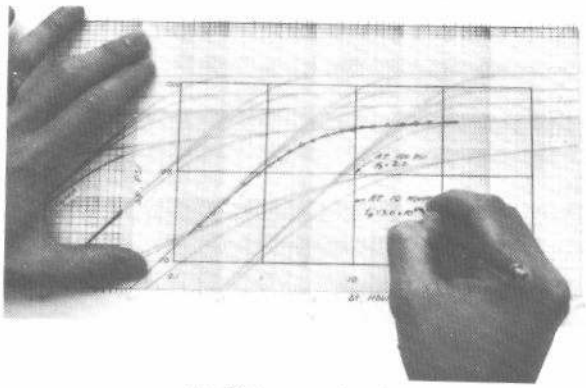

(h) Pick a match point.

Fig. 3.5 Steps in type-curve matching.

identified by a parameter, such as the dimensionless storage coefficient and the skin factor in Fig. C.6, that parameter may be used to estimate additional wellbore or reservoir properties.

Fig. C.6 is one of many useful type curves. Fig. C.8 is useful for drawdown and pressure buildup test analysis for wells with wellbore storage and skin — if the semilog straight line does not develop. The analysis procedure for this type curve, which does not use p_D and t_D, follows. The explanation becomes more understandable if the data of Example 3.2 are used to perform the process.

1a. Plot observed test data as $\Delta p/\Delta t$ (psi/hour) on the ordinate vs Δt (hours) on the abscissa on tracing paper over the grid of Fig. C.8. (Setup is similar to that illustrated in Fig. 3.5.)

1b. Estimate the wellbore storage coefficient expected from completion details (this step can be skipped and C can be estimated from Step 2b):

$$C = V_w c, \quad \ldots\ldots\ldots\ldots\ldots\ldots\ldots\ldots\ldots\ldots (3.17)$$

for a wellbore without a gas-liquid interface or,

$$C = \frac{V_u}{\left(\frac{\rho}{144}\ \frac{g}{g_c}\right)}, \quad \ldots\ldots\ldots\ldots\ldots\ldots\ldots\ldots\ldots\ldots (3.18)$$

for a wellbore with changing liquid level.

1c. Estimate the $\Delta p/\Delta t$ value where

$$\left(\frac{\Delta p}{\Delta t}\ \frac{24C}{qB}\right)_{\text{Fig. C.8}} = 1.0 . \quad \ldots\ldots\ldots\ldots\ldots\ldots\ldots (3.19)$$

This estimate is made from

$$\left(\frac{\Delta p}{\Delta t}\right)_{1.0} = \frac{qB}{24C} . \quad \ldots\ldots\ldots\ldots\ldots\ldots\ldots\ldots\ldots (3.20)$$

Align the tracing-paper data plot so the value calculated in Eq. 3.20 overlies 1.0 on the ordinate of Fig. C.8 (Eq. 3.19).

2a. Keeping the two grids parallel, slide the tracing-paper data plot *horizontally* until the best match is obtained with one of the curves in Fig. C.8. Slight vertical movement may improve the match. Trace the matched curve onto the data plot and read the value of $(C_D e^{2s})_{\text{Fig. C.8, }M}$ for the matched curve of Fig. C.8. Pick a convenient *match point* with coordinates of $(\Delta p/\Delta t)_M$, $(\Delta t)_M$ from the tracing-paper data plot; read the coordinate values lying directly under this point from Fig. C.8,

$$\left(\frac{\Delta p}{\Delta t}\ \frac{24C}{qB}\right)_{\text{Fig. C.8, }M}, \left(\frac{kh}{\mu}\ \frac{\Delta t}{C}\right)_{\text{Fig. C.8, }M}$$

2b. If any vertical movement was made during the curve-matching process, recompute the wellbore storage coefficient from the definition of the ordinate in Fig. C.8:

$$C = \frac{qB\left(\frac{\Delta p}{\Delta t}\ \frac{24C}{qB}\right)_{\text{Fig. C.8, }M}}{24\left(\frac{\Delta p}{\Delta t}\right)_M}, \quad \ldots\ldots\ldots\ldots\ldots (3.21)$$

where q and B are observed data for the test. This value of the wellbore storage coefficient should be essentially the same as the value estimated from Eq. 3.17 or 3.18. If it is not the same, search for a reason, such as washed-out sections of hole, voids connecting with the wellbore, leaking packers, etc.

3. Estimate formation permeability from the definition of the abscissa in Fig. C.8:

$$k = \frac{C\mu\left(\frac{kh}{\mu}\ \frac{\Delta t}{C}\right)_{\text{Fig. C.8, }M}}{h(\Delta t)_M} . \quad \ldots\ldots\ldots\ldots\ldots (3.22)$$

4. Estimate the skin factor from the parameter on the matched curve:

$$s = \frac{1}{2}\ln\left[\frac{\phi c_t h r_w^2 (C_D e^{2s})_{\text{Fig. C.8, }M}}{0.89359\,C}\right] . \quad \ldots\ldots\ldots (3.23)$$

This completes the analysis using Fig. C.8.

Other type curves may be used with similar analysis procedures.

Type-curve matching provides a way to analyze transient test data *when insufficient data are available for semilog analysis methods*. If sufficient data are available, semilog methods should be used because they are more accurate than type-curve matching. Nevertheless, when there is no other way to analyze data, when there is insufficient data, or when a fractured well situation is encountered, type-curve matching can provide useful, although approximate, results.

TABLE 3.1—PRESSURE DATA FOR EXAMPLE 3.2.
After Earlougher and Kersch.[8]

Time, Δt (hours)	Pressure Change, Δp (psi)	$\Delta p/\Delta t$ (psi/hr)
0.2	19.7	98.50
0.3	28.1	93.67
0.5	43.1	86.20
0.7	58.3	83.29
1.0	75.1	75.10
2.0	114.5	57.25
3.0	135.5	45.17
5.0	152.2	30.44
7.0	163.2	23.31
10.0	166.7	16.67
20.0	171.2	8.56
30.0	173.9	5.80
50.0	175.2	3.50
70.0	177.1	2.53

Example 3.2 Drawdown Test Analysis by Type-Curve Matching[8]

A pressure drawdown test on a new oil well is strongly influenced by wellbore storage. Nevertheless, enough data exist to use the semilog plot to estimate

$$\frac{kh}{\mu} = 3{,}500 \text{ md ft/cp, and}$$

$$s = 12.$$

Table 3.1 gives Δp and $\Delta p/\Delta t$ data. Other known data are

$q_o = 179$ STB/D
$B_o = 1.2$ RB/STB
$h = 35$ ft
$c_t = 8.2 \times 10^{-6}$ psi^{-1}
$r_w = 0.276$ ft
$\phi = 18$ percent.

Analyze this test using type-curve matching with Fig. C.8 and compare the results with the semilog analysis results.

Since completion details are unknown, the wellbore storage coefficient cannot be estimated. Thus, we must match without this aid (Steps 1b and 1c). We plot $(\Delta p/\Delta t)$ vs Δt on

tracing paper laid over the Fig. C.8 grid. Fig. 3.6 shows the resulting data plot. We slide the tracing-paper data plot on Fig. C.8 until a good match results. Fig. 3.7 schematically shows the data plot matched to Fig. C.8. (For clarity in printing, the grid is omitted.) Match-point data are given in Fig. 3.7.

We estimate the wellbore storage coefficient using Eq. 3.21 and the match data from Fig. 3.7:

$$C = \frac{(179)(1.2)(0.1053)}{(24)(10)} = 0.0942 \text{ RB/psi}.$$

We use a modified form of Eq. 3.22 to compute

$$\frac{kh}{\mu} = \frac{(0.0942)(49{,}000)}{(1.0)} = 4{,}620 \text{ md ft/cp}.$$

The skin factor is estimated from Eq. 3.23:

$$s = \frac{1}{2} \ln\left[\frac{(0.18)(8.2 \times 10^{-6})(35)(0.276)^2(10^{20})}{(0.89359)(0.0942)}\right]$$

$$= 18.$$

These results are approximate; the technique normally should be used *only when other analysis methods fail*. This example illustrates the analysis method and gives an indication of its accuracy. Thus, we used a test with sufficient data for a conventional, semilog analysis that allows a comparison of the two analysis methods. The kh/μ from type-curve matching is within 32 percent of the value from the semilog plot; but the skin factor is off by 50 percent. In spite of the approximate nature of the analysis technique, useful results are obtained.

The wellbore storage coefficient, $C = 0.0942$ RB/psi, appears to be within reason. Assuming an oil gravity of 30 °API ($\rho = 54.7$ lb$_m$/cu ft) and a changing liquid level, $V_u = 0.0358$ bbl/ft from Eq. 3.18. That corresponds to about a 6-in.-ID pipe ($r \simeq 0.25$ ft), and is not inconsistent with what little is known about the completion.

3.4 Pressure Drawdown Testing in Developed Systems

Slider[10,11] suggests a technique for analyzing transient tests when conditions are not constant before testing. Fig. 3.8 schematically illustrates a situation with shut-in pressure declining (solid line) before a drawdown test starts at time t_1. The dashed line, an extrapolation of that pressure behavior into the future, represents expected pressure behavior for continued shut-in. Production starts at time t_1, and pressure behaves as shown by the solid line beyond t_1.

Three steps are required to *correctly* analyze such drawdown behavior: (1) determine the correct shut-in pressure extrapolation; (2) estimate the difference between observed flowing pressure and the extrapolated pressure ($\Delta p_{\Delta t}$ in Fig. 3.8); and (3) plot $\Delta p_{\Delta t}$ vs log Δt. A semilog straight line that can be analyzed with Eqs. 3.9 and 3.10 should result.

The preceding analysis procedure usually may be modified. Consider a shut-in well in a developed reservoir with other operating wells. There is a pressure decline at the shut-in test well owing to production at the other wells. After the test well is put on production at time t_1, its pressure is

$$p_{wf} = p_i - \frac{141.2\,qB\mu}{kh}\left[p_D(\Delta t_D, r_{D1} = 1, \ldots) + s\right] - \Delta p_{ow}(t), \quad \ldots\ldots\ldots\ldots\ldots\ldots\ldots\ldots\ldots\ldots (3.24)$$

where $\Delta p_{ow}(t)$ is the pressure drop from p_i at time $t = t_1 + \Delta t$ caused by all other wells in the reservoir. That pressure drop

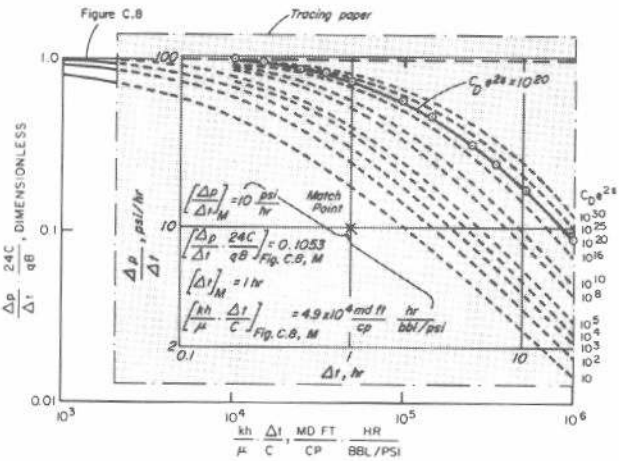

Fig. 3.7 Match of Fig. 3.6 to type curve of Fig. C.8 (part of Fig. 3.6 omitted); Example 3.2, drawdown test on a new oil well. After Earlougher and Kersch.[8]

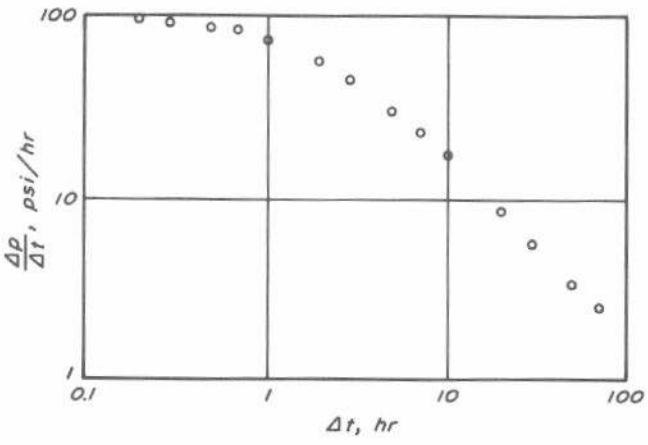

Fig. 3.6 Data plot for Example 3.2 before matching to type curve. Data plotted on tracing paper using grid of Fig. C.8.

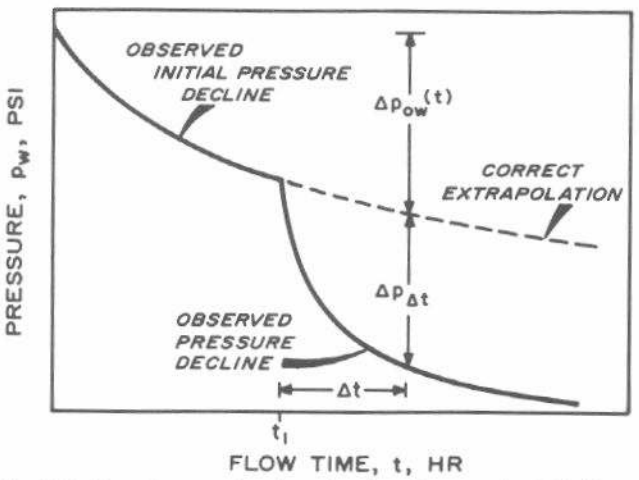

Fig. 3.8 Drawdown testing in a developed reservoir, definition of terms. After Slider.[10]

is indicated schematically in Figs. 3.8 and 3.9 and may be estimated by superposition from

$$\Delta p_{ow}(t) = p_i - p_w(t)$$

$$= \frac{141.2\mu}{kh} \sum_{j=2}^{n} q_j B_j p_D(t_D, r_{Dj}, \ldots). \quad \ldots\ (3.25)$$

Eq. 3.25 assumes that all wells start producing at a constant rate at $t = 0$. This assumption may be eliminated by a more complex superposition expression.

If the other wells in the reservoir ($j = 2, 3, \ldots n$) are operating at pseudosteady state, Eq. 3.25 takes the form

$$\Delta p_{ow}(t) = b - m^* t\ , \quad \ldots\ (3.26)$$

a straight line with slope $-m^*$ on a plot of Δp_{ow} vs t; or a straight line with slope $+m^*$ on a plot of p_w vs t. (On a reservoir-wide basis, this corresponds to the individual-well, linear, pseudosteady-state Region C of Fig. 2.1a.) The quantity m^* in Eq. 3.26 is determined before the test well starts producing from

$$m^* = \frac{dp_{ws}}{dt} = \frac{(p_{ws})_2 - (p_{ws})_1}{t_2 - t_1}\ . \quad \ldots\ (3.27)$$

For declining well pressure, m^* is negative. If pressure data are available before the drawdown test, m^* is easily estimated. It also may be estimated by using Eq. 2.23 in Eq. 3.25:

$$m^* = \frac{-0.23395}{\phi c_t h A} \sum_{j=2}^{n} q_j B_j\ , \quad \ldots\ (3.28)$$

where ϕhA is the total reservoir pore volume in cubic feet.

By appropriate combination of Eqs. 3.2, 3.3, 3.24, and 3.26, and by using $t_1 + \Delta t$ in place of t, it can be shown that

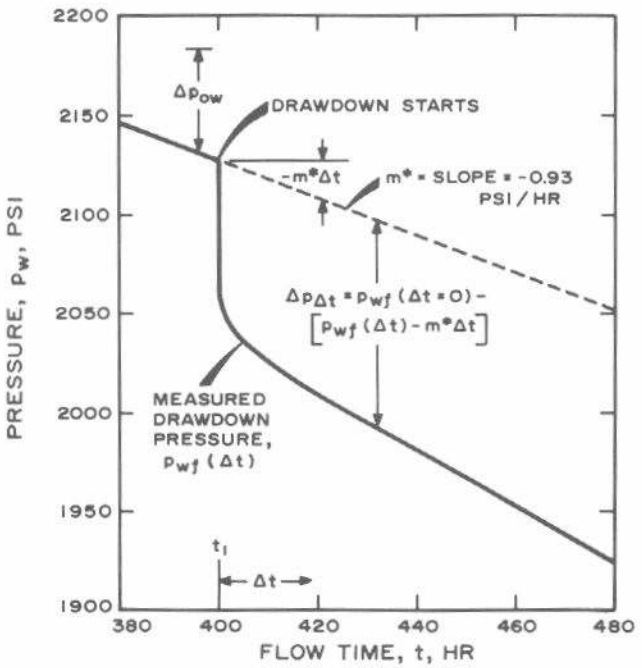

Fig. 3.9 Drawdown test for a well in a developed reservoir, data of Example 3.3.

$$p_{wf} - m^*\Delta t = m \log \Delta t + \Delta p_{1\text{hr}}\ , \quad \ldots\ (3.29)$$

where m is given by Eq. 3.6 and $\Delta p_{1\text{hr}}$ is given by the right-hand side of Eq. 3.7, with $p_{ws}(\Delta t = 0)$ in place of p_i. Eq. 3.29 indicates that a plot of $(p_{wf} - m^*\Delta t)$ vs $\log \Delta t$ should have a straight-line portion with slope m and intercept $\Delta p_{1\text{hr}}$ at $\Delta t = 1$ hour. The slope, m, can be used with Eq. 3.9 to estimate formation permeability. Skin factor is estimated from

$$s = 1.1513\left[\frac{\Delta p_{1\text{hr}} - p_{ws}(\Delta t=0)}{m} - \log\left(\frac{k}{\phi\mu c_t r_w^2}\right) + 3.2275\right]. \quad \ldots\ (3.30)$$

In Eq. 3.30, $p_{ws}(\Delta t=0)$ is the shut-in pressure at the beginning of the test.

Example 3.3 Drawdown Test Analysis in a Developed Reservoir

Fig. 3.9 shows simulated drawdown test data for a well in a relatively small multiple-well reservoir. Before the drawdown test, the pressure at the shut-in test well declines linearly, with $m^* = -0.93$ psi/hr, so the analysis method of Eq. 3.29 should apply. At $t_1 = 400$ hours, the test well started producing at 20 STB/D. The pressure response during the flow period is shown in Figs. 3.9 and 3.10. The properties used to simulate the test data are

$k = 20$ md	$B = 1.0$ RB/STB
$h = 10$ ft	$c_t = 10^{-5}$ psi^{-1}
$\mu = 1.0$ cp	$s = 0$
$\phi = 20$ percent	$p_i = 2{,}500$ psi
$r_w = 0.3535$ ft	$p_{ws}(\Delta t=0) = 2{,}127$ psi.
$q = 20$ STB/D	

To illustrate the importance of a correct analysis, we first estimate k and s from the normal semilog plot of p_{wf} vs $\log \Delta t$. From Fig. 3.10, $m = -17.1$ psi/cycle and $p_{1\text{hr}} = 2{,}051$ psi.

Using Eqs. 3.9 and 3.10,

$$k = \frac{(162.6)(20)(1.0)(1.0)}{(-17.1)(10)} = 19.0 \text{ md},$$

and

$$s = -1.1513\left\{\frac{2{,}051 - 2{,}127}{-17.1} - \log\left[\frac{19}{(0.2)(10^{-5})(1)(0.3535)^2}\right] + 3.2275\right\}$$

$$= -0.24.$$

The calculated permeability is 5 percent too low and the skin factor shows a slight improvement rather than $s = 0$.

We next estimate k and s from the plot of $(p_{wf} - m^*\Delta t)$ vs $\log \Delta t$ shown in Fig. 3.11. Data are

$m^* = -0.93$ psi/hour from Fig. 3.9,
$m = -16.3$ psi/cycle from Fig. 3.11, and
$\Delta p_{1\text{hr}} = 2{,}052$ psi from Fig. 3.11.

Using Eqs. 3.9 and 3.30,

$$k = -\frac{(162.6)(20)(1)(1)}{(-16.3)(10)} = 20.0 \text{ md.}$$

$$s = 1.1513\left\{\frac{2{,}052 - 2{,}127}{-16.3} - \log\left[\frac{20}{0.2(10^{-5})(1)(0.3535)^2}\right] + 3.2275\right\}$$

$$= -0.09.$$

A slight improvement in the estimated values of k and s is obtained by including $m^*\Delta t$. The main advantage of including $m^*\Delta t$ is the extended length of the straight line; compare Figs. 3.10 and 3.11. In many cases, the standard analysis techniques given in Section 3.2 can be used with good accuracy. The only difference is that the shut-in pressure just before starting the test rather than p_i should be used to calculate s.

As indicated in Example 3.3, the major advantage of using this kind of analysis is that it extends the length of the semilog straight line and simplifies the analysis. The method may be extended to more complicated systems, although that is beyond the scope of this monograph. The reader is referred to Slider[10,11] for additional technical details.

3.5 Reservoir Limit Testing

A drawdown test run specifically to determine the reservoir volume communicating with the well is called a *reservoir limit test*. Such a test, introduced by Jones,[12,13] uses the pseudosteady-state part of the drawdown data when

$$p_D(t_D, \ldots) = 2\pi t_{DA} + \frac{1}{2}\ln\left(\frac{A}{r_w^2}\right) + \frac{1}{2}\ln\left(\frac{2.2458}{C_A}\right). \quad \ldots\ldots\ldots\ldots (3.31)$$

The dimensionless pressure during pseudosteady-state flow is a linear function of dimensionless time. Eq. 3.31 may be combined with Eqs. 2.2 and 2.3b and simplified to

$$p_{wf} = m^* t + p_{\text{int}}, \quad \ldots\ldots\ldots\ldots\ldots\ldots\ldots (3.32)$$

where

$$m^* = -\frac{0.23395\, qB}{\phi c_t h A}, \quad \ldots\ldots\ldots\ldots\ldots\ldots (3.33)$$

and

$$p_{\text{int}} = p_i - \frac{70.60\, qB\mu}{kh}\left[\ln\left(\frac{A}{r_w^2}\right) + \ln\left(\frac{2.2458}{C_A}\right) + 2s\right]. \quad \ldots\ldots\ldots\ldots\ldots (3.34)$$

Eq. 3.32 indicates that a Cartesian plot of bottom-hole flowing pressure vs time should be a straight line during pseudosteady-state flow, with slope m^* given by Eq. 3.33 and intercept p_{int} given by Eq. 3.34. The slope may be used to estimate the connected reservoir drainage volume:

$$\phi hA = -\frac{0.23395\, qB}{c_t m^*}, \quad \ldots\ldots\ldots\ldots\ldots\ldots (3.35)$$

where the volume is in cubic feet. If ϕh is known, the drainage area may be estimated. Other techniques have been proposed[12-14] for analyzing pseudosteady-state data, but this one appears to be the simplest and least prone to errors.

If pressure data are available during both the infinite-acting period and the pseudosteady-state period, it is possible to estimate the drainage shape for the test well. The semilog plot is used to determine m and $p_{1\text{hr}}$; the Cartesian plot is used to get m^* and p_{int}. The system shape factor is estimated from[15]

$$C_A = 5.456\,\frac{m}{m^*}\exp\left[2.303\,(p_{1\text{hr}} - p_{\text{int}})/m\right]. \quad \ldots\ldots (3.36)$$

Knowing the shape factor, use Table C.1 to determine the reservoir configuration with the shape factor closest to that calculated. This process may be refined[15] by computing

$$(t_{DA})_{pss} = 0.1833\,\frac{m^*}{m}\,t_{pss}, \quad \ldots\ldots\ldots\ldots\ldots\ldots (3.37)$$

and using the "Exact for t_{DA} >" column of Table C.1. The time t_{pss} is when the Cartesian straight line starts.

Example 3.4 Reservoir Limit Test[15]

Use the long-time drawdown data of Example 3.1 to estimate the drainage area for that well. Combine the long- and short-time data to estimate the reservoir shape.

Pressure data are shown in Figs. 3.4 and 3.12. From Fig. 3.4, $m = -22$ psi/cycle and $p_{1\text{hr}} = 954$ psi. From Fig. 3.12, $m^* = -0.8$ psi/hour, $p_{\text{int}} = 940$ psi, and $t_{pss} = 11$ hours. Using Eq. 3.35,

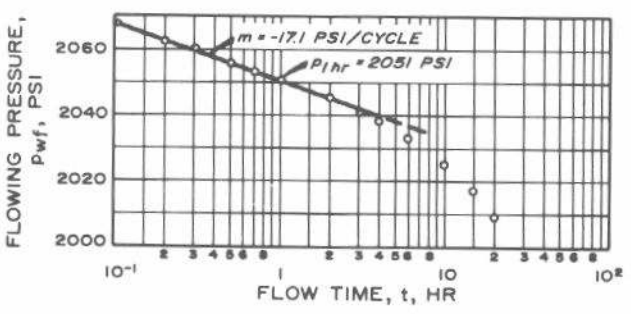

Fig. 3.10 Semilog drawdown curve for the well of Example 3.3.

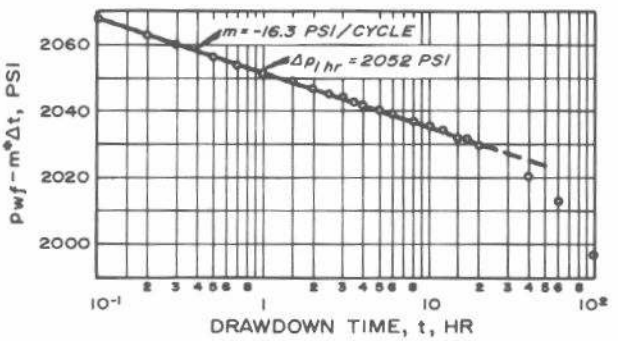

Fig. 3.11 $p_{wf} - m^*\Delta t$ vs log Δt for the well of Example 3.3.

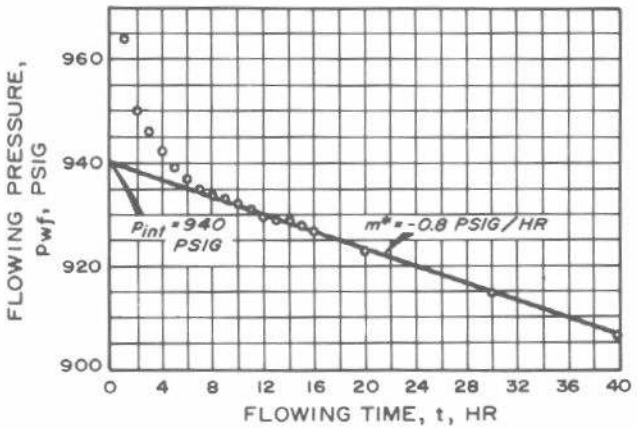

Fig. 3.12 Cartesian plot of the drawdown test data of Examples 3.1 and 3.4.

$$\phi hA = \frac{(-0.23395)(348)(1.14)}{(8.74 \times 10^{-6})(-0.8)}$$

$$= 1.33 \times 10^{7} \text{ cu ft}$$

$$= \frac{(1.33 \times 10^{7})}{5.6146} = 2.37 \times 10^{6} \text{ bbl.}$$

$$A = \frac{1.33 \times 10^{7} \text{ cu ft}}{(0.2)(130 \text{ ft})} \times \frac{1 \text{ acre}}{(43{,}560 \text{ sq ft})}$$

$$= 11.7 \text{ acres.}$$

Using Eq. 3.36,

$$C_A = \frac{(5.456)(-22)}{(-0.8)} \exp\left[(2.303)(954 - 940)/(-22)\right]$$

$$= 150.0\, e^{-1.466} = 34.6.$$

In Table C.1, $C_A = 34.6$ corresponds most closely to a well in the center of a circle, square, or hexagon.

For a circle, $C_A = 31.62$.

For a square, $C_A = 30.88$.

For a hexagon, $C_A = 31.6$.

For verification, use Eq. 3.37:

$$(t_{DA})_{pss} = (0.1833)\ \frac{(-0.8)}{(-22)}\ (11) = 0.07.$$

This agrees well with $(t_{DA})_{pss} = 0.1$ for the three shapes.

3.6 Factors Complicating Drawdown Testing

Although a properly run drawdown test yields considerable information about the reservoir, the test may be hard to control since it is a flowing test. If a constant rate cannot be maintained within a reasonable tolerance, the analysis techniques of Chapter 4 should be used. Those techniques also should be used if the well was not shut in long enough to reach static reservoir pressure before the drawdown starts.

The early part of drawdown data is influenced by wellbore storage. Sometimes it is possible to draw a straight line through the semilog plot of data taken during this time. The slope of that line gives incorrect values of permeability and skin. As discussed in Sections 2.6 and 3.2, a log-log data plot of the drawdown data must be made to select the correct semilog straight line.

References

1. Matthews, C. S. and Russell, D. G.: *Pressure Buildup and Flow Tests in Wells*, Monograph Series, Society of Petroleum Engineers of AIME, Dallas (1967) **1**, Chap. 5.

2. Papadopulos, Istavros S. and Cooper, Hilton H., Jr.: "Drawdown in a Well of Large Diameter," *Water Resources Res.* (1967) **3**, No. 1, 241-244.

3. Cooper, Hilton H., Jr., Bredehoeft, John D., and Papadopulos, Istavros S.: "Response of a Finite-Diameter Well to an Instantaneous Charge of Water," *Water Resources Res.* (1967) **3**, No. 1, 263-269.

4. Ramey, H. J., Jr.: "Short-Time Well Test Data Interpretation in the Presence of Skin Effect and Wellbore Storage," *J. Pet. Tech.* (Jan. 1970) 97-104; *Trans.*, AIME, **249.**

5. Agarwal, Ram G., Al-Hussainy, Rafi, and Ramey, H. J., Jr.: "An Investigation of Wellbore Storage and Skin Effect in Unsteady Liquid Flow: I. Analytical Treatment," *Soc. Pet. Eng. J.* (Sept. 1970) 279-290; *Trans.*, AIME, **249.**

6. Wattenbarger, Robert A. and Ramey, H. J., Jr.: "An Investigation of Wellbore Storage and Skin Effect in Unsteady Liquid Flow: II. Finite Difference Treatment," *Soc. Pet. Eng. J.* (Sept. 1970) 291-297; *Trans.*, AIME, **249.**

7. McKinley, R. M.: "Wellbore Transmissibility From Afterflow-Dominated Pressure Buildup Data," *J. Pet. Tech.* (July 1971) 863-872; *Trans.*, AIME, **251.**

8. Earlougher, Robert C., Jr., and Kersch, Keith M.: "Analysis of Short-Time Transient Test Data by Type-Curve Matching," *J. Pet. Tech.* (July 1974) 793-800; *Trans.*, AIME, **257.**

9. Gringarten, Alain C., Ramey, Henry J., Jr., and Raghavan, R.: "Pressure Analysis for Fractured Wells," paper SPE 4051 presented at the SPE-AIME 47th Annual Fall Meeting, San Antonio, Tex., Oct. 8-11, 1972.

10. Slider, H. C.: "A Simplified Method of Pressure Buildup Analysis for a Stabilized Well," *J. Pet. Tech.* (Sept. 1971) 1155-1160; *Trans.*, AIME, **251.**

11. Slider, H. C.: "Application of Pseudo-Steady-State Flow to Pressure-Buildup Analysis," paper SPE 1403 presented at the SPE-AIME Regional Symposium, Amarillo, Tex., Oct. 27-28, 1966.

12. Jones, Park: "Reservoir Limit Test," *Oil and Gas J.* (June 18, 1956) 184-196.

13. Jones, Park: "Drawdown Exploration Reservoir Limit, Well and Formation Evaluation," paper 824-G presented at the SPE-AIME Permian Basin Oil Recovery Conference, Midland, Tex., April 18-19, 1957.

14. Jones, L. G.: "Reservoir Reserve Tests," *J. Pet. Tech.* (March 1963) 333-337; *Trans.*, AIME, **228.** Also *Reprint Series, No. 9 — Pressure Analysis Methods*, Society of Petroleum Engineers of AIME, Dallas (1967) 126-130.

15. Earlougher, R. C., Jr.: "Estimating Drainage Shapes From Reservoir Limit Tests," *J. Pet. Tech.* (Oct. 1971) 1266-1268; *Trans.*, AIME, **251.**

Chapter 4

Multiple-Rate Testing

4.1 Introduction

The drawdown testing and analysis methods in Chapter 3 require a constant flow rate; however, it is often impractical or impossible to maintain a constant rate long enough to complete a drawdown test. In such a situation, multiple-(variable) rate testing and analysis techniques are applicable. A multiple-rate test may range from one with an uncontrolled, variable rate,[1,2] to one with a series of constant rates,[3,4] to testing at constant bottom-hole pressure with a continuously changing flow rate.[5] Pressure-buildup testing[1] (Chapter 5) is a special kind of multiple-rate well test. Almost any flow-rate change can be analyzed as a well test by using the concepts presented in this chapter.

Accurate flow rate and pressure measurements are essential for the successful analysis of any transient well test. Rate measurements are much more critical in multiple-rate testing, however, than in conventional, constant-rate well tests. Without good flow-rate data, good analysis of multiple-rate tests is impossible.

Multiple-rate testing has the advantage of providing transient test data while production continues. It tends to minimize changes in wellbore storage coefficient and phase segregation (humping) effects and, thus, may provide good results when drawdown or buildup testing would not.

4.2 A General Multiple-Rate Test Analysis Technique

Fig. 4.1 schematically shows a variable production-rate schedule. Although flow rate may change continuously, it is treated as a series of discrete constant rates for analysis purposes. The step-wise approximation improves as the time intervals become smaller. Section B.7 presents the derivation of a general equation for pressure behavior caused by a variable flow rate. The approach presented here requires that the log approximation to the line source (Eq. 2.5b) applies. Then,

$$\frac{p_i - p_{wf}}{q_N} = m' \sum_{j=1}^{N} \left[\frac{(q_j - q_{j-1})}{q_N} \log(t - t_{j-1}) \right] + b'. \quad \ldots\ldots\ldots\ldots\ldots\ldots\ldots\ldots\ldots\ldots\ldots\ldots\ldots\ldots (4.1)$$

Eq. 4.1 is the equation of a straight line with slope

$$m' = \frac{162.6 B\mu}{kh}, \quad \ldots\ldots\ldots\ldots\ldots\ldots\ldots\ldots\ldots\ldots\ldots\ldots\ldots\ldots (4.2)$$

and intercept

$$b' = m' \left[\log \left(\frac{k}{\phi \mu c_t r_w^2} \right) - 3.2275 + 0.86859\, s \right]. \quad \ldots\ldots\ldots\ldots\ldots\ldots\ldots\ldots\ldots\ldots\ldots\ldots\ldots\ldots (4.3)$$

Multiple-rate transient test data should appear as a straight line when plotted as

$$\frac{p_i - p_{wf}}{q_N} \text{ vs } \sum_{j=1}^{N} \left[\frac{(q_j - q_{j-1})}{q_N} \log(t - t_{j-1}) \right].$$

To make that plot correctly, it is important to understand that the rate corresponding to each plotted pressure point is q_N — the last rate that can affect that pressure. As time increases, the number of rates may increase and the last rate may change; but each pressure point is identified with the rate occurring when that pressure was measured. There may be several pressure points associated with a given rate.

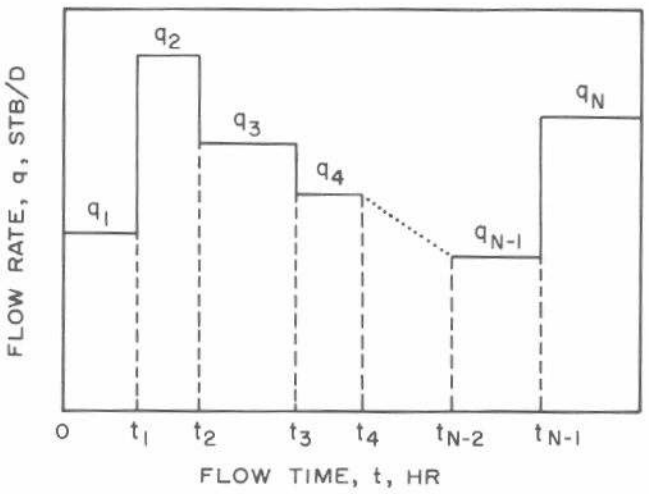

Fig. 4.1 Schematic representation of a variable production-rate schedule.

Examples 4.1 and 4.3 illustrate how the summation term in this plotting technique is calculated.

Once the data plot is made, the straight-line slope and intercept are measured. Permeability and skin factor are estimated from the slope and intercept data using Eqs. 4.2 and 4.3, rewritten as

$$k = \frac{162.6 B\mu}{m'h}, \quad \ldots\ldots\ldots\ldots\ldots\ldots\ldots\ldots\ldots\ldots (4.4)$$

and

$$s = 1.1513\left[\frac{b'}{m'} - \log\left(\frac{k}{\phi\mu c_t r_w^2}\right) + 3.2275\right]. \quad \ldots\ldots\ldots\ldots\ldots\ldots\ldots\ldots\ldots\ldots (4.5)$$

The analysis procedure is direct and simple, but the computations required to make the data plot can be tedious. The analysis has the disadvantage that the initial reservoir pressure, p_i, and the entire flow-rate history must be known; frequently, they are not. As discussed in Section 4.5, the analysis technique may be modified in some situations so that p_i is not used. If the pressure is constant during a test and the rate declines, Eqs. 4.1 through 4.5 generally are not used; instead, the techniques in Section 4.6 are preferred.

When flow-rate variation is a result of wellbore storage, a simplified plotting method, which does not require use of superposition, may be used.[6-8] In this case, one plots $(p_i - p_{wf})/q_{sf}$ vs log t. The result should be a straight line with slope m' given by Eq. 4.2 and intercept b' given by Eq. 4.3. Permeability is estimated from Eq. 4.4 and skin factor is estimated from Eq. 4.5. Ramey[8] points out that the skin factor so calculated may be low by about 0.4. We do not recommend using this analysis technique for variable-rate tests unless the variable rate results only from wellbore storage, in which case the surface rate is constant.

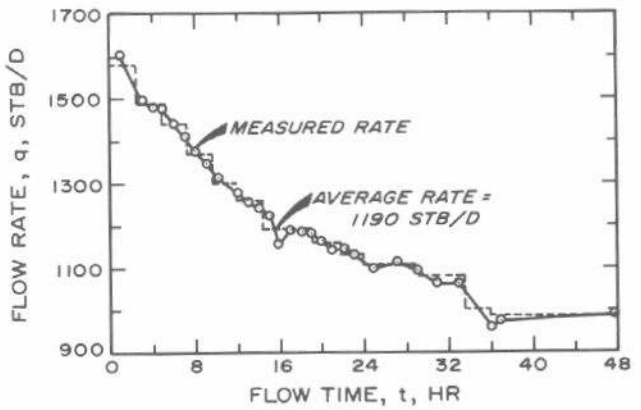

Fig. 4.2 Multiple-rate drawdown test rate history and its approximation. Data for Example 4.1.

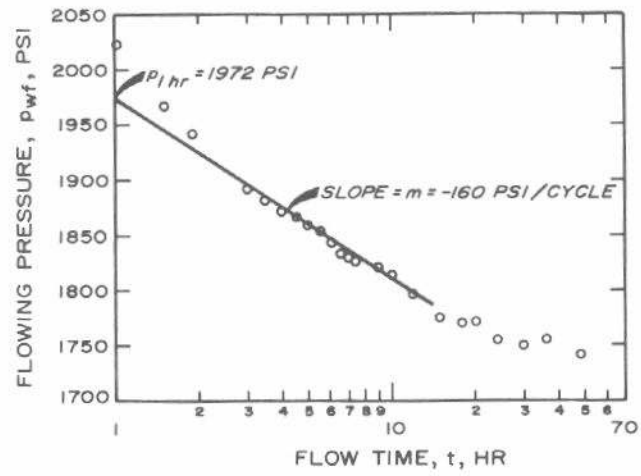

Fig. 4.3 Semilog plot of bottom-hole pressure for the multiple-rate drawdown test of Example 4.1.

Example 4.1 Multiple-Rate Drawdown Test Analysis

Production rate during a 48-hour drawdown test declined from 1,580 to 983 STB/D (Fig. 4.2). Rate and pressure data appear in Table 4.1. Reservoir data are

$p_i = 2{,}906$ psi $\qquad \mu = 0.6$ cp
$B = 1.27$ RB/STB $\qquad h = 40$ ft.

Fig. 4.3 shows flowing bottom-hole pressure vs log of flow time. That plot, which is normally used for a constant-rate drawdown test, neglects rate variations. Nevertheless, we use the straight line from 3 to 12 hours to estimate permeability. Using an average rate of 1,450 STB/D for the *first 12 hours* of the test, a slope $m = -160$ psi/cycle, and Eq. 3.9,

$$k = -\frac{(162.6)(1{,}450)(1.27)(0.6)}{(-160)(40)} = 28.1 \text{ md}.$$

Fig. 4.4 is a plot of $(p_i - p_{wf})/q_N$ vs

$$\frac{1}{q_N}\sum_{j=1}^{N}(q_j - q_{j-1})\log(t - t_{j-1})$$

for this test, using the rate breakdown shown in Table 4.1. Table 4.1 summarizes the calculations of the quantities plotted in Fig. 4.4.

To illustrate the method of computing the time summation, we calculate it at 6.05 and 12.0 hours. At 6.05 hours, $q = 1{,}440$ STB/D is the third rate observed (although the point is the ninth pressure point), so $N = 3$. Computing the summation term,

$$\begin{aligned}
&\frac{1}{q_N}\sum_{j=1}^{N}(q_j - q_{j-1})\log(t - t_{j-1}) \\
&= \frac{1}{1{,}440}\{[(1{,}580 - 0)\log(6.05 - 0)]_{j=1} \\
&+ [(1{,}490 - 1{,}580)\log(6.05 - 2.40)]_{j=2} \\
&+ [(1{,}440 - 1{,}490)\log(6.05 - 4.80)]_{j=3}\} \\
&= \frac{1}{1{,}440}\{[1{,}580\log(6.05)]_{j=1} \\
&+ [-90\log(3.65)]_{j=2} \\
&+ [-50\log(1.25)]_{j=3}\} \\
&= \frac{1}{1{,}440}\{1{,}235.17 - 50.61 - 4.85\} = 0.819.
\end{aligned}$$

Thus, the point for 6.05 hours plots at coordinates (0.819, 0.738) in Fig. 4.4. At 12.0 hours, $q = 1{,}300$ STB/D and $N = 5$. Thus,

$$\frac{1}{q_N}\sum_{j=1}^{N}(q_j - q_{j-1})\log(t - t_{j-1})$$

$$= \frac{1}{1{,}300}\left[(1{,}580 - 0)\log(12.0 - 0)\right.$$
$$+ (1{,}490 - 1{,}580)\log(12.0 - 2.40)$$
$$+ (1{,}440 - 1{,}490)\log(12.0 - 4.80)$$
$$+ (1{,}370 - 1{,}440)\log(12.0 - 7.20)$$
$$\left.+ (1{,}300 - 1{,}370)\log(12.0 - 9.60)\right]$$

$$= \frac{1}{1{,}300}\left[1{,}705.11 - 88.40 - 42.87 - 47.69 - 26.61\right]$$

$$= 1.154.$$

The point at 12.0 hours plots at coordinates (1.154, 0.853) in Fig. 4.4.

Two straight lines can be drawn through the data of Fig. 4.4. The slope of the second line is greater than that of the first, possibly indicating transition to pseudosteady state, faulting, or a decrease in permeability away from the well (see Sections 10.2 and 10.4). The incorrect semilog data plot, Fig. 4.3, has a *reduction* in slope for $t > 12$ hours that might be interpreted as increasing permeability away from the well. That is an incorrect conclusion, however, since the slope change in Fig. 4.3 is caused by the declining production rate.

Using the slope of the first straight line in Fig. 4.4 and Eq. 4.4,

$$k = \frac{(162.6)(1.27)(0.6)}{(0.227)(40)} = 13.6 \text{ md}.$$

Thus, the permeability computed from Fig. 4.3 is about 107 percent too high.

TABLE 4.1—VARIABLE FLOW RATE DRAWDOWN DATA FOR EXAMPLE 4.1.

Time, t (hours)	Rate, q (STB/D)	N	p_{wf} (psi)	$p_i - p_{wf}$ (psi)	$\frac{p_i - p_{wf}}{q_N}$ (psi/STB/D)	$\sum$
1.00	1,580	1	2,023	883	0.5589	0.000
1.50	1,580	1	1,968	938	0.5937	0.176
1.89	1,580	1	1,941	965	0.6108	0.277
2.40	1,580	1	—	—	—	—
3.00	1,490	2	1,892	1,014	0.6805	0.519
3.45	1,490	2	1,882	1,024	0.6872	0.569
3.98	1,490	2	1,873	1,033	0.6933	0.624
4.50	1,490	2	1,867	1,039	0.6973	0.673
4.80	1,490	2	—	—	—	—
5.50	1,440	3	1,853	1,053	0.7313	0.787
6.05	1,440	3	1,843	1,063	0.7382	0.819
6.55	1,440	3	1,834	1,072	0.7444	0.849
7.00	1,440	3	1,830	1,076	0.7472	0.874
7.20	1,440	3	—	—	—	—
7.50	1,370	4	1,827	1,079	0.7876	0.974
8.95	1,370	4	1,821	1,085	0.7920	1.009
9.6	1,370	4	—	—	—	—
10.0	1,300	5	1,815	1,091	0.8392	1.124
12.0	1,300	5	1,797	1,109	0.8531	1.154
14.4	1,260	6	—	—	—	—
15.0	1,190	7	1,775	1,131	0.9504	1.337
18.0	1,190	7	1,771	1,135	0.9538	1.355
19.2	1,190	7	—	—	—	—
20.0	1,160	8	1,772	1,134	0.9776	1.423
21.6	1,160	8	—	—	—	—
24.0	1,137	9	1,756	1,150	1.0114	1.485
28.8	1,106	10	—	—	—	—
30.0	1,080	11	1,751	1,155	1.0694	1.607
33.6	1,080	11	—	—	—	—
36.0	1,000	12	—	—	—	—
36.2	983	13	1,756	1,150	1.1699	1.788
48.0	983	13	1,743	1,163	1.1831	1.800

4.3 Two-Rate Testing

When a multiple-rate test consists of only two flow rates, both testing and analysis are simplified. The two-rate test provides information about k and s while production continues. Wellbore storage effects are often thought to be minimized or eliminated by two-rate tests. In fact, wellbore storage effects last just about the same amount of time in a

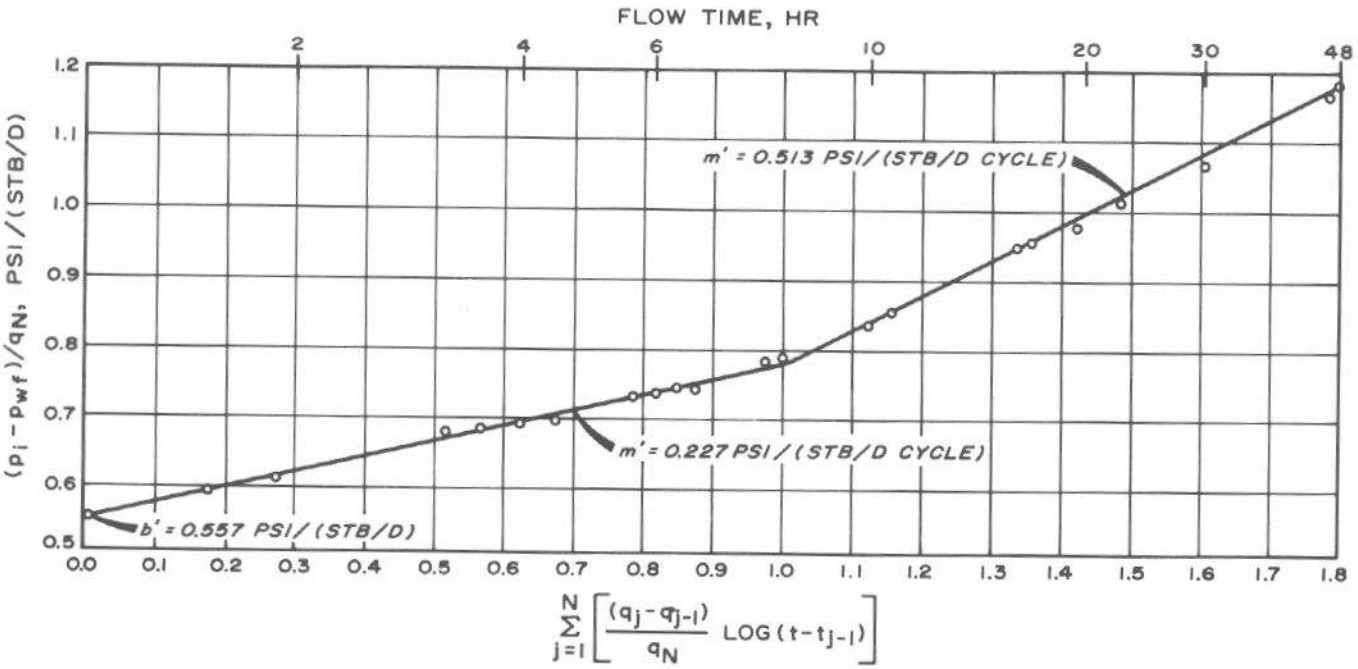

Fig. 4.4 Correct data plot for the multiple-rate drawdown test of Example 4.1; t is in hours.

two-rate test as in a normal buildup, drawdown, falloff, etc., test. However, a two-rate test often can be used to prevent a wellbore storage increase, thus providing an analyzable test when one otherwise might not be possible (see Section 11.2). The main advantage of a two-rate test over a buildup test is that deferred production is minimized.

Fig. 4.5 schematically illustrates the rate and pressure behavior for a two-rate flow test;[3] either a decreasing or increasing rate sequence may be used. Eq. 4.1 may be modified to the form presented by Russell[3] for a two-rate test:

$$p_{wf} = m_1' \left[\log \left(\frac{t_1 + \Delta t}{\Delta t} \right) + \frac{q_2}{q_1} \log \Delta t \right] + p_{int}. \quad \ldots \quad (4.6)$$

Eq. 4.6 assumes a constant flow rate, q_1, from time 0 to time t_1, at the start of the test. If, instead, the well was stabilized at rate q_1, then Eq. 4.6 is still a good approximation if t_1 is calculated from

$$t_1 = 24 \frac{(V_P)}{q_1}, \quad \ldots \quad (4.7)$$

where V_P is the cumulative volume produced since the last rate stabilization.

Eq. 4.6 implies that a graph of p_{wf} vs

$$\left[\log \left(\frac{t_1 + \Delta t}{\Delta t} \right) + \frac{q_2}{q_1} \log \Delta t \right]$$

should be a straight line with slope

$$m_1' = - \frac{162.6 q_1 B \mu}{kh}, \quad \ldots \quad (4.8)$$

and intercept

$$p_{int} = p_i + m_1' \frac{q_2}{q_1} \left[\log \left(\frac{k}{\phi \mu c_t r_w^2} \right) - 3.2275 + 0.86859 s \right]. \quad \ldots \quad (4.9)$$

Fig. 4.6 schematically shows such a data plot. Because of the choice of the abscissa variable, time increases from right to left. At long times, the data deviate from the straight line as a result of boundary and interference effects. At short times they have not yet reached the straight line because of rate restabilization and wellbore storage effects. Field test results indicate that rate restabilization is faster for a rate reduction than for a rate increase.[1,3]

Once the slope of the straight line is determined from the data plot, reservoir permeability may be estimated from

$$k = \frac{-162.6 q_1 B \mu}{m_1' h}. \quad \ldots \quad (4.10)$$

The skin factor is estimated from

$$s = 1.1513 \left[\frac{q_1}{q_1 - q_2} \left(\frac{p_{wf}(\Delta t = 0) - p_{1hr}}{m_1'} \right) - \log \left(\frac{k}{\phi \mu c_t r_w^2} \right) + 3.2275 \right]. \quad \ldots \quad (4.11)$$

The intercept of the data plot may be used to estimate the false pressure,[3]

$$p^* = p_{int} - \frac{q_2}{q_1 - q_2} \left[p_{wf}(\Delta t = 0) - p_{1hr} \right], \quad \ldots \quad (4.12)$$

which is used to estimate average reservoir pressure using methods in Chapter 6.

Example 4.2 Two-Rate Flow Test Analysis[3]

Well A is a flowing producer in a low-permeability limestone reservoir in the Permian Basin. Pressure buildup tests in this reservoir usually do not provide interpretable data because of long, low-rate afterflow periods.[3]

A two-rate flow test was run by stabilizing the flow rate at 107 STB/D for several days and then reducing the flow rate to 46 STB/D. The pressure data during the second rate are shown in Fig. 4.7. Other pertinent data are

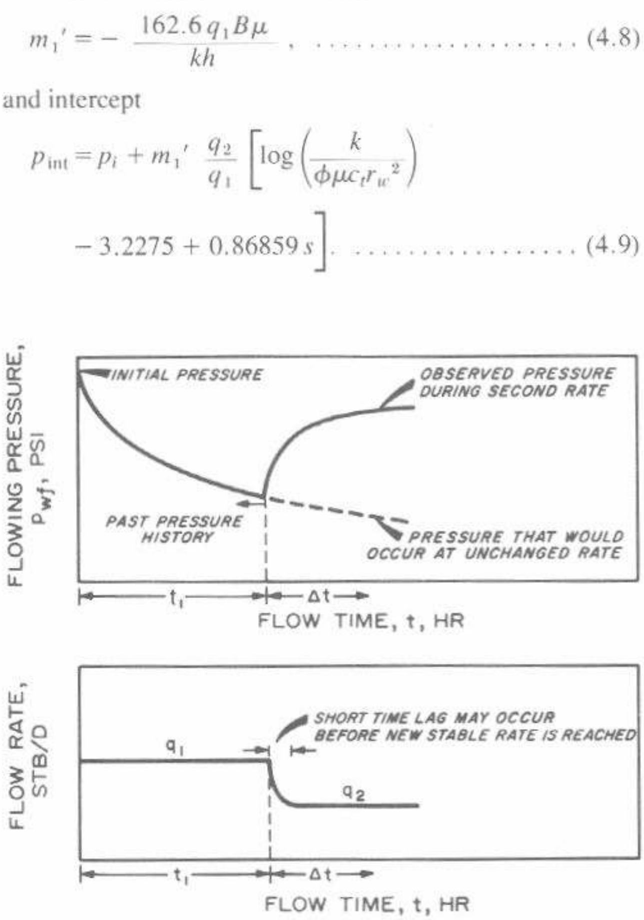

Fig. 4.5 Schematic rate and pressure history for a two-rate flow test, $q_1 > q_2$.

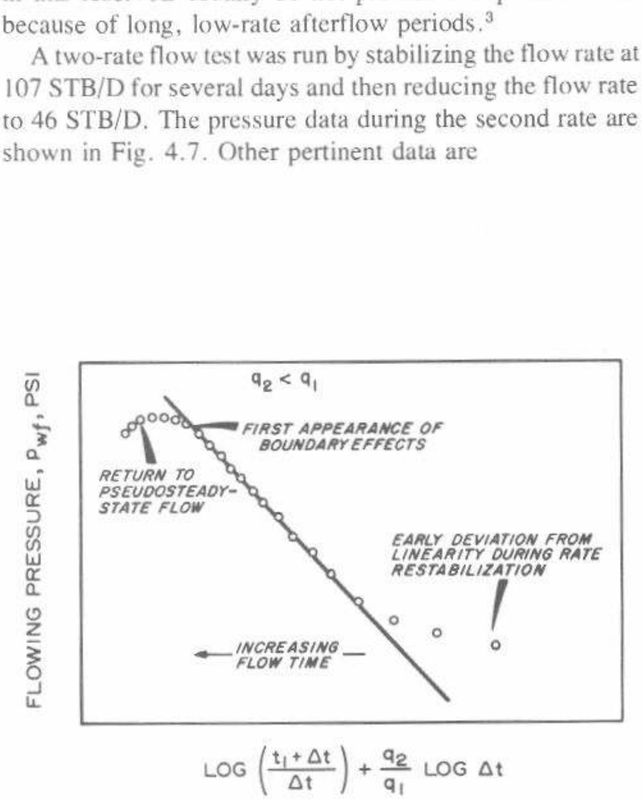

Fig. 4.6 Schematic data plot for a two-rate flow test, $q_1 > q_2$. After Russell.[3]

$B = 1.5$ RB/STB
$p_{wf}(\Delta t=0) = 3{,}118$ psi
$h = 59$ ft
$c_t = 9.32 \times 10^{-5}$ psi^{-1}
$V_p = 26{,}400$ STB
$t_1 = (26{,}400)(24)/107$
$= 5{,}921$ hours (Eq. 4.7)
$\mu = 0.6$ cp
$\phi = 0.06$
$r_w = 0.2$ ft
$m_1' = -90$ psi/cycle (Fig. 4.7)
$p_{1hr} = 3{,}169$ psi (Fig. 4.7)
$p_{int} = 3{,}510$ psi (Fig. 4.7).

Permeability is estimated from Eq. 4.10:

$$k = -\frac{(162.6)(107)(1.5)(0.6)}{(-90)(59)} = 2.9 \text{ md.}$$

The skin factor is estimated from Eq. 4.11:

$$s = 1.1513\left[\left(\frac{107}{107-46}\right)\left(\frac{3{,}118-3{,}169}{-90}\right) - \log\left(\frac{2.9}{(0.06)(0.6)(9.32\times10^{-5})(0.2)^2}\right) + 3.2275\right]$$

$$= -3.6.$$

The false pressure, p^*, is estimated from Eq. 4.12:

$$p^* = 3{,}510 - \frac{46\,(3{,}118-3{,}169)}{(107-46)}$$

$$= 3{,}548 \text{ psi.}$$

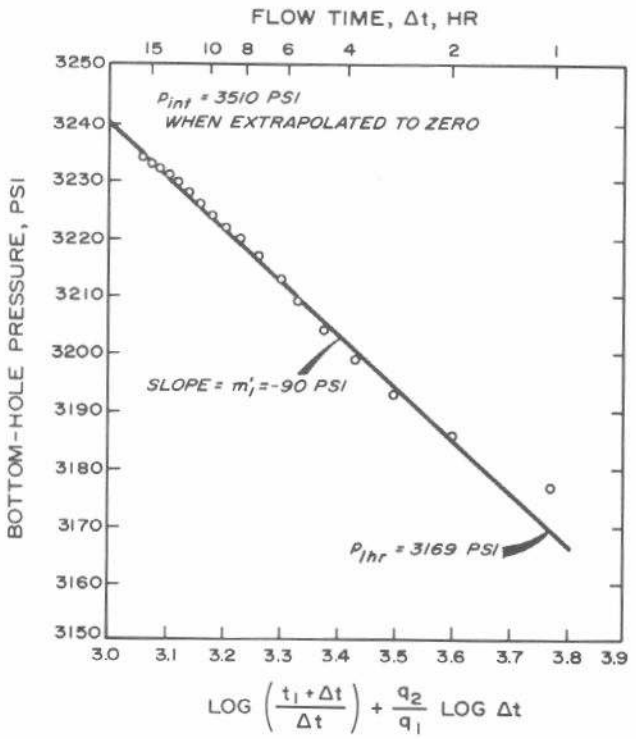

Fig. 4.7 Two-rate flow-test data plot for Example 4.2. After Russell.[3]

The p^* value may be used with material in Chapter 6 to estimate average drainage-region pressure.

In certain circumstances, the plotting technique suggested by Eq. 4.6 may be simplified.[9] When $t_1 >> \Delta t$, $\log(t_1 + \Delta t) \simeq \log t_1$ and $\log[(t_1 + \Delta t)/\Delta t] \simeq \log t_1 - \log \Delta t$. Making these approximations in Eq. 4.6 and rearranging gives

$$p_{wf} = m'' \log \Delta t + p_{int}. \quad \ldots\ldots\ldots\ldots\ldots\ldots (4.13)$$

Thus, for a two-rate test with $t_1 >> \Delta t$, a plot of p_{wf} vs $\log \Delta t$ should be a straight line with slope

$$m'' = \frac{-162.6\,(q_2 - q_1)B\mu}{kh}, \quad \ldots\ldots\ldots\ldots\ldots (4.14)$$

and intercept

$$p_{int} = p_i + \frac{m''q_2}{(q_2 - q_1)}\left[\log\left(\frac{k}{\phi\mu c_t r_w^2}\right) - 3.2275 + 0.86859\,s + \frac{q_1}{q_2}\log t_1\right]. \quad \ldots\ldots (4.15)$$

The p_{wf} vs $\log \Delta t$ data plot may be used to estimate reservoir permeability from

$$k = -\frac{162.6\,(q_2 - q_1)B\mu}{m''h}, \quad \ldots\ldots\ldots\ldots\ldots (4.16)$$

and to estimate skin factor from[9]

$$s = 1.1513\left[\frac{p_{1hr} - p_{wf}(\Delta t = 0)}{m''} - \log\left(\frac{k}{\phi\mu c_t r_w^2}\right) + 3.2275\right]. \quad \ldots\ldots\ldots\ldots\ldots\ldots (4.17)$$

The analysis suggested by Eq. 4.13 is much faster and simpler than that suggested by Eq. 4.6. However, the approximations in Eq. 4.13 cause errors in the results. The error in the permeability is[10]

$$E_k = \frac{k_E - k_{actual}}{k_{actual}}$$

$$= \frac{q_1}{q_1(T^* - 1) - q_2 T^*}, \quad \ldots\ldots\ldots\ldots\ldots (4.18)$$

while the error in skin factor is

$$E_s = s_E - s_{actual}$$

$$= \frac{-1.1513\left[p_{1hr} - p_{wf}(\Delta t = 0)\right]}{m'}\left(\frac{q_1}{q_1 - q_2}\right)\frac{1}{T^*}. \quad \ldots\ldots\ldots\ldots\ldots (4.19)$$

In Eqs. 4.18 and 4.19,

$$T^* = \frac{\log \Delta t}{\log\left(1 + \frac{\Delta t}{t_1}\right)}. \quad \ldots\ldots\ldots\ldots\ldots (4.20)$$

If the second rate of a two-rate test varies significantly, an adaptation of the multiple-rate analysis technique should be used. Odeh and Jones[11] indicate that pressure behavior for a two-rate test with a varying second rate is described by

$$\frac{p_{wf}(\Delta t=0)-p_{wf}(\Delta t)}{q_N-q_0}=m'\sum_{j=1}^{N}\left[\frac{q_j-q_{j-1}}{q_N-q_0}\times\log(\Delta t-\Delta t_{j-1})\right]+b', \quad \ldots\ldots\ldots\ldots\ldots\ldots (4.21)$$

where Δt is the time from the start of the varying second flow rate. This equation is much like Eq. 4.1 [if $q_0 = 0$ and $p_{wf}(\Delta t = 0) = p_i$, it is identical to Eq. 4.1]; the slope, m', and intercept, b', are given by Eqs. 4.2 and 4.3, respectively. If the data are plotted as the quantity on the left side of Eq. 4.21 vs the summation on the right side, permeability and skin factor may be estimated from Eqs. 4.4 and 4.5. The analysis technique suggested by Eq. 4.21 also applies to variable-rate test analysis if the well has been stabilized for a substantial time at rate q_0.

If pseudosteady state is achieved in the first flow period of a two-rate flow test, the analysis techniques of Section 4.5, Eqs. 4.30 through 4.32, should be used.

Example 4.3 Two-Rate Flow Test, Variable-Rate Case[11]

The data in Table 4.2 are for Well X of Odeh and Jones.[11] Well X was stabilized for several days at $q_0 = 1{,}103$ STB/D. Other data are

$B = 1.0$ RB/STB	$h = 18$ ft
$\mu = 1.0$ cp	$A = 28.3 \times 10^6$ sq ft
$r_w = 0.26$ ft	$\simeq 650$ acres
$c_t = 1.4 \times 10^{-5}$ psi^{-1}	$\phi = 11$ percent.

Parameters to be plotted are calculated in Table 4.2. The last value in the right-hand column is calculated as follows. (In this case, $N = 3$ since there are three rates, but five pressure data points.)

$$\sum_{j=1}^{3}\frac{q_j-q_{j-1}}{q_N-q_0}\log(\Delta t-\Delta t_{j-1})$$

$$=\left[\frac{-303}{-223}\log(10-0)\right]_{j=1}+\left[\frac{40}{-223}\log(10-4)\right]_{j=2}+\left[\frac{40}{-223}\log(10-8)\right]_{j=3}$$

$$=[(1.3587)(1)]+[(-0.1794)(0.7782)]+[(-0.1794)(0.3010)]$$

$$=1.165.$$

The data plot (Fig. 4.8) indicates the slope, m', is 0.148 psi/(STB/D cycle) and the extrapolated intercept, b', is -0.00991 psi/(STB/D). Using Eq. 4.4,

$$k=\frac{(162.6)(1)(1)}{(0.148)(18)}=61.0 \text{ md},$$

and

$$kh = 1{,}100 \text{ md ft}.$$

Using Eq. 4.5,

$$s=1.1513\left[\frac{-0.00991}{0.148}-\log\left(\frac{61.0}{(0.11)(1.0)(1.4\times10^{-5})(0.26)^2}\right)+3.2275\right]$$

$$=-6.5.$$

Odeh and Jones[11] state that pressure drawdown and buildup tests on the well indicated $kh \simeq 1{,}100$ md ft and $s \simeq -7$. They also state that they used the simplified two-rate flow-test analysis method (Eq. 4.13) with an average rate of 832 STB/D. The result was $kh \simeq 1{,}360$ md ft and $s \simeq -6.3$. Thus, the 10-percent rate variation *may have* resulted in a 23-percent error in the value calculated for kh.

Although the production time at the stabilized rate is not known for this example, the range of errors caused by using the simplified two-rate analysis may be estimated by assuming values of the stabilized production time. (This requires assuming that analysis by a two-rate technique with a constant second rate is adequate for the data of this example.) From Eq. 4.20, for $t_1 = 10$ days, and for the maximum test time of $\Delta t = 10$ hours,

$$T^*=\frac{\log 10}{\log\left(1+\frac{10}{(10)(24)}\right)}=56.4.$$

The error in kh is estimated from Eq. 4.18 with thicknesses included in the numerator and denominator:

$$E_{kh}=\frac{1{,}103}{1{,}103\,(56.4-1)-832\,(56.4)}=7.8 \text{ percent}.$$

Thus, if t_1 is indeed 10 days or more, the 23-percent error in kh when using the simplified two-rate analysis method is largely caused by the rate variation, not by the inherent errors in the simplified two-rate analysis technique. How-

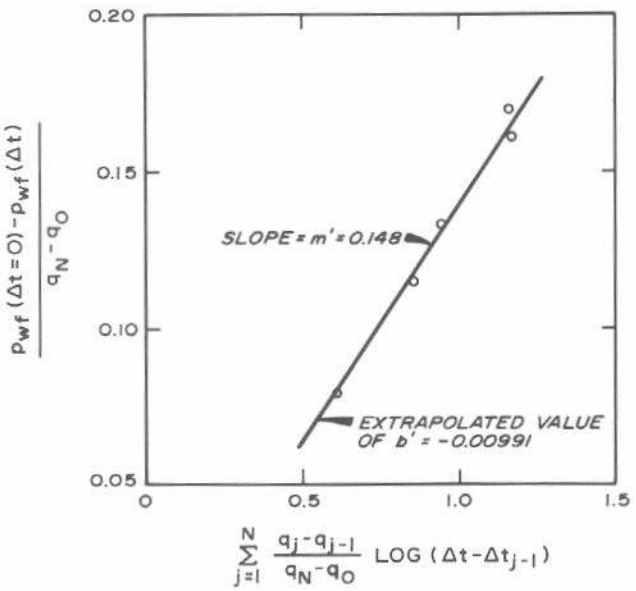

Fig. 4.8 Two-rate flow test, variable-rate case, data plot for Example 4.3. After Odeh and Jones.[11]

TABLE 4.2—SUMMARY OF CALCULATIONS FOR EXAMPLE 4.3.
After Odeh and Jones.[11]

N	j	Δt (hours)	q_j (STB/D)	$\Delta q_N = q_N - q_0$ (STB/D)	$q_j - q_{j-1}$ (STB/D)	$p_{wf}(\Delta t)$ (psi)	$\Delta p = p_{wf}(\Delta t=0) - p_{wf}(\Delta t)$ (psi)	$\frac{\Delta p}{\Delta q_N}$ (psi/STB)	$\sum_{j=1}^{N} \frac{q_j - q_{j-1}}{q_N - q_0} \log(\Delta t - \Delta t_{j-1})$
0	0	0	1,103	0	—	3,630	0	—	—
1	1	4	800	−303	−303	3,654	−24	0.0792	0.602
		6	840	−263	40	3,660	−30	0.114	0.851
2	2	8	840	−263	40	3,665	−35	0.133	0.949
		9	880	−223	40	3,666	−36	0.161	1.171
3	3	10	880	−223	40	3,668	−38	0.170	1.165

ever, the following table indicates that the error could be entirely caused by the analysis technique rather than the variable rate — if production time at the first rate is less than about 4 days.

Production Time at First Rate (days)	Error in Two-Rate Analysis (percent)
1	160
2	50
3	30
4	21
5	16
6	13
8	10
10	8

4.4 Drawdown Testing After a Short Shut-In

It is common practice to run a drawdown test after a shut-in period (pressure buildup test). If the shut-in is too short for the well pressure to stabilize at average reservoir pressure, the drawdown-test analysis techniques of Sections 3.2 and 3.4 should not be used; instead, a multiple-rate-type analysis is applicable. Fig. 4.9 schematically shows a rate history for a drawdown test after a short shut-in. Writing Eq. 4.1 for such a test and rearranging gives

$$p_{wf} = m_3' \left[\frac{q_1}{q_3} \log\left(\frac{t_1 + \Delta t_{si} + \Delta t}{\Delta t_{si} + \Delta t} \right) + \log \Delta t \right] + p_{\text{int}}. \quad \ldots\ldots\ldots\ldots\ldots\ldots\ldots\ldots\ldots\ldots (4.22)$$

Thus, a plot of p_{wf} vs $\{(q_1/q_3) \log[(t_1 + \Delta t_{si} + \Delta t)/(\Delta t_{si} + \Delta t)] + \log \Delta t\}$ should yield a straight line with slope

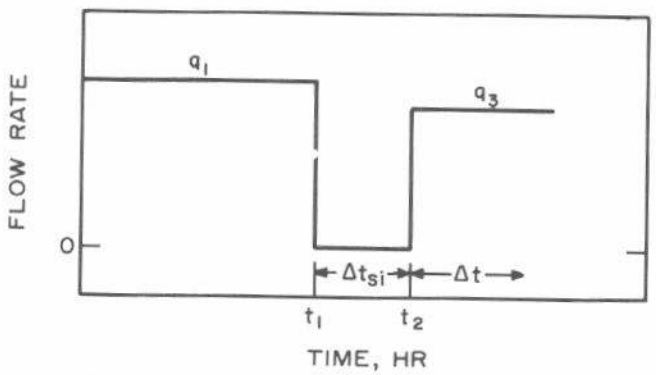

Fig. 4.9 Schematic rate history for a drawdown test after a short shut-in.

$$m_3' = \frac{-162.6\, q_3 B \mu}{kh}, \quad \ldots\ldots\ldots\ldots\ldots\ldots\ldots\ldots (4.23)$$

and intercept

$$p_{\text{int}} = p_i + m_3' \left[\log\left(\frac{k}{\phi \mu c_t r_w^2} \right) - 3.2275 + 0.86859\, s \right]. \quad \ldots\ldots\ldots\ldots\ldots\ldots (4.24)$$

Reservoir permeability can be estimated by solving Eq. 4.23. The equation is the same as the normal drawdown-test equation (Eq. 3.9), but the data plot is different. The skin factor may be estimated from the data plot with

$$s = 1.1513 \left[\frac{p_{\text{int}} - p_{wf}(\Delta t=0)}{m_3'} + \frac{q_1}{q_3} \log\left(\frac{t_1 + \Delta t_{si}}{\Delta t_{si}} \right) - \log\left(\frac{k}{\phi \mu c_t r_w^2} \right) + 3.2275 \right]. \quad \ldots\ldots\ldots\ldots\ldots (4.25)$$

Eq. 4.25 is similar to Eq. 3.10 for estimating skin factor from a normal drawdown test, with the exception of the additional logarithmic term. The skin factor computed from a drawdown test after a buildup test often does not agree with that computed from the buildup test because the correct data plot and the correct equation (Eq. 4.25) were not used in the analysis. That is particularly true in drillstem-test data analysis.

4.5 Developed Reservoir Effects

When bottom-hole pressure is declining as a result of withdrawals from the test well or from other wells in the reservoir, the analysis methods presented earlier in this chapter must be modified.[12,13] Such modified analysis techniques become increasingly important as the depletion rate increases and as test duration increases. The modifications presented in this section apply when pressure decline at the test well is caused by production from other wells or from the test well itself; the cause of the pressure decline is not important.

Fig. 4.10 illustrates bottom-hole pressure from a tested well in a developed reservoir. The solid line is the observed pressure behavior, while the dashed line represents the pressure that would have been observed had there been no flow-rate change at the well at time t_1. The pressure along the dashed line for the "no test" case is called $p_{w\text{ext}}$. Using the approaches outlined by Slider[12,13] (similar to those in Section 3.4), Eq. 4.1 may be modified to

$$\frac{p_{w\text{ext}}(t_1+\Delta t)-p_{wf}(t_1+\Delta t)}{q_N} = m'\sum_{j=1}^{N}\left[\frac{q_j-q_{j-1}}{q_N}\log(\Delta t-\Delta t_{j-1})\right]+b', \quad (4.26)$$

where m' and b' are given by Eqs. 4.2 and 4.3, respectively. The analysis is the same as outlined in Section 4.2 except that the pressure quantity used is $p_{w\text{ext}} - p_{wf}$, the vertical distance between the solid and dashed curves in Fig. 4.10. If the test starts at time zero from p_i in a reservoir with no other operating wells, Eq. 4.26 is identical to Eq. 4.1. A similar equation can be used in place of Eq. 4.21 with $p_{w\text{ext}}$ replacing $p_{wf}(\Delta t=0)$.

For the two-rate test of Section 4.3, the applicable equation is

$$p_{w\text{ext}}(t_1+\Delta t)-p_{wf}(t_1+\Delta t) = -m_1'\left[\log\left(\frac{t_1+\Delta t}{\Delta t}\right)+\frac{q_2}{q_1}\log\Delta t\right]-\Delta p_{\text{int}}. \quad (4.27)$$

In this case the data plot has slope m_1', given by Eq. 4.8, and an intercept

$$\Delta p_{\text{int}} = m_1'\frac{q_2}{q_1}\left[\log\left(\frac{k}{\phi\mu c_t r_w^2}\right)-3.2275+0.86859\,s\right]. \quad (4.28)$$

Reservoir permeability is estimated from Eq. 4.10 and skin factor from

$$s = 1.1513\left[\frac{\Delta p_{\text{int}}}{m_1'}\frac{q_1}{q_2}-\log\left(\frac{k}{\phi\mu c_t r_w^2}\right)+3.2275\right]. \quad (4.29)$$

If pseudosteady-state conditions exist during the first flow period in a two-rate flow test, then Eq. 4.27 becomes

$$p_{w\text{ext}}(t_1+\Delta t)-p_{wf}(t_1+\Delta t) = \Delta p_{1\text{hr}} - m''\log\Delta t. \quad (4.30)$$

This indicates that a plot of the extrapolated pressure difference vs log Δt should be a straight line with slope $= -m''$, where m'' is given by Eq. 4.14. The intercept is

$$\Delta p_{1\text{hr}} = -m''\left[\log\left(\frac{k}{\phi\mu c_t r_w^2}\right)-3.2275+0.86859\,s\right]. \quad (4.31)$$

Permeability would be estimated from Eq. 4.16 and skin factor would be estimated from

$$s = 1.1513\left[\frac{-\Delta p_{1\text{hr}}}{m''}-\log\left(\frac{k}{\phi\mu c_t r_w^2}\right)+3.2275\right]. \quad (4.32)$$

This analysis for pseudosteady-state flow during the first rate can be simplified even further, since

$$p_{w\text{ext}}(t_1+\Delta t) = p_{wf}(\Delta t=0)+m^*\Delta t, \quad (4.33)$$

where

$$m^* = \frac{dp_{wf}}{dt}, \quad (4.34)$$

is estimated from the slope of a Cartesian plot of p_{wf} vs t before the second rate starts. By using Eq. 4.33, Eq. 4.30 may be rewritten:

$$p_{wf}(t_1+\Delta t)-m^*\Delta t = \Delta p_{1\text{hr}}+m''\log\Delta t, \quad (4.35)$$

where m^* is given by Eq. 4.34 and m'' is given by Eq. 4.14. A plot of $(p_{wf} - m^*\Delta t)$ vs log Δt would be a straight line with slope m'' and intercept

$$\Delta p_{1\text{hr}} = \left[p_{wf}(t_1+\Delta t)-m^*\Delta t\right]_{1\text{hr}} = p_{wf}(\Delta t=0)+m''\left[\log\left(\frac{k}{\phi\mu c_t r_w^2}\right)-3.2275+0.86859\,s\right]. \quad (4.36)$$

The skin factor may be estimated from Eq. 4.17 with $\Delta p_{1\text{hr}}$ in place of $p_{1\text{hr}}$.

The main difference between equations in this section and in Sections 4.2 and 4.3 is that this section does not assume the system pressure is infinite-acting at the time the two-rate or variable-rate test *begins*. In particular, if pseudosteady-state conditions exist at the start of the test, the analysis technique can be expected to give results different from those of the techniques in Sections 4.2 and 4.3.

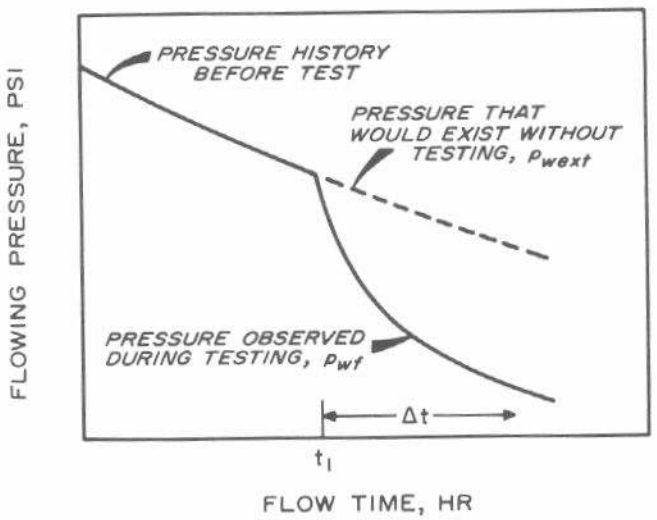

Fig. 4.10 Schematic pressure history for variable-rate testing in a developed reservoir.

4.6 Constant-Pressure Flow Testing

The transient behavior of a well operating at constant sand-face pressure is analogous to that of a well operating at a constant flow rate. In a constant-pressure flow test, the well produces at a constant bottom-hole pressure and flow rate is recorded with time. Constant bottom-hole pressure test data are not influenced by wellbore storage. However, if the *surface* pressure is maintained constant, the frictional pressure drop in the flow tubing may act in a manner similar

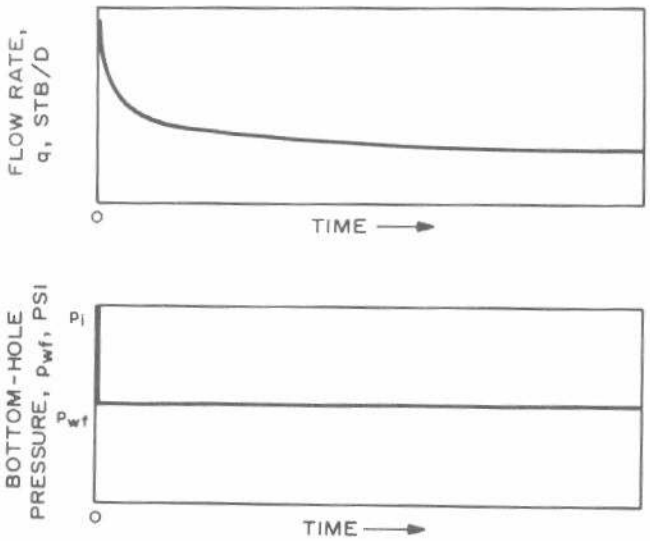

Fig. 4.11 Schematic representation of rate and pressure histories during a constant-pressure test.

to wellbore storage, causing bottom-hole pressure to vary during the test.

Fig. 4.11 schematically represents pressure and rate behavior in a constant-pressure drawdown test. Such a test is seldom performed since it is much easier to measure pressure accurately than it is to measure flow rate accurately. However, constant-rate tests may inadvertently become constant-pressure tests, so it is desirable to have a method for analyzing such tests.

In a manner similar to that used to express pressure as a function of flow rate and time, we may express flow rate as a function of pressure drop and time by

$$q = \frac{kh\,(p_i - p_{wf})}{141.2\,B\mu}\,q_D(t_D)\,. \quad \ldots\ldots\ldots\ldots\ldots\ldots\ldots (4.37)$$

Dimensionless time has its usual definition:

$$t_D = 0.0002637\,\frac{kt}{\phi\mu c_t r_w{}^2}\,. \quad \ldots\ldots\ldots\ldots\ldots\ldots\ldots (4.38)$$

The principle of superposition may be used with Eq. 4.37 to compute the flow rate resulting from a series of pressure drops during pressure-controlled flow. The calculations are analogous to those given in Section 2.9.

Fig. 4.12,* showing dimensionless rate as a function of dimensionless time for an infinite-acting system,[5] is useful for test analysis by type-curve matching. The technique is similar to that outlined in Section 3.3. Briefly, test data are plotted on tracing paper laid over the grid of Fig. 4.12, with flow rate on the ordinate and the time on the abscissa. The tracing-paper data plot is moved horizontally and vertically until the data match the curve in Fig. 4.12. Then, q_M and t_M are read from an arbitrary match point on the tracing paper and $(q_D)_M$ and $(t_D)_M$ are read from the corresponding point on Fig. 4.12. Reservoir permeability is estimated from

*See footnote on Page 24.

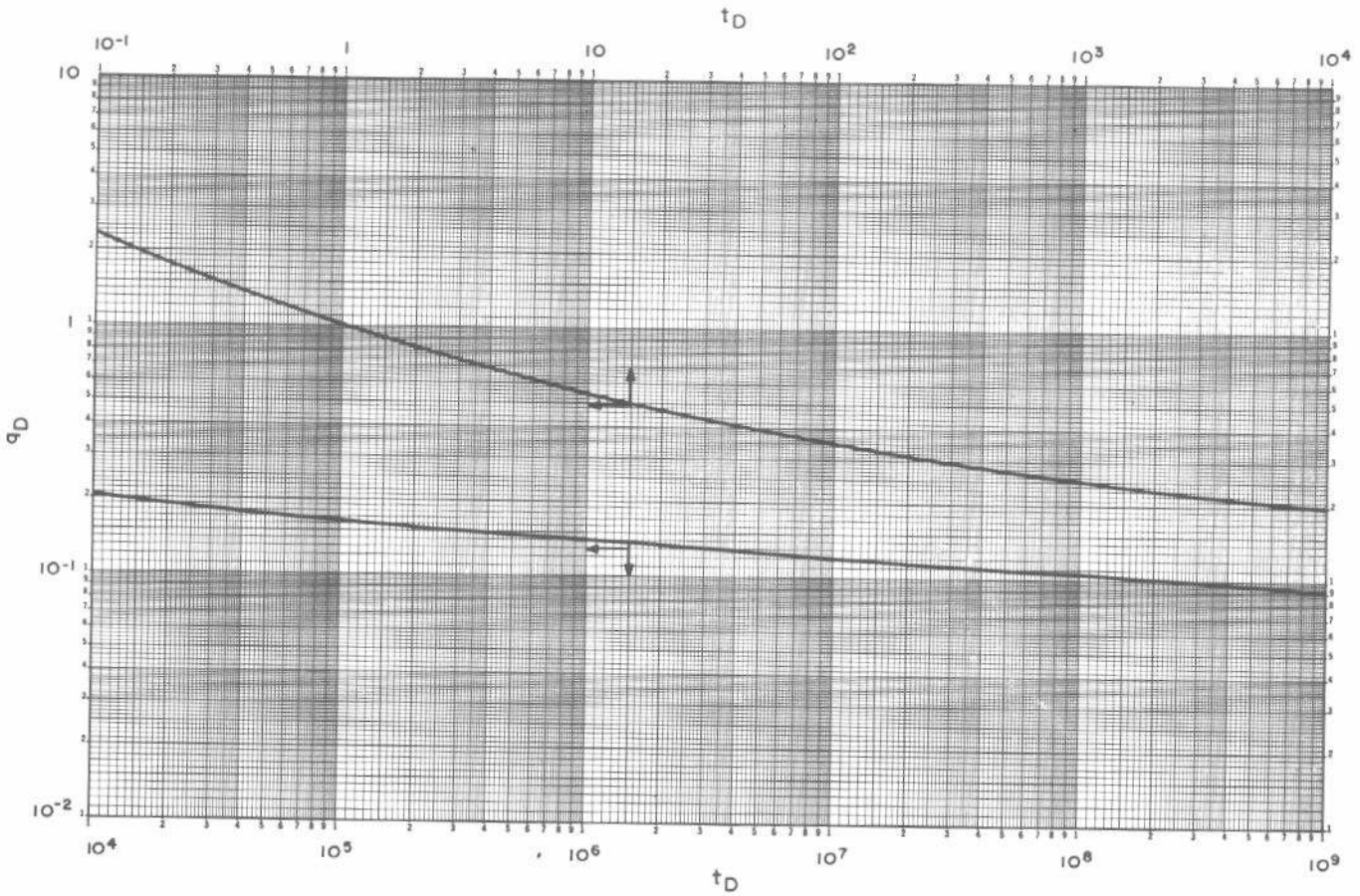

Fig. 4.12 Dimensionless rate for a single well in an infinite system. Data of Jacob and Lohman.[5]

$$k = \frac{141.2 B\mu}{(p_i - p_{wf})h}\left[\frac{q_M}{(q_D)_M}\right], \quad \ldots\ldots\ldots\ldots\ldots (4.39)$$

and reservoir porosity-compressibility-thickness is estimated from

$$\phi c_t h = 0.0002637 \frac{kh}{\mu r_w^2}\left[\frac{t_M}{(t_D)_M}\right]. \quad \ldots\ldots\ldots (4.40)$$

The curve-matching process *assumes a zero skin factor*.

Jacob and Lohman[5] show that, at long times, q_D may be approximated by

$$q_D = \frac{2}{\ln(t_D) + 0.80907}. \quad \ldots\ldots\ldots\ldots\ldots (4.41)$$

Eq. 4.41, which applies only to infinite-acting systems, is correct within 0.1 percent for $t_D \geq 5 \times 10^{11}$. The error is only 1 percent when $t_D \geq 8 \times 10^4$ and is 2 percent when $t_D \geq 5 \times 10^3$. If Eq. 4.41 is used in Eq. 4.37, and if the skin factor is included in the pressure-drop calculation, the result is

$$\frac{1}{q} = m_q \log t + (1/q)_{1hr}. \quad \ldots\ldots\ldots\ldots\ldots (4.42)$$

This equation indicates that a graph of $(1/q)$ vs $\log t$ should be a straight line with slope

$$m_q = \frac{162.6 B\mu}{kh(p_i - p_{wf})}, \quad \ldots\ldots\ldots\ldots\ldots (4.43)$$

and intercept (at $t = 1$ hour)

$$(1/q)_{1hr} = m_q\left[\log\left(\frac{k}{\phi\mu c_t r_w^2}\right) - 3.2275 + 0.86859 s\right]. \quad \ldots\ldots\ldots\ldots\ldots (4.44)$$

Permeability may be estimated from the slope of a $(1/q)$ vs $\log t$ data plot with

$$k = \frac{162.6 B\mu}{m_q (p_i - p_{wf})h}. \quad \ldots\ldots\ldots\ldots\ldots (4.45)$$

Skin factor may be estimated from a rearranged form of Eq. 4.44:

$$s = 1.1513\left[\frac{(1/q)_{1hr}}{m_q} - \log\left(\frac{k}{\phi\mu c_t r_w^2}\right) + 3.2275\right]. \quad \ldots\ldots\ldots\ldots\ldots (4.46)$$

Example 4.4 Constant-Pressure Testing in an Infinite-Acting Reservoir

The flow-rate data shown in Fig. 4.13 are from a simulated constant-pressure drawdown test. Data used to simulate the test are

$k = 6.5$ md	$\phi c_t = 2.05 \times 10^{-6}$ psi^{-1}
$\mu = 1.35$ cp	$p_i - p_{wf} = 1{,}000$ psi
$h = 190$ ft	$r_w = 1$ ft
$B = 1.0$ RB/STB	$s = 0$.

The data of Fig. 4.13 were type-curve matched to Fig. 4.12. Match-point data are

$q_M = 1{,}720$ STB/D	$(q_D)_M = 0.27$
$t_M = 1.0$ hour	$(t_D)_M = 600$.

Using Eq. 4.39,

$$k = \frac{(141.2)(1.0)(1{,}720)(1.35)}{(1{,}000)(0.27)(190)} = 6.4 \text{ md},$$

an error of 1.5 percent. Reservoir porosity-compressibility is estimated from Eq. 4.40:

$$\phi c_t h = \frac{0.0002637\,(6.4)(190)(1)}{(1.35)(1)^2(600)}$$

$$= 3.96 \times 10^{-4} \text{ ft/psi},$$

or

$$\phi c_t = \frac{3.96 \times 10^{-4}}{190} = 2.08 \times 10^{-6} \text{ psi}^{-1},$$

an error of 1.5 percent.

An alternate analysis uses Fig. 4.14, a plot of $(1/q)$ vs log t. The slope of the straight line drawn through the data for $0.1 < t < 10$ hours is

$$m_q = 1.7 \times 10^{-4} \text{ (D/STB)/cycle}.$$

Using Eq. 4.45,

$$k = \frac{(162.6)(1.0)(1.35)}{(1{,}000)(1.7 \times 10^{-4})(190)} = 6.8 \text{ md},$$

an error of 4.6 percent. The skin factor is estimated from Fig. 4.14 and Eq. 4.46. From Fig. 4.14, $(1/q)_{1hr} = 0.000578$ D/STB.

$$s = 1.1513\left[\frac{0.000578}{1.7 \times 10^{-4}} - \log\left(\frac{6.8}{(1.35)(2.08 \times 10^{-6})(1)^2}\right) + 3.2275\right]$$

$$= 0.28.$$

This compares with the actual value of 0.

As opposed to constant-rate testing, the analog to pseudosteady-state flow does not develop during constant-pressure testing. When boundary effects influence behavior during the constant-pressure test, there is a rapid decline of flow rate caused by declining reservoir pressure. Flow rate goes to zero as reservoir pressure approaches the wellbore pressure.

4.7 Reservoir Limit Testing When Rate Varies

Section 3.5 discusses reservoir limit testing for constant-rate production; however, it may be difficult to maintain a constant flow rate during long production periods. If flow rate varies in a cyclic or oscillatory manner, reservoir limit testing techniques still can be used.[14,15] The analysis technique is similar to that for constant-rate reservoir limit tests, but the results are less accurate.

To analyze a variable-rate reservoir limit test, one plots observed flowing pressure vs time on Cartesian paper. Pressure points must be segregated by the rate occurring when the pressure measurement was made. Fig. 4.15 is such a plot for a waste-water injection well; the three sets of pressure points occur at three different injection rates. Such a data

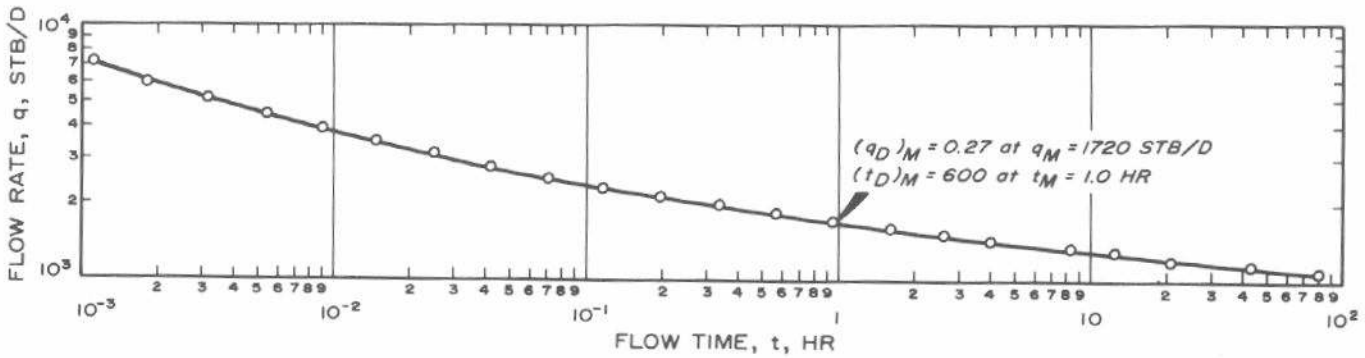

Fig. 4.13 Flow rate-time data for constant-pressure drawdown test of Example 4.4.

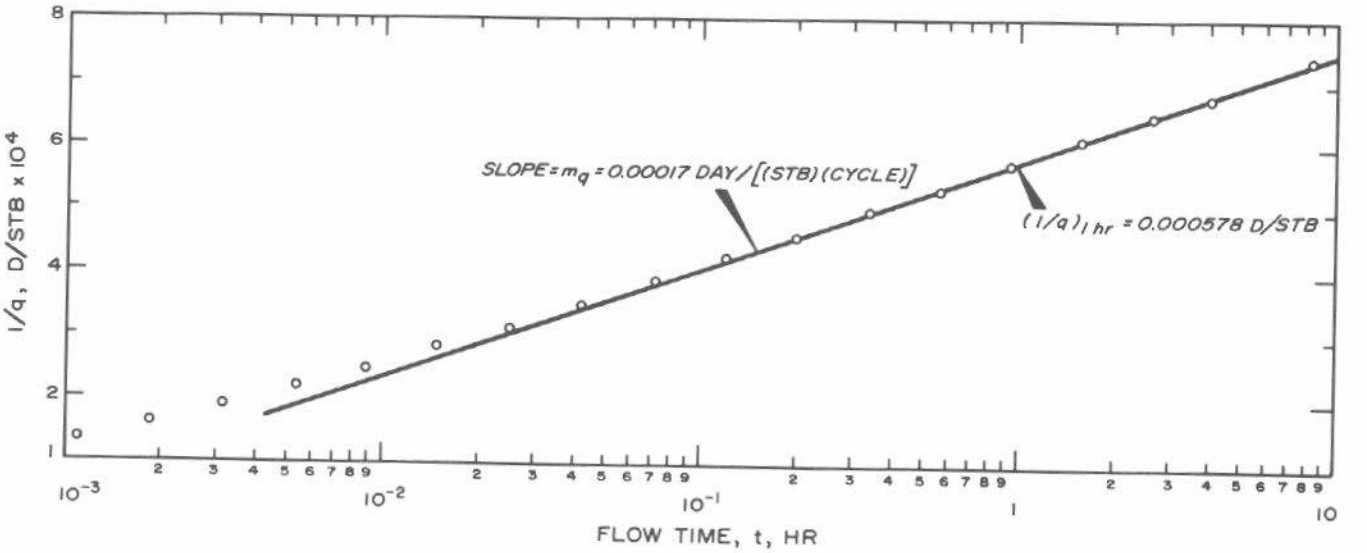

Fig. 4.14 Plot of $1/q$ vs $\log t$ for constant-pressure drawdown test of Example 4.4.

plot should have a straight-line section. Because of flow-rate variation, there is actually never a definite straight line, but a least-squares straight line usually can be fit to the pressure points observed at one of the rates. The slope, m^*, of the straight line may be used to estimate reservoir drainage volume:

$$A\phi h = \frac{-0.23395\,\bar{q}B}{m^* c_t} \quad \ldots\ldots\ldots\ldots\ldots\ldots\ldots (4.47)$$

Eq. 4.47 is identical to Eq. 3.35 except that the over-all average flow rate is used. Even though the pressure points are segregated by the rate in effect at the time the pressure was measured, the *total average flow rate* is used to estimate reservoir volume.

Example 4.5 Variable-Rate Reservoir Limit Test

Fig. 4.15 shows pressure data from Ref. 14 for the last 5 years of the 11-year life of an industrial waste-disposal well. Although the data are for injection, the methods of this section can be applied by using a negative rate (see Chapter 7).

The well, with casing set at 1,800 ft, is completed open hole to about 3,000 ft, just into basement. Only a part of the 1,200-ft section is porous and permeable, but porosity and net interval are not known. The injection horizon is known to be of large extent.

Injection is with one, two, or three pumps, so the rate is −5,140, −10,280, or −15,420 STB/D. Pressure and rate data are reported by month only without indication of how long the rate had applied when the pressure was measured. Cumulative fluid injected is known accurately. The average injection rate is −9,660 STB/D for the period shown in Fig. 4.15. The formation volume factor, B, is 1.0; system total compressibility, c_t, is unknown, but is estimated to be about 5×10^{-6} psi^{-1}.

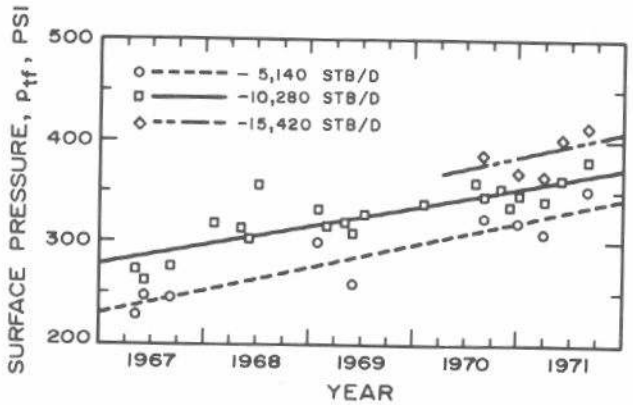

Fig. 4.15 Long-term, variable-rate reservoir limit test of Example 4.5. Five years of injection history for a disposal well with three injection rates; $\bar{q} = -9{,}660$ STB/D during period shown. After Earlougher.[14]

The lines in Fig. 4.15 are least-squares fits to the pressure data for each of the three rates. The slopes, m^*, are $+2.62 \times 10^{-3}$ psi/hr, $+2.15 \times 10^{-3}$ psi/hr, and $+3.16 \times 10^{-3}$ psi/hr for the $-5{,}140$, $-10{,}280$, and $-15{,}420$ STB/D rates, respectively. We estimate the pore volume from Eq. 4.47, being certain to use the average injection rate, $\bar{q} = -9{,}660$ STB/D.

$$A\phi h = \frac{-0.23395\,(-9{,}660)(1)}{(2.62 \times 10^{-3})(5 \times 10^{-6})}$$

$$= 1.73 \times 10^{11} \text{ cu ft}$$

$$= 30.7 \times 10^{9} \text{ STB},$$

for the circular data points. Similarly, the estimated pore volume is 37.4×10^9 STB for the square data points and 25.5×10^9 STB for the diamond-shaped data points. These volumes do not contradict the known geology of the formation. The results for the diamond-shaped points ($q = -15{,}420$ STB/D) should be considered the least reliable since there are only five data points, and they are scattered. The value of 37.4×10^9 STB may be the most reliable, since most data points are for $q = -10{,}280$ STB/D.

These calculations require that flow be pseudosteady state. A long period of apparently linear pressure increase with time is a good indicator of pseudosteady-state conditions. If this assumption is incorrect, estimated pore volume is too small.

4.8 Deliverability Testing of Oil Wells

Deliverability testing has long been used to predict the capability of a gas well to deliver against a specific flowing bottom-hole pressure.[1,16-19] Fetkovich[20] demonstrates that such testing can be used for oil wells. It is particularly useful for reservoir systems operating below the bubble point, when fluid properties and relative permeabilities vary with distance from the well. Oil flow rate (at surface conditions) has been empirically related to flowing bottom-hole pressure and average reservoir pressure by

$$q_o = J_o'\,(\bar{p}^2 - p_{wf}^2)^n, \quad \ldots\ldots\ldots\ldots\ldots\ldots\ldots\ldots\ldots\ldots (4.48)$$

where J_o' is a form of productivity index and n is an empirically determined exponent. Fetkovich[20] states that field tests indicate $0.5 \leq n \leq 1.0$. Eq. 4.48 is similar to the deliverability equation used in gas well testing.

Two important deliverability tests are the flow-after-flow test and the modified isochronal test. Fig. 4.16 schematically demonstrates the rate and pressure behavior of a flow-after-flow test. The well is produced at rate q_1 until the pressure stabilizes at p_{wf1}. Then the rate is changed to q_2 until the pressure stabilizes at p_{wf2}, and so on. Normally, four rates are run but any number greater than three may be used. Flow rate may be either increased or decreased. The major disadvantage of the flow-after-flow test is that each rate must remain constant until pressure stabilizes. The time required may be estimated from Eq. 2.40,

$$t_s \simeq 380\,\frac{\phi\mu c_t A}{k} \quad \ldots\ldots\ldots\ldots\ldots\ldots\ldots\ldots\ldots\ldots (4.49)$$

For systems that are large or have low permeability, stabilization time can be very long.

To avoid problems with long stabilization times, Cullender[18] proposed the isochronal flow test for gas wells. A shortened version, the modified isochronal flow test,[19] was later suggested and is generally preferred. Fig. 4.17 schematically illustrates flow-rate and pressure histories for a modified isochronal flow test. The well is produced at rate q_1 for time t_1 and the final flowing pressure, p_{wf1}, is observed. Then the well is shut in for time t_1 and the final shut-in pressure, p_{ws2}, is observed. The procedure is repeated at rates q_2, q_3, q_4, etc. The well is usually produced to a stabilized pressure at the final rate, so one stabilized pressure point, $(p_{wf})_{pss}$, is available.

Fig. 4.18 illustrates the analysis method for a modified isochronal deliverability test; $\log(\bar{p}^2 - p_{wf}^2)$ is plotted vs $\log q$. The points usually fall on a straight line with slope $1/n$. The location of the line depends on the flow-period duration. Thus, in normal analysis, the points for the four rates define the straight line and the single stabilized point defines location of the stabilized deliverability curve. The stabilized deliverability curve may be entered at set values of $(\bar{p}^2 - p_{wf}^2)$ to estimate the well's deliverability (flow rate) at a given drawdown. Alternatively, the data plot (Fig. 4.18) may be used to estimate J_o' and n and the flow rate may be estimated from Eq. 4.48. Fig. 4.18 and Eq. 4.48 are written with average reservoir pressure, the pressure used for flow-after-flow and normal isochronal flow tests. *The data plot for a modified isochronal flow test uses the shut-in pressure occurring immediately before the flow rate instead of the average reservoir pressure.*

Fetkovich[20] provides data for many flow-after-flow and isochronal flow tests in several oil wells. Fig. 4.19 demonstrates that the isochronal and flow-after-flow tests can give the same results in oil wells producing from a saturated (both oil and free gas present) reservoir.

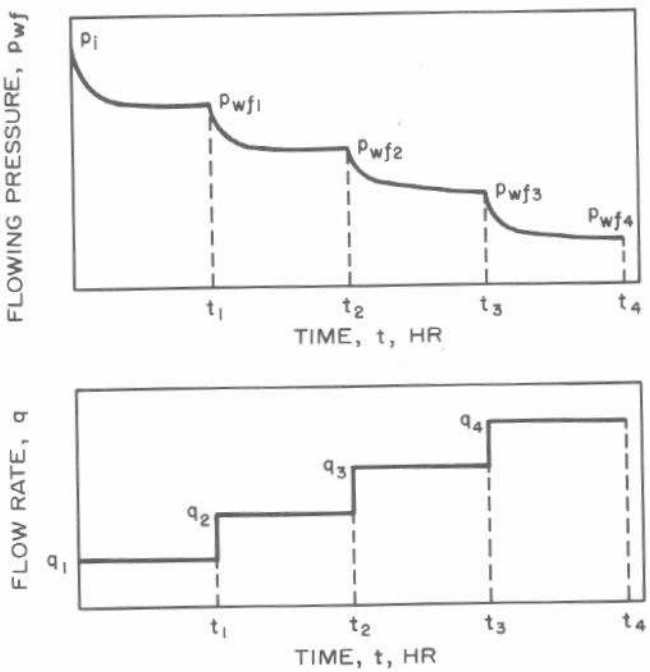

Fig. 4.16 Pressure-rate history for a flow-after-flow test.

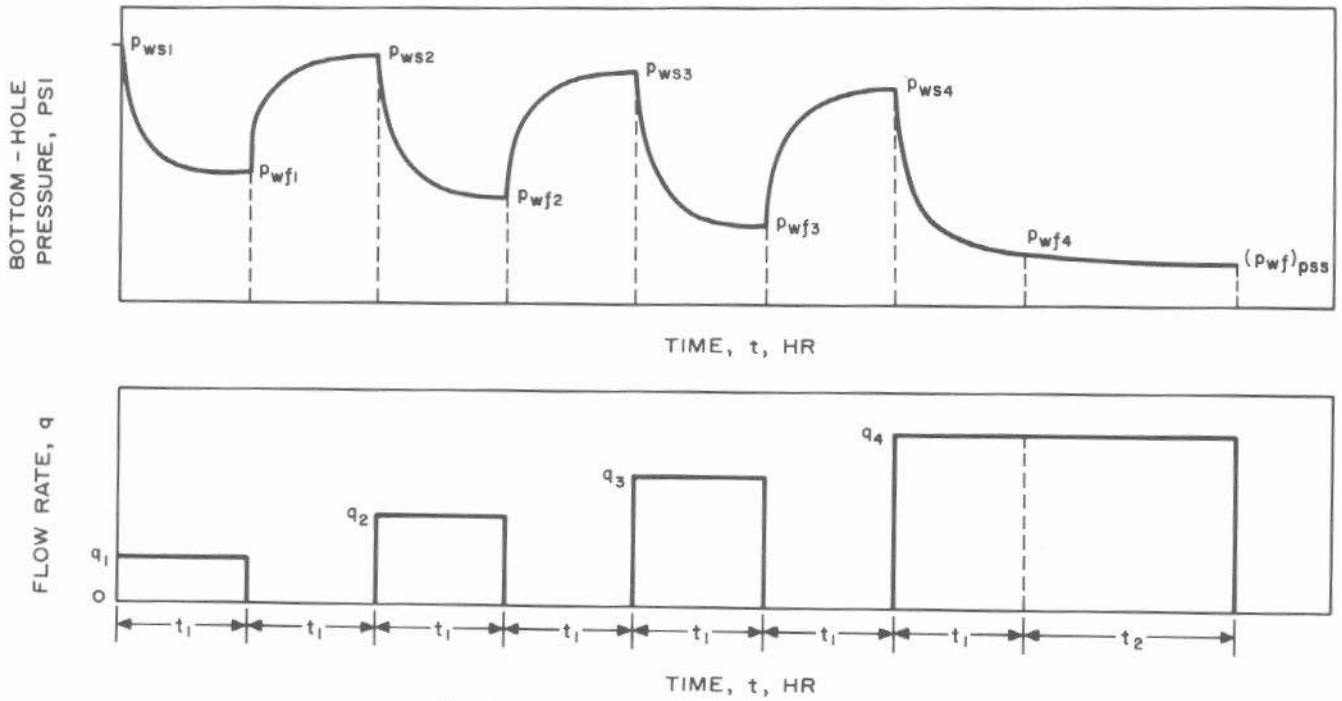

Fig. 4.17 Pressure-rate history for a modified-isochronal-flow test.

If deliverability test data are not available for a solution gas drive reservoir, it still may be possible to predict a well's deliverability by using the "inflow performance relationship" (IPR) proposed by Vogel[21] and the modification to the IPR proposed by Standing.[22] Vogel used computer simulation techniques to demonstrate that many solution gas drive reservoirs operating below the bubble point have an inflow performance relationship given by

$$q_o = \frac{J^* \bar{p}}{1.8}\left[1 - 0.2\left(\frac{p_{wf}}{\bar{p}}\right) - 0.8\left(\frac{p_{wf}}{\bar{p}}\right)^2\right], \quad \ldots (4.50)$$

where q_o is the oil flow rate (STB/D) occurring at bottomhole pressure p_{wf} and J^* is a productivity index. Given a stabilized q_o and the corresponding $\bar{p}$ and p_{wf}, it is possible to calculate J^* from Eq. 4.50. Then, to estimate q_o at another stabilized pressure, one uses Eq. 4.50 with the experimentally determined J^*. Standing[22] indicated that, as the reservoir is depleted, it is necessary to modify Eq. 4.50 because of changes in relative permeability and fluid properties. He suggested estimating a future value of the productivity index from the present value by using

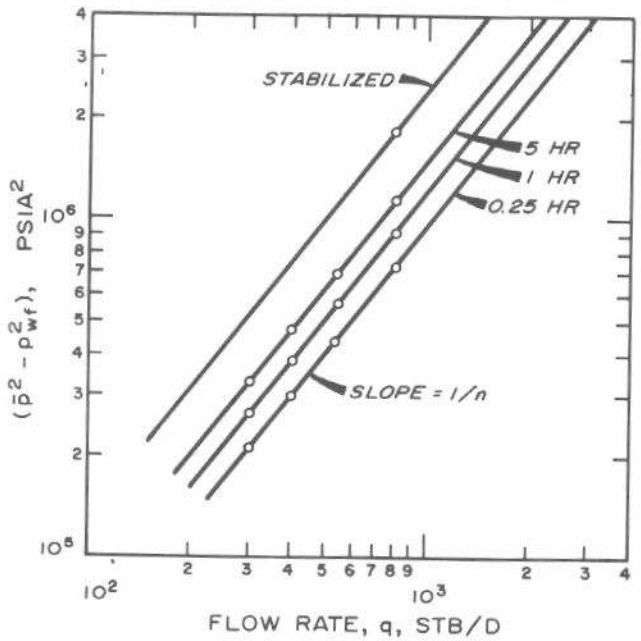

Fig. 4.18 Schematic example of a modified-isochronal-test data plot.

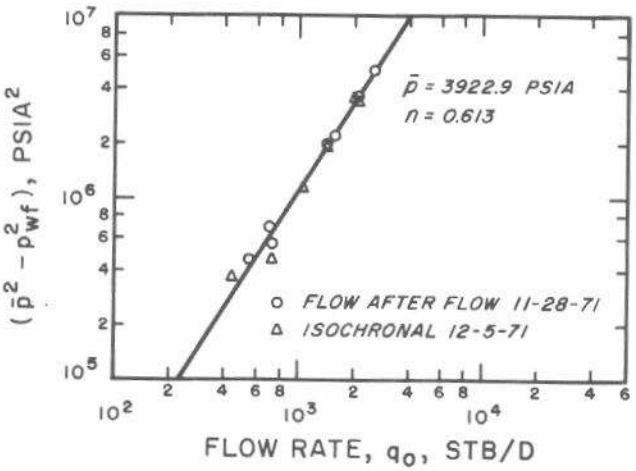

Fig. 4.19 Four-hour modified-isochronal and flow-after-flow deliverability curves. Field data from a saturated reservoir. After Fetkovich.[20]

$$J_F^* = J_p^* \frac{\left(\frac{k_{ro}}{\mu_o B_o}\right)_F}{\left(\frac{k_{ro}}{\mu_o B_o}\right)_p} \quad \ldots\ldots\ldots\ldots\ldots\ldots\ldots\ldots (4.51)$$

where the subscript F refers to some time in the future and the subscript p refers to data at the present time. Values of k_{ro}, μ_o, and B_o in the future are estimated from material balance relationships. The procedure for developing a future IPR is (1) estimate J_p^* from current production data and Eq. 4.50; (2) estimate J_F^* from Eq. 4.51; and (3) estimate the future IPR (q_o) by using J_F^* in Eq. 4.50. Standing[22] gives an example calculation.

It is emphasized that deliverability tests are not transient well tests. They do not yield estimates of skin and formation permeability; rather, they provide empirical relationships between flow rate and drawdown for stabilized oil wells. They do include the nonideal conditions existing in the reservoir, particularly saturation distributions and variation of fluid properties with pressure. Deliverability testing thus may be valuable in helping predict future production rates as a function of available pressure differential.

4.9 Factors Complicating Multiple-Rate Testing

Multiple-rate tests exhibit their greatest advantage when changing wellbore storage makes normal transient test analysis difficult or impossible. That is because such tests can eliminate changes in the wellbore storage coefficient — even though the effects of wellbore storage still exist. Multiple-rate tests also reduce the loss of current production. However, such tests are difficult to control since they are flowing tests. Rate fluctuations are difficult to measure, especially on a continuous basis. The analysis techniques are much more bothersome and difficult than those for constant-rate tests; they frequently require the use of a computer.

To assure the best possible multiple-rate test, the engineer must have an idea of a well's flow characteristics. The rate change imposed must be large enough to give significant change in a pressure transient behavior of the well. The effect of rate change on pressure response must be estimated from Eq. 4.1, Eq. 4.6, or Eq. 4.13. Normally, rate is changed by a factor of two or more.

References

1. Matthews, C. S. and Russell, D. G.: *Pressure Buildup and Flow Tests in Wells*, Monograph Series, Society of Petroleum Engineers of AIME, Dallas (1967) **1**, Chap. 6.
2. Odeh, A. S. and Jones, L. G.: "Pressure Drawdown Analysis, Variable-Rate Case," *J. Pet. Tech.* (Aug. 1965) 960-964; *Trans.*, AIME, **234.** Also *Reprint Series, No. 9 — Pressure Analysis Methods*, Society of Petroleum Engineers of AIME, Dallas (1967) 161-165.
3. Russell, D. G.: "Determination of Formation Characteristics From Two-Rate Flow Tests," *J. Pet. Tech.* (Dec. 1963) 1347-1355; *Trans.*, AIME, **228.** Also *Reprint Series, No. 9 — Pressure Analysis Methods*, Society of Petroleum Engineers of AIME, Dallas (1967) 136-144.
4. Doyle, R. E. and Sayegh, E. F.: "Real Gas Transient Analysis of Three-Rate Flow Tests," *J. Pet. Tech.* (Nov. 1970) 1347-1356.
5. Jacob, C. E. and Lohman, S. W.: "Nonsteady Flow to a Well of Constant Drawdown in an Extensive Aquifer," *Trans.*, AGU (Aug. 1952) 559-569.
6. Gladfelter, R. E., Tracy, G. W., and Wilsey, L. W.: "Selecting Wells Which Will Respond to Production-Stimulation Treatment," *Drill. and Prod. Prac.*, API (1955) 117-129.
7. Winestock, A. G. and Colpitts, G. P.: "Advances in Estimating Gas Well Deliverability," *J. Cdn. Pet. Tech.* (July-Sept. 1965) 111-119.
8. Ramey, H. J., Jr.: "Verification of the Gladfelter-Tracy-Wilsey Concept for Wellbore Storage Dominated Transient Pressures During Production," *J. Cdn. Pet. Tech.*, (April-June 1976) 84-85.
9. Pinson, A. E., Jr.: "Conveniences in Analyzing Two-Rate Flow Tests," *J. Pet. Tech.* (Sept. 1972) 1139-1141.
10. Earlougher, R. C., Jr.: "Estimating Errors When Analyzing Two-Rate Flow Tests," *J. Pet. Tech.* (May 1973) 545-547.
11. Odeh, A. S. and Jones, L. G.: "Two-Rate Flow Test, Variable-Rate Case — Application to Gas-Lift and Pumping Wells," *J. Pet. Tech.* (Jan. 1974) 93-99; *Trans.*, AIME, **257.**
12. Slider, H. C.: "Application of Pseudo-Steady-State Flow to Pressure-Buildup Analysis," paper SPE 1403 presented at the SPE-AIME Regional Meeting, Amarillo, Tex., Oct. 27-28, 1966.
13. Slider, H. C.: "A Simplified Method of Pressure Buildup Analysis for a Stabilized Well," *J. Pet. Tech.* (Sept. 1971) 1155-1160; *Trans.*, AIME, **251.**
14. Earlougher, Robert C., Jr.: "Variable Flow Rate Reservoir Limit Testing," *J. Pet. Tech.* (Dec. 1972) 1423-1429.
15. Kazemi, Hossein: "Discussion of Variable Flow Rate Reservoir Limit Testing," *J. Pet. Tech.* (Dec. 1972) 1429-1430.
16. Rawlins, E. L. and Schellhardt, M. A.: "Back-Pressure Data on Natural-Gas Wells and Their Application to Production Practices," *Monograph 7*, USBM (1936).
17. *Theory and Practice of the Testing of Gas Wells*, 3rd ed., Pub. ERCB-75-34, Energy Resources and Conservation Board, Calgary, Alta., Canada (1975).
18. Cullender, M. H.: "The Isochronal Performance Method of Determining the Flow Characteristics of Gas Wells," *Trans.*, AIME (1955) **204,** 137-142. Also *Reprint Series, No. 9 — Pressure Analysis Methods*, Society of Petroleum Engineers of AIME, Dallas (1967) 203-208.
19. Katz, Donald L., Cornell, David, Kobayashi, Riki, Poettmann, Fred H., Vary, John A., Elenbaas, John R., and Weinaug, Charles F.: *Handbook of Natural Gas Engineering*, McGraw-Hill Book Co., Inc., New York (1959) Chap. 11.
20. Fetkovich, M. J.: "The Isochronal Testing of Oil Wells," paper SPE 4529 presented at the SPE-AIME 48th Annual Fall Meeting, Las Vegas, Nev., Sept. 30-Oct. 3, 1973.
21. Vogel, J. V.: "Inflow Performance Relationships for Solution-Gas Drive Wells," *J. Pet. Tech.* (Jan. 1968) 83-92; *Trans.*, AIME, **243.**
22. Standing, M. B.: "Concerning the Calculation of Inflow Performance of Wells Producing Solution Gas Drive Reservoirs," *J. Pet. Tech.* (Sept. 1971) 1141-1142.

Chapter 5

Pressure Buildup Testing

5.1 Introduction

Pressure buildup testing, probably the most familiar transient well testing technique, has been treated widely in the literature.[1-10] This type of testing was first introduced by the groundwater hydrologists,[2] but has been used extensively in the petroleum industry.

Pressure buildup testing requires shutting in a producing well. The most common and simplest analysis techniques require that the well produce at a constant rate, either from startup or long enough to establish a stabilized pressure distribution (t_{pss}), before shut-in. Fig. 5.1 schematically shows rate and pressure behavior for an ideal pressure buildup test. In that figure, and throughout this monograph, t_p is the production time and Δt is running shut-in time. The pressure is measured immediately before shut-in and is recorded as a function of time during the shut-in period. The resulting pressure buildup curve is analyzed for reservoir properties and wellbore condition; the methods used most are described in this chapter.

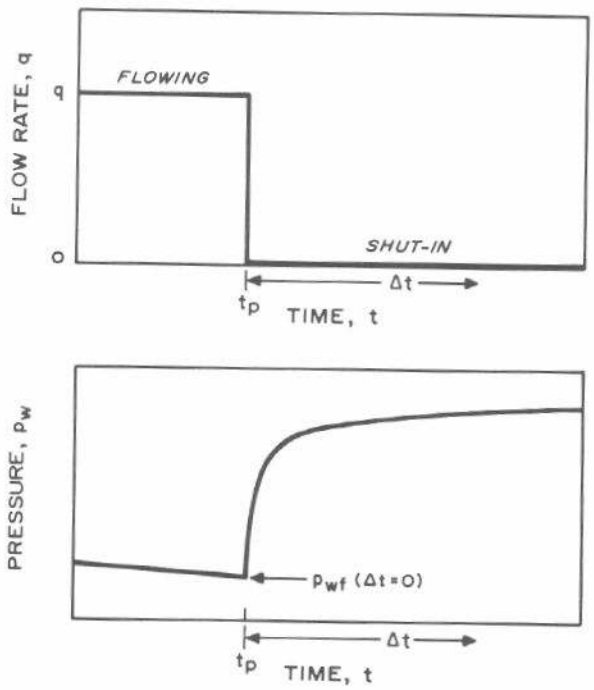

Fig. 5.1 Idealized rate and pressure history for a pressure buildup test.

As in all transient well tests, knowledge of surface and subsurface mechanical conditions is important in buildup-test data interpretation. Therefore, it is recommended that tubing and casing sizes, well depth, packer locations, etc., be determined before data interpretation starts. Short-time pressure observations usually are necessary for complete delineation of wellbore storage effects. Data may be needed at intervals as short as 15 seconds for the first few minutes of some buildup tests. As the test progresses, the data-collection interval can be expanded.

Stabilizing the well at a constant rate before testing is an important part of a pressure buildup test. If stabilization is overlooked or is impossible, standard data analysis techniques may provide erroneous information about the formation. Thus, it is important to determine the degree and adequacy of the stabilization; one way is to check the length of the pre-shut-in constant-rate period against the time required for stabilization, as given by Eqs. 2.40 and 2.42. For wells with significantly varying rates, buildup test analysis is still possible using the variable-rate methods of Chapter 4 or the modifications of those methods presented in Section 5.4.

5.2 Pressure Buildup Test Analysis During the Infinite-Acting Period

For any pressure-buildup testing situation, bottom-hole shut-in pressure in the test well may be expressed by using the principle of superposition for a well producing at rate q until time t_p, and at zero rate thereafter. At any time after shut-in,

$$p_{ws} = p_i - \frac{141.2\,qB\mu}{kh}\left\{p_D\left(\left[t_p + \Delta t\right]_D\right) - p_D(\Delta t_D)\right\}, \quad \ldots\ldots\ldots\ldots\ldots\ldots\ldots\ldots (5.1)$$

where p_D is the applicable dimensionless-pressure function and t_D is as defined by Eq. 2.3a:

$$t_D = \frac{0.0002637\,kt}{\phi\mu c_t r_w^{\,2}} \quad \ldots\ldots\ldots\ldots\ldots\ldots\ldots\ldots (5.2)$$

During the infinite-acting time period, after wellbore storage effects have diminished and providing there are no major induced fractures, p_D in Eq. 5.1 may be replaced by the logarithmic approximation to the exponential integral, Eq. 2.5b:

$$p_D = \frac{1}{2}(\ln t_D + 0.80907) \quad \ldots\ldots\ldots\ldots\ldots\ldots (5.3)$$

Eq. 5.3 applies when $t_D > 100$, which occurs after a few minutes for most unfractured systems. By using Eqs. 5.2 and 5.3, Eq. 5.1 may be rewritten:

$$p_{ws} = p_i - m \log\left(\frac{t_p + \Delta t}{\Delta t}\right) \quad \ldots\ldots\ldots\ldots\ldots\ldots (5.4)$$

Eq. 5.4 describes a straight line with intercept p_i and slope $-m$, where

$$m = \frac{162.6\, qB\mu}{kh} \quad \ldots\ldots\ldots\ldots\ldots\ldots\ldots\ldots (5.5)$$

Eq. 5.4 indicates that a plot of observed shut-in bottom-hole pressure, p_{ws}, vs $\log\left[(t_p + \Delta t)/\Delta t\right]$ should have a straight-line portion with slope $-m$ that can be used to estimate reservoir permeability,

$$k = \frac{162.6\, qB\mu}{mh} \quad \ldots\ldots\ldots\ldots\ldots\ldots\ldots\ldots (5.6)$$

Both Theis[2] and Horner[6] proposed estimating permeability in this manner. The p_{ws} vs $\log\left[(t_p + \Delta t)/\Delta t\right]$ plot is commonly called the Horner plot (graph, method) in the petroleum industry; that terminology is used in this monograph.

Fig. 5.2 is a schematic Horner plot of pressure buildup data. The straight-line section is shown. As indicated by Eq. 5.4, this straight-line portion of the Horner plot may be extrapolated to $(t_p + \Delta t)/\Delta t = 1$, $\{\log\left[(t_p + \Delta t)/\Delta t\right] = 0\}$, the equivalent of infinite shut-in time, to obtain an estimate of p_i. That is an accurate estimate only for short production periods. However, the extrapolated pressure value is useful for estimating average reservoir pressure, as indicated in Chapter 6.

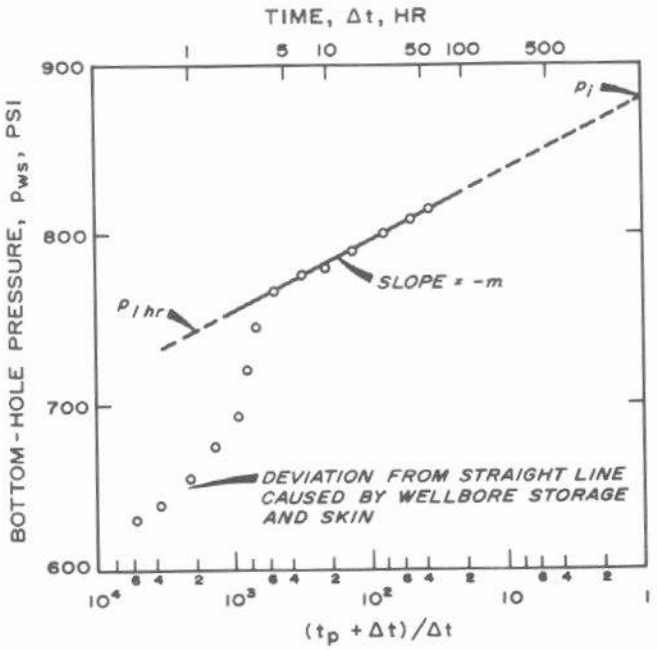

Fig. 5.2 Horner plot of pressure buildup data showing effects of wellbore storage and skin.

In Fig. 5.2, as in all other Horner plots in this monograph, the abscissa has been reversed so it increases from right to left in keeping with common practice. The reverse plotting, which is mathematically equivalent to plotting $\log\left[\Delta t/(t_p + \Delta t)\right]$, causes time to increase from left to right (see upper scale in Fig. 5.2) and gives the buildup curve the shape one would expect. However, it means that the slope, which normally would be thought of as positive, *is negative*. In Fig. 5.2, the slope is -42 psi/cycle, so $m = 42$ psi/cycle.

A result of using the superposition principle is that the skin factor, s, does not appear in the general pressure-buildup equation, Eq. 5.1. As a result, skin factor does not appear in the simplified equation for the Horner plot, Eq. 5.4. That means the Horner-plot slope is not affected by the skin factor; however, the skin factor still *does* affect the *shape* of the pressure buildup data. In fact, an early-time deviation from the straight line can be caused by skin factor as well as by wellbore storage, as indicated in Fig. 5.2 (also see Fig. E.1). The deviation can be significant for the large negative skins that occur in hydraulically fractured wells. In any case, the skin factor does affect flowing pressure before shut-in, so skin may be estimated from the buildup test data plus the flowing pressure immediately before the buildup test:[1,8,11]

$$s = 1.1513\left[\frac{p_{1\text{hr}} - p_{wf}(\Delta t = 0)}{m} - \log\left(\frac{k}{\phi\mu c_t r_w^2}\right) + 3.2275\right]. \quad \ldots\ldots\ldots\ldots\ldots\ldots (5.7)$$

In Eq. 5.7, $p_{wf}(\Delta t = 0)$ is the observed flowing bottom-hole pressure immediately before shut-in and $-m$ is the slope of the Horner plot. As a result of assumptions made in deriving Eq. 5.7,[1,8] the value of $p_{1\text{hr}}$ must be taken from the Horner straight line. Frequently, pressure data do not fall on the straight line at 1 hour because of wellbore storage effects that allow afterflow into the well, or large negative skin factors resulting from induced fracturing, etc. In that case, the semilog line must be extrapolated to 1 hour and the pressure read. Fig. 5.2 shows the correct way to determine $p_{1\text{hr}}$.

In different types of transient test analysis, the slope is sometimes $+m$ and sometimes $-m$; additionally, m sometimes includes a minus sign (compare Eq. 3.6 for drawdown testing with Eq. 5.5 for buildup). This may cause some confusion in transient well test analysis. Confusion may be avoided by realizing (1) permeability must always be positive, so the sign of m may be determined from Eq. 5.5 (or its equivalent for other types of testing); (2) the first term inside the brackets of the skin equation, $[p_{1\text{hr}} - p_{wf}(\Delta t = 0)]/m$, is usually positive (the exception occurs in hydraulically fractured wells with $s << 0$); and (3) production rates are positive while injection rates are negative. There should not be a problem with analysis equations if the correct definition of m and its relation to the slope of the data

plot are used with the correct signs in the analysis equations. Appendix E gives appropriate signs for common analysis techniques for different tests.

Eq. 5.7 provides a good estimate of the skin factor as long as $t_p >> 1$ hour. But when t_p is on the order of 1 hour (for example, in drillstem testing), Eq. 5.7 should be replaced by

$$s = 1.1513 \left[\frac{p_{1\text{hr}} - p_{wf}(\Delta t=0)}{m} + \log\left(\frac{t_p + 1}{t_p}\right) - \log\left(\frac{k}{\phi\mu c_t r_w^2}\right) + 3.2275 \right]. \quad \ldots\ldots\ldots\ldots (5.8)$$

The proper t_p to use for a given well in a multiple-well reservoir has been a matter of frequent concern to practicing engineers. Eqs. 5.1 and 5.4 assume a constant production rate from time 0 to time t_p, not often a realistic assumption. Horner[6] indicated that t_p often can be approximated as the cumulative production since completion divided by the rate immediately before shut-in (when rate varies). Except shortly after well completion, it appears desirable as a matter of general practice to approximate t_p using cumulative production since the last pressure equalization (or some other convenient, relatively short time in terms of reservoir depletion) rather than total cumulative production:

$$t_p = \frac{24\,V_P}{q}. \quad \ldots\ldots\ldots\ldots\ldots\ldots\ldots\ldots\ldots\ldots\ldots\ldots (5.9)$$

In Eq. 5.9, V_P is the cumulative volume produced since the *last pressure equalization* and q is the constant rate just before shut-in. If t_p on this basis is significantly greater than t_{pss}[12,13] (for example, by a factor of 2), then replotting using t_{pss} (Eq. 2.24 for a closed boundary or Eq. 2.42 for a constant-pressure boundary) may be justified. For closed boundary conditions, a Horner plot *using* t_{pss} as opposed to a Miller-Dyes-Hutchinson (MDH) plot (Section 5.3) tends to prolong the straight-line portion of the buildup curve. However, the principal importance of using t_{pss} usually is in minimizing errors in estimating average reservoir pressure (Section 6.3).

When the time at constant rate immediately before shut-in is significantly less than t_{pss} and the rate variation is significant (for example, 20 to 50 percent), accurate values of permeability, skin, and static pressure generally can be obtained only by using the methods of superposition discussed in Section 5.4. When the time at a constant production rate is significantly less than t_{pss}, but is still large (more than about four times the buildup time of interest), reasonably accurate values of skin and permeability should still be obtainable with the normal Horner plot using Eq. 5.9, even though values of estimated static pressure could be poor. This comment applies to systems with negligible fracturing in which wellbore storage effects either have died out or have been properly adjusted for (Section 11.2).

Even though the well is shut in during pressure buildup testing, the afterflow caused by wellbore storage has a significant influence on pressure buildup data. Fig. 5.2 schematically shows that pressure points fall below the semilog straight line while wellbore storage is important. The duration of those effects may be estimated by making the log-log data plot described in Section 2.6. For pressure buildup testing, plot $\log[p_{ws} - p_{wf}(\Delta t=0)]$ vs $\log \Delta t$. When wellbore storage dominates, that plot will have a unit-slope straight line; as the semilog straight line is approached, the log-log plot bends over to a gently curving line with a low slope (see Fig. 2.10). In all pressure-buildup test analyses, the log-log data plot should be made before the straight line is chosen on the semilog data plot, since it is often possible to draw a semilog straight line through wellbore-storage-dominated data. This phenomenon occurs because wellhead shut-in does not correspond to sand-face shut-in. When the surface valve is closed, fluid continues to flow into the wellbore from the formation. Thus, pressure does not build up as fast as we might expect. As the flow rate drops off to zero, the pressure increases rapidly to approach the theoretically predicted level. The semilog data plot is steep and nearly linear during this time, and may be analyzed incorrectly. The analyzable data occur after the data-plot slope has become less steep, as indicated in Fig. 5.2.

When wellbore storage effects last so long that the semilog straight line does not develop, it may be possible to analyze the test data by using type-curve matching techniques in a manner similar to that described in Section 3.3, with $\Delta p = p_{ws} - p_{wf}(\Delta t = 0)$. The type curves of Figs. C.6,[14] C.8,[15] and C.9[16,17] are particularly useful for pressure buildup testing, providing a significant change in wellbore storage coefficient is not involved (see Section 11.2). It cannot be overemphasized that type-curve matching *should not be used for test analysis if semilog analysis techniques can be applied.* Type-curve matching generally gives only approximate results (within a factor of 2 or 3). Refs. 15 and 16 give examples of type-curve matching for pressure buildup analysis. The Gladfelter-Tracy-Wilsey[1,18] or Russell[1,9] approaches can also give good results for data nearing the semilog straight line (after q is less than 20 percent of the previous rate). However, curve-matching techniques, particularly Fig. C.8, can also give good quantitative results in this region.

Example 5.1 Pressure Buildup Test Analysis—Horner Method

Table 5.1 shows pressure buildup data from an oil well with an estimated drainage radius of 2,640 ft. Before shut-in the well had produced at a stabilized rate of 4,900 STB/D for 310 hours. Known reservoir data are

$$\begin{aligned} \text{depth} &= 10{,}476 \text{ ft} \\ r_w &= (4.25/12) \text{ ft} \\ c_t &= 22.6 \times 10^{-6} \text{ psi}^{-1} \\ q_o &= 4{,}900 \text{ STB/D} \\ h &= 482 \text{ ft} \\ p_{wf}(\Delta t = 0) &= 2{,}761 \text{ psig} \\ \mu_o &= 0.20 \text{ cp} \\ \phi &= 0.09 \\ B_o &= 1.55 \text{ RB/STB} \\ \text{casing ID} &= (6.276/12) \text{ ft} \\ t_p &= 310 \text{ hours.} \end{aligned}$$

Wellbore storage affects transient pressure behavior and,

therefore, should be considered in all transient test analyses. Failure to do so may result in analyzing the wrong portion of the data. Fig. 5.3, the log-log plot of the buildup data in Table 5.1, is used to check the significance of wellbore storage. Since there is no unit-slope line, we conclude that dominant wellbore storage has ended by 0.1 hour. However, the rapid pressure increase shown in Fig. 5.4 does indicate that wellbore storage or skin effects are significant until about 0.75 hour. The data obtained after 0.75 hour can be analyzed.

The Horner plot is shown as Fig. 5.4. Residual wellbore storage or skin effects at shut-in times of less than 0.75 hour are apparent. The straight line, drawn after $\Delta t = 0.75$ hour, has a slope of -40 psig/cycle, so $m = 40$ psig/cycle.

Eq. 5.6 is used to estimate permeability:

$$k = \frac{162.6(4{,}900)(1.55)(0.20)}{(40)(482)} = 12.8 \text{ md}.$$

Skin factor is estimated from Eq. 5.7 using $p_{1\text{hr}} = 3{,}266$ psig from Fig. 5.4:

$$s = 1.1513\left[\frac{3{,}266 - 2{,}761}{40} - \log\left(\frac{(12.8)(12)^2}{(0.09)(0.20)(22.6 \times 10^{-6})(4.25)^2}\right) + 3.2275\right] = 8.6.$$

We can estimate Δp across the skin from Eq. 2.9:

$$\Delta p_s = \frac{(141.2)(4{,}900)(1.55)(0.20)(8.6)}{(12.8)(482)} = 300 \text{ psi}.$$

TABLE 5.1—PRESSURE BUILDUP TEST DATA FOR EXAMPLE 5.1, $t_p = 310$ HOURS.

Δt (hours)	$t_p+\Delta t$ (hours)	$\frac{(t_p+\Delta t)}{\Delta t}$	p_{ws} (psig)	$p_{ws} - p_{wf}$ (psig)
0.0	—	—	2,761	—
0.10	310.10	3,101	3,057	296
0.21	310.21	1,477	3,153	392
0.31	310.31	1,001	3,234	473
0.52	310.52	597	3,249	488
0.63	310.63	493	3,256	495
0.73	310.73	426	3,260	499
0.84	310.84	370	3,263	502
0.94	310.94	331	3,266	505
1.05	311.05	296	3,267	506
1.15	311.15	271	3,268	507
1.36	311.36	229	3,271	510
1.68	311.68	186	3,274	513
1.99	311.99	157	3,276	515
2.51	312.51	125	3,280	519
3.04	313.04	103	3,283	522
3.46	313.46	90.6	3,286	525
4.08	314.08	77.0	3,289	528
5.03	315.03	62.6	3,293	532
5.97	315.97	52.9	3,297	536
6.07	316.07	52.1	3,297	536
7.01	317.01	45.2	3,300	539
8.06	318.06	39.5	3,303	542
9.00	319.00	35.4	3,305	544
10.05	320.05	31.8	3,306	545
13.09	323.09	24.7	3,310	549
16.02	326.02	20.4	3,313	552
20.00	330.00	16.5	3,317	556
26.07	336.07	12.9	3,320	559
31.03	341.03	11.0	3,322	561
34.98	344.98	9.9	3,323	562
37.54	347.54	9.3	3,323	562

Thus, pressure drop across the skin in this damaged well is about one-half the total pressure drop. The flow efficiency may be estimated from Eq. 2.12, using $\bar{p} = 3{,}342$ psig (as estimated in Example 6.1, Section 6.3). Flow efficiency is calculated as

$$\frac{3{,}342 - 2{,}761 - 300}{3{,}342 - 2{,}761} = 0.48.$$

This suggests that the production rate could be more than doubled by simply removing the damage, or possibly could be tripled with an acid or fracture treatment, depending on conditions around the well and on rock type.

5.3 Pressure Buildup Test Analysis in Finite and Developed Reservoirs

When wells being tested do not act like a single well in an infinite system, the equations in Section 5.2 require modification. In this section, we consider pressure buildup testing of a single well in a bounded reservoir and of a well in a developed reservoir. During the initial discussion, we will not consider the effects of changing offset-well drainage areas on the developed reservoir situation.

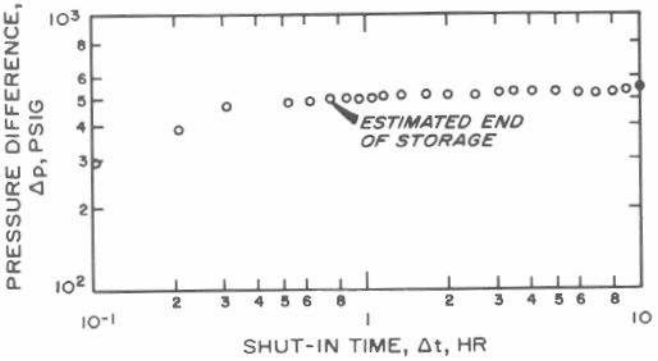

Fig. 5.3 Log-log data plot for the buildup test of Example 5.1.

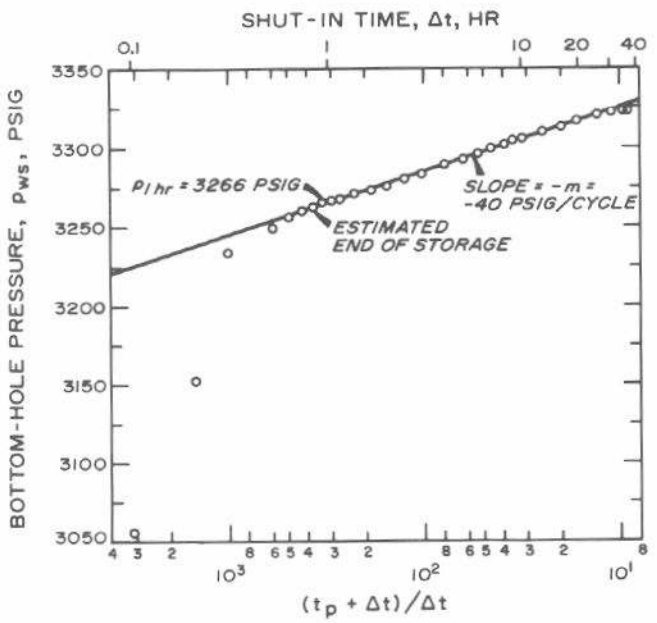

Fig. 5.4 Horner plot of pressure buildup data for Example 5.1.

Horner Plot

The Horner pressure-buildup test data analysis can be used to estimate permeability and skin in finite reservoirs just as in infinite-acting reservoirs, since boundary effects influence only late-time data. The data plot is as described in Section 5.2 and Fig. 5.2; Eqs. 5.6, 5.7, and 5.9 apply. Section 5.2 states that an estimate of p_i is obtained by extrapolating the straight-line section of the Horner plot to infinite shut-in time. For finite and developed reservoirs, the extrapolated pressure is not a good estimate of p_i and generally has been called the "false pressure," p^*.[1,6,9,10] Fig. 5.5 shows pressure buildup data for a well in a finite reservoir. The extrapolated false pressure, p^*, is higher than the average pressure at the instant of shut-in unless the drainage region is highly skewed.

Using the concept of the false pressure, we may rewrite Eq. 5.4:

$$p_{ws} = p^* - m \log\left(\frac{t_p + \Delta t}{\Delta t}\right) . \quad \ldots\ldots\ldots\ldots (5.10)$$

Ramey and Cobb[10] show that p^* is related to p_i by

$$p^* = p_i - \frac{141.2\,qB\mu}{kh}\left[p_D(t_{pD}) - \frac{1}{2}(\ln t_{pD} + 0.80907)\right] . \quad \ldots\ldots\ldots\ldots (5.11)$$

When the logarithmic approximation, Eq. 5.3, can be used for $p_D(t_{pD})$ in Eq. 5.11, p^* is identical to p_i.

Eq. 5.10 indicates that the normal Horner plot, p_{ws} vs $\log[(t_p + \Delta t)/\Delta t]$, should have a straight-line section with slope $-m$, as schematically illustrated in Figs. 5.2 and 5.5. Although it is commonly believed that the Horner plot should be used only for new wells or when t_p is relatively small, Ramey and Cobb[10] and Cobb and Smith[19] indicate that the Horner plot may *always* be used for pressure-buildup data analysis. However, since it requires more work than the Miller-Dyes-Hutchinson method, the Horner plot is generally not used unless $t_p < t_{pss}$.

Miller-Dyes-Hutchinson Analysis

The Horner plot may be simplified if $\Delta t << t_p$. In that case, $t_p + \Delta t \simeq t_p$ and

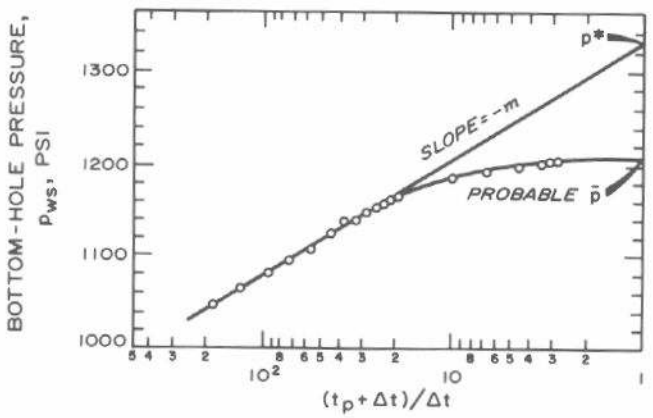

Fig. 5.5 Horner plot of typical pressure buildup data from a well in a finite reservoir. After Matthews and Russell.[1]

$$\log\left(\frac{t_p + \Delta t}{\Delta t}\right) \simeq \log t_p - \log \Delta t . \quad \ldots\ldots\ldots (5.12)$$

If Eq. 5.12 is used in Eq. 5.10, then

$$p_{ws} = p_{1hr} + m \log \Delta t . \quad \ldots\ldots\ldots\ldots (5.13)$$

Eq. 5.13 indicates that a plot of p_{ws} vs $\log \Delta t$ should be a straight line with slope $+m$, where m is given by Eq. 5.5. Permeability may be estimated from Eq. 5.6, and the skin factor may be estimated from Eq. 5.7. The p_{ws} vs $\log \Delta t$ plot is commonly called the Miller-Dyes-Hutchinson (MDH) plot.[1,10] We use this terminology throughout this monograph. The false pressure may be estimated from the MDH plot by using

$$p^* = p_{1hr} + m \log(t_p + 1) \simeq p_{1hr} + m \log(t_p) . \quad \ldots\ldots\ldots\ldots (5.14)$$

Fig. 5.2 indicates that some minimum shut-in time is required before pressure-buildup data fall on the Horner straight line. The same is true for the MDH plot. The beginning of the MDH semilog straight line may be estimated by making the log-log data plot and observing when the data points reach the slowly curving low-slope line, about 1 to 1.5 cycles in time after the end of the unit-slope straight line. Alternatively, the time to the beginning of the semilog straight line for either the Horner or the MDH plot may be estimated from Eq. 2.22.[20]

$$\Delta t_D = 50\,C_D e^{0.14s} , \quad \ldots\ldots\ldots\ldots (5.15a)$$

or, in hours,

$$\Delta t = \frac{170{,}000\,C e^{0.14s}}{(kh/\mu)} . \quad \ldots\ldots\ldots\ldots (5.15b)$$

For fractured wells, Δt estimated using a C based on wellbore storage volume rather than a C derived from a log-log plot unit slope (see Eq. 2.20) will tend to be a minimum value owing to neglect of any fracture storage volume.

Fig. 5.5 indicates that after some shut-in time, the pressure begins to fall below the semilog straight line. This is true for both Horner- and MDH-type plots. The end time of the semilog straight line may be estimated from

$$\Delta t = \frac{\phi\mu c_t A}{0.0002637\,k}(\Delta t_{DA})_{esl} , \quad \ldots\ldots\ldots\ldots (5.16)$$

where $(\Delta t_{DA})_{esl}$, the dimensionless shut-in time at the end of the semilog straight line, depends on reservoir shape and well location. Ramey and Cobb[10] and Cobb and Smith[19] present $(\Delta t_{DA})_{esl}$ data for a variety of shapes and well locations for both Horner- and MDH-type plots. Fig. 5.6 gives $(t_{DA})_{esl}$ data for a Horner plot for the shapes and well locations in Table 5.2. Fig. 5.7 gives the information for an MDH plot. Both figures identify the time when the data-plot slope deviates from the correct slope by about 5 percent. Cobb and Smith[19] (preprint version only) also give the time to the end of the semilog straight line for 2-, 10-, 15-, 20-, and 40-percent deviation. Similar data for a square with constant-pressure boundaries and the well at the center are available[21,22] and are included as Shape 7 in Figs. 5.6 and 5.7.

A comparison of Fig. 5.6 with Fig. 5.7 shows that, in closed systems, $(\Delta t_{DA})_{esl}$ is never longer for an MDH plot than for a Horner plot. For symmetric closed systems, the straight line will be prolonged by the Horner plot for producing times t_p up to $4t_{pss}$. For asymmetrical systems, the advantage is not so great. Practically speaking, the Horner plot is superior from the standpoint of straight-line duration for $t_p < t_{pss}$; otherwise, the MDH plot is equally good and is much easier to prepare. However, the figures do show that the MDH plot has a longer straight line than the Horner plot for a square with constant-pressure boundaries when $t_{pDA} > 0.15$.

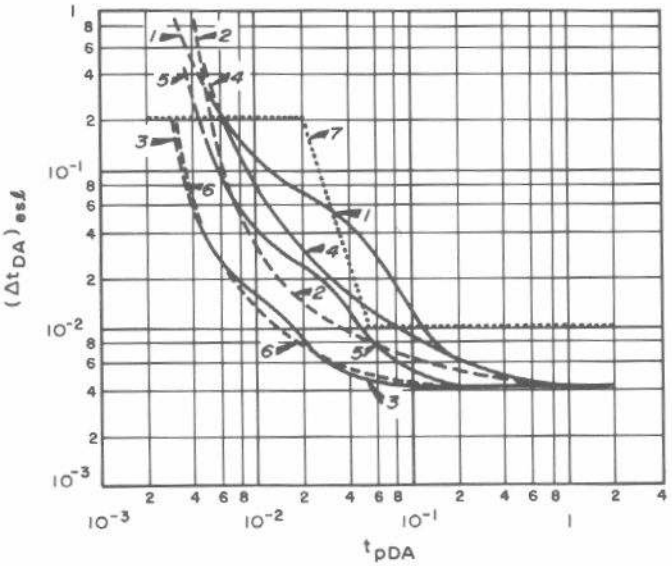

Fig. 5.6 Dimensionless time to end of Horner straight line for shapes identified in Table 5.2. Data of Cobb and Smith[19] and Kumar and Ramey.[22]

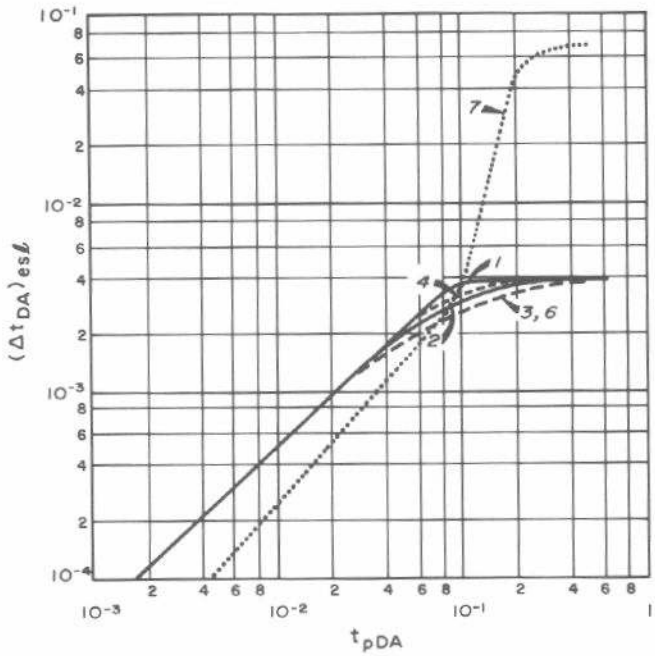

Fig. 5.7 Dimensionless time to end of Miller-Dyes-Hutchinson straight line for shapes identified in Table 5.2. Data of Cobb and Smith[19] and Kumar and Ramey.[22]

For the closed systems given in Table 5.2, Cobb and Smith[19] show that the average reservoir pressure is reached after a dimensionless shut-in time given by

$$\Delta t_{DA} = (t_{DA})_{pss}, \quad \ldots\ldots\ldots\ldots\ldots\ldots\ldots\ldots (5.17)$$

where $(t_{DA})_{pss}$ is given in Table C.1. In highly asymmetrical systems, or in systems with eccentric well locations, $\bar{p}$ is reached slightly before this time.

Example 5.2 Pressure Buildup Test Analysis—Miller-Dyes-Hutchinson Method

We use the buildup test data of Example 5.1 shown in Table 5.1. The log-log data plot, Fig. 5.3, shows that wellbore storage effects have died out after 0.75 hour. The MDH plot, p_{ws} vs log Δt, shown in Fig. 5.8 has a straight line with

$$m = 40 \text{ psig/cycle},$$

and,

$$p_{1hr} = 3{,}266 \text{ psig}.$$

Using Eq. 5.6,

$$k = \frac{162.6(4{,}900)(1.55)(0.20)}{(40)(482)} = 12.8 \text{ md},$$

the result obtained in Example 5.1. The skin factor may be estimated as in Example 5.1 to give the same result.

TABLE 5.2—SHAPES USED IN FIGS. 5.6 AND 5.7.

CURVE NUMBER	SHAPE
1	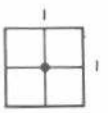
2	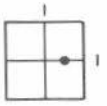
3	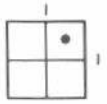
4	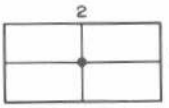
5	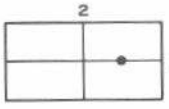
6	
7	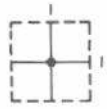

NO FLOW

CONSTANT PRESSURE

The end of the MDH straight line may be estimated with Eq. 5.16 and Fig. 5.7. Using Eq. 2.3b and data from Example 5.1,

$$t_{pDA} = \frac{(0.0002637)(12.8)(310)}{(0.09)(0.20)(22.6 \times 10^{-6})(\pi)(2{,}640)^2}$$

$$= 0.117.$$

For Curve 1 in Fig. 5.7, $(\Delta t_{DA})_{esl} \simeq 0.004$. We approximate the well in the center of a circle by a well in the center of a square, since the two systems behave similarly (see Table C.1). Using Eq. 5.16,

$$\Delta t = \frac{(0.09)(0.20)(22.6 \times 10^{-6})(\pi)(2{,}640)^2(0.004)}{(0.0002637)(12.8)}$$

$$= 10.6 \text{ hours}.$$

The straight line chosen uses more than a full cycle of data before 10 hours, so the analysis should be correct. Actually, the straight line in Fig. 5.8 appears to last to about 20 hours. This may indicate that Fig. 5.7 provides conservative estimates, or that the value of A or c_t used in this example is too small. The end of the straight line for the Horner plot is estimated in a similar manner to be about 26 hours, which agrees well with Fig. 5.4.

Extended Muskat Analysis

In 1937, Muskat[3] proposed plotting pressure buildup data as $\log(\bar{p} - p_{ws})$ vs Δt. Subsequent theoretical studies[10,19,21] indicate that this graph should be used with caution and only as a *late-time* analysis method. Because of the long shut-in times usually required for pressure buildup data to reach the Muskat straight line, the method has limited value for pressure-buildup test analysis. However, it appears to be more practical for analyzing pressure buildup data in producing wells in water-drive reservoirs and filled-up waterfloods because of the longer duration of the Muskat straight line in those systems.[21,22]

The Muskat method uses a trial-and-error plot with several $\bar{p}$ estimates; a straight line is obtained for the correct $\bar{p}$. Fig. 5.9 is a schematic illustration of the extended Muskat data plot.[1,9,10] If the assumed $\bar{p}$ is too high, the plot will be concave upward; if $\bar{p}$ is too low, the plot will be concave downward.

The intercept at $\Delta t = 0$, $(\bar{p} - p_{ws})_{\text{int}}$, of the correct straight line of an extended Muskat plot may be used to estimate reservoir permeability from[10]

$$k = \frac{141.2\, qB\mu}{h(\bar{p} - p_{ws})_{\text{int}}} p_{D\,\text{Mint}}(t_{pDA}). \quad \ldots\ldots\ldots\ldots \quad (5.18)$$

The dimensionless Muskat intercept, $p_{D\,\text{Mint}}$, which is a function of dimensionless producing time, is given by Ramey and Cobb[10] for a single unfractured well in the center of a closed-square drainage system, and by Kumar and Ramey[22] for a square with a constant-pressure boundary. Fig. 5.10 shows the data for both systems. For the closed-square system,

$$p_{D\,\text{Mint}}(t_{pDA} > 0.1) = 0.67, \quad \ldots\ldots\ldots\ldots \quad (5.19a)$$

if producing time exceeds the time to pseudosteady state. For the constant-pressure boundary system,

$$p_{D\,\text{Mint}}(t_{pDA} > 0.25) = 1.34, \quad \ldots\ldots\ldots\ldots \quad (5.19b)$$

when producing time exceeds the time required to reach steady state. Matthews and Russell[1] (Page 31) and Russell[9] give data indicating that $p_{D\,\text{Mint}}(t_{pDA} > 0.1) = 0.84$ for a closed circular system. The large difference between values of 0.67 and 0.84 for a square and a circular system operating at pseudosteady state is cause for concern. Under most circumstances, those two systems should behave almost identically. Yet, for the Muskat method of analysis, the appropriate factor to use in the analysis varies by about 25 percent. This is definitely an indication that the accuracy of the method is open to question.

The value of the Muskat intercept for the square with the constant-pressure boundary (Fig. 5.10) is significantly different from the value for the closed square. That results from the different behavior of the systems and because the Muskat plot for the constant-pressure boundary system uses p_e, the constant-boundary pressure, rather than $\bar{p}$, the average pressure at the time of shut-in.

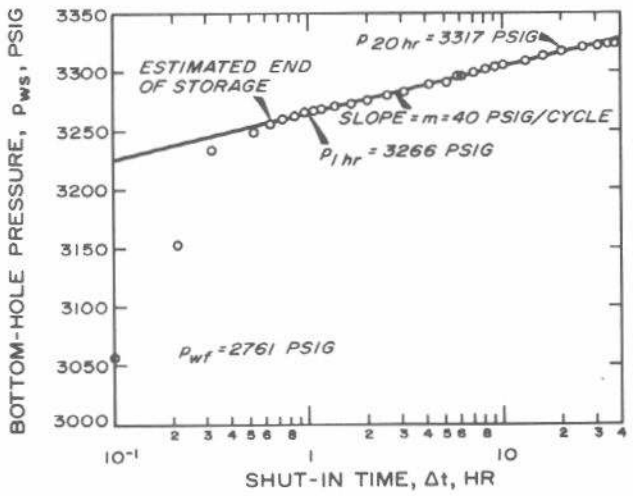

Fig. 5.8 Miller-Dyes-Hutchinson plot for the buildup test of Example 5.2.

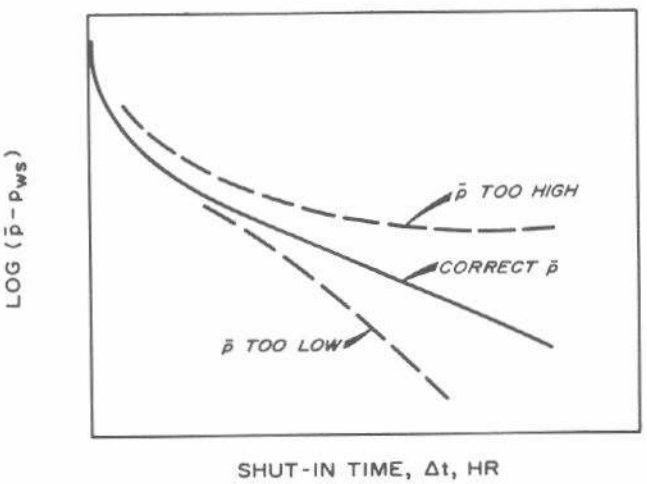

Fig. 5.9 Schematic extended Muskat data plot for pressure buildup test analysis.

The slope of the Muskat-plot straight line may be used to estimate drainage area. For a closed square,[10]

$$A = \frac{-0.00471\,k}{\phi\mu c_t m_M}, \quad \ldots\ldots\ldots\ldots\ldots\ldots\ldots\ldots \quad (5.20a)$$

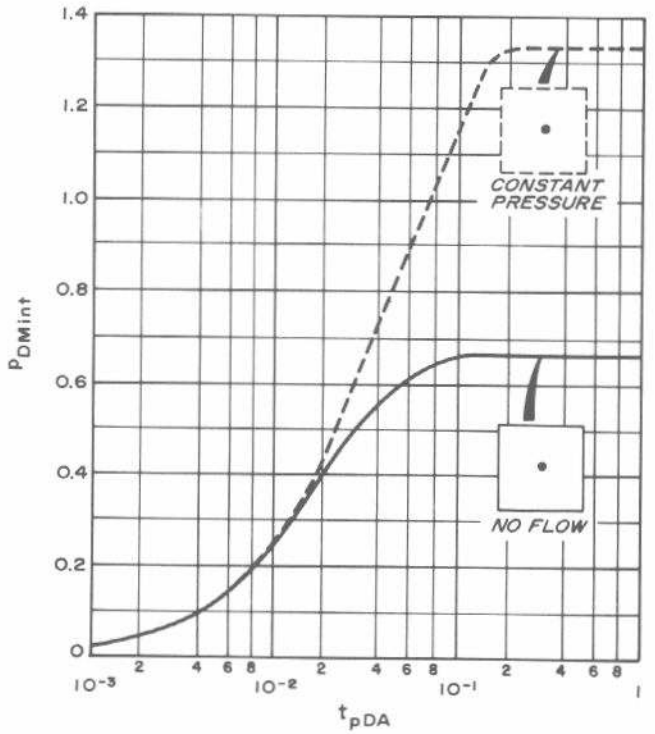

Fig. 5.10 Muskat dimensionless-intercept pressure for a well in the center of a closed or constant-pressure-boundary square. Data of Ramey and Cobb[10] and Kumar and Ramey.[22]

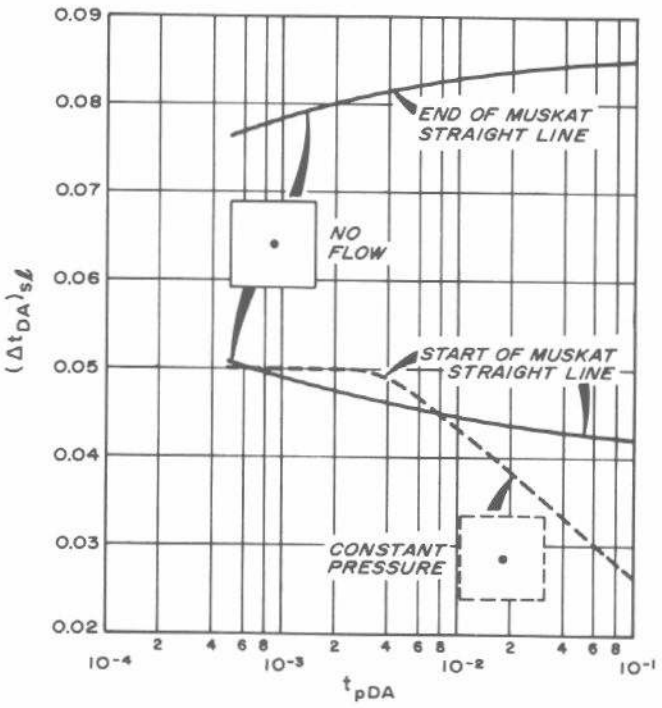

Fig. 5.11 Time to beginning and end of the Muskat straight line for a well in the center of a closed or constant-pressure boundary square. Data of Ramey and Cobb[10] and Kumar and Ramey.[22]

and for a square with constant pressure boundaries,

$$A = \frac{-0.00233\,k}{\phi\mu c_t m_M} \quad \ldots\ldots\ldots\ldots\ldots\ldots\ldots\ldots \quad (5.20b)$$

In Eq. 5.20, m_M is the slope of the Muskat plot and is a negative number. Matthews and Russell[1] (Page 31) and Russell[9] indicate that the constant in Eq. 5.20a is −0.00528 for a closed circular system with the well at the center. Again, we see a large discrepancy in the values used for analyzing pressure buildup data in square and circular systems. That discrepancy in both Eqs. 5.19a and 5.20a may indicate that very accurate results should not be expected when using the Muskat analysis method.

The beginning and end of the Muskat straight line may be estimated from

$$\Delta t = \frac{\phi\mu c_t A}{0.0002637\,k}(\Delta t_{DA})_{sl}, \quad \ldots\ldots\ldots\ldots\ldots\ldots \quad (5.21)$$

where $(\Delta t_{DA})_{sl}$ is shown in Fig. 5.11. Data for both the start and the end of the straight line are given for the closed square. For the square with constant-pressure boundaries, Fig. 5.11 indicates only the start of the straight line; it can be expected to end at $\Delta t_{DA} = 0.25$.[21,22]

Example 5.3 Pressure Buildup Test Analysis—Extended Muskat Method

A Muskat plot of the pressure data of Example 5.1 is shown in Fig. 5.12. Only four points define the straight line in Fig. 5.12, so we should immediately be suspicious of analysis results. From Fig. 5.12,

$$(\bar{p} - p_{ws})_{int} = 31.4 \text{ psig},$$

and

$$m_M = -0.00586 \text{ cycle/hr}.$$

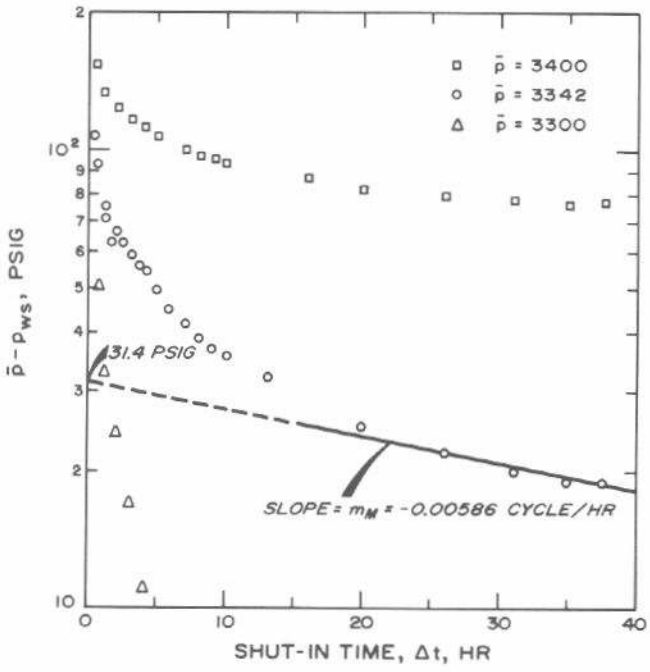

Fig. 5.12 Extended Muskat data plot for Example 5.3.

We will use Eq. 5.18 to estimate permeability from the intercept, but we must first obtain $p_{D\text{Mint}}$ (t_{pDA}) from Fig. 5.10. Thus, we assume a single well in the center of a closed square; normally, that would be a reasonable approximation to the circular system, but as shown with Eqs. 5.19 and 5.20, it may not be so reasonable for the extended Muskat analysis. Using Eq. 2.3b and an estimated permeability of 12 md,

$$t_{pDA} \simeq \frac{(0.0002637)(12)(310)}{(0.09)(0.20)(22.6 \times 10^{-6})(\pi)(2{,}640)^2}$$
$$\simeq 0.11.$$

Thus, for a first estimate, $p_{D\text{Mint}} = 0.67$ from Eq. 5.19a and Fig. 5.10. Using Eq. 5.18,

$$k = \frac{(141.2)(4{,}900)(1.55)(0.67)(0.20)}{(31.4)(482)} = 9.5 \text{ md.}$$

Since this is lower than the value used to estimate t_{pDA}, we need to iterate. Repeating the computations, $t_{pDA} \simeq 0.087$, $p_{D\text{Mint}} \simeq 0.665$, and $k = 9.4$, which is acceptable agreement.

This value of k is about 27 percent lower than estimated by the Horner and MDH methods. This is because the Muskat straight line is poorly defined in this case and apparently is not drawn through data from the correct time interval (estimated to be about 150 to 300 hours later in this example). Ramey and Cobb[10] indicate that only *very* late buildup data are straightened by the Muskat plot; we may not have enough of those data. Unfortunately, data at such times also may be influenced by interference from other wells or other boundary effects.

In spite of the problems with the data, we estimate A and the duration of the straight line to illustrate the method. Using Eq. 5.20 and the slope of the straight line in Fig. 5.12,

$$A = \frac{(-0.00471)(9.4)}{(-0.00586)(0.20)(0.09)(22.6 \times 10^{-6})}$$
$$= 18.6 \times 10^6 \text{ sq ft.}$$

From data provided for Example 5.1,

$$A = \pi\,(2{,}640)^2 = 21.9 \times 10^6 \text{ sq ft.}$$

So, the extended Muskat analysis is low by about 15 percent.

Fig. 5.11 indicates that for $t_{pDA} = 0.09$, the straight line should meet the requirement $0.042 < (\Delta t_{DA})_{st} < 0.085$. Using Eq. 5.21,

$$\left[\frac{(0.09)(0.20)(22.6 \times 10^{-6})(\pi)(2{,}640)^2}{(0.0002637)(9.4)}\right](0.042)$$
$$< \Delta t < \left[3{,}590\right](0.085).$$

Thus,

$$151 < \Delta t < 305 \text{ hours.}$$

This clearly indicates that even though the extended Muskat plot *appears* to have a straight line, that straight line does not occur at the right shut-in time for analysis. In this case, careful analysis (using Eq. 5.21 and Fig. 5.11 to check the limits on the straight line) indicates that the results should be considered as incorrect — at least when analysis techniques for a closed square are used.

If, instead of using the Ramey and Cobb[10] data for a closed square system, we use the Matthews and Russell[1] data for a closed circular system, we would estimate

$$k = 11.9 \text{ md,}$$

using a value of 0.84 in Eq. 5.19 rather than 0.67. Using a value of -0.00528 as the constant in Eq. 5.20a, we estimate

$$A = 20.8 \times 10^6 \text{ sq ft.}$$

These values are within 7 and 5 percent of the correct values, respectively. Thus, we see that we get much better results by using the analysis method for the closed circle than the closed square. This may or may not be coincidental. Unfortunately, little information is available for analyzing Muskat plots for closed, circular, or other systems.

Example 5.3 illustrates that results from the extended Muskat analysis method may be incorrect. Fig. 5.11 shows that it takes a long time for the extended Muskat straight line to develop; for a well in the center of a closed square, the well must be shut in almost half as long as it would take for that well to reach pseudosteady state under producing conditions. Detailed data are not available for shut-in requirements for other well locations and drainage shapes, but we can expect the requirements to be as severe as those for a well in a closed square. The relatively large difference in the analysis constants for the square and circular systems is an indication that systems with other shapes may have significantly different constants in the analysis equations. That can be expected because the Muskat analysis technique applies to data taken late in the buildup period, when the system boundaries have their largest effect on pressure behavior.

Fig. 5.12 also indicates the difficulty of identifying the Muskat straight line. The uppermost set of points, with $\bar{p} =$ 3,400 psi, appears to be straight for the last four points. Certainly it is as straight as the line for the assumed correct $\bar{p}$ in Example 5.3. The set of points for the assumed correct $\bar{p}$ appears to have a second straight-line section from about 8 to 20 hours. Only experience and the use of Eq. 5.21 and Fig. 5.11 would prevent drawing and analyzing that straight line. Eqs. 5.18 and 5.20 indicate that a straight line drawn from 8 to 20 hours would yield even lower permeability and drainage area.

Because of the long time required for pressure buildup data to reach the Muskat straight line, and because small geometry differences have a large effect on analysis results, the Muskat method has limited value for pressure-buildup test analysis.

Developed Reservoir Effects

When the test well is producing at pseudosteady state before a buildup test, or when it is experiencing a pressure decline because of production from other wells in the reservoir, the analysis methods discussed previously may give incorrect results. In such cases, it is best to use Eq. 5.1 in a more general form. Slider[23,24] has suggested analysis techniques that apply in these situations; Sections 3.4 and 4.5 give them for drawdown and multiple-rate testing. A similar

approach is used for pressure buildup testing, as explained below.

Extrapolate the flowing pressure into the buildup period to estimate $p_{wf\,ext}$. (Fig. 3.8 gives nomenclature for a flowing test.) Then estimate the difference between the observed shut-in pressure and the extrapolated flowing pressure, $\Delta p_{\Delta t}$, and plot $\Delta p_{\Delta t}$ vs log Δt. The data plotted should follow the relationship

$$\Delta p_{\Delta t} = p_{ws} - p_{wf\,ext} = \Delta p_{1hr} + m \log \Delta t, \quad \ldots\ldots (5.22)$$

a straight line on a $\Delta p_{\Delta t}$ vs log Δt plot with slope m given by Eq. 5.5 and intercept given by

$$\Delta p_{1hr} = m\left[\log\left(\frac{k}{\phi\mu c_t r_w^2}\right) - 3.2275 + 0.86859\,s\right]. \quad \ldots\ldots (5.23)$$

Permeability is estimated from Eq. 5.6 and skin factor is estimated from

$$s = 1.1513\left[\frac{\Delta p_{1hr}}{m} - \log\left(\frac{k}{\phi\mu c_t r_w^2}\right) + 3.2275\right]. \quad \ldots\ldots (5.24)$$

If pressure decline at the test well is linear before the buildup test, then Eq. 5.22 becomes

$$p_{ws} - m^*\Delta t = \Delta p_{1hr}^* + m \log \Delta t, \quad \ldots\ldots (5.25)$$

where m^* is the linear rate of pressure change before the buildup test:

$$m^* = \frac{dp_{wf}}{dt} \text{ when } t < t_p. \quad \ldots\ldots (5.26)$$

Normally, m^* is a negative number. The value of Δp_{1hr}^* in Eq. 5.25 is derived from Eq. 5.23 and the equation for the extrapolated linear pressure behavior:

$$\Delta p_{1hr}^* = p_{wf}(\Delta t = 0) + m\left[\log\left(\frac{k}{\phi\mu c_t r_w^2}\right) - 3.2275 + 0.86859\,s\right]. \quad \ldots\ldots (5.27)$$

Thus, when pressure declines linearly before testing, a plot of $(p_{ws} - m^*\Delta t)$ vs log Δt should be a straight line. Skin factor may be estimated from Eq. 5.7 with Δp_{1hr}^* in place of p_{1hr}. Permeability is obtained from Eq. 5.6.

Example 5.4 Pressure Buildup Test Analysis—Developed System Analysis

Figs. 5.13 and 5.14 show simulated pressure buildup data for a well in a developed reservoir. All wells were produced at a constant rate for 15 days; then, one well was shut in for buildup while the others continued to produce. Known data are

$k = 15$ md	$q = 51$ STB/D
$h = 11$ ft	$B = 1.21$ RB/STB
$\mu = 1.37$ cp	$c_t = 26.7 \times 10^{-6}$ psi^{-1}
$\phi = 0.173$	$s = 0$
$r_w = 0.286$ ft	$p_{wf}(\Delta t{=}0) = 2{,}634$ psig.

Just before shut-in, bottom-hole flowing pressure was declining linearly at 7.836 psi/D, so $m^* = -0.3265$ psi/hr.

Fig. 5.13 is a plot of $\log[p_{ws} - p_{wf}(\Delta t = 0)]$ vs log Δt. It shows that wellbore storage effects are important initially, but die out after about 4 hours of shut-in time. The first two data points are on the unit-slope straight line; thus, Eq. 2.20 can be used to estimate the wellbore storage coefficient. From Fig. 5.13, $\Delta p = 20$ psig at $\Delta t = 0.1$ hour. Then,

$$C = \frac{(51)(1.21)}{24}\,\frac{0.1}{20} = 0.0129 \text{ RB/psig}.$$

For an oil gravity of 30 °API, $\rho = 54.7$ lb$_m$/cu ft and Eq. 2.16 may be used to estimate pipe size for a rising fluid level:

$$V_u = (0.0129)\,\frac{54.7}{144}\,\frac{32.17}{32.17} = 0.0049 \text{ bbl/ft}.$$

This corresponds roughly to 2-in. tubing.

Fig. 5.14 is a semilog plot of data from this test. Both the correct quantity accounting for the declining reservoir pres-

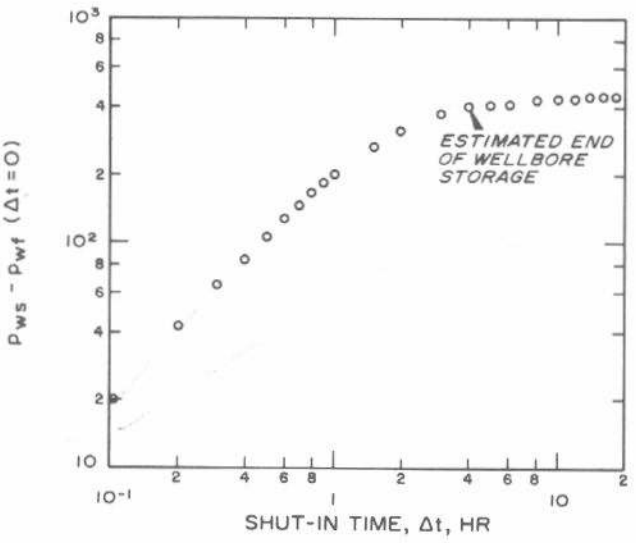

Fig. 5.13 Log-log data plot for a pressure buildup test in a developed reservoir, Example 5.4.

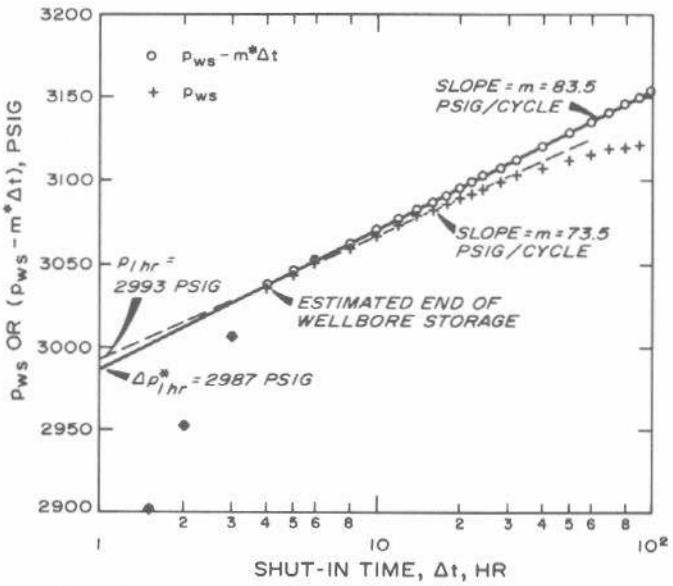

Fig. 5.14 Data plot for a pressure buildup test in a developed reservoir, Example 5.4.

sure, $p_{ws} - m^*\Delta t$, and the normal MDH plot are shown. For the correct data plot (circles in Fig. 5.14),

$m = 83.5$ psig/cycle,

and

$\Delta p_{1hr}{}^* = 2{,}987$ psig.

We estimate permeability from Eq. 5.6:

$$k = \frac{(162.6)(51)(1.21)(1.37)}{(83.5)(11)} = 14.97 \text{ md}.$$

This is within 0.2 percent of the input value, 15 md. The skin factor is estimated from Eq. 5.7 using $\Delta p_{1hr}{}^*$ in place of p_{1hr}:

$$s = 1.1513\left[\frac{2{,}987-2{,}634}{83.5} - \log\left(\frac{14.97}{(0.173)(1.37)(26.7\times 10^{-6})(0.286)^2}\right) + 3.2275\right] = -0.007.$$

The input value is zero.

If the MDH plot (+'s in Fig. 5.14) is analyzed with Eqs. 5.6 and 5.7, we obtain $k = 17.0$ (a 13.3-percent error) and $s = 0.7$. In addition to providing more correct results, the $(p_{ws} - m^*\Delta t)$ plot has a semilog straight line of longer duration than the MDH plot. In this example, the line ends after about 24 hours for the MDH plot while data still fall on the semilog straight line after 100 hours for the correct data plot.

5.4 Buildup Test Analysis When Rate Varies Before Testing

Strictly speaking, the Horner and Miller-Dyes-Hutchinson plotting techniques apply only for a constant production rate preceding the buildup test. However, as indicated by Eq. 5.9, variable-rate conditions may be handled approximately in many circumstances. Nevertheless, in buildup tests with relatively short flow periods or with widely varying rate before shut-in, it is important to include the effects of rate variation on test analysis. For *infinite-acting systems* and unfractured wells, a variation of Eq. 4.1 may be used:

$$p_{ws} = p_i - m\sum_{j=1}^{N}\frac{q_j}{q_N}\log\left(\frac{t_N - t_{j-1} + \Delta t}{t_N - t_j + \Delta t}\right). \quad \ldots\ldots\ldots\ldots\ldots\ldots\ldots\ldots\ldots\ldots (5.28)$$

Fig. 5.15 identifies the nomenclature for the variable-rate period. Eq. 5.28 indicates that a plot of p_{ws} vs the summation term on the right-hand side should yield a straight-line portion with slope $-m$ given by Eq. 5.5 (with the final rate, q_N, used in place of q) and intercept p_i. Permeability is estimated from Eq. 5.6, and skin factor from Eq. 5.7 if $(t_N - t_{N-1}) >> 1$ hour or from Eq. 5.8 with t_p replaced by $(t_N - t_{N-1})$.

Odeh and Selig[25] propose a method similar to the Horner method for analyzing variable-rate buildup tests when the production period is shorter than the shut-in period. They suggest calculating a modified production time,

$$t_p{}^* = 2\left\{t_p - \frac{\sum_{j=1}^{N} q_j(t_j{}^2 - t_{j-1}{}^2)}{2\sum_{j=1}^{N} q_j(t_j - t_{j-1})}\right\}, \quad \ldots\ldots\ldots (5.29)$$

and a modified flow rate

$$q^* = \frac{1}{t_p{}^*}\sum_{j=1}^{N} q_j(t_j - t_{j-1}). \quad \ldots\ldots\ldots\ldots\ldots\ldots (5.30)$$

The summation term in Eq. 5.30 is the total stock-tank volume produced. The normal Horner analysis is used with $t_p{}^*$ and q^* in place of t_p and q.

Example 5.5 Pressure Buildup Test Analysis—Variable-Rate Analysis

Odeh and Selig[25] give the pressure buildup and pretest rate data in Table 5.3. They also indicate that

$B = 1.0$ RB/STB and $\mu = 0.6$ cp.

Fig. 5.16 is a plot of the data in Table 5.3, using Eq. 5.28. The summation term in that equation is written as follows for those data ($N = 3$):

$$\sum_{j=1}^{N}\frac{q_j}{q_N}\log\left(\frac{t_N - t_{j-1} + \Delta t}{t_N - t_j + \Delta t}\right) = \frac{478.5}{159.5}\log\left(\frac{9-0+\Delta t}{9-3+\Delta t}\right) + \frac{319.0}{159.5}\log\left(\frac{9-3+\Delta t}{9-6+\Delta t}\right) + \frac{159.5}{159.5}\log\left(\frac{9-6+\Delta t}{9-9+\Delta t}\right)$$

$$= 3\log\left(\frac{9+\Delta t}{6+\Delta t}\right) + 2\log\left(\frac{6+\Delta t}{3+\Delta t}\right) + \log\left(\frac{3+\Delta t}{\Delta t}\right).$$

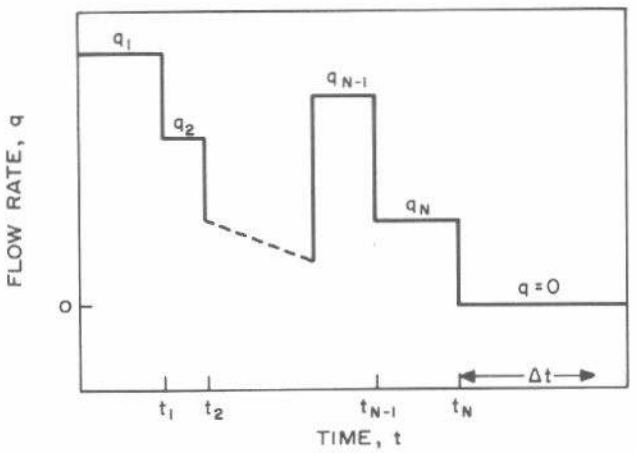

Fig. 5.15 Schematic of rate variation preceding a pressure buildup test.

For $\Delta t = 2$, this becomes

$$3 \log \left(\frac{9+2}{6+2}\right) + 2 \log \left(\frac{6+2}{3+2}\right) + \log \left(\frac{3+2}{2}\right)$$
$$= 0.4149 + 0.4082 + 0.3979$$
$$= 1.2210.$$

Table 5.3 summarizes the calculations. The slope in Fig. 5.16 gives $m = 153$ psi/cycle. Using Eq. 5.6 with the last rate,

$$kh = \frac{(162.6)(159.5)(1.0)(0.6)}{153} = 102 \text{ md ft.}$$

Odeh and Selig[25] indicate that the correct result for these simulated data is 106 md ft. They used the Horner plot to get 77 md ft and the modified analysis method of Eqs. 5.29 and 5.30 to get 97 md ft. It does appear that the varying rate before shut-in must be considered in analyzing this test.

Example 5.5 demonstrates that applying Eq. 5.28 can be tedious. Generally, a computer would be used to calculate the summation term in that equation.

5.5 Choice of Analysis Techniques

From a practical viewpoint, the Miller-Dyes-Hutchinson analysis technique is preferred because of its ease of use. When $t_p > t_{pss}$, the MDH method gives answers for permeability and skin that are just as good as those given by the Horner method. However, for short production times, the Horner method should be used since the semilog straight line with the correct slope is longer than the MDH plot. Recommended engineering practice is the following:

1. Use the MDH method as a first-pass method unless $t_p < t_{pss}$, or unless the system can be approximated by a well in the center of a square with constant-pressure boundaries (as in a five-spot, filled-up waterflood).

2. Use the Horner method for a second pass if circumstances dictate, or as a first pass if t_p is small.

When a test well in a developed reservoir has an extrapolatable flowing pressure decline, the developed-reservoir test analysis methods, Eqs. 5.22 and 5.25, should be used. Significant analysis errors can result if normal Horner or MDH plotting is used in such cases. When flow rate varies significantly before buildup testing, a variable flow-rate analysis technique, such as Eqs. 5.28 through 5.30, should be used.

The extended Muskat analysis method uses pressure buildup data occurring in the transition between the normal Horner or MDH straight line and the onset of average reservoir pressure.[10] This technique is not recommended except in unusual circumstances because of (1) the long testing time required for the extended Muskat method to exhibit the straight line; (2) the ease of observing an apparent straight line at incorrect average pressures or at times before the straight line actually starts; (3) frequent distortion caused by interference effects of other wells; and (4) the significant effect of system shape on the coefficients in the analysis equations. The extended Muskat method appears to be more applicable to wells in waterfloods and in water-drive reservoirs that more closely approach constant pressure than a no-flow boundary condition.[21,22]

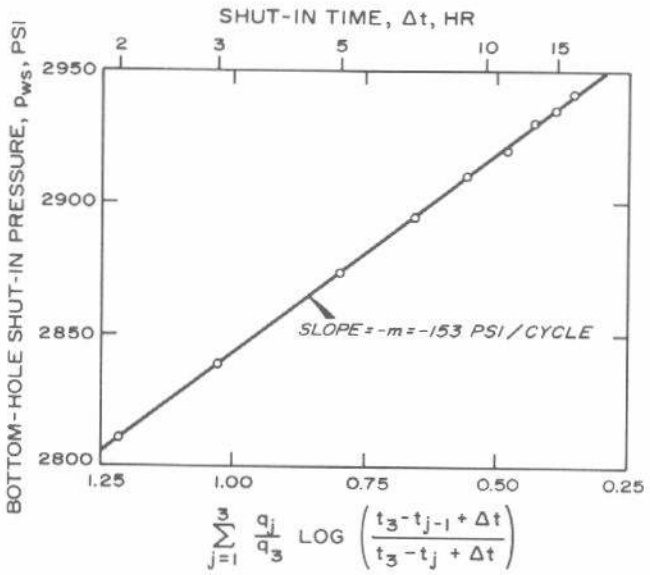

Fig. 5.16 Variable-rate pressure-buildup analysis plot for Example 5.5. Data of Odeh and Selig.[25]

5.6 Factors Complicating Pressure Buildup Testing

Frequently, pressure buildup tests are not as simple as discussed in the preceding examples. Many factors can influence the shape of a pressure buildup curve. An unusual shape may require explanation to complete a proper analysis, or it may prevent a proper analysis. In addition to wellbore storage effects, hydraulic fractures, particularly in low-permeability formations, can have a major effect on buildup-curve shape and analysis. Chapter 11 gives a more detailed discussion of both these factors.

One example of a pressure buildup curve that has an unusual shape when analyzed by the Horner or Miller-Dyes-Hutchinson methods is a test run with a nonstabilized rate before testing. It is important to recognize that condition

TABLE 5.3—RATE AND PRESSURE DATA FOR EXAMPLE 5.5. Data of Odeh and Selig.[25]

Rate History

j	t_j (hours)	q_j (STB/D)
0	0	0
1	3	478.5
2	6	319.0
3	9	159.5

Buildup Data and Computations

Δt (hours)	$3 \log \left(\frac{9+\Delta t}{6+\Delta t}\right)$	$2 \log \left(\frac{6+\Delta t}{3+\Delta t}\right)$	$\log \left(\frac{3+\Delta t}{\Delta t}\right)$	Σ	p_{ws} (psig)
2	0.4149	0.4082	0.3979	1.2210	2,813
3	0.3748	0.3522	0.3010	1.0280	2,838
5	0.3142	0.2766	0.2041	0.7949	2,872
7	0.2705	0.2279	0.1549	0.6533	2,895
9	0.2375	0.1938	0.1249	0.5563	2,910
11	0.2117	0.1686	0.1047	0.4851	2,919
13	0.1910	0.1493	0.0902	0.4305	2,930
15	0.1740	0.1339	0.0792	0.3871	2,935
17	0.1597	0.1214	0.0706	0.3517	2,942

and consider it in the analysis, as discussed in Section 5.4. Other practical problems also can be troublesome. These include a bottom-hole pressure gauge in poor working condition, a leaking pump or lubricator, problems resulting from pump pulling before gauge placement, etc. Additionally, wells with a high gas-oil ratio can exhibit humping during pressure buildup[26] (see Fig. 2.13). In such cases, the bottom-hole pressure increases to a peak, decreases, and finally increases in a normal manner. In some situations, segregation of water and oil in the wellbore can produce a hump.

The shape of the pressure buildup curve also can be affected by fluid and rock interfaces, water-oil contacts, layering, and lateral fluid or rock heterogeneities. (See Chapter 10.) Wellbore storage, wellbore damage or improvement, and geometry of the drainage area can also affect the shape of a buildup curve. For examples, see Refs. 19, 20, and 27, as well as Chapter 11.

References

1. Matthews, C. S. and Russell, D. G.: *Pressure Buildup and Flow Tests in Wells*, Monograph Series, Society of Petroleum Engineers of AIME, Dallas (1967) **1,** Chap. 3.
2. Theis, Charles V.: "The Relation Between the Lowering of the Piezometric Surface and the Rate and Duration of Discharge of a Well Using Ground-Water Storage," *Trans.*, AGU (1935) 519-524.
3. Muskat, Morris: "Use of Data on the Build-Up of Bottom-Hole Pressures," *Trans.*, AIME (1937) **123,** 44-48. Also *Reprint Series, No. 9 — Pressure Analysis Methods*, Society of Petroleum Engineers of AIME, Dallas (1967) 5-9.
4. van Everdingen, A. F. and Hurst, W.: "The Application of the Laplace Transformation to Flow Problems in Reservoirs," *Trans.*, AIME (1949) **186,** 305-324.
5. Miller, C. C., Dyes, A. B., and Hutchinson, C. A., Jr.: "The Estimation of Permeability and Reservoir Pressure From Bottom-Hole Pressure Build-Up Characteristics," *Trans.*, AIME (1950) **189,** 91-104. Also *Reprint Series, No. 9 — Pressure Analysis Methods*, Society of Petroleum Engineers of AIME, Dallas (1967) 11-24.
6. Horner, D. R.: "Pressure Build-Up in Wells," *Proc.*, Third World Pet. Cong., The Hague (1951) Sec. II, 503-523. Also *Reprint Series, No. 9 — Pressure Analysis Methods*, Society of Petroleum Engineers of AIME, Dallas (1967) 25-43.
7. Perrine, R. L.: "Analysis of Pressure Buildup Curves," *Drill. and Prod. Prac.*, API (1956) 482-509.
8. Matthews, C. S.: "Analysis of Pressure Build-Up and Flow Test Data," *J. Pet. Tech.* (Sept. 1961) 862-870. Also *Reprint Series, No. 9 — Pressure Analysis Methods*, Society of Petroleum Engineers of AIME, Dallas (1967) 111-119.
9. Russell, D. G.: "Extensions of Pressure Build-Up Analysis Methods," *J. Pet. Tech.* (Dec. 1966) 1624-1636; *Trans.*, AIME, **237.** Also *Reprint Series, No. 9 — Pressure Analysis Methods*, Society of Petroleum Engineers of AIME, Dallas (1967) 175-187.
10. Ramey, H. J., Jr., and Cobb, William M.: "A General Buildup Theory for a Well in a Closed Drainage Area," *J. Pet. Tech.* (Dec. 1971) 1493-1505; *Trans.*, AIME, **251.**
11. van Everdingen, A. F.: "The Skin Effect and Its Influence on the Productive Capacity of a Well," *Trans.*, AIME (1953) **198,** 171-176. Also *Reprint Series, No. 9 — Pressure Analysis Methods*, Society of Petroleum Engineers of AIME, Dallas (1967) 45-50.
12. Pinson, A. E., Jr.: "Concerning the Value of Producing Time Used in Average Pressure Determinations From Pressure Buildup Analysis," *J. Pet. Tech.* (Nov. 1972) 1369-1370.
13. Kazemi, Hossein: "Determining Average Reservoir Pressure From Pressure Buildup Tests," *Soc. Pet. Eng. J.* (Feb. 1974) 55-62; *Trans.*, AIME, **257.**
14. Agarwal, Ram G., Al-Hussainy, Rafi, and Ramey, H. J., Jr.: "An Investigation of Wellbore Storage and Skin Effect in Unsteady Liquid Flow: I. Analytical Treatment," *Soc. Pet. Eng. J.* (Sept. 1970) 279-290; *Trans.*, AIME, **249.**
15. Earlougher, Robert C., Jr., and Kersch, Keith M.: "Analysis of Short-Time Transient Test Data by Type-Curve Matching," *J. Pet. Tech.* (July 1974) 793-800; *Trans.*, AIME, **257.**
16. McKinley, R. M.: "Wellbore Transmissibility From Afterflow-Dominated Pressure Buildup Data," *J. Pet. Tech.* (July 1971) 863-872; *Trans.*, AIME, **251.**
17. McKinley, R. M.: "Estimating Flow Efficiency From Afterflow-Distorted Pressure Buildup Data," *J. Pet. Tech.* (June 1974) 696-697.
18. Gladfelter, R. E., Tracy, G. W., and Wilsey, L. E.: "Selecting Wells Which Will Respond to Production-Stimulation Treatment," *Drill. and Prod. Prac.*, API (1955) 117-129.
19. Cobb, William M. and Smith, James T.: "An Investigation of Pressure Buildup Tests in Bounded Reservoirs," paper SPE 5133 presented at the SPE-AIME 49th Annual Fall Meeting, Houston, Oct. 6-9, 1974 (an abridged version appears in *J. Pet. Tech.*, Aug. 1975, 991-996; *Trans.*, AIME, **259**).
20. Chen, Hsiu-Kuo and Brigham, W. E.: "Pressure Buildup for a Well With Storage and Skin in a Closed Square," paper SPE 4890 presented at the SPE-AIME 44th Annual California Regional Meeting, San Francisco, April 4-5, 1974.
21. Ramey, Henry J., Jr., Kumar, Anil, and Gulati, Mohinder S.: *Gas Well Test Analysis Under Water-Drive Conditions*, AGA, Arlington, Va. (1973).
22. Kumar, Anil and Ramey, Henry J., Jr.: "Well-Test Analysis for a Well in a Constant-Pressure Square," paper SPE 4054 presented at the SPE-AIME 47th Annual Fall Meeting, San Antonio, Tex., Oct. 8-11, 1972 (an abridged version appears in *Soc. Pet. Eng. J.*, April 1974, 107-116).
23. Slider, H. C.: "Application of Pseudo-Steady-State Flow to Pressure-Buildup Analysis," paper SPE 1403 presented at SPE-AIME Regional Meeting, Amarillo, Tex., Oct. 27-28, 1966.
24. Slider, H. C.: "A Simplified Method of Pressure Buildup Analysis for a Stabilized Well," *J. Pet. Tech.* (Sept. 1971) 1155-1160; *Trans.*, AIME, **251.**
25. Odeh, A. S. and Selig, F.: "Pressure Build-Up Analysis, Variable-Rate Case," *J. Pet. Tech.* (July 1963) 790-794; *Trans.*, AIME, **228.** Also *Reprint Series, No. 9 — Pressure Analysis Methods*, Society of Petroleum Engineers of AIME, Dallas (1967) 131-135.
26. Stegemeier, G. L. and Matthews, C. S.: "A Study of Anomalous Pressure Build-Up Behavior," *Trans.*, AIME (1958) **213,** 44-50. Also *Reprint Series, No. 9 — Pressure Analysis Methods*, Society of Petroleum Engineers of AIME, Dallas (1967) 75-81.
27. Ramey, H. J., Jr., and Earlougher, R. C., Jr.: "A Note on Pressure Buildup Curves," *J. Pet. Tech.* (Feb. 1968) 119-120.

Chapter 6

Estimating Average Reservoir Pressure

6.1 Introduction

Average reservoir pressure, $\bar{p}$, is used for characterizing a reservoir, computing oil in place, and predicting future reservoir behavior. It is fundamental in understanding much reservoir behavior in primary recovery, secondary recovery, and pressure-maintenance projects.

Average pressure for a reservoir without water influx is sometimes defined as the pressure the reservoir would reach if all wells were shut in for infinite time. An equivalent definition, assuming uniform compressibility, is the average pressure obtained by planimetering an isobaric map of the reservoir. For some purposes, such a volumetrically weighted average pressure over the entire productive area is satisfactory. In some applications, separate volumetrically weighted average pressures are desired for gas cap and oil areas using appropriate volumes and compressibilities. At other times, the average pressure at a boundary is desired for computing influx. In yet other situations, other types of averages for various areas or fluid types may be desired for use in models that use different reservoir-performance prediction techniques. Thus, the method of averaging can depend on the use intended.

In high-permeability reservoirs, observed pressures after 24 to 72 hours of shut-in sometimes may be used as control points for isobaric maps with acceptable accuracy. However, most situations require some correction of observed pressures to estimate average pressure near the well. In this regard, one common estimate is the average pressure for a well's drainage region. With the increasing use of reservoir simulation, it is often necessary to estimate average pressure around a well in an area equivalent to the model's grid blocks. In general, only drainage-region average pressure can be estimated from well tests in developed reservoirs.

If a single well in a multiple-well reservoir is shut in, its pressure will eventually decline as a result of withdrawals from other wells, so its pressure will not level out at the true average pressure of the well's drainage region at the instant of shut-in. Nevertheless, each well's drainage region — or, for that matter, any other composite region — does have an average pressure at a given time.

Section 5.2 indicates that the average reservoir pressure in an infinite-acting reservoir ($p^* = p_i = \bar{p}$) may be estimated by extrapolating the straight-line portion of a Horner plot for a shut-in well to $\left[(t_p + \Delta t)/\Delta t\right] = 1$, as indicated in Fig. 6.1. Estimating $\bar{p}$ is more complex for bounded drainage regions since the pressure normally falls below the semilog straight line. This chapter presents methods for estimating average drainage-region pressure from individual-well pressure buildup data.

6.2 Estimating Drainage Volume

Most reservoirs are depleted by several producing wells. In closed, single-phase, constant-compressibility systems containing only production wells, each well drains only a portion of the reservoir.[1,2] At any given time the drainage limits of a well are, from a mathematical standpoint, equivalent to physical barriers to flow located around the well. The average pressure estimate for a well applies only to its drainage region as it existed at the instant of shut-in. Matthews and Russell[1] and Matthews and Lefkovits[2] treat the concept of drainage volume in detail.

In single-phase depletion systems, for wells put on production at the same time, each well initially drains an equal *volume* of the reservoir without regard to production rate. Matthews and Russell[1] present a series of figures showing drainage boundary movement from initial production to

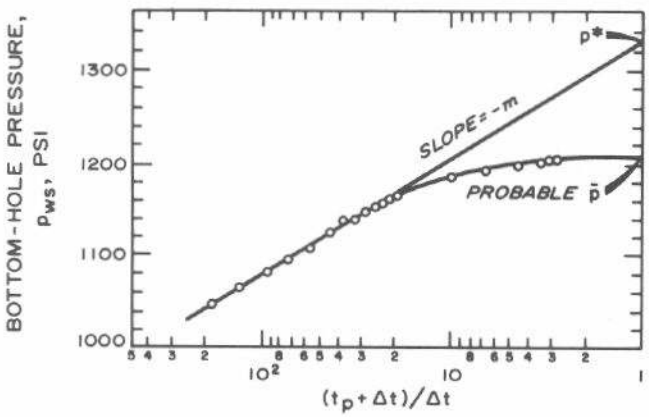

Fig. 6.1 Typical pressure-buildup curve for a well in a finite reservoir. After Matthews and Russell.[1]

pseudosteady-state conditions for unequal well production rates. Under pseudosteady-state conditions, the reservoir pore volume drained by a well is proportional to that well's production rate:[1,2]

$$V_{pi} = \frac{V_{pt}\, q_i}{q_t} \quad \ldots\ldots\ldots\ldots\ldots\ldots\ldots\ldots\ldots\ldots\ldots\ldots (6.1)$$

This concept is based on pore volume and *not* on area; variations in thickness, porosity, and fluid saturation must be considered when changing drainage volumes estimated from Eq. 6.1 to drainage areas. *Eq. 6.1 applies to single-phase, constant-compressibility systems only.* When two or three fluid phases are present, the relationship between drainage volume and production rate may be much more complex because of (1) the complex nature of multiple-phase fluid flow through porous media; and (2) the possibility that some fluids may be produced from portions of the reservoir where other fluids are not mobile. For example, a well producing oil, water, and gas may produce oil (plus solution gas) from a portion of the pay section; water from below the water-oil contact, from the transition zone, or from coning; and gas from the gas cap, from the transition zone, or from coning. Under such conditions, it should be apparent that the simple approach indicated by Eq. 6.1 would not be necessarily correct.

Drainage regions in water-drive and pressure-maintained reservoirs are considerably more complex than those in depletion-type reservoirs. This subject is discussed in more detail in Section 6.4.

In spite of the difficulties of defining drainage volumes, there appear to be many situations where weighting estimated average drainage-region pressures proportional to production rates will provide workable estimates of volumetrically weighted average reservoir pressure. Using such a procedure, the drainage-region average pressure at the instant of shut-in would be estimated using methods presented in Sections 6.3 and 6.4. For that computation, individual-well drainage regions of an assumed nominal shape are required. The size of those regions would be estimated by using a fraction of the total reservoir hydrocarbon pore volume based on representative production rates before shut-in, as indicated by Eq. 6.1.[2] Then, the over-all average volumetrically weighted reservoir pressure would be estimated by weighting each drainage-region average pressure by the production rate in that drainage region.

Normally, pressure surveys include only a portion of the wells in a given reservoir. In such a case, it is often acceptable to compute average pressures based on nominal drainage areas related to the well pattern (for example, a 40-acre square). Such pressures then can be spotted on maps and contoured to obtain a volumetrically weighted average reservoir pressure. The desired pressure for contouring purposes is the average pressure in the vicinity of each well at some point in time. That pressure will differ from the pressure over the well's actual drainage region when the drainage region is highly skewed as the result of unequal production rates, irregular well locations, incomplete reservoir development, water influx, etc. Both approaches to estimating average reservoir pressure are pragmatic; in many cases, a result with a possible ±20-percent error is better than no result at all. It is hoped that the errors resulting from inaccuracies in evaluating drainage-region shapes will be in both directions and will tend to be self-cancelling on an over-all reservoir basis.

6.3 Estimating Drainage-Region Average Pressure

In his classic paper, Horner[3] presented a method for estimating average or initial reservoir pressure in an infinite system. That technique provides realistic estimates of average pressure for tests with short production periods, such as drillstem tests (see Chapter 8). Horner stated, however, that the extrapolation method does not apply to closed or multiple-well systems without correction. He said that, in closed, single-well reservoirs, the average pressure generally would be below the extrapolated false pressure, p^*, shown in Fig. 6.1. In fact, $\bar{p}$ is usually less than p^*, but it may be greater than p^* in highly skewed drainage shapes. This section presents several methods for using observed pressure-buildup data to estimate drainage-region average pressures. Those drainage-region average pressures then may be used to estimate a volumetrically weighted average reservoir pressure, as outlined in Section 6.2.

Matthews-Brons-Hazebroek Method

In 1954, Matthews, Brons, and Hazebroek[4] presented a technique for estimating average reservoir pressure from buildup tests in bounded drainage regions. The limitations of the method result from assumptions of no variation in drainage region, fluid mobility, or fluid compressibility. However, those limitations can be overcome effectively in multiple-well reservoirs (as discussed in Section 5.2 and later in this section) by using a production time, t_p, equal to t_{pss} rather than the longer actual production time. The Matthews-Brons-Hazebroek (MBH) technique does provide a way to estimate $\bar{p}$ for a well in almost any position within a variety of bounded drainage shapes. In using the method, the engineer ideally would divide the reservoir into drainage *areas*. Such division can be quite time-consuming, so nominal drainage regions based on well spacing or some other convenient parameter are often used in practice. When that is done, it should be recognized that significant differences in late-time buildup-curve appearance can result from unusually shaped drainage regions (normally, a result of high degrees of production imbalance or very irregular well spacing). Such circumstances could justify more precise evaluation of drainage-area shape as outlined in Section 6.2 and by Matthews, Brons, and Hazebroek,[4] depending on the intended use of the resulting average pressures.

To estimate drainage-volume average pressure by the MBH method, first extrapolate the Horner pressure-buildup plot (Section 5.2) to obtain the false pressure, p^* (Fig. 6.1). (Or p^* may be estimated from the Miller-Dyes-Hutchinson plot and Eq. 5.14). Then, average pressure is estimated from

$$\bar{p} = p^* - \frac{m}{2.3025}\, p_{DMBH}(t_{pDA}), \quad \ldots\ldots\ldots\ldots (6.2)$$

where m is from the slope of the Horner (or Miller-Dyes-Hutchinson) straight line, Eq. 5.5:

$$m = \frac{162.6\,qB\mu}{kh} \quad \ldots\ldots\ldots\ldots\ldots\ldots\ldots\ldots\ldots\ldots (6.3)$$

In Eq. 6.2, $p_{D\text{MBH}}(t_{pDA})$ is the MBH dimensionless pressure determined at the dimensionless time corresponding to t_p:

$$t_{pDA} = \frac{0.0002637\,kt_p}{\phi\mu c_t A} \quad \ldots\ldots\ldots\ldots\ldots\ldots\ldots\ldots\ldots\ldots (6.4)$$

Figs. 6.2 through 6.5 give MBH dimensionless pressures for several drainage-area shapes and well locations.

As in the normal Horner analysis technique, we have assumed that the well produces at constant rate q from time zero to t_p, when the well is shut in for buildup testing. If the rate is not constant, t_p is estimated as discussed in Section 5.2 (before Eq. 5.9). In such a case, one normally estimates t_p from Eq. 5.9:

$$t_p = \frac{24\,V_p}{q} \quad \ldots\ldots\ldots\ldots\ldots\ldots\ldots\ldots\ldots\ldots\ldots\ldots (6.5)$$

where V_P is the cumulative volume produced since the *last pressure equalization* and q is the constant rate just before shut-in. Cumulative production from the last pressure survey is normally used because it is convenient. The important fact is that the Horner plot is based on superposition for an infinite-acting system, both *before* and *after* shut-in. If the system is not infinite-acting before shut-in, that must be considered in analysis, and either t_p or the analysis technique must be modified. The $p_{D\text{MBH}}$ values from Figs. 6.2 through 6.5 include such a consideration.

Pinson[5] and Kazemi[6] indicate that t_p should be compared with the time required to reach pseudosteady state:

$$t_{pss} = \frac{\phi\mu c_t A}{0.0002637\,k}(t_{DA})_{pss} \quad \ldots\ldots\ldots\ldots\ldots\ldots\ldots (6.6)$$

$(t_{DA})_{pss} \simeq 0.1$ for a symmetric closed square or circle with the well at the center and is given in the "Exact for $t_{DA} >$" column of Table C.1 for other shapes. If $t_p >> t_{pss}$, then t_{pss} should ideally replace t_p both for the Horner plot and in Eqs. 6.2 and 6.4 for use with the MBH dimensionless-pressure curves, Figs. 6.2 through 6.5.

Practically, substituting t_{pss} for a t_p usually will not significantly improve estimates of static pressure unless t_p is greater than about five to ten times t_{pss}, although results are relatively more sensitive with high rates. As discussed in Chapter 5, for a closed boundary condition, use of t_{pss} with the Horner method can increase the duration of the semilog straight line as opposed to an MDH plot, and may sometimes be a justification for a Horner plot using t_{pss} in place of t_p, where t_p is only 1.5 to 2 times t_{pss}.

Because of compensating factors (lower value of p^* and corresponding smaller correction), any value of t_p used with the Matthews-Brons-Hazebroek approach theoretically will give identical results for average pressure.[5] Practically, a relatively short t_p can eliminate serious numerical errors in calculated static pressures. That includes errors caused by long extrapolations and deviations from theoretical assumptions, such as (1) lack of rate stabilization before shut-in; (2) migration and changing drainage areas in multiple-well reservoirs; and (3) time variations in system compressibility and mobility.

Example 6.1 Average Drainage-Region Pressure—Matthews-Brons-Hazebroek Method

We use the pressure-buildup test data of Examples 5.1 through 5.3 (Table 5.1). Pressure buildup data are plotted in Figs. 5.3 and 5.4. Other data are

$\phi = 0.09$
$c_t = 22.6 \times 10^{-6}$ psi^{-1}
$k = 12.8$ md (Example 5.1)
$\mu = 0.20$ cp
$m = 40$ psig/cycle (Fig. 5.4)
$t_p = 310$ hours
$A = \pi r_e^2 = \pi(2{,}640)^2$ sq ft.

To see if we should use $t_p = 310$ hours, we estimate t_{pss} from Eq. 6.6 using $(t_{DA})_{pss} = 0.1$ from Table C.1:

$$t_{pss} = \frac{(0.09)(0.2)(22.6 \times 10^{-6})(\pi)(2{,}640)^2(0.1)}{(0.0002637)(12.8)}$$

$$= 264 \text{ hours.}$$

Thus, we could replace t_p by 264 hours in the analysis. However, since t_p is only about 1.17 t_{pss}, we expect no difference in $\bar{p}$ from the two methods,[6] so we use $t_p = 310$ hours. As a result, Fig. 5.4 applies.

Fig. 5.4 does not show p^* since $(t_p + \Delta t)/\Delta t$ does not go to 1.0. However, we may compute p^* from p_{ws} at $(t_p + \Delta t)/\Delta t = 10$ by extrapolating one cycle:

$$p^* = 3{,}325 + (1 \text{ cycle})(40 \text{ psi/cycle})$$

$$= 3{,}365 \text{ psig.}$$

Using Eq. 6.4,

$$t_{pDA} = \frac{(0.0002637)(12.8)(310)}{(0.09)(0.20)(22.6 \times 10^{-6})(\pi)(2{,}640)^2}$$

$$= 0.117.$$

From the curve for the circle in Fig. 6.2, $p_{D\text{MBH}}(t_{pDA} = 0.117) = 1.34$. Eq. 6.2 gives the average pressure:

$$\bar{p} = 3{,}365 - \frac{40}{2.3025}(1.34)$$

$$= 3{,}342 \text{ psig.}$$

This is 19 psi higher than the maximum pressure recorded.

Dietz Method

Dietz[7] presents a slightly different approach for estimating $\bar{p}$. He suggests extrapolating the straight-line portion of an MDH plot (p_{ws} vs log Δt) directly to $\bar{p}$. The Dietz approach assumes that the well has been produced at a constant rate long enough to reach pseudosteady state before shut-in,[7] and that a semilog straight line of appropriate slope will develop (for wells that are not highly stimulated, $s > -3$). Dietz determined the time when $\bar{p}$ may be read *directly* from the extrapolated semilog straight line:

$$(\Delta t)_{\bar{p}} = \frac{t_p}{C_A t_{pDA}} = \frac{\phi\mu c_t A}{0.0002637\,C_A k} \quad \ldots\ldots\ldots (6.7a)$$

For a well centrally located in a closed-square drainage area, $C_A = 30.8828$, so

$$(\Delta t)_{p_{\text{square}}} = 122.8\,\frac{\phi\mu c_t A}{k} \quad \ldots\ldots\ldots\ldots\ldots (6.7b)$$

For other shapes, the shape factor, C_A, is taken from Table

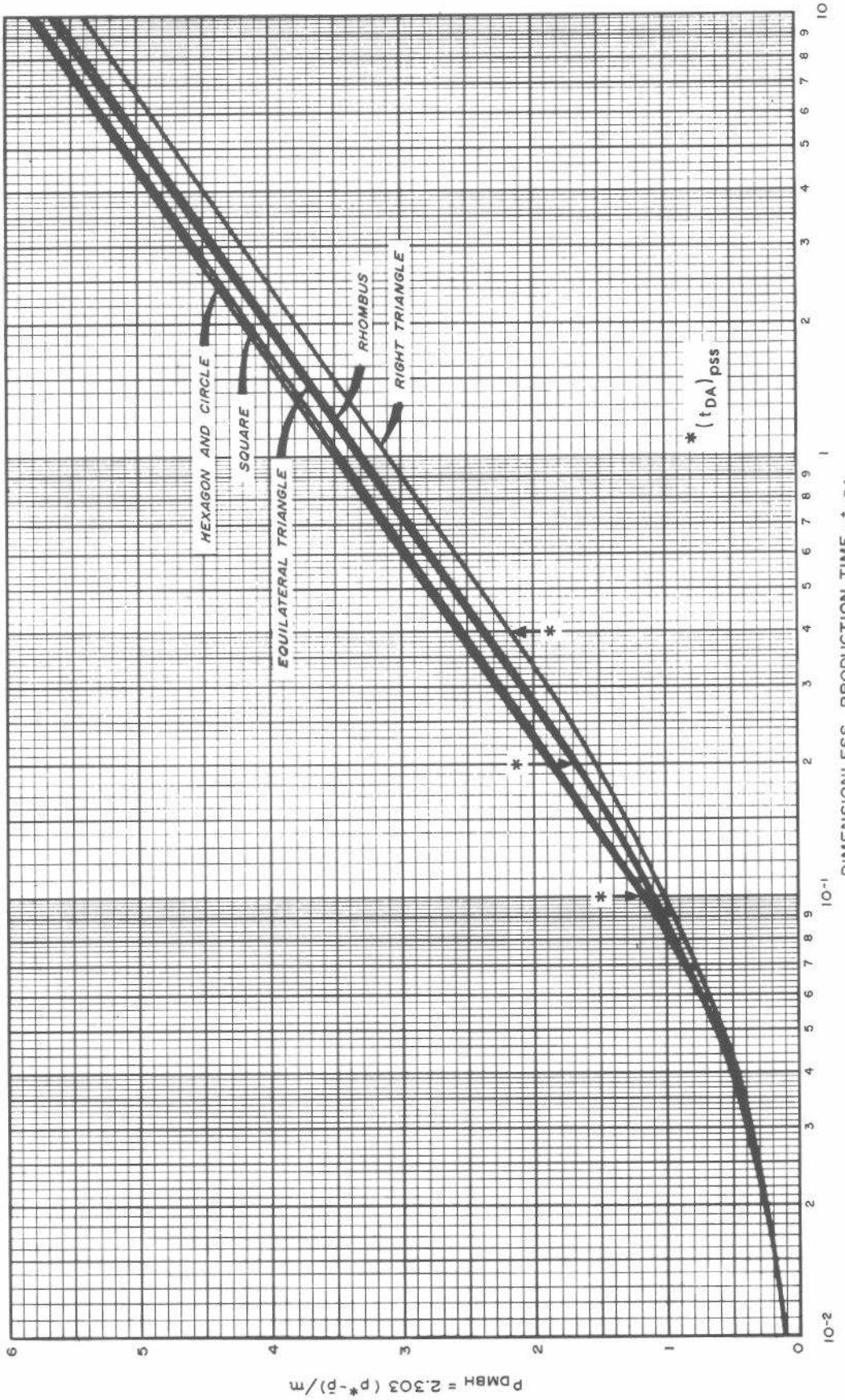

Fig. 6.2 Matthews-Brons-Hazebroek dimensionless pressure for a well in the center of equilateral drainage areas. After Matthews, Brons, and Hazebroek.[4]

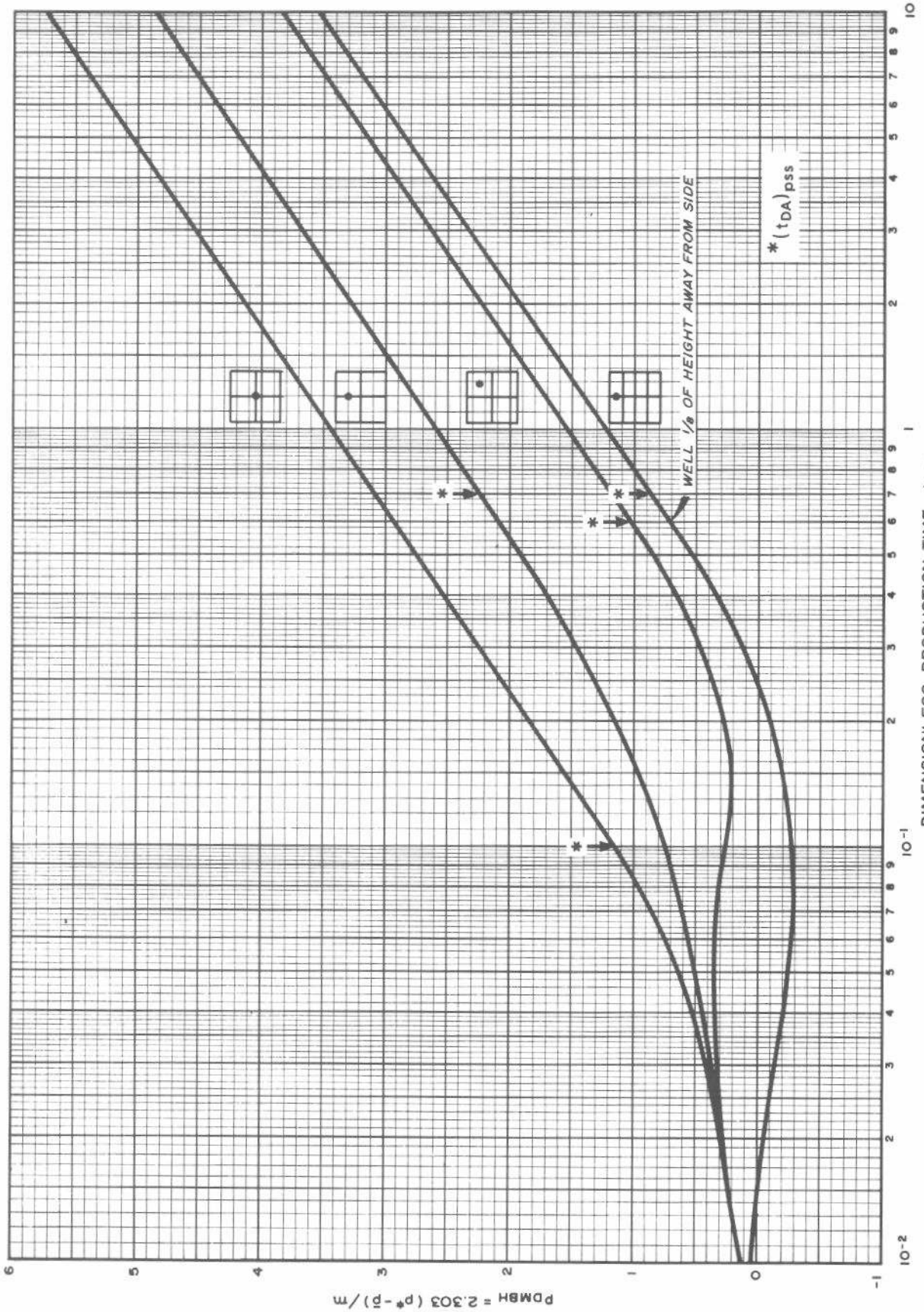

Fig. 6.3 Matthews-Brons-Hazebroek dimensionless pressure for different well locations in a square drainage area. After Matthews, Brons, and Hazebroek.[1]

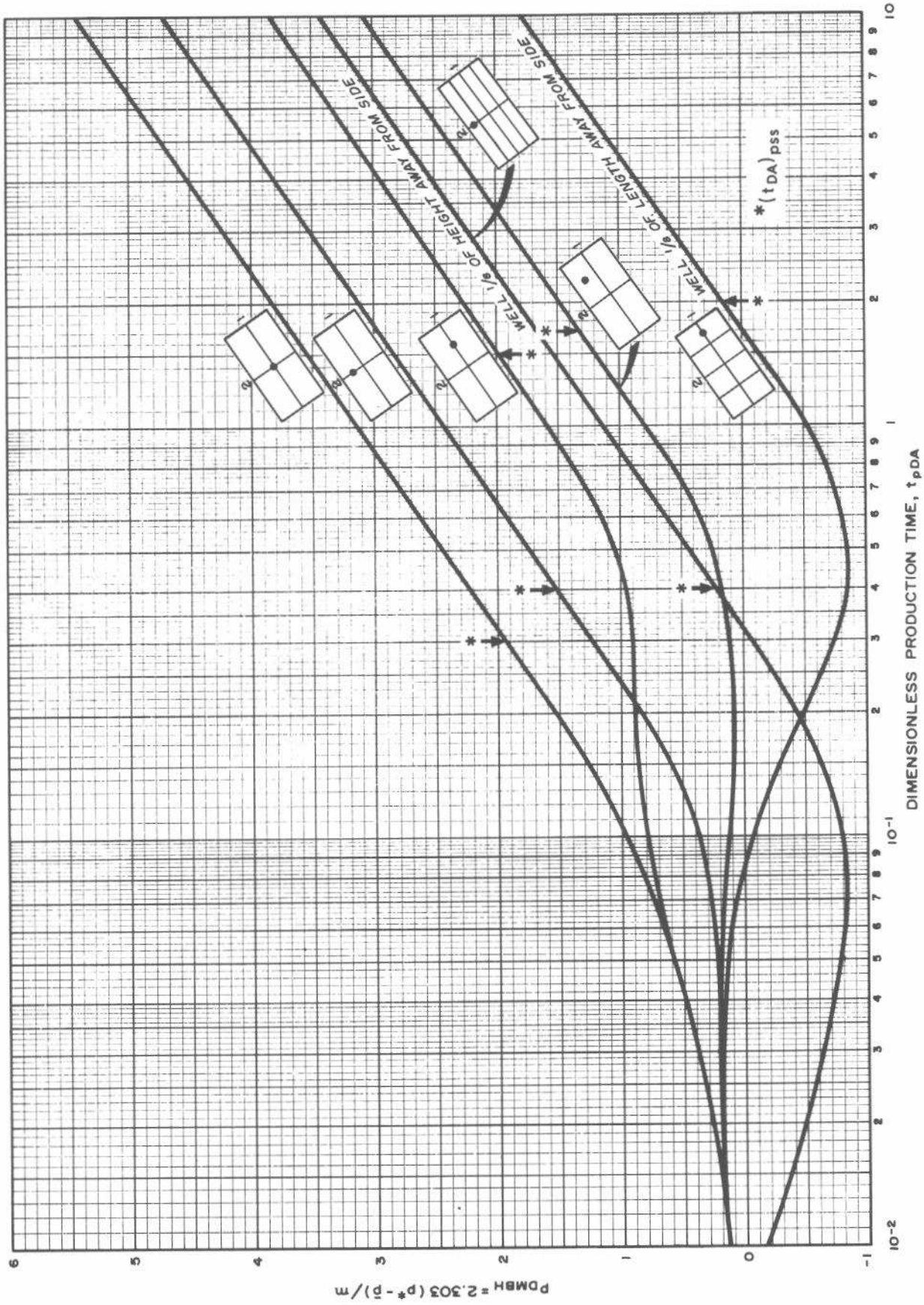

Fig. 6.4 Matthews-Brons-Hazebroek dimensionless pressure for different well locations in a 2:1 rectangular drainage area. After Matthews, Brons, and Hazebroek.[4]

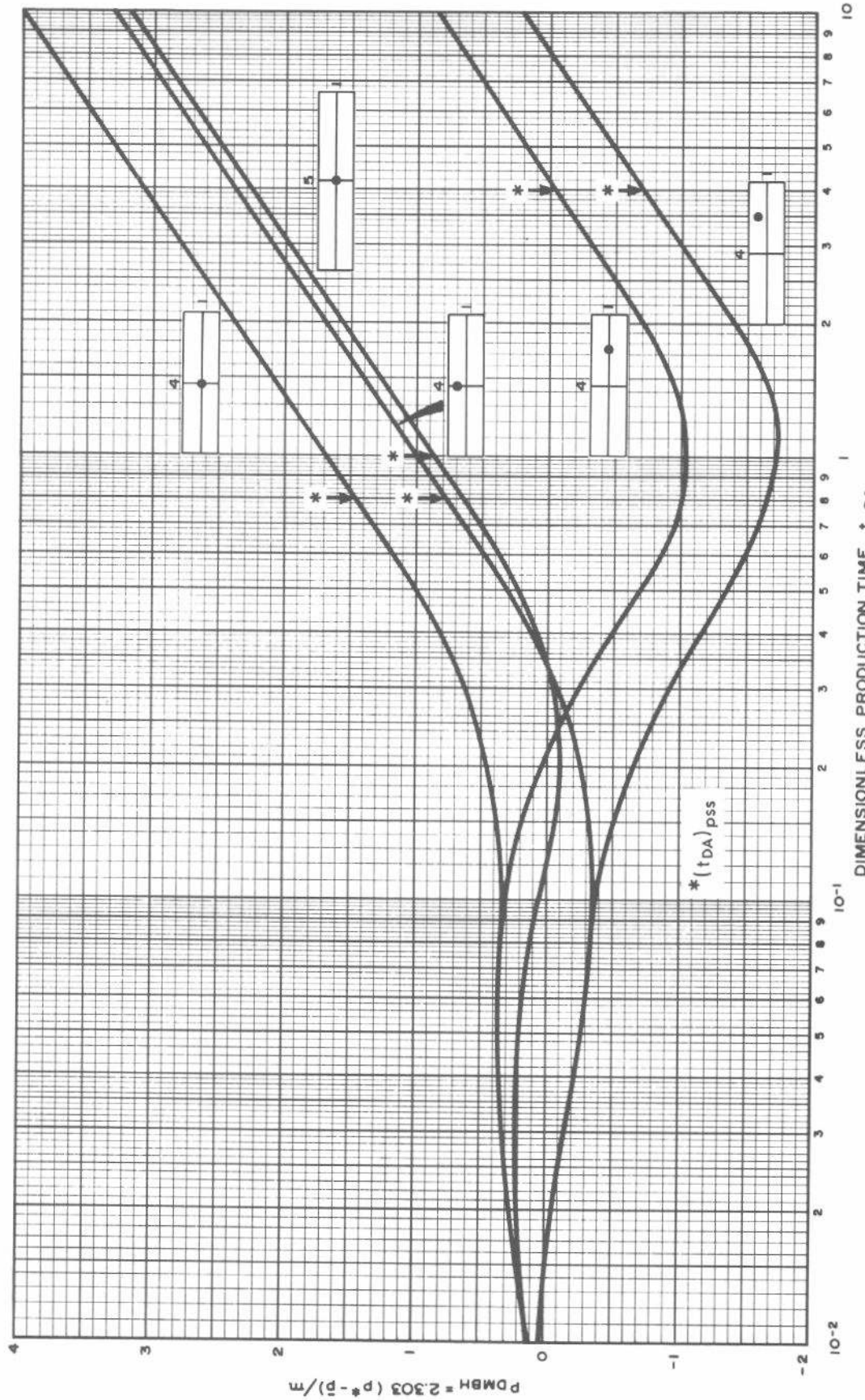

Fig. 6.5 Matthews-Brons-Hazebroek dimensionless pressure for different well locations in 4:1 and 5:1 rectangular drainage areas. After Matthews, Brons, and Hazebroek.[4]

C.1. The Dietz method has the advantage of being quick and simple, and usually is the preferred method for wells without a significant skin factor ($s > -3$ or $r_{wa} < 0.05\,r_e$) caused by acidizing or fracturing.

Ramey and Cobb[8] describe a method for extrapolating a *Horner plot* straight line to average reservoir pressure. For $t_p \geq t_{pss}$, they show that

$$\left(\frac{t_p + \Delta t}{\Delta t}\right)_{\bar{p}} = C_A t_{pDA} = \frac{0.0002637\,kt_pC_A}{\phi\mu c_t A} \quad \ldots\ldots (6.8a)$$

For a centrally located well in a closed-square drainage area, $C_A = 30.8828$ and

$$\left(\frac{t_p + \Delta t}{\Delta t}\right)_{\bar{p}} = \frac{0.008144\,kt_p}{\phi\mu c_t A} \quad \ldots\ldots (6.8b)$$

Eq. 6.8 reduces to Eq. 6.7 when $(t_p + \Delta t) \simeq t_p$. When $t_p < t_{eia}$, which may be estimated from Eq. 2.8, Ramey and Cobb show[8]

$$\left(\frac{t_p + \Delta t}{\Delta t}\right)_{\bar{p}} = e^{4\pi t_{pDA}} \quad \ldots\ldots (6.9)$$

The Matthews-Brons-Hazebroek,[4] Dietz,[7] and Ramey-Cobb[8] methods for estimating average reservoir pressure require a certain amount of knowledge about the drainage region. In particular, one must be able to approximate the boundary shape and well location and know that the boundary is effectively a no-flow boundary at the time the well is shut in. In many cases, one does not have such information with any degree of accuracy. Fortunately, under most circumstances it is permissible to assume a regular drainage shape based on the well pattern and use that when estimating average reservoir pressure with any of the three methods.

Example 6.2 Average Drainage-Region Pressure—Dietz Method

We again use the buildup test of Examples 5.1 through 5.3 and Example 6.1. Pertinent data are given in Example 6.1. The shape factor, C_A, for a closed circular reservoir is 31.62 (Table C.1). Using Eq. 6.7a,

$$(\Delta t)_{\bar{p}} = \frac{(0.09)(0.20)(22.6 \times 10^{-6})(\pi)(2{,}640)^2}{(0.0002637)(12.8)(31.62)}$$

$$= 83.5 \text{ hours.}$$

The MDH plot, Fig. 5.8, does not extend to 83.5 hours, but the straight line may be extrapolated to that time. From Fig. 5.8, $p_{ws} = 3{,}302$ psig at 8.35 hours, so extrapolating 1 cycle to 83.5 hours,

$$\bar{p} = 3{,}302 + (1 \text{ cycle})(40 \text{ psig/cycle})$$

$$= 3{,}342 \text{ psig,}$$

the result obtained in Example 6.1.

The equation proposed by Ramey and Cobb,[8] Eq. 6.8a, also may be used:

$$\left(\frac{t_p + \Delta t}{\Delta t}\right)_{\bar{p}} = \frac{(0.0002637)(12.8)(310)(31.62)}{(0.09)(0.20)(22.6 \times 10^{-6})(\pi)(2{,}640)^2}$$

$$= 3.71.$$

Extrapolating the Horner-plot straight line from 37.1 to 3.71 (Fig. 5.4) gives

$$\bar{p} = 3{,}302 + (1 \text{ cycle})(40 \text{ psig/cycle})$$

$$= 3{,}342 \text{ psig.}$$

Miller-Dyes-Hutchinson Method

Miller, Dyes, and Hutchinson[9] published a technique for estimating $\bar{p}$ for closed circular drainage regions from the MDH data plot (p_{ws} vs log Δt). The MDH average reservoir-pressure analysis method applies directly only to wells operating at pseudosteady state before the buildup test. (Ramey and Cobb[8] show how to use the MDH method for a closed square drainage region when $t_p < t_{pss}$.)

To use the MDH method to estimate average drainage-region pressure for a circular or square system producing at pseudosteady state before shut-in, choose *any convenient time* on the *semilog straight line*, Δt, and read the corresponding pressure, p_{ws}. Then calculate the dimensionless shut-in time based on the drainage area:

$$\Delta t_{DA} = \Delta t_D \left(\frac{r_w^2}{A}\right) = \frac{0.0002637\,k(\Delta t)}{\phi\mu c_t A} \quad \ldots\ldots (6.10)$$

That dimensionless time is used with the upper curve of Fig. 6.6 to determine an MDH dimensionless pressure, $p_{D\text{MDH}}$. (Note that Fig. 6.6 is based on Δt_{DA} rather than on Δt_{De}, as is commonly done. That allows inclusion of the square systems.) The average reservoir pressure in the closed drainage region is estimated from

$$\bar{p} = p_{ws} + \frac{m\,p_{D\text{MDH}}(\Delta t_{DA})}{1.1513} \quad \ldots\ldots (6.11)$$

In Eq. 6.11, p_{ws} is the pressure read from the MDH semilog straight line at any convenient shut-in time, Δt, and $p_{D\text{MDH}}$ is taken from the upper curve in Fig. 6.6 for the same Δt. The lower curves in Fig. 6.6 apply for estimating boundary pressures, p_e, in water-drive reservoirs and are discussed in Section 6.4.

Example 6.3 Average Drainage-Region Pressure—Miller-Dyes-Hutchinson Method

We consider the same buildup test as in Examples 6.1 and 6.2. The drainage area of the well is approximated by a circle with $r_e = 2{,}640$ ft. We choose $\Delta t = 20$ hours on the straight-line section of the MDH buildup curve in Fig. 5.8. From Eq. 6.10,

$$\Delta t_{DA} = \frac{(0.0002637)(12.8)(20)}{(0.09)(0.20)(22.6 \times 10^{-6})(\pi)(2{,}640)^2}$$

$$= 0.0076.$$

From the upper curve in Fig. 6.6, $p_{D\text{MDH}}$ at $\Delta t_{DA} = 0.0076$ is 0.78. From Fig. 5.8, p_{ws} at $\Delta t = 20$ hours is 3,317 psig and $m = 40$ psig/cycle. Then, using Eq. 6.11,

$$\bar{p} = 3{,}317 + (40)(0.78)/1.1513$$

$$= 3{,}344 \text{ psig.}$$

This compares with an average reservoir pressure of 3,342 psig estimated by the other methods.

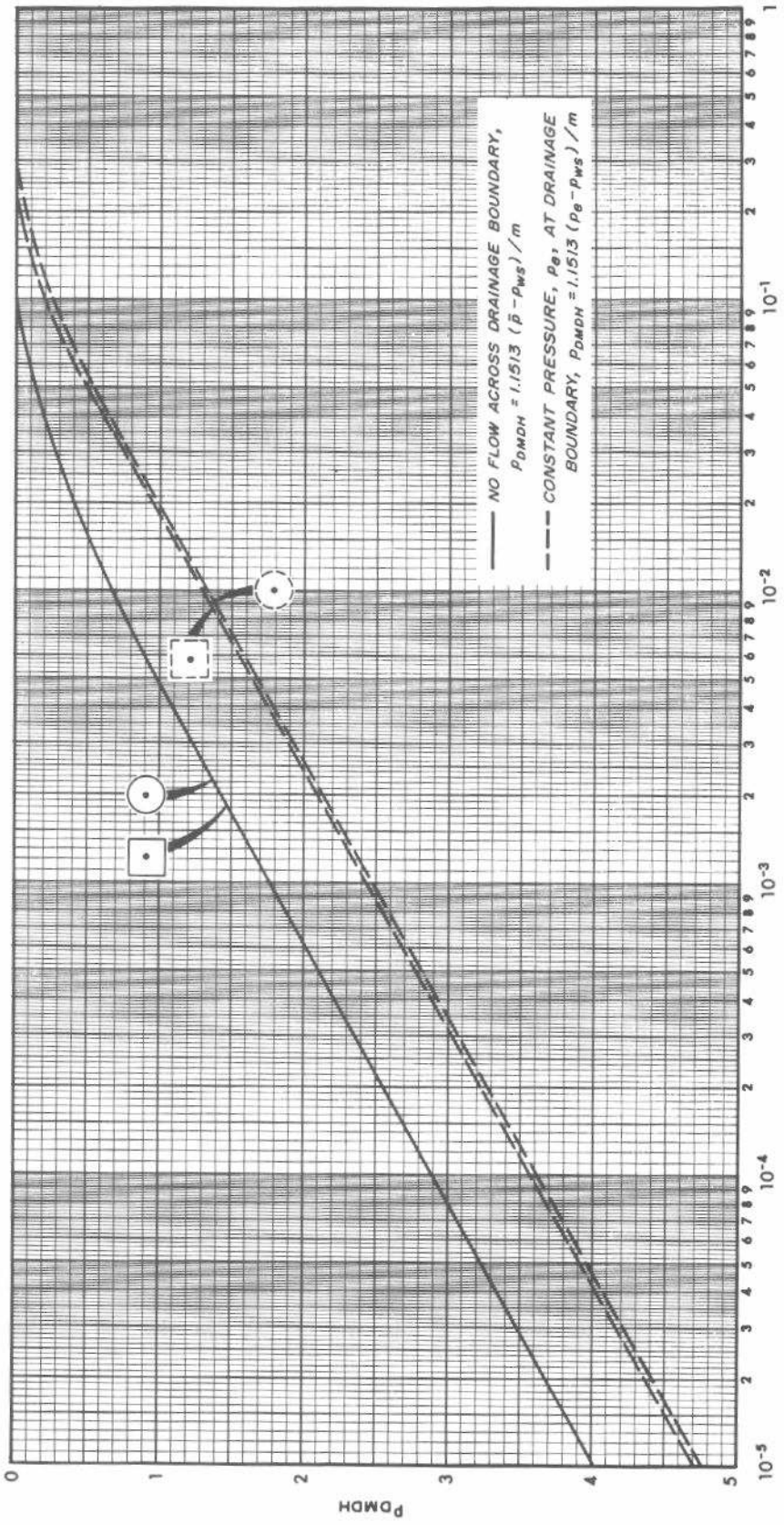

Fig. 6.6 Miller-Dyes-Hutchinson dimensionless pressure for circular and square drainage areas. Data of Miller, Dyes, and Hutchinson,[9] Perrine,[10] and Kumar and Ramey.[11]

Correcting Spot Pressure Readings to Average Drainage-Region Pressure

There are a surprising number of situations where a single pressure point, or "spot pressure," is the only pressure information available about a well. In older fields, the areal and chronological pressure coverage often consists only of spot readings. Brons and Miller[12] show two ways to estimate average pressure for single-well, closed drainage areas from such measurements. Their method is similar to the Dietz method in that it assumes the wells are producing at pseudosteady state before shut-in. It also assumes that the spot pressure measurement falls on the semilog straight-line portion of the buildup curve (that is, it is between the wellbore- and boundary-effects portions of the buildup curve). The technique requires knowledge or reasonable estimates of the shut-in time when pressure was measured, the flow rate, formation thickness, formation volume factor, fluid viscosity, and drainage-region shape and well location. Two approaches can be used. In the first, an estimate of formation permeability is required. When that approach is used, average drainage-region pressure is estimated from the spot pressure reading at shut-in time, Δt, using

$$\bar{p} = p_{ws}(\Delta t) + \frac{162.6\,qB\mu}{kh} \log\left(\frac{1}{\Delta t_{DA}\,C_A}\right), \quad \ldots\ldots\ldots\ldots\ldots\ldots (6.12a)$$

or

$$\bar{p} = p_{ws}(\Delta t) + \frac{162.6\,qB\mu}{kh} \log\left(\frac{\phi\mu c_t A}{0.0002637\,k\,\Delta t\,C_A}\right). \quad \ldots\ldots\ldots\ldots\ldots\ldots (6.12b)$$

For a closed square drainage region, $C_A = 30.8828$ and

$$\bar{p} = p_{ws}(\Delta t) + \frac{162.6\,qB\mu}{kh} \log\left(\frac{122.8\,\phi\mu c_t A}{k\,\Delta t}\right). \quad \ldots\ldots\ldots\ldots\ldots\ldots (6.12c)$$

Note that Eq. 6.12 is independent of skin factor or apparent wellbore radius. However, it should not be expected to apply when $s < -3$.

If an estimate of permeability is not available, another approach may be used. That approach does have the drawback of requiring knowledge of both the skin factor (or apparent wellbore radius) and the flowing pressure before shut-in. Brons and Miller[12] showed that the k/μ term could be eliminated, so

$$\log\left(\frac{qB}{h}\right) = \log\left[(\bar{p} - p_{ws}) + (p_{ws} - p_{wf})\right] + \log\left(\frac{23.32\,\phi c_t A}{C_A f}\right) - \log(\Delta t) - \frac{f(\bar{p} - p_{ws})}{(\bar{p} - p_{ws}) + (p_{ws} - p_{wf})}, \quad \ldots\ldots (6.13a)$$

where

$$f = \log\left(\frac{2.2458\,A}{r_w^2\,C_A}\right) + 0.86859\,s. \quad \ldots\ldots\ldots (6.13b)$$

Unfortunately, solving Eq. 6.13 for $\bar{p}$ is difficult without a computer, or at least a programmable calculator. Brons and Miller suggested a graphical approach. Fig. 6.7 is a graphical representation of Eq. 6.13a (although different from the one proposed by Brons and Miller[12]). That figure applies only for the reservoir properties indicated on it, but the technique is general. To estimate $\bar{p}$, choose values for the reservoir properties indicated in Fig. 6.7 and calculate qB/h for a series of assumed values of $(p_{ws} - p_{wf})$ and $(\bar{p} - p_{ws})$. Once a figure like Fig. 6.7 has been constructed, qB/h and $(p_{ws} - p_{wf})$ are entered to determine $\bar{p} - p_{ws}$ (and, thus, $\bar{p}$). Fig. 6.7 is shown only for illustrative purposes; it is not meant to apply for general analyses.

Typical or average values for compressibility, porosity, and shape factor (commonly 30.8 to 31.6) often can be used with acceptable accuracy in the Brons-Miller technique in a given field situation. That is especially true since only average pressure in the vicinity of the well is usually desired for contouring. Engineering judgment is involved in any simplification and allowances should always be made for major changes in compressibility and mobility. Thus, λ_t and c_t should be used for multiple-phase reservoir flow, as indicated in Section 2.11. Normally, one or several simple graphs similar to Fig. 6.7 (for different skin factors) can be constructed for a given reservoir. Then, average pressure

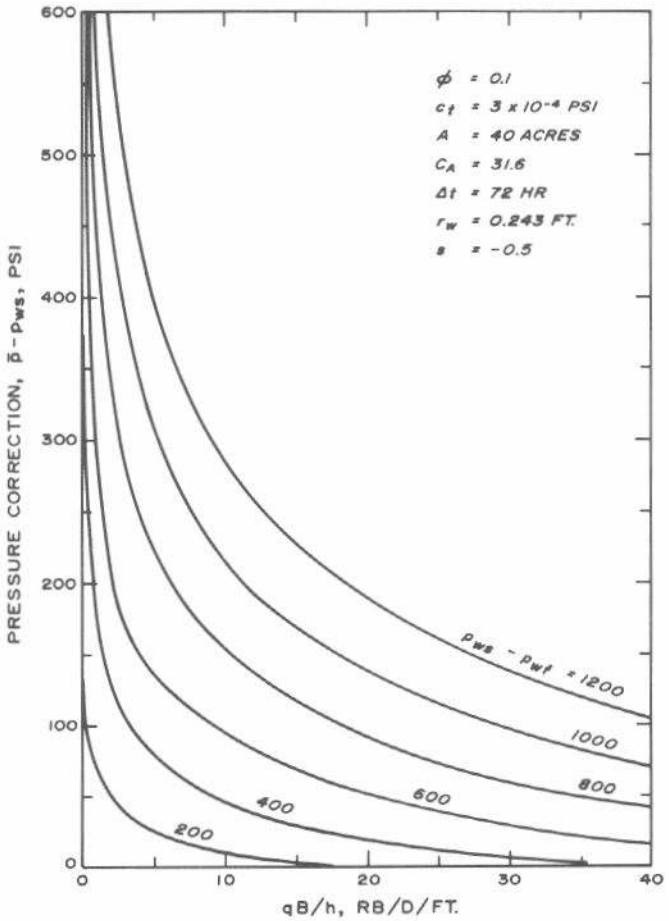

Fig. 6.7 Graph for estimating correction to a spot pressure reading to estimate average reservoir pressure. Brons-Miller[12] data and method.

may be estimated using the equivalent of Fig. 6.7, or Eq. 6.13a may be used with actual data. Of course, if an estimate of mobility is available, Eq. 6.12 may be used, thus greatly simplifying the analysis.

The method of Eq. 6.13a and Fig. 6.7 does not require knowledge of k/μ because that has been implicitly developed from previous flow rate and observed pressure data. The merit of such an approach is that it offers a way to correct spot pressure readings to average drainage-region pressures with limited data. The major disadvantages are the inherent inaccuracy in the implicitly estimated k/μ and that skin factor must be estimated.

An approach somewhat similar to the Brons-Miller approach may be devised that uses the MDH dimensionless pressure. To use that approach, we write the expression for k/μ used implicitly by Brons and Miller:[12]

$$\frac{k}{\mu} = \frac{162.6\,qB}{(p_{ws} - p_{wf})h} f, \quad \ldots\ldots\ldots\ldots\ldots\ldots\ldots (6.14)$$

where f is given by Eq. 6.13b. In Eq. 6.14, p_{ws} is the observed spot-pressure reading and, *for purposes of this equation,* is taken to be equivalent to the average reservoir pressure. We assume that p_{ws} is on the semilog straight line and use the MDH method to estimate average reservoir pressure. Thus, Eq. 6.11,

$$\bar{p} = p_{ws} + \frac{m\,p_{D\,\mathrm{MDH}}(\Delta t_{DA})}{1.1513}, \quad \ldots\ldots\ldots\ldots\ldots\ldots (6.11)$$

is used to estimate $\bar{p}$. To obtain $p_{D\,\mathrm{MDH}}$, use Fig. 6.6 where Δt_{DA} is estimated from

$$\Delta t_{DA} \simeq \frac{(0.0002637)(162.6\,qB)f}{(p_{ws} - p_{wf})\,h\phi c_t A}\,\Delta t, \quad \ldots\ldots\ldots (6.15a)$$

$$\simeq \frac{0.04288\,qBf}{(p_{ws} - p_{wf})\,h\phi c_t A}\,\Delta t, \quad \ldots\ldots\ldots\ldots (6.15b)$$

and p_{ws} is the shut-in pressure observed at time Δt; f is given by Eq. 6.13b. The slope used in Eq. 6.11 is estimated from

$$m = \frac{p_{ws} - p_{wf}}{f}. \quad \ldots\ldots\ldots\ldots\ldots\ldots\ldots (6.16)$$

It should be clear that $\bar{p}$ estimated by this method is only an approximation, and applies only to a circular or square drainage region. If there is a significant difference between $\bar{p}$ and p_{ws}, a second iteration should be made. In that iteration, the value for $\bar{p}$ just estimated replaces p_{ws} in Eqs. 6.15 and 6.16. Then, a new value of $p_{D\,\mathrm{MDH}}$ can be obtained from Fig. 6.6 and a second estimate of $\bar{p}$ can be made using Eq. 6.11. Normally, a second iteration is not warranted, given the imprecision of other data used. Note that the f term in Eqs. 6.14 through 6.16 does depend on drainage area, wellbore radius, skin factor, and shape factor.

The Extended Muskat Method

As indicated in Section 5.3, Muskat[13] showed that a plot of $\log(\bar{p} - p_{ws})$ vs Δt should give a straight line that can be used for analyzing pressure buildup data. That plot uses late-time pressure data corresponding to the curved tail-end seen on the Horner and MDH plots when the well is shut in long enough. The Muskat technique has been discussed and extended by others.[8,14,15] Section 5.3 explains the technique for estimating permeability and average reservoir pressure. The extended Muskat analysis applies for any length of producing time before shut-in, but requires very long shut-in times for the straight line to develop. Thus, the straight line is frequently not observed. Fig. 5.11 and Eq. 5.21 may be used to estimate the physical time range during which the Muskat straight line will occur. Example 5.3 illustrates the Muskat analysis technique for the data of Examples 6.1 through 6.3. For those examples, shut-in time was insufficient to develop the correct Muskat straight line, so an incorrect result was obtained.

Other Methods

Based on Muskat's work, Arps and Smith[16] suggest plotting dp_{ws}/dt vs p_{ws} during the late-transient buildup period to estimate average reservoir pressure. The plot should yield a straight line that, when extrapolated to zero, provides an estimate of $\bar{p}$. When applicable, the Arps-Smith technique should give reliable results. However, it suffers from the same problem as the Muskat technique: it requires a very long shut-in period.

Recommended Methods

In general, the Matthews-Brons-Hazebroek method for estimating average reservoir pressure can be expected to give the most reliable results for a variety of drainage shapes and production times, providing a t_p on the order of t_{pss} is used where production time is large. It is superior to the other methods discussed in its flexibility and is the only method that encompasses the entire range of t_p from infinite-acting through pseudosteady state. The Dietz-type methods of Eqs. 6.7 through 6.9 are also valid when production is at pseudosteady state before shut-in. The Dietz method appears to be the more practical for routine engineering application except for a short period immediately after well completion. For wells with a skin factor more negative than about -3, both methods require further modification since the correct semilog straight line may not develop for normal data plots (see Chapter 11).

Dynamic Pressure Used for Numerical Reservoir Simulation

One current common use of reservoir pressure data is for comparison with numerical simulator results during a history-matching process.[17] The pressure computed by a reservoir simulator to be compared with reservoir pressure is not usually a well's drainage-region average pressure. Rather, it is the average pressure of the *node* (grid block) that contains the well in the reservoir simulator.[17] The corresponding reservoir pressure may be estimated from pressure buildup tests by extrapolating the semilog straight line to the correct time and directly reading the "dynamic" pressure. The time is given by[17]

$$\Delta t_{\mathrm{dyn}} = \frac{200\,\phi c_t \Delta x^2}{(k/\mu)_t}, \quad \ldots\ldots\ldots\ldots\ldots\ldots (6.17)$$

where Δx is the length of the side of a square node in the reservoir simulator. Although Eq. 6.17 assumes that the well is in the center of a square node that is relatively small with respect to the well's drainage region, the equation may be used with reasonable accuracy for wells slightly off center in rectangular nodes. In that case, Δx^2 is replaced by $\Delta x \Delta y$, the product of the length and width of the node.

If a complete pressure buildup curve is not available, Eq. 6.17 cannot be used directly. However, if a single (spot) shut-in pressure reading is available for the well and that pressure point is assumed to be on the semilog straight line, Eq. 6.17 still may be used in modified form, and the dynamic pressure may be estimated from[18]

$$(p_{ws})_{dyn} = (p_{ws})_{OB} + \frac{162.6\, qB}{(k/\mu)_t\, h} \log\left(\frac{200\, \phi c_t \Delta x^2}{(k/\mu)_t\, (\Delta t)_{OB}}\right). \quad \ldots\ldots\ldots\ldots\ldots\ldots (6.18)$$

Eq. 6.18 assumes that a reasonable value of total mobility is known. It should be used only when no better method is available for estimating the dynamic pressure for history-matching purposes. Clearly, the approach of Eq. 6.18 could be modified to be similar to the Brons-Miller method, thus eliminating the need for an estimate of k/μ.

6.4 Water-Drive Reservoirs

Water-drive reservoirs (that is, reservoirs in direct communication with an active aquifer) behave quite differently from closed reservoirs, particularly with respect to well drainage regions and flow patterns. Water-drive reservoirs range from those with complete pressure maintenance (equivalent to a constant pressure at the reservoir aquifer boundary with a nearby replenishable outcrop) to those that provide only a small amount of water influx to the producing reservoir. The analysis techniques in this section apply only to those edge water-drive reservoirs that provide complete pressure maintenance. In practice, pressure at the reservoir-aquifer boundary is generally neither constant nor uniform. It changes in time as a result of (1) movement of the reservoir transient into the aquifer, (2) finite aquifer extent, and (3) interference from withdrawals or injection in the aquifer. However, the concepts presented here are usually applied when the pressure at the water-oil contact has stabilized at nearly a constant value or when further declines in field boundary pressure and internal pressure are in step so that the internal field pressure distribution is constant. Material in this section is directly applicable only to constant-compressibility and unit-mobility-ratio, water-oil systems.

Estimating Drainage Volume

Steady-state drainage regions for wells in a water-drive reservoir do not resemble drainage areas during pseudosteady-state conditions in closed systems.[1,2,19] Ramey, Kumar, and Gulati[19] have studied steady-state drainage areas in water-drive reservoirs with from 1 to 35 production wells. Two general conclusions apply to all unit-mobility-ratio reservoir-aquifer systems with constant pressure at the oil-water contact: (1) flow near each well is radial — but the radial flow pattern may not extend for a very great distance; and (2) all producing wells have *direct* communication with the constant-pressure boundary in some way. Matthews and Russell[1] suggest techniques for estimating drainage areas under water-drive conditions; Ramey, Kumar, and Gulati[19] propose more accurate techniques for idealized cases and present results for many systems. Their results for a square with constant-pressure boundaries may be most directly applicable to injection and production wells in five-spot waterfloods with near unit mobility ratio, and for nominal well drainage areas in strong water-drive reservoirs.

Fig. 6.8 shows steady-state drainage regions for a 15-well, water-drive reservoir with wells producing at different rates. While that is an extreme case, each well's drainage area does extend to the constant-pressure boundary. Because of such behavior, individual-well drainage regions in water-drive reservoirs tend to be more irregular than those in reservoirs with no influx. Similar drainage-area distortions also may occur in reservoirs with incomplete development and highly imbalanced withdrawal rates with respect to total fluids in place.

Estimating Permeability, Skin Factor, and End of the Semilog Straight Line

Pressure-buildup analysis methods for permeability and skin factor are the same for water-drive reservoirs as for closed reservoirs. Either the Horner- or the MDH-type plot may be used. The slope and p_{1hr} values from the data plot are used to estimate permeability from Eq. 5.6 and skin factor from Eq. 5.7. Kumar and Ramey[11] show that, for a square with constant-pressure boundaries (equal influx on all sides), with the well in the center, the MDH straight line lasts longer than the Horner straight line if production time before shut-in is long enough ($t_{pDA} > 0.25$). This is in contrast to the behavior of closed systems. However, because of highly irregular drainage areas, which can change

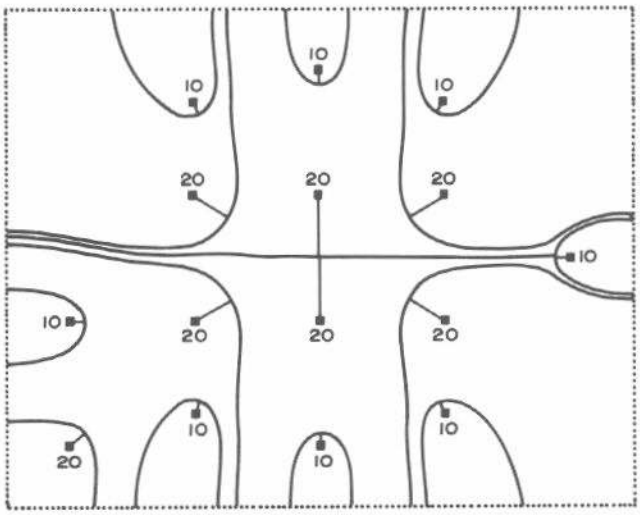

Fig. 6.8 Steady-state drainage regions for a 15-well, nonideal water-drive reservoir, wells producing at rates shown, dotted boundary at constant pressure. After Ramey, Kumar, and Gulati,[19] courtesy AGA.

fairly rapidly when a well is shut in, the semilog straight line of the infinite-acting period usually ends earlier for wells in water-drive reservoirs than for wells with no-flow boundaries. Eq. 5.16 and Figs. 5.6 and 5.7 provide a way to estimate the shut-in time when the semilog straight line ends for this system and for closed systems. The extended Muskat method may be used to estimate k by using Eq. 5.18 and Fig. 5.10. Refs. 11 and 19 give additional information, and Ref. 19 considers other fixed shapes and mixed boundary conditions.

Estimating Boundary and Average Pressure

Several pressures are important in water-drive systems, including the initial pressure and the average pressure for the hydrocarbon producing area as a function of time. In addition, the average pressure as a function of time at the original water-oil contact may be useful. In other instances, separate average pressures over some encroached area or produced inner area may be needed for past-performance matching and predictions depending on the technique used. Several techniques may be used to estimate average and boundary pressures for water-drive systems. For short production times, the Horner and Matthews-Brons-Hazebroek methods are probably the best. The Dietz and Miller-Dyes-Hutchinson methods both apply for $t_{pDA} > 0.25$ and $s > -3$. The Muskat method also applies and may have more utility for water-drive systems than for closed systems.

The *Matthews-Brons-Hazebroek* method is applied to a square with constant-pressure boundaries in much the same way as it is applied to a closed system. Pressure buildup data are plotted on semilog paper vs $[(t_p + \Delta t)/\Delta t]$. The resulting semilog straight line is extrapolated to $[(t_p + \Delta t)/\Delta t] = 1$ to obtain p^*. Then, the boundary pressure is computed from

$$p_e = p^* - \frac{m\, p_{D\,\mathrm{MBH}e}(t_{pDA})}{2.3025} \quad \ldots\ldots\ldots\ldots \quad (6.19a)$$

and the average pressure at the instant of shut-in is computed from

$$\bar{p} = p^* - \frac{m\, \bar{p}_{D\,\mathrm{MBH}}(t_{pDA})}{2.3025} \quad \ldots\ldots\ldots\ldots \quad (6.19b)$$

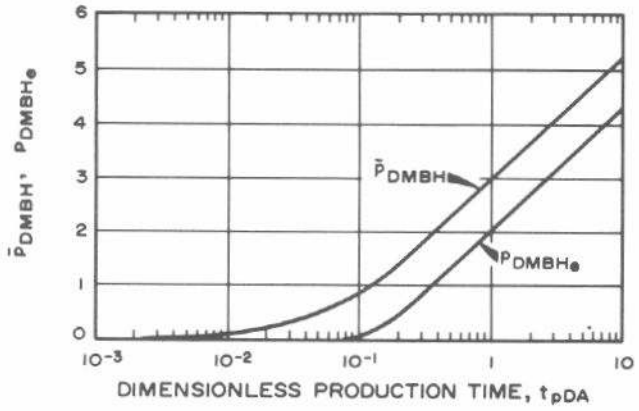

Fig. 6.9 Matthews-Brons-Hazebroek dimensionless pressures for a well in the center of a constant-pressure square. Upper curve is based on $\bar{p}$ at time of shut-in; lower curve is based on p_e, the pressure at the boundary. After Kumar and Ramey.[11]

The MBH dimensionless pressures, $p_{D\,\mathrm{MBH}e}$ and $\bar{p}_{D\,\mathrm{MBH}}$, are given in Fig. 6.9. Unfortunately, such data are not available for systems other than a well centered in a square with a constant-pressure boundary.

The *Dietz* method also may be applied to water-drive reservoirs. The semilog straight line is extrapolated to a time given by Eq. 6.7a, and $\bar{p}$ is read directly from the graph at that time. Table C.1 shows that the appropriate shape factor for a circular reservoir with constant-pressure boundaries is 19.1. Ref. 11 indicates that the shape factor for a square, constant-pressure-boundary reservoir is 19.5. Using the latter value in Eq. 6.7, the time to read $\bar{p}$ for a square system with constant-pressure boundaries from the extrapolated semilog straight line is given by

$$(\Delta t)_{\bar{p}} = 195\, \frac{\phi \mu c_t A}{k} \quad \ldots\ldots\ldots\ldots\ldots\ldots \quad (6.20)$$

Shape factors are not available for other shapes with constant-pressure boundaries. The Dietz method applies only when $t_{pDA} > 0.25$ and $s > -3$.

The *Miller-Dyes-Hutchinson* approach also may be used for water-drive systems. A normal MDH plot of buildup pressure vs log Δt is made and the system boundary pressure is then estimated from

$$p_e = p_{ws}(\Delta t) + \frac{m\, p_{D\,\mathrm{MDH}}(\Delta t_{DA})}{1.1513} \quad \ldots\ldots\ldots\ldots \quad (6.21)$$

In Eq. 6.21, $p_{ws}(\Delta t)$ is the shut-in pressure at any time, Δt, on the semilog straight line; m is from the slope of the semilog straight line; Δt_{DA} is from Eq. 6.10; and $p_{D\,\mathrm{MDH}}$ is from the dashed curve on Fig. 6.6 for either the circular or square system. The calculation technique is the same as the MDH method, Section 6.3.

The *extended Muskat method* also may be used to estimate p_e for closed systems. Kumar and Ramey[11] show empirically that this method does give valid results for p_e when late-time data are analyzed. They also state that the method seems to be more applicable in water-drive reservoirs than in closed reservoirs. The method is basically the same as described in Section 6.3. Kumar and Ramey give techniques for estimating formation permeability using the Muskat plot.

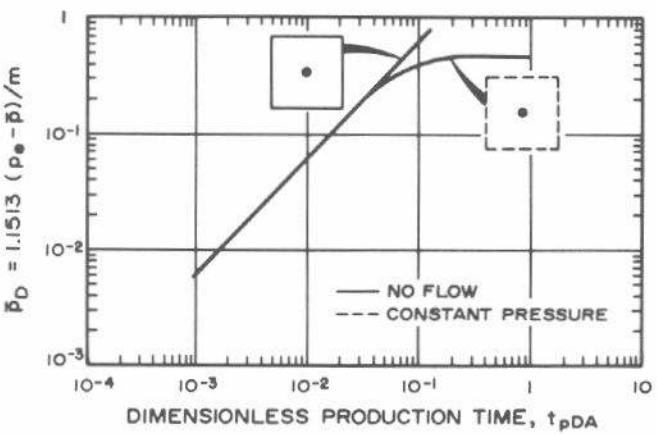

Fig. 6.10 Dimensionless average pressures for square systems. After Kumar and Ramey.[11]

Several other techniques also may be used to estimate average system pressures and boundary pressures. Given a boundary pressure, the average system pressure at the instant of shut-in may be estimated from[11]

$$\bar{p} = p_e - \frac{m\,\bar{p}_D(t_{pDA})}{1.1513}, \quad \ldots\ldots\ldots\ldots\ldots\ldots\ldots (6.22)$$

where the average dimensionless pressure, $\bar{p}_D$, is given in Fig. 6.10. Another approach uses the well's flowing pressure, the buildup slope, and other data in

$$\bar{p} = p_{wf}(\Delta t = 0) + m\left[\log\left(\frac{A}{r_w^2}\right) + \log\left(\frac{2.2458}{C_A'}\right) + 0.86859\,s\right], \quad \ldots\ldots\ldots\ldots\ldots\ldots\ldots (6.23)$$

For this equation to give acceptable results, it is important that the skin factor be included. The shape factor, C_A', is 19.1 or 19.5 for a circular or square system.[11] Eq. 6.23 applies only when t_{pDA} (Eq. 6.4) is greater than 0.25.

Kumar and Ramey indicate that the drainage-region average pressure at the time of shut-in may be read directly from the semilog straight line at the value of Δt or $(t_p + \Delta t)/\Delta t$ obtained from Fig. 6.11. t_{pDA} is calculated from Eq. 6.4. For the MDH plot, it is necessary to estimate Δt from $(\Delta t_{DA})_{\bar{p}}$ by using Eq. 2.3b.

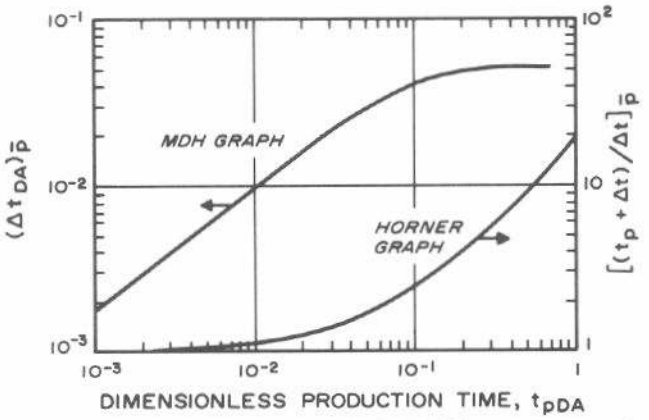

Fig. 6.11 Time when semilog straight-line buildup pressure equals average pressure at instant of shut-in. Constant-pressure square system. After Kumar and Ramey.[11]

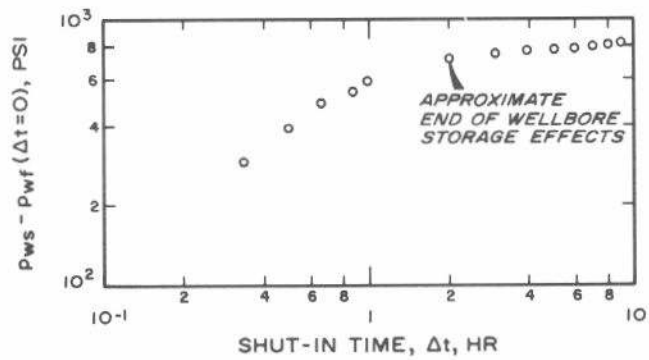

Fig. 6.12 Log-log data plot for a buildup test on a well in a constant-pressure square. Example 6.4. Data from Kumar and Ramey.[11]

TABLE 6.1—PRESSURE BUILDUP DATA FOR A WELL IN THE CENTER OF A SQUARE WITH CONSTANT-PRESSURE BOUNDARIES.[11] EXAMPLE 6.4.

Shut-in Time, Δt (hours)	Pressure, p_{ws} (psi)
0	3,561
0.333	3,851
0.500	3,960
0.667	4,045
0.883	4,104
1.0	4,155
2.0	4,271
3.0	4,306
4.0	4,324
5.0	4,340
6.0	4,352
7.0	4,363
8.0	4,371
9.0	4,380
10.0	4,387
20.0	4,432

Example 6.4 Average Drainage-Region Pressure and Pressure Buildup Analysis for a Water-Drive Reservoir

Kumar and Ramey[11] provide the simulated pressure buildup data in Table 6.1 for a well in the center of a square drainage area with constant-pressure boundaries. Other pertinent data are

$t_p = 4{,}320$ hours $= 180$ days
$q = 350$ STB/D
$\mu = 0.80$ cp
$c_t = 17 \times 10^{-6}$ psi^{-1}
$B = 1.136$ RB/STB
$h = 49$ ft
$r_w = 0.29$ ft
$\phi = 0.23$
$A = 7.72$ acres, well in center of a square with constant-pressure boundaries, 580×580 ft
$= 336{,}400$ sq ft.

Fig. 6.12 is the log-log plot of data from Table 6.1. Wellbore storage effects appear to diminish after about 2 hours of shut-in. Because of the long production time, the MDH plot shown in Fig. 6.13 is adequate for analysis. Fig. 6.13 indicates

$$m = 152 \text{ psi/cycle}, \quad \text{and} \quad p_{1hr} = 4{,}236 \text{ psi}.$$

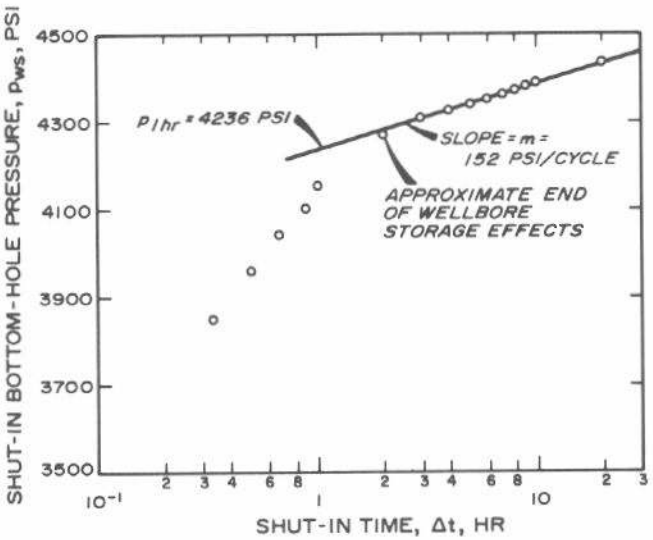

Fig. 6.13 Miller-Dyes-Hutchinson data plot for a pressure buildup test on a well in a constant-pressure square. Example 6.4. Data from Kumar and Ramey.[11]

We estimate permeability from Eq. 5.6:

$$k = \frac{(162.6)(350)(1.136)(0.80)}{(152)(49)}$$

$$= 6.9 \text{ md}.$$

Skin factor is estimated from Eq. 5.7:

$$s = 1.1513 \left[\frac{4{,}236 - 3{,}561}{152} - \log\left(\frac{6.9}{(0.23)(0.80)(17 \times 10^{-6})(0.29)^2} \right) + 3.2275 \right]$$

$$= 0.3.$$

We may estimate the system boundary pressure, p_e, by the MDH method, Eq. 6.21. We use the square-drainage-region, constant-pressure-boundary curve of Fig. 6.6 to get $p_{D\text{MDH}}$. In this case, we use $\Delta t = 10$ hours and Eq. 6.4 to calculate

$$\Delta t_{DA} = \frac{(0.0002637)(6.9)(10)}{(0.23)(0.80)(17 \times 10^{-6})(336;400)}$$

$$= 0.0173.$$

Fig. 6.6 indicates that $p_{D\text{MDH}} = 1.01$ at $\Delta t_{DA} = 0.0173$. Using Eq. 6.21 and $p_{ucs} = 4{,}388$ psi (Fig. 6.13) at $\Delta t = 10$ hours,

$$p_e = 4{,}388 + \frac{(152)(1.01)}{1.1513}$$

$$= 4{,}521 \text{ psi},$$

which is 89 psi higher than the maximum recorded pressure.

The average pressure at the time of shut-in is estimated from Eq. 6.22 and Fig. 6.10. To use Fig. 6.10, we estimate t_{pDA} from Eq. 6.4.

$$t_{pDA} = \frac{(0.0002637)(6.9)(4{,}320)}{(0.23)(0.80)(17 \times 10^{-6})(336{,}400)}$$

$$= 7.47.$$

From Fig. 6.10, $\bar{p}_D = 0.478$ for $t_{pDA} > 1$, so using Eq. 6.22,

$$\bar{p} = 4{,}521 - \frac{(152)(0.478)}{1.1513}$$

$$= 4{,}458 \text{ psi}.$$

Alternatively, we could use Fig. 6.11 to get $(\Delta t_{DA})_{\bar{p}} = 0.0513$. This implies that

$$(\Delta t)_{\bar{p}} = \frac{(0.23)(0.80)(17 \times 10^{-6})(336{,}400)(0.0513)}{(0.0002637)(6.9)}$$

$$= 29.7 \text{ hours}.$$

Extrapolating the straight line in Fig. 6.13, $\bar{p} = 4{,}458$ psi.

Kumar and Ramey[11] illustrate Horner plotting and the Matthews-Brons-Hazebroek method (Fig. 6.9) for this example.

6.5 Factors Complicating Average-Pressure Estimation

Since most reservoirs have many wells, the general pressure level in the reservoir usually continues to decrease during buildup tests on a single well. That is not important in the early stages of a buildup test; however, if the well is shut in for several days, readjustment of the drainage areas of offsetting wells and the general pressure decline may begin to affect the buildup response at the shut-in well. Methods for analysis under such conditions are given in Section 5.3. The fact that this happens indicates that an average pressure for a well's drainage region or an entire reservoir applies only at a point in time. In particular, as a result of changing drainage regions and continued reservoir depletion, we cannot expect a single well in a developed reservoir to reach the average pressure applicable to its drainage area at the instant of shut-in. The alternative is estimating drainage-region average pressure by using the Matthews-Brons-Hazebroek approach and then *volumetrically* averaging the pressures for each drainage region to obtain the over-all reservoir average pressure. Such an approach may not be viable as normal engineering practice because of practical difficulties in estimating drainage areas, since they vary in response to changing operating practices. Fortunately, pressure buildup is usually rapid in high-permeability reservoirs, so observed pressures may be representative of drainage-region average pressure. In lower-permeability reservoirs, wells tend to have slower and more incomplete buildups during reasonable shut-in periods. Therefore, a different approach is indicated in such reservoirs. The most general approach is either full or key-well buildup surveys to estimate average reservoir pressures for each well's nominal drainage region (40-acre square, for example) using techniques given in this chapter. The resulting pressures may be contoured, assuming them to be at the well points, and then volumetrically weighed by any of several acceptable techniques.

A common mistake made in pressure buildup analysis is to begin thinking that the mathematical conveniences used in analysis exist in reality. In fact, in any developed reservoir, the only true no-flow boundaries are the physical boundaries. While there may be effective no-flow boundaries between producing wells when all wells are producing, those boundaries move (drainage shapes change) as flow rates vary and as wells are shut in and put back on production. It is a common error in pressure analysis methods to assume that when one well is shut in, it will always act like a well in a closed drainage system; in fact, that only happens for single wells in very small reservoirs.

References

1. Matthews, C. S. and Russell, D. G.: *Pressure Buildup and Flow Tests in Wells*, Monograph Series, Society of Petroleum Engineers of AIME, Dallas (1967) **1**, Chap. 4.

2. Matthews, C. S. and Lefkovits, H. C.: "Studies on Pressure Distribution in Bounded Reservoirs at Steady State," *Trans.*, AIME (1955) **204**, 182-189.

3. Horner, D. R.: "Pressure Build-Up in Wells," *Proc.*, Third World Pet. Cong., The Hague (1951) Sec. II, 503-523. Also *Reprint Series, No. 9 — Pressure Analysis Methods*, Society of Petroleum Engineers of AIME, Dallas (1967) 25-43.

4. Matthews, C. S., Brons, F., and Hazebroek, P.: "A Method for Determination of Average Pressure in a Bounded Reservoir," *Trans.*, AIME (1954) **201**, 182-191. Also *Reprint Series No. 9 — Pressure Analysis Methods*, Society of Petroleum Engineers of AIME, Dallas (1967) 51-60.

5. Pinson, A. E., Jr.: "Concerning the Value of Producing Time Used in Average Pressure Determinations From Pressure Buildup Analysis," *J. Pet. Tech.* (Nov. 1972) 1369-1370.

6. Kazemi, Hossein: "Determining Average Reservoir Pressure From Pressure Buildup Tests," *Soc. Pet. Eng. J.* (Feb. 1974) 55-62; *Trans.*, AIME, **257.**

7. Dietz, D. N.: "Determination of Average Reservoir Pressure From Build-Up Surveys," *J. Pet. Tech.* (Aug. 1965) 955-959; *Trans.*, AIME, **234.**

8. Ramey, H. J., Jr., and Cobb, William M.: "A General Buildup Theory for a Well in a Closed Drainage Area," *J. Pet. Tech.* (Dec. 1971) 1493-1505; *Trans.*, AIME, **251.**

9. Miller, C. C., Dyes, A. B., and Hutchinson, C. A., Jr.: "The Estimation of Permeability and Reservoir Pressure From Bottom-Hole Pressure Build-Up Characteristics," *Trans.*, AIME (1950) **189,** 91-104. Also *Reprint Series, No. 9 — Pressure Analysis Methods*, Society of Petroleum Engineers of AIME, Dallas (1967) 11-24.

10. Perrine, R. L.: "Analysis of Pressure Buildup Curves," *Drill. and Prod. Prac.*, API (1956) 482-509.

11. Kumar, Anil and Ramey, Henry J., Jr.: "Well-Test Analysis for a Well in a Constant-Pressure Square," paper SPE 4054 presented at the SPE-AIME 47th Annual Fall Meeting, San Antonio, Tex., Oct. 8-11, 1972 (an abridged version appears in *Soc. Pet. Eng. J.*, April 1974, 107-116).

12. Brons, F. and Miller, W. C.: "A Simple Method for Correcting Spot Pressure Readings," *J. Pet. Tech.* (Aug. 1961) 803-805; *Trans.*, AIME, **222.**

13. Muskat, Morris: "Use of Data on the Build-Up of Bottom-Hole Pressures," *Trans.*, AIME (1937) **123,** 44-48. Also *Reprint Series, No. 9 — Pressure Analysis Methods*, Society of Petroleum Engineers of AIME, Dallas (1967) 5-9.

14. Matthews, C. S.: "Analysis of Pressure Build-Up and Flow Test Data," *J. Pet. Tech.* (Sept. 1961) 862-870. Also *Reprint Series, No. 9 — Pressure Analysis Methods*, Society of Petroleum Engineers of AIME, Dallas (1967) 111-119.

15. Russell, D. G.: "Extensions of Pressure Build-Up Analysis Methods," *J. Pet. Tech.* (Dec. 1966) 1624-1636; *Trans.*, AIME, **237.** Also *Reprint Series, No. 9 — Pressure Analysis Methods*, Society of Petroleum Engineers of AIME, Dallas (1967) 175-187.

16. Arps, J. J. and Smith, A. E.: "Practical Use of Bottom-Hole Pressure Buildup Curves," *Drill. and Prod. Prac.*, API (1949) 155-165.

17. van Poollen, H. K., Breitenbach, E. A., and Thurnau, D. H.: "Treatment of Individual Wells and Grids in Reservoir Modeling," *Soc. Pet. Eng. J.* (Dec. 1968) 341-346.

18. Earlougher, Robert C., Jr.: "Comparing Single-Point Pressure Buildup Data With Reservoir Simulator Results," *J. Pet. Tech.* (June 1972) 711-712.

19. Ramey, Henry J., Jr., Kumar, Anil, and Gulati, Mohinder S.: *Gas Well Test Analysis Under Water-Drive Conditions*, AGA, Arlington, Va. (1973) Chaps. 4-7.

Chapter 7

Injection Well Testing

7.1 Introduction

In many reservoirs, the number of injection wells approaches the number of producing wells, so the topic of testing those wells is important. That is particularly true when tertiary recovery projects are being considered or are in progress. When an input well receives an expensive fluid, its ability to accept that fluid uniformly for a long time is important to the economics of the tertiary recovery project. In particular, increasing wellbore damage must be detected and corrected promptly.

The information available about injection well testing is much less abundant than information about production well testing. Matthews and Russell[1] summarize injection well testing, but emphasize falloff testing. Injectivity testing is rarely discussed in the literature, but it can be important.[2] Falloff testing is treated[3-7] rather thoroughly, particularly for systems with unit mobility ratio. Gas-well falloff testing, especially in association with in-situ combustion, also has been discussed.[8,9]

Injection-well transient testing and analysis are basically simple — as long as the *mobility ratio* between the injected and the in-situ fluids is about unity. Fortunately, that is a reasonable approximation for many waterfloods. It also is a reasonable approximation in watered-out waterfloods that initially had mobility ratios significantly different from unity, and early in the life of tertiary recovery projects when so little fluid has been injected that it appears only as a skin effect. When the unit-mobility-ratio condition is satisfied, injection well testing for liquid-filled systems is analogous to production well testing. Injection is analogous to production (but the rate, q, used in equations is negative for injection while it is positive for production), so an injectivity test (Section 7.2) parallels a drawdown test (Chapter 3). Shutting in an injection well results in a pressure falloff (Section 7.3) that is analogous to a pressure buildup (Chapter 5). The equations for production well testing in Chapters 3 through 5 apply to injection well testing as long as sign conventions are observed. The analogy should become clear in the next two sections.

When the unit-mobility-ratio assumption is not satisfied, the analogy between production well testing and injection well testing is not so complete. In that situation, analysis depends on the relative sizes of the water bank and the oil bank; generally, analysis is possible only when $r_{ob} > 10r_{wb}$ (see Section 7.5). Fracturing effects, which can have a significant effect on analysis, are discussed in Section 11.3.

Reservoirs with injection wells can reach true steady-state conditions when total injection rate equals total production rate. In that situation, or when the situation is approached, the steady-state analysis techniques of Section 7.7 may be useful.

7.2 Injectivity Test Analysis in Liquid-Filled, Unit-Mobility-Ratio Reservoirs

Injectivity testing is pressure transient testing during injection into a well. It is analogous to drawdown testing, for both constant and variable injection rates. Although sometimes called "injection pressure buildup" or simply "pressure buildup," we prefer to use the term "injectivity testing" to avoid confusion with production-well pressure buildup testing. This section applies to liquid-filled reservoirs with mobility of the injected fluid essentially equal to the mobility of the in-situ fluid. If the unit-mobility-ratio condition is not satisfied, results of analysis by techniques in this section may not be valid. Even in that situation, if the radius of investigation is not beyond the water (injected-fluid) bank, valid analysis can be made for permeability and skin, but not necessarily for static reservoir pressure.

Fig. 7.1 shows an ideal rate schedule and pressure response for injectivity testing. The well is initially shut in and pressure is stabilized at the initial reservoir pressure, p_i. At time zero, injection starts at constant rate, q. Fig. 7.1 illustrates the convention that $q < 0$ for injection. It is advisable to monitor the injection rate carefully so the methods of Chapter 4 (variable-rate analysis) may be applied if the rate varies significantly.

Since unit-mobility-ratio injection well testing is analogous to production well testing, the analysis methods in Chapters 3 and 4 for drawdown and multiple-rate testing may be applied directly to injection well testing. Of course, while pressure at a production well declines during drawdown, pressure at an injection well increases during injec-

tion. That difference is accounted for in the analysis methods by using $q < 0$ for injection and $q > 0$ for production.

For the constant-rate injectivity test illustrated in Fig. 7.1, the bottom-hole injection pressure is given by Eq. 3.5:

$$p_{wf} = p_{1hr} + m \log t. \quad \ldots\ldots\ldots\ldots\ldots\ldots\ldots\ldots\ldots (7.1)$$

Eq. 7.1 indicates that a plot of bottom-hole injection pressure vs the logarithm of injection time should have a straight-line section, as shown in Fig. 7.2. The intercept, p_{1hr}, is given by Eq. 3.7; the slope is m and is given by Eq. 3.6:

$$m = \frac{-162.6\,qB\mu}{kh} \quad \ldots\ldots\ldots\ldots\ldots\ldots\ldots\ldots\ldots (7.2)$$

As in drawdown testing, wellbore storage may be an important factor in injection well testing. Often, reservoir pressure is low enough so that there is a free liquid surface in the shut-in well. In that case, the wellbore storage coefficient is given by Eq. 2.16 and can be expected to be relatively large. Therefore, we recommend that all injectivity test analyses start with the $\log(p_{wf} - p_i)$ vs $\log t$ plot so the duration of wellbore storage effects may be estimated as explained in Sections 2.6 and 3.2. As indicated in Fig. 7.2, wellbore effects may appear as a semilog straight line on the p_{wf} vs $\log t$ plot; if such a line is analyzed, low values of permeability will be obtained and calculated skin factor will be shifted in the negative direction. Eq. 3.8 may be used to estimate the beginning of the semilog straight line shown in Fig. 7.2:

$$t > \frac{(200{,}000 + 12{,}000\,s)\,C}{(kh/\mu)} \quad \ldots\ldots\ldots\ldots\ldots\ldots\ldots (7.3)$$

Once the semilog straight line is determined, reservoir permeability is estimated from Eq. 3.9:

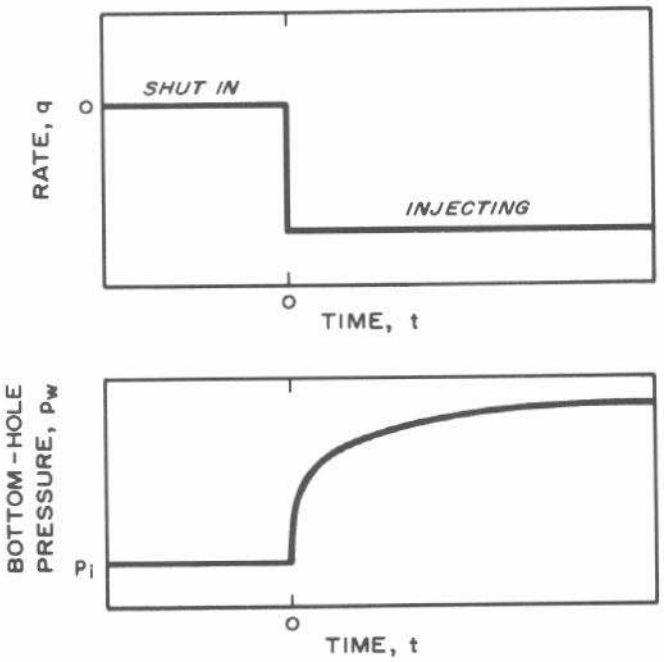

Fig. 7.1 Idealized rate schedule and pressure response for injectivity testing.

$$k = \frac{-162.6\,qB\mu}{mh} \quad \ldots\ldots\ldots\ldots\ldots\ldots\ldots\ldots\ldots (7.4)$$

Skin factor is estimated with Eq. 3.10:

$$s = 1.1513\left[\frac{p_{1hr} - p_i}{m} - \log\left(\frac{k}{\phi\mu c_t r_w^2}\right) + 3.2275\right]. \quad \ldots\ldots\ldots\ldots\ldots\ldots\ldots\ldots\ldots (7.5)$$

Example 7.1 Injectivity Test Analysis in an Infinite-Acting Reservoir

Figs. 7.3 and 7.4 show pressure response data for an injectivity test in a waterflooded reservoir. Before the test, all wells in the reservoir had been shut in for several weeks and pressure had stabilized. Known reservoir data are

depth = 1,002 ft	$h = 16$ ft
$c_t = 6.67 \times 10^{-6}$ psi^{-1}	$\mu = 1.0$ cp
$\phi = 0.15$	$B = 1.0$ RB/STB
$\rho_w = 62.4$ lb$_m$/cu ft	$q = -100$ STB/D
$p_i = 194$ psig	$r_w = 0.25$ ft.

The well is completed with 2-in. tubing set on a packer. The reservoir had been under waterflood for several years. We can safely assume that the unit-mobility-ratio assumption is satisfied, since the test radius of investigation is less than the distance to the water bank, as shown by calculations later in this example.

The log-log data plot, Fig. 7.3, indicates that wellbore storage is important for about 2 to 3 hours. The deviation of the data above the unit-slope line suggests that the wellbore storage coefficient decreased at about 0.55 hour. Sections 2.6 and 11.2 and Figs. 2.12 and 11.5 through 11.7 discuss such changing wellbore storage conditions. The data in Fig. 7.3 start deviating upward from the unit-slope straight line when $\Delta p = 230$ psi and $p_{wf} = 424$ psig. Since the column of water in the well is equivalent to about 434 psi, it appears that the apparent decrease in storage coefficient corresponds to fillup of the tubing.

From the unit-slope portion of Fig. 7.3, $\Delta p = 408$ psig when $\Delta t = 1$ hour. Using Eq. 2.20, we estimate the apparent wellbore storage coefficient:

$$C = \frac{(100)(1.0)}{24}\,\frac{(1.0)}{(408)} = 0.0102 \text{ bbl/psi}.$$

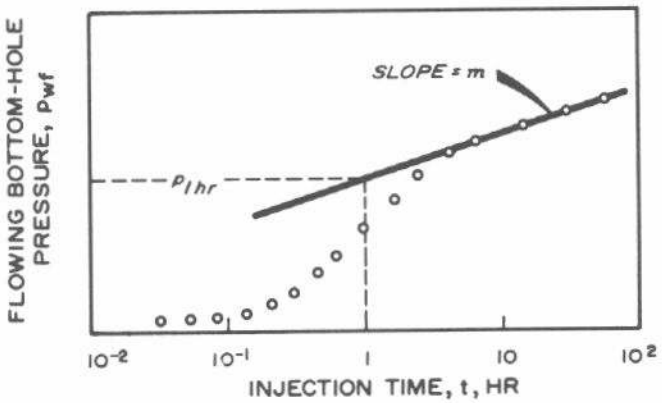

Fig. 7.2 Semilog plot of typical injectivity test data.

(C is always positive.) Wellbore capacity for a rising fluid level can be estimated (from Eq. 2.16) to get $V_u = 0.0044$ bbl/ft. Two-inch tubing has a capacity of about 0.004 bbl/ft, so the unit-slope straight line does correspond to a rising fluid level in the tubing. If we use $C = 0.0102$ in Eq. 7.3, or if we go 1 to 1.5 cycles in Δt after the data start deviating from the unit-slope line (Section 2.6), we would decide that the semilog straight line should not start for 5 to 10 hours of testing. Those rules indicate too long a time for a *decreasing* wellbore storage condition. Figs. 7.3 and 7.4 clearly show that wellbore storage effects have died out after about 2 to 3 hours.

Fig. 7.4 shows a semilog straight line through the data after 3 hours of injection. From this line, $m = 80$ psig/cycle and $p_{1\text{hr}} = 770$ psig. Permeability is estimated using Eq. 7.4:

$$k = \frac{-(162.6)(-100)(1.0)(1.0)}{(80)(16)} = 12.7 \text{ md.}$$

We may now determine if the unit-mobility-ratio analysis applies. The estimated permeability is used to estimate a radius of investigation from Eq. 2.41:

$$r_d \simeq 0.029\sqrt{\frac{kt}{\phi\mu c_t}}$$

$$\simeq 0.029\sqrt{\frac{(12.7)(7)}{(0.15)(1.0)(6.67\times 10^{-6})}}$$

$$\simeq 273 \text{ ft.}$$

A volumetric balance provides an estimate of the distance to the water bank. The volume injected is

$$W_i = \frac{\pi r_{wb}^2 h\phi\Delta S_w}{5.6146},$$

so

$$r_{wb} = \sqrt{\frac{5.6146\, W_i}{\pi h\phi\Delta S_w}}.$$

Assuming that $\Delta S_w = 0.4$ and that injection has been under way for at least 2 years,

$$W_i \simeq (100 \text{ STB/D})(1.0 \text{ RB/STB})(2 \text{ years})(365 \text{ D/year})$$

$$\simeq 73{,}000 \text{ res bbl}$$

and

$$r_{wb} = \sqrt{\frac{(5.6146)(73{,}000)}{\pi(16)(0.15)(0.4)}} \simeq 369 \text{ ft.}$$

Since $r_d < r_{wb}$, we are justified in using the unit-mobility-ratio analysis.

Eq. 7.5 provides an estimate of the skin factor:

$$s = 1.1513\left\{\frac{770-194}{80} - \log\left[\frac{12.7}{(0.15)(1.0)(6.67\times 10^{-6})(0.25)^2}\right] + 3.2275\right\}$$

$$= 2.4.$$

The well is damaged; the pressure drop across the skin may be estimated from Eq. 2.9:

$$\Delta p_s = \frac{(141.2)(-100)(1.0)(1.0)(2.4)}{(12.7)(16)}$$

$$= -167 \text{ psi.}$$

The negative sign here indicates damage since the pressure decreases away from the well (in the positive r direction) for injection while it increases for production. This is seen by computing the flow efficiency from Eq. 2.12. Assume $\bar{p} = p_i = 194$ psi, since the reservoir is stabilized before injection. Using $p_{wf} = 835$ psig from the last available data point, the *flow efficiency* is

$$\frac{194 - 835 - (-167)}{194 - 835} = 0.74.$$

If we had ignored the sign on q when estimating Δp_s, we would have incorrectly computed a flow efficiency of 1.26, indicating improvement instead of damage.

Multiple-rate injection testing, constant-pressure injection testing, injectivity testing after falloff testing, etc., are all performed and analyzed as explained for production well

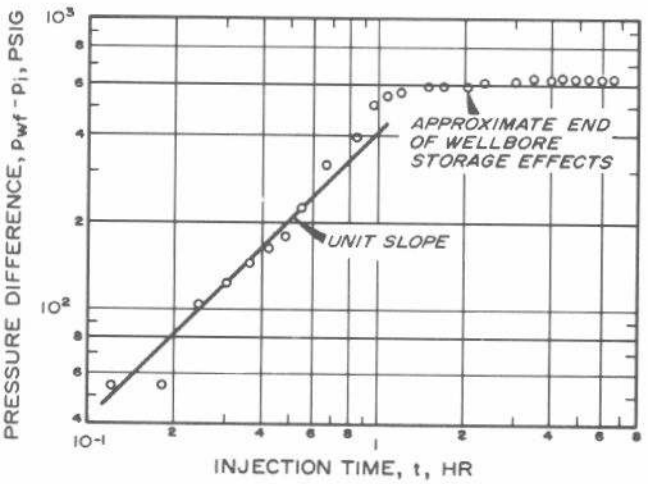

Fig. 7.3 Log-log data plot for the injectivity test of Example 7.1. Water injection into a reservoir at static conditions.

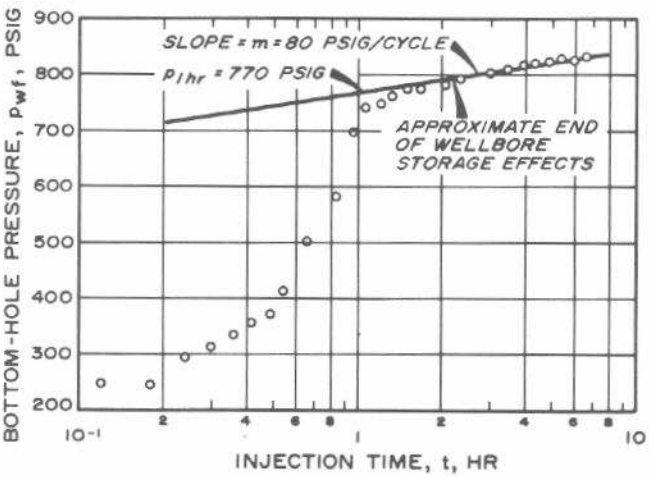

Fig. 7.4 Semilog plot for the injectivity test of Example 7.1. Water injection into a reservoir at static conditions.

testing in Chapters 3 and 4. Type-curve matching for injection well testing is done just as it is for production well testing (Section 3.3); the Δp used must be positive for plotting the log scale, although it is actually a negative number. The signs must be considered in analysis.

Eqs. 7.1 through 7.5 apply to injectivity testing in infinite-acting reservoirs, just as do Eqs. 3.5 through 3.10 for drawdown testing. When an injection well in a developed reservoir shows the effects of interference from other wells, the infinite-acting analysis may not be strictly applicable. In that case, the techniques presented in Section 3.4 should be used.

7.3 Falloff Test Analysis for Liquid-Filled, Unit-Mobility-Ratio Reservoirs

Falloff testing, illustrated schematically in Fig. 7.5, is analogous to pressure buildup testing in a production well. Injection is at a constant rate, q, until the well is shut in at time t_p. Pressure data taken immediately before and during the shut-in period are analyzed as pressure buildup data are analyzed. The pressure falloff behavior can be expressed by Eq. 5.10 for both infinite-acting and developed reservoirs:

$$p_{ws} = p^* - m \log\left(\frac{t_p + \Delta t}{\Delta t}\right) \quad \ldots\ldots\ldots\ldots\ldots\ldots (7.6)$$

The false pressure, p^*, is equivalent to the initial pressure, p_i, for an infinite-acting system. As illustrated in Fig. 7.6, Eq. 7.6 indicates that a plot of p_{ws} vs $\log[(t_p + \Delta t)/\Delta t]$ should have a straight-line portion with intercept p^* at infinite shut-in time $[(t_p + \Delta t)/\Delta t = 1]$ and with slope $-m$, where m is given by Eq. 5.5:

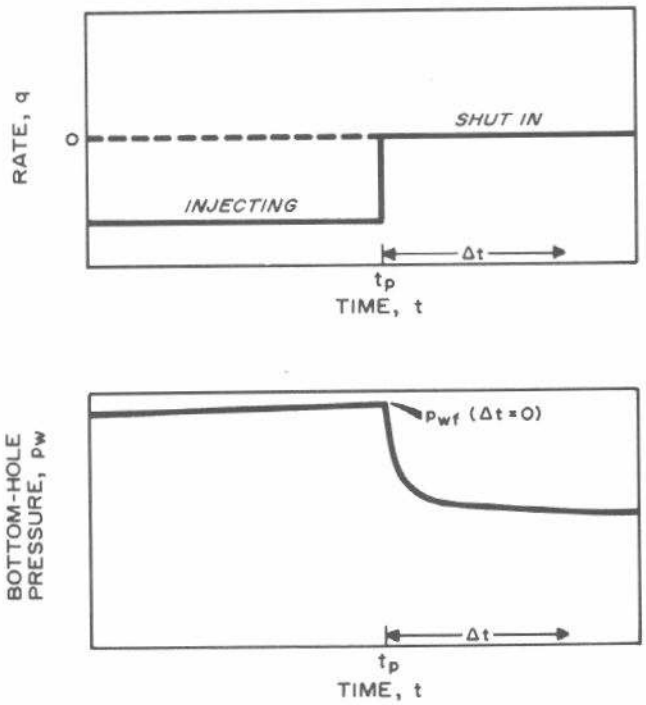

Fig. 7.5 Idealized rate schedule and pressure response for falloff testing.

$$m = \frac{162.6\,qB\mu}{kh} \quad \ldots\ldots\ldots\ldots\ldots\ldots (7.7)$$

As in buildup testing, the Horner graph is plotted with the horizontal scale increasing from right to left (Fig. 7.6). Thus, although the slope appears to be negative, it is actually positive because of the reverse plotting; m is negative since $m = -\text{slope}$.

As for other transient well tests, the log-log data plot should be made so the end of wellbore storage effects may be estimated and the proper semilog straight line (Fig. 7.6) can be chosen. Eq. 5.15b may be used to estimate the beginning of the semilog straight line for falloff testing:

$$t = \frac{170{,}000\,Ce^{0.14s}}{(kh/\mu)} \quad \ldots\ldots\ldots\ldots\ldots\ldots (7.8)$$

but the log-log plot is preferred.

Once the correct semilog straight line has been determined, reservoir permeability and skin factor are estimated from Eqs. 5.6 and 5.7:

$$k = \frac{162.6\,qB\mu}{mh} \quad \ldots\ldots\ldots\ldots\ldots\ldots (7.9)$$

and

$$s = 1.1513\left[\frac{p_{1hr} - p_{wf}(\Delta t = 0)}{m} - \log\left(\frac{k}{\phi\mu c_t r_w^2}\right) + 3.2275\right] \quad \ldots\ldots\ldots\ldots\ldots\ldots (7.10)$$

As is the case in pressure buildup testing, if the injection rate varies before the falloff test, the equivalent injection time may be approximated from Eq. 5.9:

$$t_p = \frac{24\,V_P}{q} \quad \ldots\ldots\ldots\ldots\ldots\ldots (7.11)$$

where V_P is the cumulative volume injected since the *last pressure equalization* and q is the constant rate just before shut-in. Comments made in Sections 5.2 and 6.3 about the proper t_p to use for a Horner-type analysis also apply here. In Eq. 7.11, the numerator is usually the cumulative injection since the last pressure equalization rather than the cumula-

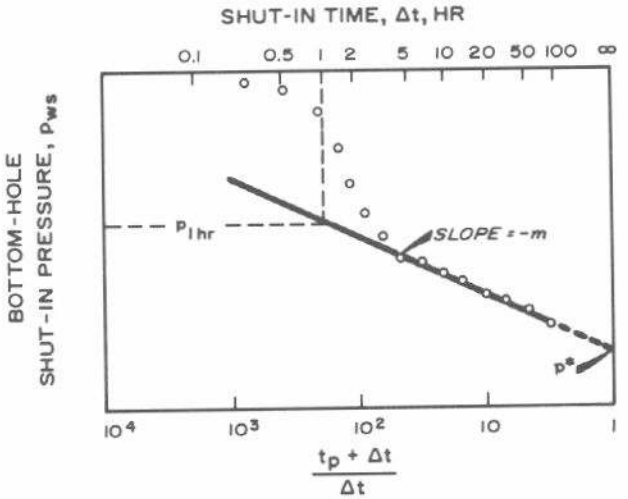

Fig. 7.6 Horner plot of a typical falloff test.

tive injection since the well was put on injection. If $t_p > 2t_{pss}$, then, for reasons discussed in Sections 5.2 and 6.3, the time to reach pseudosteady state (or steady state, which for a five-spot system[10] occurs at $t_{DA} = 0.25$ with A = the area per well, not per pattern) should be used[11,12] in place of t_p.

Miller-Dyes-Hutchinson-type plotting of falloff data, as suggested by Eq. 5.13,

$$p_{ws} = p_{1hr} + m \log \Delta t \ , \quad \ldots\ldots\ldots\ldots\ldots\ldots \quad (7.12)$$

also applies to falloff testing. The analysis method of Section 5.3 applies: m in Eq. 7.12 is the slope of the p_{ws} vs log Δt straight line and is defined by Eq. 7.7; k is estimated from Eq. 7.9; skin factor is estimated from Eq. 7.10; and the false pressure, p^*, may be estimated from Eq. 5.14. The end of the semilog straight line (either Horner or MDH) may be estimated by using Eq. 5.16 and Figs. 5.6 and 5.7. Because it is less work, the MDH plot is more practical unless t_p is less than about twice the maximum shut-in time. If necessary, the Horner plot may be used for a second pass to estimate average pressure.

Muskat-type plotting may be used to analyze pressure falloff tests, but this is generally not recommended since the boundary conditions in injection well testing are more complicated than the simple single-well closed systems assumed in the analysis technique described in Section 5.3. The information in Section 6.4 indicates that a Muskat plot may provide good results if there is essentially a constant-pressure boundary between production and injection wells.

Example 7.2 Pressure Falloff in a Liquid-Filled, Infinite-Acting Reservoir

During a stimulation treatment, brine was injected into a well and the falloff data shown in Figs. 7.7 through 7.9 were taken.[6] Other data include

$t_p = 6.82$ hours

total falloff time = 0.67 hour

$p_{tf}(\Delta t = 0) = 1{,}310$ psig
$q_w = -807$ STB/D
$B_w = 1.0$ RB/STB
$\mu_w = 1.0$ cp
$c_t = 1.0 \times 10^{-5}$ psi^{-1}
$c_w = 3.0 \times 10^{-6}$ psi^{-1}
$\phi = 0.25$
$r_w = 0.4$ ft
$\rho_w = 67.46$ lb$_m$/cu ft
$h = 28$ ft
depth = 4,819 ft
$A = 20$ acres = 871,200 sq ft.

Fig. 7.7 is the log-log plot for the test data. From the shape of the curve, it appears that the semilog straight line should begin by 0.1 to 0.2 hour. Using $\Delta p = 238$ psi and $\Delta t = 0.01$ hour from the unit-slope straight line, we estimate the wellbore storage coefficient from Eq. 2.20:

$$C = \frac{(807)(1.0)(0.01)}{(24)(238)} = 0.0014 \text{ RB/psi}.$$

C must be positive, so we disregard the sign convention here. Since wellhead pressure was always above atmospheric, the wellbore remained full during the test. Thus, Eq. 2.17 and a wellbore compressibility of $c_w = 3.0 \times 10^{-6}$ psi^{-1} can be used to estimate the wellbore volume corresponding to $C = 0.0014$ bbl/psi: $V_w = 467$ bbl. Using the depth of 4,819 ft, we compute a casing radius of 0.42 ft, which is too large for a hole of radius 0.4 ft. Nevertheless,

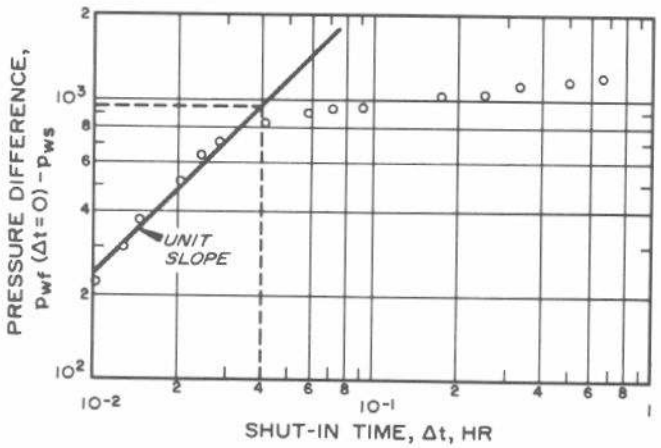

Fig. 7.7 Log-log data plot for a falloff test after brine injection, Example 7.2.

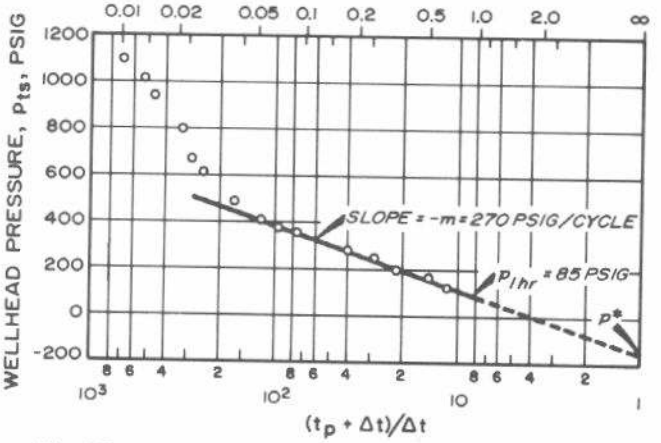

Fig. 7.8 Horner plot of pressure falloff after brine injection, Example 7.2.

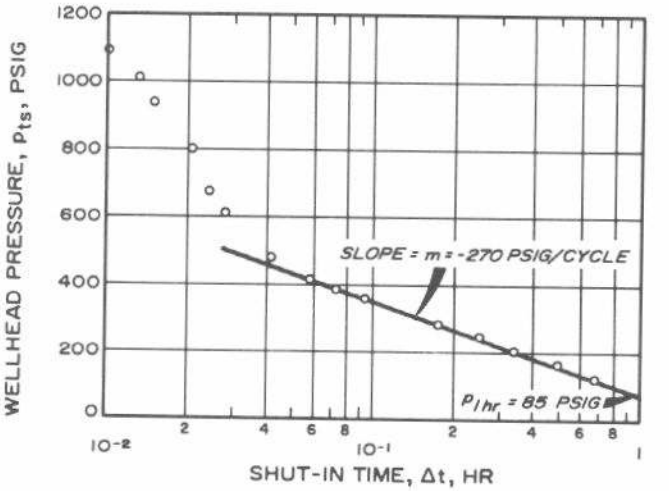

Fig. 7.9 Miller-Dyes-Hutchinson plot of pressure falloff after brine injection, Example 7.2.

the agreement is within reason. If the well was shut in at the injection pump rather than at the wellhead, the connecting lines would cause the storage coefficient to be larger than that resulting from the wellbore only. Unfortunately, we do not have all the information necessary to know if such speculation is correct. This clearly indicates the *need* for a diagram or a sketch of the well completion equipment and surface connecting lines.

Wellhead pressures are plotted vs $\log[(t_p + \Delta t)/\Delta t]$ in Fig. 7.8. That Horner plot can be used to estimate k, s, and p^*. Since the falloff time (0.67 hour) is much smaller than the flow time (6.82 hours), the log Δt (MDH) plot shown in Fig. 7.9 also may be used. The correct straight line in Figs. 7.8 and 7.9 indicates $m = -270$ psig/cycle and $p_{1hr} = 85$ psig. Thus, using Eq. 7.9,

$$k = \frac{(162.6)(-807)(1.0)(1.0)}{(-270)(28)} = 17.4 \text{ md}.$$

The skin factor is estimated from Eq. 7.10:

$$s = 1.1513\left\{\frac{85 - 1{,}310}{-270} - \log\left[\frac{17.4}{(0.25)(1.0)(1.0 \times 10^{-5})(0.4)^2}\right] + 3.2275\right\}$$

$$= 0.15.$$

From Fig. 7.8, $p_{ts}^* = -151$ psig. This is the false pressure at the *surface*. Using the hydrostatic gradient of 0.4685 psi/ft and the depth of 4,819 ft, the initial bottom-hole pressure is estimated:

$$p^* = (4{,}819)(0.4685) - 151 = 2{,}107 \text{ psig}.$$

Since injection time t_p is short, we can safely assume that $p^* = \bar{p}$, so $\bar{p} = 2{,}107$ psig.

When the test well is operating at true steady state, falloff test analysis by the MDH technique *should be sufficient* and, thus, is the preferred method from the practical standpoint of less work. Shutting in the well will disturb steady-state conditions in the reservoir, and adjacent producing wells will eventually cause pressure decline in the test well. The pressure does not level off in a falloff test as it does in a buildup test. Pressure falloff will continue for a time, then the pressure will deviate *below* the semilog straight line rather than above it, as might be expected by analogy to pressure buildup testing. This is not a violation of the analogy between the tests — but is caused by interference from adjacent withdrawal wells; indeed, data in a pressure buildup test in an injection project will deviate *above* the semilog straight line when injection at adjacent wells continues.

If there is a general pressure increase or decrease at the injection well before falloff testing, the techniques described in the "Developed Reservoir Effects" portion of Section 5.3 may be applied. It is necessary, however, to recognize the basic differences in behavior between a reservoir with only producing wells and a reservoir with both injection and producing wells.

As indicated in Section 7.2, multiple-rate testing of injection wells is analogous to multiple-rate testing in production wells. Two-rate testing (two-rate falloff testing) is appropriate to eliminate changing wellbore storage during a falloff test (Section 11.2). A two-rate falloff test is run by injecting at a relatively high rate (but below parting pressure) and then decreasing the injection rate while observing the pressure decrease as a result of the rate decrease. If rates are chosen correctly, surface pressure is maintained and changing wellbore storage effects are eliminated. That can be important because injection wells frequently go on vacuum during a falloff test, resulting in an increasing wellbore storage condition (see Sections 2.6 and 11.2 and Figs. 2.12, 11.2, and 11.3, and Ref. 13) and essentially unanalyzable test data. A two-rate falloff test is analyzed like the two-rate production-well test described in Section 4.3. The data plot is made as suggested by Eq. 4.6 and the analysis is based on Eqs. 4.10 and 4.11. The simplified analysis technique in Section 4.3 also may be used when the conditions it assumes are satisfied.

Example 7.3 Two-Rate Falloff Test

An injectivity test was started on an injection well in a waterflooded reservoir before a tertiary recovery test. After a few hours of injection, it was evident that the −100 STB/D injection rate could not be maintained without exceeding fracture pressure, so the rate was reduced. Since an injectivity test had been planned, a bottom-hole pressure gauge was operating and the pressure data in Table 7.1 were obtained. Other data are

$t_1 = 371$ minutes $= 6.183$ hours
$q_1 = -100$ STB/D
$q_2 = -48.5$ STB/D
$B_w = 1.0$ RB/STB
$\mu_w = 1.0$ cp.
$h = 20$ ft
$r_w = 0.39$ ft
$c_t = 7.0 \times 10^{-6}$ psi^{-1}
$\phi = 0.20$
$p_{wf}(\Delta t = 0) = 832$ psi.

The log-log data plot in Fig. 7.10 indicates that wellbore storage effects are insignificant after the first data point.

We analyze test data for formation properties by using equations for multiple-rate production-well testing. Eq. 4.6 applies for a two-rate test and the pressure data should be plotted vs $\left\{\log[(t_1 + \Delta t)/\Delta t] + (q_2/q_1)\log \Delta t\right\}$. Fig. 7.11 is

TABLE 7.1—TWO-RATE FALLOFF TEST DATA FOR EXAMPLE 7.3.
$q_1 = -100$ STB/D, $q_2 = -48.5$ STB/D, $t_1 = 6.183$ hours.

Δt (hours)	p_w (psi)	$\log\left(\frac{t_1 + \Delta t}{\Delta t}\right)$	$\log \Delta t$	$\log\left(\frac{t_1 + \Delta t}{\Delta t}\right) + \frac{q_2}{q_1}\log \Delta t$
0	831.8	—	—	—
0.167	661.3	1.580	−0.777	1.203
0.333	640.6	1.292	−0.478	1.060
0.500	631.3	1.126	−0.301	0.980
0.667	630.3	1.012	−0.176	0.927
0.833	625.1	0.925	−0.079	0.887
1.000	623.1	0.856	0.000	0.856
1.333	621.0	0.751	0.125	0.812
1.667	620.0	0.673	0.222	0.781
2.000	620.0	0.612	0.301	0.758
3.000	611.7	0.486	0.477	0.717
4.000	611.7	0.406	0.602	0.698
5.000	611.7	0.350	0.699	0.689

such a plot; it has a slope of $m_1' = 81$ psi/cycle and $p_{1hr} = 624$ psi. Using Eq. 4.10,

$$k = \frac{(-162.6)(-100)(1.0)(1.0)}{(81)(20)} = 10.0 \text{ md}.$$

The skin factor is estimated using Eq. 4.11:

$$s = 1.1513 \left\{ \left[\frac{-100}{-100 - (-48.5)} \right] \left[\frac{832 - 624}{81} \right] - \log \left[\frac{10.0}{(0.2)(1.0)(7.0 \times 10^{-6})(0.39)^2} \right] + 3.2275 \right\}$$

$$= 0.6.$$

The two-rate falloff test in Example 7.3 eliminated high wellbore storage that had been previously observed in the well. Wellbore storage effects in that two-rate test were insignificant after about 15 minutes. That was accomplished with only a 6-hour duration for the initial rate; the entire test lasted only 12 hours.

7.4 Average and Interwell Reservoir Pressure

In finite, liquid-filled reservoirs of uniform mobility and $\phi c_t h$, the false pressure is obtained by extrapolating the straight-line portion of the Horner plot to $(t_p + \Delta t)/\Delta t = 1$. In new wells or wells with short injection times, $p^* \simeq p_i$. However, as is the case in pressure buildup analysis, p^* must be corrected to average reservoir pressure for finite reservoirs. A Matthews-Brons-Hazebroek-type[14] dimensionless pressure may be used to correct the false pressure to average pressure, as given by Eq. 6.2:

$$\bar{p} = p^* - \frac{m\, p_{D\text{MBH}}(t_{pDA})}{2.3025} \quad \ldots\ldots\ldots\ldots\ldots\ldots (7.13)$$

Fig. 7.12 is the MBH dimensionless pressure correlation for a five-spot waterflood.[1] The area per well (one-half the five-spot area) is used in t_{pDA}. Similar correlations are not available for other waterflooding patterns.

Caution should be exercised in applying Eq. 7.13 and Fig. 7.12, and in attempting to apply the methods of Chapter 6 to falloff test analysis. Those methods apply only if (1) the reservoir behaves as if it is lithologically homogeneous and there is a single homogeneous fluid present (that is, the unit mobility ratio assumption must be satisfied); (2) no marked contrast in $\phi c_t h$ exists between the injected and original fluid; (3) noncommunicating layers of markedly different properties are not present; and (4) limited hydraulically induced fractures are present.

In reservoirs with composite fluid banks (Section 7.5), Eq. 7.13 and the methods of Chapter 6 yield incorrect results, especially before fillup. To remedy this situation, Hazebroek, Rainbow, and Matthews[4] proposed a procedure for estimating $\bar{p}$ from falloff tests run before fillup. Their procedure is essentially the same as the extended Muskat method in that $\log(p_{ws} - p_e)$ is plotted vs shut-in time, Δt. At late times, a straight line results when the correct value of p_e has been assumed. The approach must be applied to late-time data; in general, the time restrictions for the beginning of the Muskat straight line given by Eq. 5.21 and Fig. 5.11 for the square with constant-pressure boundaries must be satisfied. The actual numerical values may differ somewhat because of the circular nature of an expanding oil bank, but quantitative methods for estimating the beginning of the Muskat straight line for that situation are not available.

The interwell reservoir pressure sometimes may be used as an approximation of average reservoir pressure. In a five-spot pattern with unit mobility ratio, the pressure halfway between the injector and the producer is

$$\bar{p} = p_{wf}(\Delta t = 0) + \frac{162.6\, qB\mu}{kh} \left[\log \left(\frac{A}{r_w^2} \right) - 0.83867 + 0.86859\, s \right]$$

$$= p_{wf}(\Delta t = 0) + m \left[\log \left(\frac{A}{r_w^2} \right) - 0.83867 + 0.86859\, s \right], \quad \ldots\ldots\ldots\ldots (7.14)$$

where A is the area within the five-spot pattern. If the skin

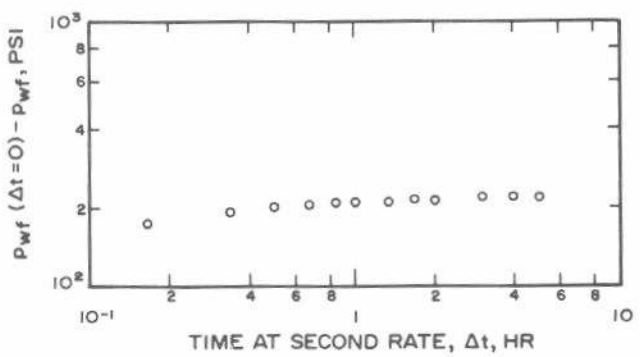

Fig. 7.10 Log-log data plot for the two-rate falloff test of Example 7.3. Water injection in a waterflooded reservoir.

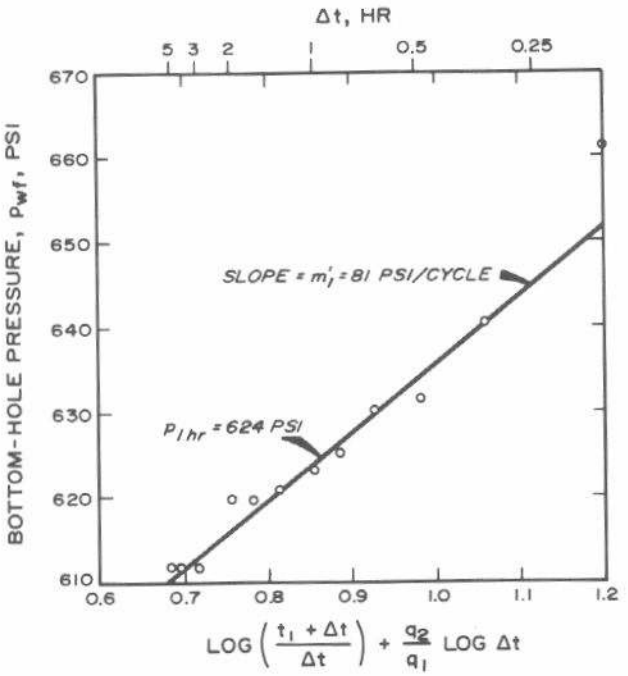

Fig. 7.11 Two-rate falloff-test data plot for Example 7.3. Water injection into a waterflooded reservoir.

factor is not the same in the production and injection wells, replace s in Eq. 7.14 by the average of the two skin factors for theoretically correct results. If the wellbore radii differ, replace r_w^2 by the product of the two r_w values. The coefficient in front of the brackets in Eq. 7.14 is m, obtained from the falloff curve, Eq. 7.7.

Another approximation to the interwell average pressure after fillup is just the arithmetic average of the pressures outside the skin zones at the stabilized injection well and the adjacent stabilized production wells. This pressure may be estimated from

$$\bar{p} \simeq \frac{1}{2}\left[(p_{wf} - \Delta p_s)_{\text{inj}} + \frac{1}{n}\sum_{i=1}^{n}(p_{wf} + \Delta p_s)_{\text{prod},i}\right], \quad \ldots\ldots\ldots\ldots\ldots\ldots\ldots\ldots\ldots\ldots (7.15)$$

where n is the number of producers surrounding the injector. Note that the pressure drop across the skin must be removed before the average reservoir (interwell) pressure is estimated. This is done because injectors and producers can be expected to have different skins and rates because of different wellbore conditions, net sand variations, or different operating practices. As used in Eq. 7.15, Δp_s is positive for damage and negative for improvement. This is a minor deviation from the strict sign interpretation used in Example 7.1.

Example 7.4 Estimating Average Pressure From a Falloff Test—Unit-Mobility-Ratio, Liquid-Filled System

The falloff test of Example 7.2 can be used to illustrate estimating $\bar{p}$ even though the injection time is very short. From Example 7.2, $p^* = -151$ psig at the surface or 2,107 psig at reservoir datum. Using Eq. 2.3b,

$$t_{pDA} = \frac{(0.0002637)(17.4)(6.82)}{(0.25)(1.0)(10^{-5})(871{,}200)} = 0.0144.$$

From Fig. 7.12, $p_{D\text{MBH}}(t_{pDA} = 0.0144) \simeq 0.001$ (read non-zero for illustrative purposes only). Then, applying Eq. 7.13,

$$\bar{p} = 2{,}107 - \frac{(-270)(0.001)}{2.3025}$$

$$= 2{,}107 + 0.12$$

$$= 2{,}107 \text{ psi}.$$

Thus, the p^* value for this short injection time is a usable estimate of $\bar{p}$. Note that the correction to p^* is positive,

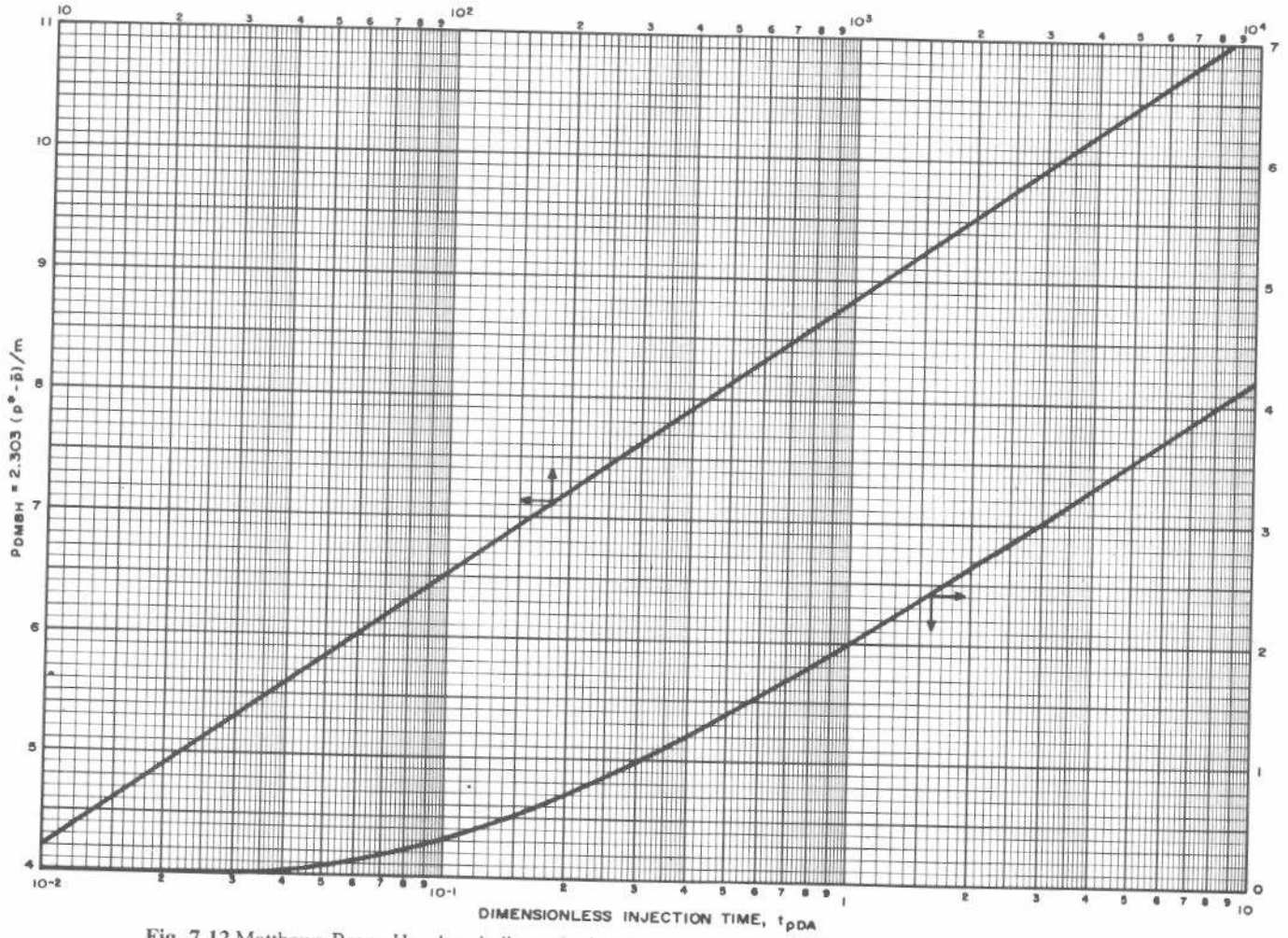

Fig. 7.12 Matthews-Brons-Hazebroek dimensionless pressure for the injection well of a five-spot waterflood, unit mobility ratio. After Matthews and Russell.[1]

indicating that $\bar{p} > p^*$ for falloff.

Eq. 7.14 cannot be used for this example since it assumes a steady-state pressure profile in the formation, which as previously noted, would not occur until a t_{pDA} of about 0.25 based on the area per well (not per pattern).

7.5 Composite System Testing—Non-Unit Mobility Ratio

This section considers transient test analysis for an injection well with the fluid distribution shown in Fig. 7.13. For injection wells, the locations of the banks shown in Fig. 7.13 move; we refer to such a moving bank system as a "composite system." Odeh[15] and Bixel and van Poollen[16] have studied production-well transient test behavior in reservoirs with physical radial discontinuities similar to those indicated in Fig. 7.13. They were concerned with physical discontinuities in the rock system rather than with moving fluid banks. Nevertheless, the analysis methods they present may be useful for injection well testing. Their results can be used to examine the effects of a wide range of porosity-compressibility (ϕc_t) products and mobility (k/μ) ratios or permeability changes when the second bank radius is large compared with the first bank.

Hazebroek, Rainbow, and Matthews[4] have presented material specifically for injection wells before fillup. They assume a significant gas saturation ahead of the oil bank and that the pressure at the leading edge of the oil bank is constant and dominated by the pressure in the gas phase. Although that assumption is not strictly correct, their method may be applied to estimate permeability, skin factor, and average drainage-area pressure from falloff test analysis. The analysis uses an extended Muskat-type plot of $\log(p_{ws} - p_e)$ vs Δt, with p_e being varied until a straight line is obtained with late-time falloff data. The slope and intercept of that plot may be used with correlations to estimate permeability and skin factor. If an independent estimate of the mobility ratio and the ϕc_t ratio between the two banks can be made, the permeability in each bank may be estimated. The Hazebroek-Rainbow-Matthews method is covered in detail in Chapter 8 of Ref. 1, and, therefore, is not repeated here. Hazebroek, Rainbow, and Matthews[4] conclude that permeability and skin factor for the zone near the well may be estimated equally well by their method or by the MDH and Horner techniques. It must be realized, however, that those two methods give the properties of the fluid bank within the radius of investigation given by Eq. 2.41. If the boundary between the inner and outer banks does not exceed that radius of investigation for the portion of the data analyzed, incorrect results will be obtained. When the distance to the boundary between the two regions is small compared with the radius of investigation, the permeability of the outer region will be obtained by transient data analysis; the skin factor will reflect the presence of the inner bank.

For very small injected volumes, the Hazebroek-Rainbow-Matthews technique is probably superior to normal techniques for estimating permeability of the inner zone and actual damage skin factor — when the important assumption of constant pressure at the outer edge of the oil bank is satisfied. For systems with large injection volumes, normal analysis methods should provide equally reliable data, with the possible exception of estimates of average reservoir pressure. In that case, the Hazebroek-Rainbow-Matthews method (or equivalently, the extended Muskat method) should be used for estimating average pressure if the methods of Section 7.4 cannot be applied. The following analysis approach[17,18] is preferred for fluid-filled systems, when it is applicable, to that of Hazebroek, Rainbow, and Matthews.

Fig. 7.14 shows typical expected injection well falloff behavior in a two-bank system, as presented by Merrill,

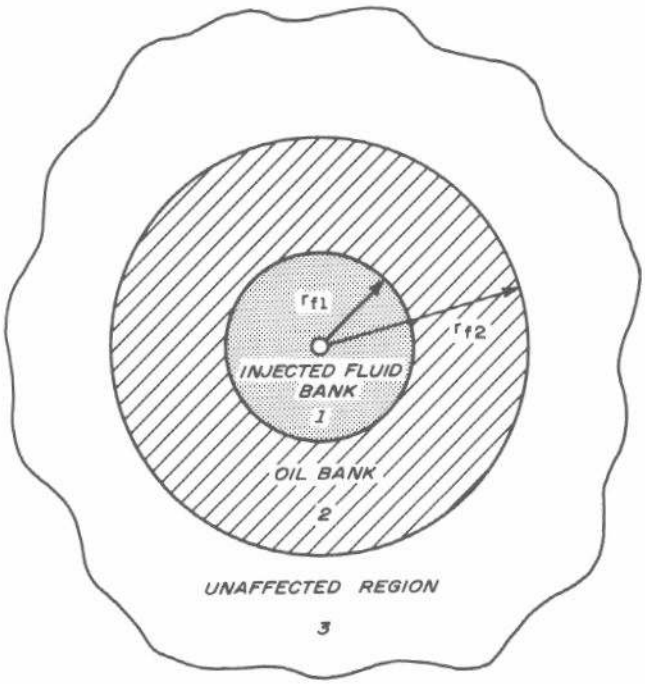

Fig. 7.13 Schematic diagram of fluid distribution around an injection well (composite reservoir).

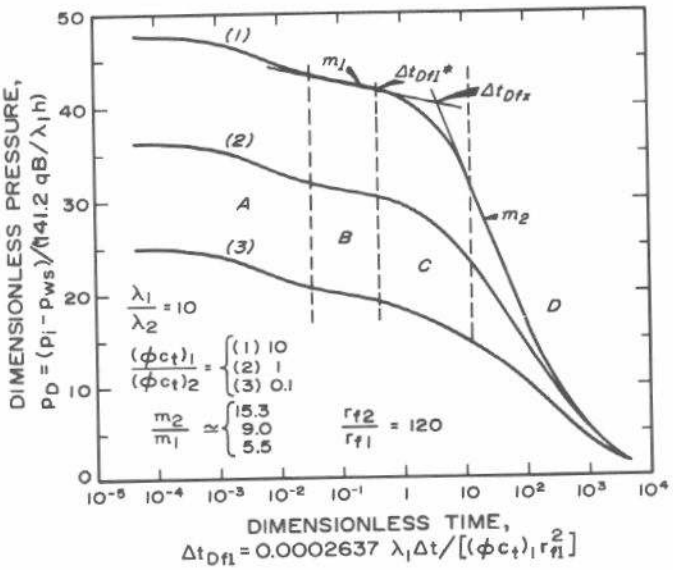

Fig. 7.14 Simulated pressure falloff data for a two-zone system. After Merrill, Kazemi, and Gogarty.[18]

Kazemi, and Gogarty[18] for a liquid-filled system. The three falloff curves apply for a mobility ratio $[M = \lambda_1/\lambda_2 = (k/\mu)_1/(k/\mu)_2]$ of 10 between the first and second bank; there is no third bank. The three curves apply for different ratios of porosity-compressibility product (ϕc_t) between the two zones. Wellbore storage effects are included. The "A" portion of Fig. 7.14 is dominated by wellbore storage effects; the "B" portion is a semilog straight line that provides information about the injected fluid bank, Region 1; the "C" portion is a transition as the second fluid bank begins to exert its influence on the falloff behavior; and the "D" portion of the curve includes a second semilog straight line whose slope is determined by properties of Regions 1 and 2.

Merrill, Kazemi, and Gogarty[18] propose methods for estimating both the location of the front of Region 1 in Fig. 7.13 and the permeability of the two fluid banks in a two-zone system. Their approach does not require previous knowledge of the mobility ratio, although an estimate of the ϕc_t ratio must be available. The data presented in Ref. 18 and here are based on computer simulations for which $r_{f2}/r_{f1} > 50$. Practically speaking, if $r_{f2}/r_{f1} > 10$, the techniques probably still apply. However, for lower values of r_{f2}/r_{f1}, chances of successful analysis are poor. The Merrill-Kazemi-Gogarty approach differs from the Hazebroek-Rainbow-Matthews approach in that it requires knowledge of neither the mobility ratio nor the location of the interior fluid front.

Merrill, Kazemi, and Gogarty[18] proposed two ways for estimating the distance to the front of Region 1 from a p_{ws} vs log Δt plot of falloff data. One approach is to use the extrapolated intersection time of the two semilog straight lines on the MDH plot, Δt_{fx}, with

$$r_{f1} = \sqrt{\frac{0.0002637\,(k/\mu)_1}{(\phi c_t)_1}\,\frac{\Delta t_{fx}}{\Delta t_{Dfx}}}\ . \quad \ldots\ldots\ldots (7.16)$$

Fig. 7.15 correlates Δt_{Dfx} with the ratio of the two semilog slopes from the falloff curve and the ϕc_t ratio in the two fluid banks. The second method uses the point of deviation of the observed pressure data from the first semilog straight line, $\Delta t_{f1}{}^*$, with

$$r_{f1} = \sqrt{\frac{0.0002637\,(k/\mu)_1}{(\phi c_t)_1}\,\frac{\Delta t_{f1}{}^*}{\Delta t_{Df1}{}^*}}\ . \quad \ldots\ldots\ldots (7.17)$$

Merrill, Kazemi, and Gogarty[18] show that $0.13 < \Delta t_{Df1}{}^* < 1.39$, with an average value of 0.389. This agrees quite well with an interpretive rule of thumb that the water-bank (first bank) slope normally will be valid to a time equivalent to Δt_{Df1} (based on r_{f1}, see Fig. 7.13) of about 0.25. $\Delta t_{Df1}{}^*$ does not correlate well with slope and specific storage ratios, so we do not recommend using Eq. 7.17 unless insufficient data are available to estimate Δt_{fx} for use in Eq. 7.16.

The permeability in the injected fluid bank may be estimated from the slope $(\pm m_1)$ of the first semilog straight line and Eq. 7.9. Skin factor is estimated from m_1, p_{1hr}, and Eq. 7.10. If $r_{f2} > 10r_{f1}$, the mobility in the second zone may be estimated from

$$\left(\frac{k}{\mu}\right)_2 = \frac{(k/\mu)_1}{(\lambda_1/\lambda_2)}\ , \quad \ldots\ldots\ldots\ldots\ldots\ldots\ldots (7.18)$$

where the mobility ratio, (λ_1/λ_2), is from either Fig. 7.16 or Fig. 7.17.[18] If both semilog straight lines appear and if it is possible to estimate the ratio of specific storage capacities, it is possible to estimate mobility or permeability in each zone. A common error in transient test analysis is to assume that each slope indicates the mobility of a particular fluid zone. Figs. 7.14, 7.16, and 7.17, and Eq. 7.18 clearly show this is not the case for the second zone. Further modifications are needed when $r_{f2} < 10r_{f1}$, even for a liquid-filled, two-bank system. Unfortunately, it seems that reservoir simulation

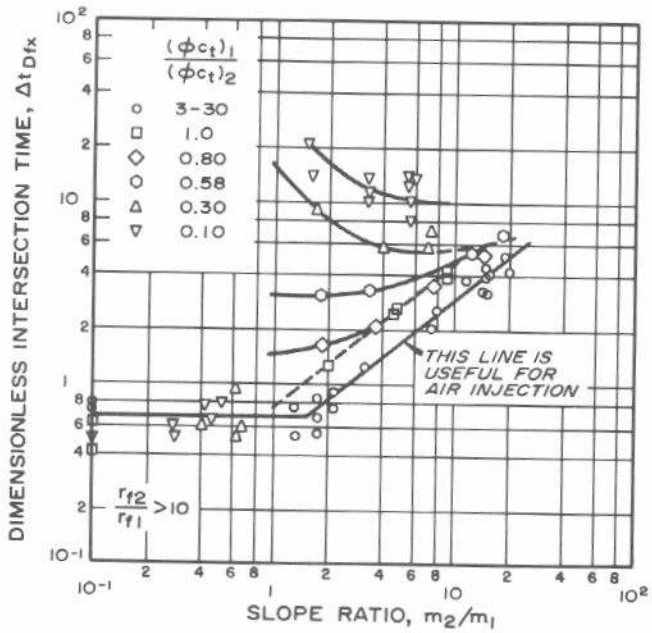

Fig. 7.15 Correlation of dimensionless intersection time, Δt_{Dfx}, for falloff data from a two-zone reservoir. After Merrill, Kazemi, and Gogarty.[18]

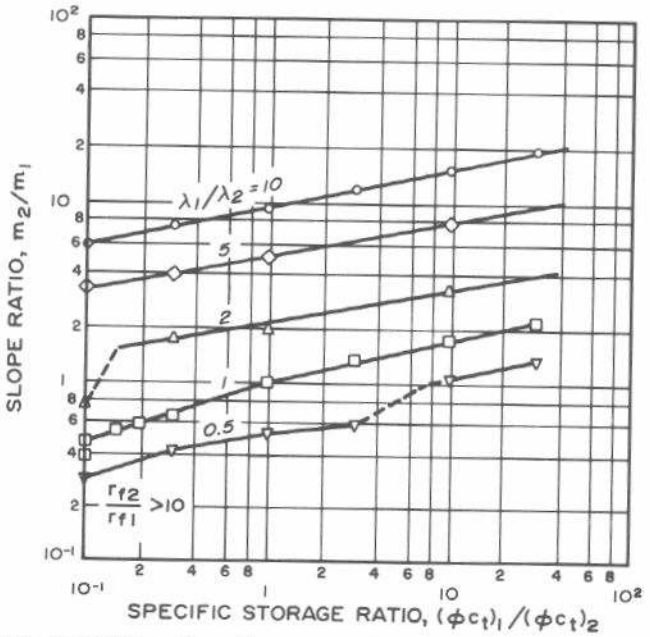

Fig. 7.16 Effect of specific storage ratio and mobility ratio on the slope ratio for falloff testing in a two-zone reservoir. After Merrill, Kazemi, and Gogarty.[18]

approaches are required for analysis of that common situation.

Merrill, Kazemi, and Gogarty[18] suggest a way to estimate the maximum wellbore storage coefficient that still allows the first semilog straight line to be observed. By using their approach, but substituting Eq. 2.22b as the criterion for the end of wellbore storage effects for pressure falloff testing, we see that

$$C \leq 5.9 \times 10^{-7} \left(\frac{k}{\mu}\right)_1 h \Delta t_{f1}^* e^{-0.14s}, \quad \ldots\ldots\ldots (7.19)$$

for the first semilog straight line to be detected. Eq. 7.19 allows for about 1 cycle of semilog straight line between die-out of afterflow and initial deviation caused by second-bank effects. That is a difficult criterion to achieve, especially if the boundary between the first and second banks is relatively close to the injection well.

Example 7.5 Pressure Falloff Analysis in a Two-Zone System

Fig. 7.18 is a semilog plot of simulated falloff data for a two-zone waterflood from Merrill, Kazemi, and Gogarty.[18] Data used in the simulation were

$r_w = 0.25$ ft
$r_{f1} = 30$ ft
$r_{f2} = r_e = 3{,}600$ ft, so $r_{f2}/r_{f1} = 120$
$(k/\mu)_1 = \lambda_1 = 100$ md/cp
$(k/\mu)_2 = \lambda_2 = 50$ md/cp
$(\phi c_t)_1 = 8.95 \times 10^{-7}$ psi^{-1}
$(\phi c_t)_2 = 1.54 \times 10^{-6}$ psi^{-1}
$q = -400$ STB/D
$B_w = 1.0$ RB/STB
$h = 20$ ft
$s = 0$
$C = 0$.

Since the data were simulated with no wellbore storage effect, we need not make the log-log data plot. Fig. 7.18, the MDH plot of the data, shows that $m_1 = -32.5$ psi/cycle and $m_2 = -60.1$ psi/cycle. Also,

$$m_2/m_1 = -60.1/(-32.5) = 1.85,$$

and

$$(\phi c_t)_1/(\phi c_t)_2 = 8.95 \times 10^{-7}/1.54 \times 10^{-6} = 0.581.$$

To estimate k/μ for Region 1 we use Eq. 7.9:

$$\left(\frac{k}{\mu}\right)_1 = \frac{162.6(-400)(1.0)}{(-32.5)(20)} = 100 \text{ md/cp},$$

the correct result.

To estimate $(k/\mu)_2$ we enter Fig. 7.17 with the slope and ϕc_t ratios above and read $\lambda_1/\lambda_2 = 2.0$. Then, from Eq. 7.18,

$$\left(\frac{k}{\mu}\right)_2 = \frac{100}{2.0} = 50 \text{ md/cp}.$$

We may use either Eq. 7.16 or Eq. 7.17 to estimate the location of the front of the water bank. From Fig. 7.18, the falloff plot, $\Delta t_{Dfx} = 0.095$ hour and $\Delta t_{f1}^* = 0.013$ hour. Using Fig. 7.15 with $m_2/m_1 = 1.85$ and $(\phi c_t)_2/(\phi c_t)_1 = 0.58$, we get $\Delta t_{Dfx} = 3.05$. Using Eq. 7.16,

$$r_{f1} = \sqrt{\frac{(0.0002637)(100)(0.095)}{(8.95 \times 10^{-7})(3.05)}} = 30 \text{ ft},$$

the value set in the simulation. To use Eq. 7.17 we must assume a value or a range for t_{Df1}^*. Using $0.13 \leq t_{Df1}^* \leq 1.39$ and $\bar{t}_{Df1}^* = 0.389$, we get

$$54 > r_{f1} > 17,$$

and

$$\bar{r}_{f1} = 31 \text{ ft}.$$

In this case the average value of t_{Df1}^* gave quite acceptable results, but that may be a coincidence.[18]

Although there is no wellbore storage in this example, we can estimate the maximum wellbore storage coefficient that

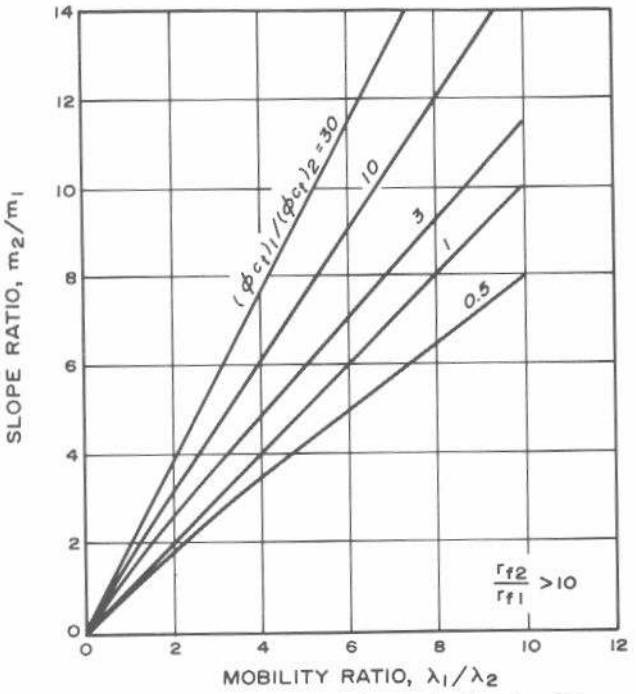

Fig. 7.17 Crossplot of data in Fig. 7.16. After Merrill, Kazemi, and Gogarty.[18]

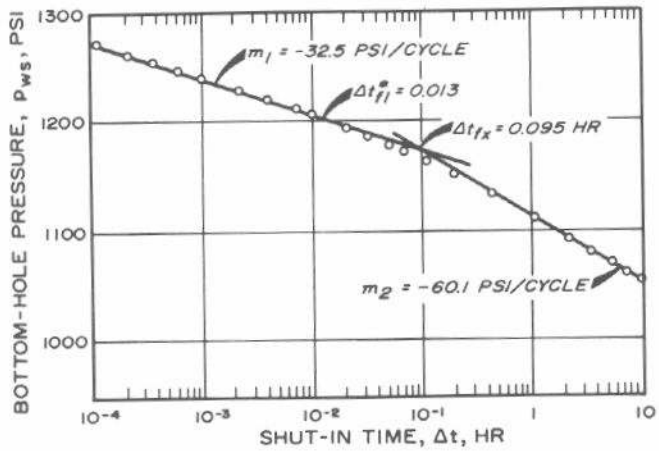

Fig. 7.18 Falloff test data for Example 7.5. After Merrill, Kazemi, and Gogarty.[18]

would not have obscured the first straight line on Fig. 7.18. Using Eq. 7.19 with $s = 0$,

$$C \leq 5.9 \times 10^{-7}(100)(20)(0.013)e^{(-0.14)(0)}$$

$$\leq 1.53 \times 10^{-5} \text{ RB/psi.}$$

If we assume that the wellbore is full of water of compressibility, $c_w = 3.0 \times 10^{-6}$ psi^{-1}, then from Eq. 2.17,

$$V_w \leq \frac{1.53 \times 10^{-5}}{3.0 \times 10^{-6}} = 5.1 \text{ bbl.}$$

Thus, if the well is completed with 2-in. tubing on a packer ($V_u \simeq 0.004$ bbl/ft), the maximum depth to meet the restriction on the wellbore storage coefficient would be about 1,300 ft — and this is assuming zero skin. For 3-in. tubing the depth must not exceed about 570 ft. If the skin factor had been 5.0, the depths for 2- and 3-in. tubing would be 635 and 282 ft, respectively.

This material applies to composite systems with two radial fluid zones, with the second zone large compared with the first. Based on a study of three-zone systems, Merrill, Kazemi, and Gogarty[18] conclude that the *only useful information* obtainable in such reservoirs is the mobility of the first zone and a rough estimate of its extent if there is a distinct contrast of mobility ratios. Reliable estimates of the mobilities and the locations of the second and third zones cannot be made with currently available technology. It is likely that the only way such estimates could be made would be by a matching process using a reservoir simulator such as that discussed in Ref. 17.

Merrill, Kazemi, and Gogarty[18] and Dowdle[19] propose methods for estimating the water saturation in the injected-fluid zone by combining Eq. 7.16, Fig. 7.15, and the material-balance equation. These methods apply at a fairly early stage of water injection into a previously liquid-filled reservoir as a result of the restriction $r_{f2} > 10r_{f1}$.

Type-curve matching may be applied to composite systems under certain circumstances. Bixel and van Poollen[16] propose such a method for analyzing pressure buildup tests with widely varying ϕc_t and k/μ ratios where the second zone is large.

One characteristic of water injection with a non-unit mobility ratio is that the injectivity tends to change as water enters the formation.[20] During the early stages of injection, this will appear as a changing skin factor. When enough fluid is injected to form a significantly large fluid bank around the injection well, the mobility of that bank will be detected by transient tests, and skin factor computed from the first-bank slope should not change unless the injected fluid is actually damaging or stimulating the wellbore.

7.6 A Pragmatic Approach to Falloff Test Analysis

From a practical point of view, a stepwise approach to pressure falloff analysis usually can be applied with acceptable results. The procedure is as follows:

1. Plot log Δp vs log Δt to determine when wellbore storage effects cease to be important. Use that plot to select the semilog straight line for the following step.

2. Regardless of the mobility ratio and whether the reservoir is filled up or not, make the MDH plot. Choose what appears to be the correct semilog straight line and estimate permeability and skin factor.

3. Calculate the expected end of the semilog straight line, assuming that it corresponds to

$$\Delta t_{Df1}{}^* \simeq 0.25 \; . \qquad (7.20)$$

Thus, the approximate end time of the semilog straight line may be estimated from

$$\Delta t^* \simeq \frac{950\,(\phi c_t)_1 r_{f1}{}^2}{(k/\mu)_1}, \qquad (7.21)$$

where $(k/\mu)_1$ is estimated from the MDH slope and r_{f1} is estimated independently such as by material balance. Eq. 7.21 is a reasonable rule-of-thumb estimate for both unfilled and filled systems operating at steady or pseudosteady conditions before shut-in.

4. If the apparent end of the MDH straight line does not correspond approximately to the time estimated in Step 3, additional steps can be taken to complete the process. This might include using the Horner method with t_p computed by normal methods, and t_{pss} computed from $(t_{DA})_{pss}$ using the area to the front of the oil bank. Also, the Hazebroek-Rainbow-Matthews method could be applied at this point, if necessary.

5. The average pressure, $\bar{p}$, may be estimated using the Matthews-Brons-Hazebroek, Fig. 7.12, or Hazebroek-Rainbow-Matthews (extended Muskat plot) methods. When the oil bank is relatively thin, the mobility ratio is near unity, and wellbore effects have died out, a simple Dietz-type extrapolation of the MDH straight line equivalent to a dimensionless time of 0.445 (based on radius of the oil bank) may be made to estimate $\bar{p}$:

$$(\Delta t)_{\bar{p}} = \frac{1{,}690\,(\phi c_t)_1 r_{f2}{}^2}{(k/\mu)_1} \qquad (7.22)$$

Eq. 7.22 can give a reasonable estimate of the reservoir pressure at the leading edge of the oil bank, assuming a constant pressure beyond that point.

6. When applicable, the Merrill-Kazemi-Gogarty[18] method can be used to estimate the second-bank mobility.

There can be errors in all the methods because of imprecise boundary conditions and assumptions used in deriving those techniques. Generally, the MDH method does give quite good values for mobility, unless the mobility ratio between the banks varies significantly from unity and the inner and outer banks are about the same size. The Hazebroek-Rainbow-Matthews approach is a late-time method based on a constant-pressure outer boundary condition. The worst errors in application of that method can be expected to occur when $t_{DAf2} < 0.44$. The calculation of the dimensionless time can prevent or reveal such application.

7.7 Series-of-Steady-State Analysis

Hall[20] proposed a technique for analyzing injection wells that basically assumes a series of steady-state injection conditions. Required data are cumulative volume injected

and a good record of injection pressure. The technique presented here is a modified version of Hall's technique.[20] Eq. 2.2 is written for steady-state flow conditions and p_D is assumed to be independent of time. That assumption is not correct for long periods of time, but it is a workable approximation over reasonable time periods and does provide a simple method for monitoring injection-well performance. Using the constant p_D assumption, both sides of Eq. 2.2 can be multiplied by dt and integrated from time 0 to time t. The result is

$$\int_0^t p_{wf}dt - p_e t = \frac{141.2\mu\,(p_D+s)}{kh} W_i \,, \quad \ldots\ldots (7.23)$$

where W_i is the cumulative fluid injected at time t, a positive number. Usually, the integral on the left side of Eq. 7.23 can be approximated by a summation using wellhead pressure, p_{tf}, plus a constant fluid head term, Δp_{tw}, to approximate bottom-hole pressure, p_{wf}. Alternatively, it can be evaluated by planimetering a graph of injection pressure vs time. If p_{wf} on the left side of Eq. 7.23 is approximated by the surface injection pressure plus a constant fluid head term, the equation may be written as

$$\int_0^t p_{tf}dt - (p_e - \Delta p_{tw})t = \frac{141.2\mu\,(p_D+s)}{kh} W_i \,, \quad \ldots\ldots (7.24)$$

where Δp_{tw} is the constant fluid head between surface and bottom hole. If $(p_e - \Delta p_{tw})t$ is small compared with the integral in Eq. 7.24, as it often is for pumped-off waterfloods, a plot of the integral (or its approximation) vs cumulative water injection (called a "Hall plot") should give a straight line with slope

$$m_H = \frac{141.2\mu\,(p_D+s)}{kh} \text{ psi/(B/D)} \,, \quad \ldots\ldots (7.25)$$

as illustrated in Fig. 7.19. Eq. 7.25 assumes the integral term has units psi × days (not hours). If p_D and s are known, we should be able to estimate k/μ from Eq. 7.25. Or, if p_D and k/μ are known, we should be able to estimate s. However, we must obtain at least k/μ or s from a transient test to use Eq. 7.25 and we must be able to estimate p_D. If $(p_e - \Delta p_{tw})t$ is about 15 percent or more of the integral, its effect should be included in the data plot, or serious quantitative errors can result. In most cases, little error is caused by neglecting $(p_e - \Delta p_{tw})$. The error may be estimated by using two or three values in making the plot and observing the effect.

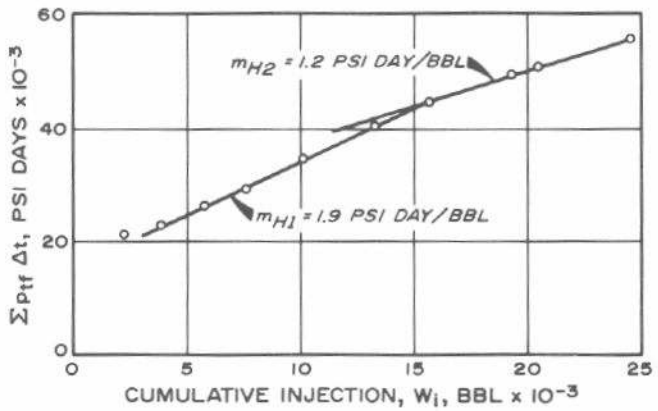

Fig. 7.19 Hall plot for a water injection well showing the effects of stimulation, Example 7.6.

The major benefit of the Hall plot is not from the single straight line, but from changes in the slope of the line. Changes in the slope of the Hall plot can be caused by changes in k/μ, s, or p_D. In any fluid injection operation, we expect k/μ to change in the vicinity of the well as fluid is injected and as the gas volume in the reservoir is filled up. As that happens, both k/μ and p_D change. In addition, p_D may change as a result of changes in operating practices or the addition of new offset production wells. Actual changes in the skin factor will also affect the slope of the Hall plot. Since Eq. 2.10 indicates that any change in permeability in the vicinity of the wellbore can be expressed as skin, we choose to show how to use the Hall plot to estimate changes in skin factor. Nevertheless, the plot can be used to estimate changes in any of the quantities of the right side of Eq. 7.25. The change in skin factor is estimated from the change in slope of the Hall plot:

$$s_2 = s_1 + \frac{kh}{141.2\mu}(m_{H2} - m_{H1}) \,, \quad \ldots\ldots (7.26)$$

where k/μ is supplied from transient test data. Another approach is to use the two slopes on a Hall plot, such as in Fig. 7.19, to estimate the ratio of the new flow efficiency to the old flow efficiency:

$$\frac{E_{f2}}{E_{f1}} = \frac{m_{H1}}{m_{H2}} \,. \quad \ldots\ldots (7.27)$$

While always in the right direction, the amount of change in the flow efficiency can be somewhat distorted if p_{tf} used in the Hall plot is significantly different from the true differential $(p_{wf} - p_e)$; that is, if $(p_e - \Delta p_{tw}) > 0.15\,p_{tf}$.

Example 7.6 Hall Method Steady-State Analysis

Fig. 7.19 is a Hall plot for a water injection well in a 1,000-ft deep, filled-up Illinois reservoir. In that reservoir $(p_e - \Delta p_{tw})$ is very small compared with p_{tf}, so the data plot shown is adequate. The injection well was shot with nitroglycerin on completion. It was stimulated with micellar solution[21] after a cumulative water injection of about 15,000 bbl. From transient testing before stimulation,

$$\left(\frac{kh}{\mu}\right)_1 = 280 \text{ md ft/cp},$$

and

$$s_1 = -1.12.$$

From transient testing several weeks after stimulation,

$$\left(\frac{kh}{\mu}\right)_2 = 290 \text{ md ft/cp},$$

and

$$s_2 = -2.3.$$

From Fig. 7.19,

$$m_{H1} = 1.9 \text{ psi/(B/D)},$$

and

$$m_{H2} = 1.2 \text{ psi/(B/D)}.$$

Applying Eq. 7.26,

$$s_2 = -1.12 + \frac{280}{141.2}(1.2 - 1.9)$$

$$= -2.5.$$

This compares favorably with $s = -2.3$ determined by transient testing several weeks after stimulation.

Muskat[22] has devised a method for analyzing water injection well data when the injection pressure, p_{wf}, is constant. He suggests that a plot of $1/q$, where q is the time varying injection rate, vs log W_i, where W_i is the cumulative volume injected, should be a straight line. The slope of the line is related to the permeability of the injected fluid, while the intercept is related to mobility ratio and saturations in the various bank areas.

7.8 Step-Rate Testing

A step-rate injectivity test is normally used to estimate fracture pressure in an injection well.[23] Such information is useful in waterfloods and is critically important in tertiary floods where it is important to avoid injecting expensive fluids through uncontrolled, artificially induced fractures.

A step-rate injectivity test is simple, inexpensive, and fast. Fluid is injected at a series of increasing rates, with each rate preferably lasting the same length of time. In relatively low-permeability formations ($k < 5$ md), each injection rate should last about 1 hour; 30-minute injection times are adequate for formations with permeability exceeding 10 md.[23] As few as four rates may be used, but normally

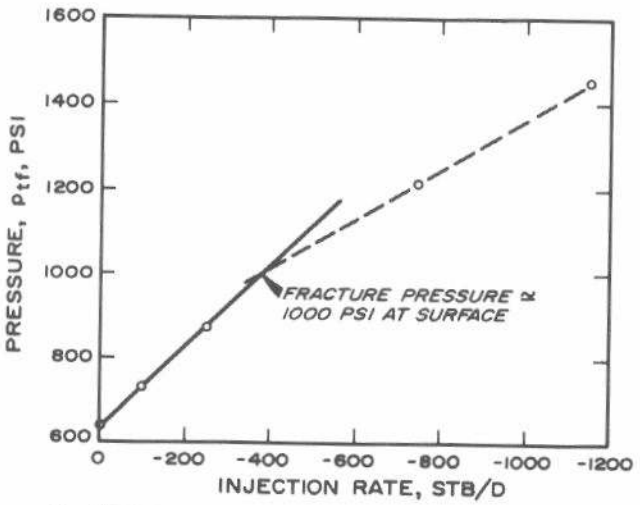

Fig. 7.20 Step-rate injectivity data plot for Example 7.7. Data of Felsenthal.[23]

TABLE 7.2—PRESSURE AND RATE DATA FOR A STEP-RATE INJECTIVITY TEST,[23] EXAMPLE 7.6.

t (hours)	q (STB/D)	p_{tf} (psi)	$\sum$ term, Eq. 4.1	$(p_i - p_{tf})/q$ (psi/STB/D)
0	0	642	—	—
0.5	−100	720	−0.301	0.780
1.0	−100	730	0.000	0.880
1.5	−250	856	−0.110	0.856
2.0	−250	874	0.120	0.928
2.25	−750	1,143	−0.335	0.668
2.50	−750	1,182	−0.112	0.720
3.00	−750	1,216	0.124	0.765
4.00	−1,150	1,450	0.246	0.703

six, seven, or eight rates are preferred. The analysis consists of plotting injection pressure at the end of each rate vs injection rate. It is preferable to plot bottom-hole pressure, but surface pressure may be used if it is positive throughout the test and friction effects are not significant. The plot should have two straight-line segments, as illustrated in Fig. 7.20. The break in the line indicates formation fracture pressure. (Unfortunately, it can also indicate the breakdown pressure of the cement bond. When the cement bond fails, the slope of the second straight line in Fig. 7.20 usually continues below the fracture pressure as the rate is decreased.) The fracture pressure may vary depending on fluid saturation conditions in the formation and long-term variations in reservoir pressure level with time.[23]

Pressure data taken during each rate may be analyzed with a multiple-rate transient technique (Section 4.2) to estimate formation permeability and skin factor. Eqs. 4.1, 4.4, and 4.5 can be used, providing the effective wellbore radius was not already large because of previous fracture stimulation, thus making the line-source log approximation an inappropriate solution.

Example 7.7 Step-Rate Analysis

Felsenthal[23] provides the data in Table 7.2 for a step-rate test in a reservoir with the following properties:

$B_w = 1.0$ RB/STB
$\mu_w = 0.45$ cp
$h = 270$ ft
$\phi = 0.186$
$c_t = 1.5 \times 10^{-5}$ psi^{-1}
$r_w = 0.25$ ft
Depth = 7,260 ft
Injected-fluid pressure gradient = 0.433 psi/ft.

Fig. 7.20 shows the normal step-rate data plot, p_{tf} vs q. The break in the data indicates a surface fracture pressure of about 1,000 psi. The fracture gradient is estimated by dividing the bottom-hole fracture pressure by the depth. The fracture gradient is

$$[(0.433)(7{,}260) + 1{,}000]/7{,}260 = 0.57 \text{ psi/ft}.$$

The data in Table 7.2 also may be analyzed for formation properties by using the methods described in Section 4.2. The two right-hand columns in Table 7.2 contain the data to be plotted according to Eq. 4.1. Fig. 7.21 shows the data plot. The first four points, for the rates before the fracture was induced, fall on the expected straight line. That line has the properties

$$m' = 0.357\ [\text{psi/(STB/D)}]/\text{cycle},$$

and

$$b' = 0.885\ \text{psi/(STB/D)}.$$

We estimate formation permeability from Eq. 4.4:

$$k = \frac{(162.6)(1.0)(0.45)}{(0.357)(270)} = 0.76\ \text{md}.$$

The skin factor is estimated from Eq. 4.5:

$$s = 1.1513\left\{\frac{0.885}{0.357} - \log\left[\frac{0.76}{(0.186)(0.45)(1.5 \times 10^{-5})(0.25)^2}\right] + 3.2275\right\}$$

$$= -1.5.$$

In Fig. 7.21, the data points for $q = -750$ and $q = -1{,}150$ STB/D do not fall on the straight line. Those points correspond to data taken after the formation fractured (see Fig. 7.20). They do not fall on the initial straight line in Eq. 7.25 because the assumptions of radial, infinite-acting flow (used in Eq. 4.1) are not satisfied after the formation is fractured.

In this multiple-rate analysis, we have assumed a unit mobility ratio; there are no data to indicate the accuracy of that assumption.

References

1. Matthews, C. S. and Russell, D. G.: *Pressure Buildup and Flow Tests in Wells*, Monograph Series, Society of Petroleum Engineers of AIME, Dallas (1967) **1**, Chap. 8.

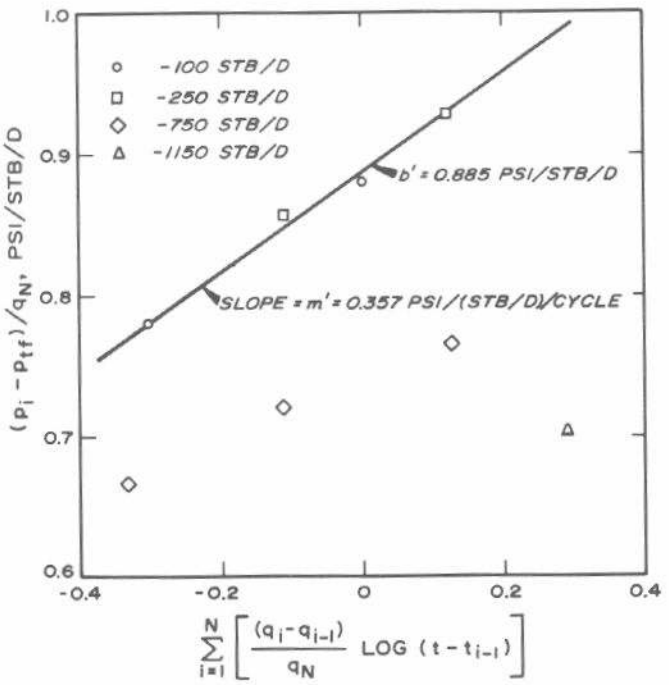

Fig. 7.21 Multiple-rate-type data plot for Example 7.7. Data of Felsenthal.[23]

2. Morse, J. V. and Ott, Frank III: "Field Application of Unsteady-State Pressure Analysis in Reservoir Diagnosis," *J. Pet. Tech.* (July 1967) 869-876.
3. Nowak, T. J. and Lester, G. W.: "Analysis of Pressure Fall-Off Curves Obtained in Water Injection Wells to Determine Injective Capacity and Formation Damage," *Trans.*, AIME (1955) **204**, 96-102. Also *Reprint Series, No. 9 — Pressure Analysis Methods*, Society of Petroleum Engineers of AIME, Dallas (1967) 61-67.
4. Hazebroek, P., Rainbow, H., and Matthews, C. S.: "Pressure Fall-Off in Water Injection Wells," *Trans.*, AIME (1958) **213**, 250-260.
5. Clark, K. K.: "Transient Pressure Testing of Fractured Water Injection Wells," *J. Pet. Tech.* (June 1968) 639-643; *Trans.*, AIME, **243.**
6. McLeod, H. O., Jr., and Coulter, A. W., Jr.: "The Stimulation Treatment Pressure Record — An Overlooked Formation Evaluation Tool," *J. Pet. Tech.* (Aug. 1969) 951-960.
7. Robertson, D. C. and Kelm, C. H.: "Injection-Well Testing To Optimize Waterflood Performance," *J. Pet. Tech.* (Nov. 1975) 1337-1342.
8. van Poollen, H. K.: "Transient Tests Find Fire Front in an In-Situ Combustion Project," *Oil and Gas J.* (Feb. 1, 1965) 78-80.
9. Kazemi, Hossein: "Locating a Burning Front by Pressure Transient Measurements," *J. Pet. Tech.* (Feb. 1966) 227-232; *Trans.*, AIME, **237.**
10. Ramey, Henry J., Jr., Kumar, Anil, and Gulati, Mohinder S.: *Gas Well Test Analysis Under Water-Drive Conditions*, AGA, Arlington, Va. (1973).
11. Pinson, A. E., Jr.: "Concerning the Value of Producing Time Used in Average Pressure Determinations From Pressure Buildup Analysis," *J. Pet. Tech.* (Nov. 1972) 1369-1370.
12. Kazemi, Hossein: "Determining Average Reservoir Pressure From Pressure Buildup Tests," *Soc. Pet. Eng. J.* (Feb. 1974) 55-62; *Trans.*, AIME, **257.**
13. Earlougher, Robert C., Jr., Kersch, K. M., and Ramey, H. J., Jr.: "Wellbore Effects in Injection Well Testing," *J. Pet. Tech.* (Nov. 1973) 1244-1250.
14. Matthews, C. S., Brons, F., and Hazebroek, P.: "A Method for Determination of Average Pressure in a Bounded Reservoir," *Trans.*, AIME (1954) **201**, 182-191. Also *Reprint Series, No. 9 — Pressure Analysis Methods*, Society of Petroleum Engineers of AIME, Dallas (1967) 51-60.
15. Odeh, A. S.: "Flow Test Analysis for a Well With Radial Discontinuity," *J. Pet. Tech.* (Feb. 1969) 207-210; *Trans.*, AIME, **246.**
16. Bixel, H. C. and van Poollen, H. K.: "Pressure Drawdown and Buildup in the Presence of Radial Discontinuities," *Soc. Pet. Eng. J.* (Sept. 1967) 301-309; *Trans.*, AIME, **240.** Also *Reprint Series, No. 9 — Pressure Analysis Methods*, Society of Petroleum Engineers of AIME, Dallas (1967) 188-196.
17. Kazemi, Hossein, Merrill, L. S., and Jargon, J. R.: "Problems in Interpretation of Pressure Fall-Off Tests in Reservoirs With and Without Fluid Banks," *J. Pet. Tech.* (Sept. 1972) 1147-1156.
18. Merrill, L. S., Jr., Kazemi, Hossein, and Gogarty, W. Barney: "Pressure Falloff Analysis in Reservoirs With Fluid Banks," *J. Pet. Tech.* (July 1974) 809-818; *Trans.*, AIME, **257.**
19. Dowdle, Walter L.: "Discussion of Pressure Falloff Analysis in Reservoirs With Fluid Banks," *J. Pet. Tech.* (July 1974) 818.

20. Hall, H. N.: "How to Analyze Waterflood Injection Well Performance," *World Oil* (Oct. 1963) 128-130.

21. Gogarty, W. B., Kinney, W. L., and Kirk, W. B.: "Injection Well Stimulation With Micellar Solutions," *J. Pet. Tech.* (Dec. 1970) 1577-1584.

22. Muskat, Morris: *Physical Principles of Oil Production,* McGraw-Hill Book Co., Inc., New York (1949) 682-686.

23. Felsenthal, Martin: "Step-Rate Tests Determine Safe Injection Pressures in Floods," *Oil and Gas J.* (Oct. 28, 1974) 49-54.